BOREAL ECOSYSTEM CHANGES DUE TO PERMAFROST THAW ACROSS THE DISCONTINUOUS TO SPORADIC PERMAFROST ZONE

LINDA FLADE

Master of Science, Ludwig Maximilians University, Munich, Germany, 2017

A thesis submitted
in partial fulfillment of the requirements for the degree of

DOCTOR OF PHILOSOPHY

in

EARTH, SPACE, AND PHYSICAL SCIENCE

Department of Geography & Environment
University of Lethbridge
LETHBRIDGE, ALBERTA, CANADA

BOREAL ECOSYSTEM CHANGES DUE TO PERMAFROST THAW ACROSS THE DISCONTINUOUS TO SPORADIC PERMAFROST ZONE

LINDA FLADE

Date of Defense: December 16th, 2024

Dr. Laura Chasmer	Associate Professor	Ph.D.
Dr. Chris Hopkinson	Professor	Ph.D.
Thesis Co-Supervisors		
Dr. Derek Peddle	Professor	Ph.D.
Thesis Examination Committee Member		
Dr. Larry Flanagan	Professor	Ph.D.
Thesis Examination Committee Member		
Dr. Aaron Berg	Professor	Ph.D.
External Examiner		
Geography, Environment & Geomatics, University of Guelph		
Dr. Kevin McGeough	Professor	Ph.D.
Chair of Thesis Examination Committee		

DEDICATION

To my grandfather, for opening my childhood eyes and heart to nature on our wanderings through Germany's last primary forests, to my late grandmother for ensuring there always was a beloved home waiting for us on our returns, and to my late mother-in-law for making me feel at home anew in Canada.

ABSTRACT

This PhD thesis developed a framework to model, quantify, and improve understanding of spatially explicit changes in short-to-tall-stature vegetation structure in the southern Taiga of northwestern Canada. This region is still changing due to the retreat of the Laurentide Ice Sheet since the last glacial maximum (~22.1 cal ka BP). In addition, climate change has caused rapid ecosystem changes, for example due to permafrost thaw, with implications to carbon sink strength and wildland fire susceptibility, amongst others. Regional allometric equations for shrubs and short-stature trees were developed to estimate aboveground biomass (AGB) and live aboveground plant carbon stocks using 1D, 2D, and 3D field measurements. Spatially coincident bi-temporal airborne lidar data were used to develop a single AGB model applicable across changing relationships between lidar point clouds and AGB magnitudes as ecosystems change form, ecosystem boundaries expand and recede, and airborne lidar technologies evolve. By fusing field data with bi-temporal airborne lidar data, the study quantified and analyzed changes in vegetation structure and aboveground plant carbon stocks. By employing geospatial statistical analysis and machine learning the underlying important drivers of these changes were identified.

Key findings of this thesis were the following: (1) the developed framework has improved understanding of the magnitudes and directions of short-to-tall-stature vegetation structural changes over the past decade (2010 to 2019); (2) increases in the growth and abundance of short-stature vegetation were substantial across the study region and need to be integrated into carbon accounting frameworks with extension to unmanaged forest and peatland ecosystems. Overall, the established framework could aid in the modelling of

wildland fire fuel dynamics and fire behavior also in peatlands, which could reduce community risk to fire in this region.

CONTRIBUTION OF AUTHORS

This dissertation consists of four scientific manuscripts, of which to date three are published within peer-reviewed, open access academic journals. Thesis Chapters 2 to 4 were published as open-access, peer-reviewed journal articles. Thesis Chapter 5 will be submitted for publication after thesis defense. All thesis chapters can be read in stand-alone form. Thesis chapters can further be understood as hierarchical framework whereby latter chapters use and expand upon findings of previous chapters. As such, there is repetition in the description of study areas, field and remote sensing data, and data processing steps. Finally, this work is the result of multiple collaborative efforts, with specific contributions listed below.

Chapter 2: Allometric Equations for Shrub and Short-Stature Tree Aboveground Biomass within Boreal Ecosystems of Northwestern Canada

Authors: Flade, L.; Hopkinson, C.; Chasmer, L.

Published on November 16th, 2020 in Forests – Special Issue on Forest Biomass and Carbon Estimation (MDPI)

Citation: Flade, L.; Hopkinson, C.; Chasmer, L. Allometric Equations for Shrub and Short-Stature Tree Aboveground Biomass within Boreal Ecosystems of Northwestern Canada. Forests 2020, 11, 1207. https://doi.org/10.3390/f11111207.

Author Contributions:

Conceptualization: Flade, Hopkinson, Chasmer

Methodology: Flade, Hopkinson, Chasmer

Validation: Flade

Formal analysis: Flade

Data curation: Flade, Chasmer

Writing—original draft preparation: Flade

Writing—review and editing: Flade, Hopkinson, Chasmer

Visualization: Flade

Supervision: Hopkinson, Chasmer

Project administration: Chasmer, Hopkinson

Funding acquisition: Chasmer, Hopkinson

All authors have read and agreed to the published version of the manuscript. The authors declare no conflicts of interest.

Chapter 3: Aboveground Biomass Allocation of Boreal Shrubs and Short-Stature Trees in Northwestern Canada. Forests

Authors: Flade, L.; Hopkinson, C.; Chasmer, L.

Published on February 18th, 2021 in Forests – Special Issue on Forest Biomass and Carbon Estimation (MDPI).

Citation: Flade, L.; Hopkinson, C.; Chasmer, L. Aboveground Biomass Allocation of Boreal Shrubs and Short-Stature Trees in Northwest-ern Canada. Forests 2021, 12, 234. https://doi.org/10.3390/f12020234.

Author Contributions:

Conceptualization: Flade, Hopkinson, Chasmer

Methodology: Flade, Hopkinson, Chasmer

Validation: Flade

Formal analysis: Flade

Investigation: Flade, Hopkinson, Chasmer

Resources: Chasmer, Hopkinson

Data curation: Flade, Chasmer

Writing—original draft preparation: Flade

Writing—review and editing: Chasmer, Hopkinson, Flade

Visualization: Flade

Supervision: Chasmer, Hopkinson

Project administration: Chasmer, Hopkinson

Funding acquisition: Chasmer, Hopkinson

All authors have read and agreed to the published version of the manuscript. The authors declare no conflicts of interest.

Chapter 4: A bi-temporal airborne lidar shrub-to-tree aboveground biomass model for the Taiga of western Canada

Authors: Flade, L.; Hopkinson, C.; Chasmer, L.

Published on June 21st, 2024 in the Canadian Journal of Remote Sensing – 44th Canadian Symposium in Remote Sensing Special Issue (Taylor & Francis Group). https://www.tandfonline.com/doi/full/10.1080/07038992.2024.2379915.

Author Contributions:

Conceptualization: Flade, Hopkinson, Chasmer

Methodology: Flade, Hopkinson

Validation: Flade

Formal analysis: Flade

Data curation: Hopkinson, Flade, Chasmer

Writing—original draft preparation: Flade

Writing—review and editing: Flade, Hopkinson, Chasmer

Visualization: Flade

Supervision: Chasmer, Hopkinson

Project administration: Hopkinson, Chasmer

Funding acquisition: Hopkinson, Chasmer

All authors have read and agreed to the published version of the manuscript. The authors declare no conflicts of interest.

Chapter 5: Hydroclimatic shifts in ecosystems in the southern Taiga of western Canada: Woody aboveground biomass gains exceeding losses due to mortality

Authors: Flade, L.; Hopkinson, C.; Chasmer, L., et al.

Author Contributions:

Conceptualization: Flade, Chasmer, Hopkinson

Methodology: Flade, Chasmer, Hopkinson

Validation: Flade

Formal analysis: Flade

Data curation: Hopkinson, Flade, Chasmer

Writing—original draft preparation: Flade

Writing—review and editing: Flade, Chasmer, Hopkinson

Visualization: Flade

Supervision: Chasmer, Hopkinson

Project administration: Chasmer, Hopkinson

Funding acquisition: Hopkinson, Chasmer

The authors declare no conflicts of interest.

ACKNOWLEDGEMENTS

I would like to express my sincerest gratitude and heartfelt thanks to my co-supervisor Dr. Laura Chasmer. A supervisor so devoted to the success of her students in their current and future careers is a rare find and a true gift. I have learned immensely from Laura's unparalleled expertise because she has invested a great amount of time and resources in teaching and guiding me, provided numerous opportunities/challenges, and has given me space to learn and grow independently. Laura's way of leading and inspiring her students has made a lasting impact on me, providing a role-model from which to draw from in the future. I would also like to express my sincerest gratitude to my co-supervisor Dr. Chris Hopkinson for the inspirational and challenging discussions on my research. I have learned immensely from Chris' guidance, expertise, input of ideas, and his way of making connections between research aspects and formulating complex research concepts. Laura and Chris were an outstanding team of supervisors, and I had the greatest time exploring hundreds of different remote northern peatlands together or sit in the office with a cup of coffee discussing research. The support and trust I have received from Laura and Chris have transformed this chapter in my life to a once-in-a-lifetime experience of learning and growing. A time for me to follow my aspirations. A time, I will always cherish.

I would also like to thank my PhD thesis committee, Dr. Derek Peddle and Dr. Larry Flanagan, for providing invaluable feedback during Progress and Standing meetings, for asking questions that inspired me to new ways of thinking, for joining in celebrating my professional successes, and for always being supportive in every way. I would also like to express my sincerest gratitude to Dr. Bill Quinton (Wilfrid Laurier University), and the Dehcho Collaborative on Permafrost for the monthly invitations to the Scotty Creek gatherings that provide a space for knowledge transfer between researchers and community, which is so

important. Bill's support to collect data at the Scotty Creek research station and the permitted access to these lands by the Dehcho Collaborative on Permafrost was substantial for this thesis and my understanding of the variability of these landscapes. Thank you also to Megan Herbert for introducing me to the trickle-down effects of supportive and respectful peer-mentorship, which came exactly when I needed it. To my peers at the University of Lethbridge, who helped me with field work, research discussions, and by simply being in this space collectively: Kailyn Nelson, Emily Jones, Celeste Barnes, Maxim Okhrimenko, Tristan Skretting, Jessica Van Gaalen, Italo Rodrigues, Danika King, Farnoosh Aslami, Saeid Parsian, Amanda Bakalarczyk, Natalie Krizan, Joe Silva, and many others – thank you.

Lastly, this thesis came to completion because of the unwavering support of my family and friends. Words cannot express, how grateful I am for my grandfather, for believing in me, for my mother and stepfather for doing the same and more, for my brother and his partner for being ready to jump into the arena with me at any moment, for my partner's family for integrating me into their lives, for my GOLF club for cheering me on and making me laugh since childhood days, for Lavinia Haase for the many road trips along Highway 22, and for the supportive community in Lethbridge on treaty 7 – Sikoohkotoki – from neighbors to closest friends. At the very end and at the center of my heart, I am immensely grateful for my partner Steven Foord. From making a fresh cup of coffee in the morning, to pushing me down the street in a wheelchair, to transforming camping into glamping, to stepping in during periods of financial drought, to skating with me through German castles, Steve is the mechanism strengthening resilience in my ecosystem. His infinite support for me is like blue grama grass in a Prairie field, like spotting a snowy owl high up in the tree, like the bluish green in a braided mountain stream, like hearing a long-forgotten song playing in the radio – with all my heart and always, thank you.

TABLE OF CONTENTS

LIST OF FIGURES

LIST OF TABLES

LIST OF EQUATIONS

LIST OF ABBREVIATIONS

ABoVE	Arctic-Boreal Vulnerability Experiment
AGB	aboveground biomass
ALTM	airborne laser terrain mapper
C	carbon
cal ka BP	calibrated 1000 years before present
CCI	Climate Change Initiative
CF	correction factor
CHM	canopy height model
CI	confidence interval
dAGB	aboveground biomass change
DBH	diameter at breast height
DEM	digital elevation model
dIQR	change in the interquartile range
DSM	digital surface model
ECV	essential climate variable
ESA	European Space Agency
GCOS	Global Climate Observing System
GEDI	Global Ecosystem Dynamics Instrument
GLAS	Geoscience Laser Altimeter System
GNSS	global navigation satellite system
GPP	gross primary production
HAGL	height above ground level
ICESat-2	Ice, Cloud, and Land Elevation Satellite 2
IPCC	Intergovernmental Panel on Climate Change
IQR	interquartile range
ISRO	Indian Space Research Organization
LIDAR	light detection and ranging
LLR	linear logarithmic regression
LLRC	linear logarithmic regression with correction
MAAT	mean annual air temperature
MOLI	Multi-footprint Observation LIDAR and Imager mission
MSE	mean square error
NASA	National Aeronautics and Space Administration

NLS	nonlinear least squares regression
NWT	Northwest Territories
OOB	out-of-bag
PF	permafrost plateau forest
PFG	plant functional group
PI	prediction interval
PPP	precise point positioning
PSPs	permanent sampling plots
RMSE	root mean square error
SAR	synthetic aperture radar
SD	standard deviation
SE	standard error
TAP	total annual precipitation
TIN	triangulated irregular network
TPI	topographical position index
TWI	topographical wetness index
UF	upland forest

CHAPTER 1: INTRODUCTION

1.1. Boreal ecosystem succession and landscape evolution

In the southern Taiga of northwestern Canada widespread and rapid permafrost thaw due to climate change and other natural/anthropogenic disturbances has resulted in large-area landscape evolution (Baltzer et al., 2014; Camill & Clark, 2000; Carpino et al., 2021; Chasmer & Hopkinson, 2017). This is in addition to dynamic land cover changes still occurring since the onset of the deglaciation of the Laurentide Ice Sheet after the last glacial maximum (~22.1 cal ka BP) and the subsequent establishment of an ice-free corridor in the interior Taiga Plains (Figure 1.1) (Dulfer et al., 2023; Stoker et al., 2022). These landcover change dynamics have resulted in extensive changes to ecosystem function in the zone of sporadic to discontinuous permafrost extent (Helbig et al., 2022; Loudermilk et al., 2022; Reisen et al., 2015; See et al., 2024). Here, permafrost, which formed during a colder climate of the late Pleistocene, is relatively thin (< 10 m) and warm (permafrost temperatures close to 0°C) and in disequilibrium with the current climate (Shur & Jorgenson, 2007; Wright et al., 2022). Its persistence at the southern extent is therefore dependent on specific ecosystem properties (Shur & Jorgenson, 2007). For example, deep and dry organic soils insulate permafrost from sensible heat inputs in the summer due to a low thermal conductivity, while saturated organic soils (high thermal conductivity) promote ground cooling in the winter (Shur & Jorgenson, 2007; Wright et al., 2022). In addition, ground shading from incoming solar radiation by tree and shrub canopies in the summer and interception of snow by evergreen tree canopy in the winter promote permafrost maintenance (Disher et al., 2021; Shur & Jorgenson, 2007). In the sporadic to discontinuous permafrost zone of the southern Taiga of western Canada, these conditions are commonly

found in slightly raised permafrost plateaus perched above the water table of adjacent lower lying permafrost free wetlands (Chasmer et al., 2011; Wright et al., 2022). Permafrost is also found in mixed-wood upland forests with soil organic layer depths > 0.3 m (Wright et al., 2022).

However, changes to ecosystem properties such as removal of evergreen tree canopy (e.g. due to mortality or disturbance) and an increased abundance of shrubs (insultation of the ground from cold air temperatures in the spring due to snow cover dynamics) can initiate and/or accelerate permafrost thaw (Camill, 1999b; Chasmer et al., 2011; Gibson et al., 2018; Wilcox et al., 2019; Zoltai, 1993). In addition, heat conduction into permafrost plateaus from adjacent water bodies and wetlands, or the ground surface (Connon et al., 2014; Devoie et al., 2021; Shur & Jorgenson, 2007; Wright et al., 2022), leads to a net permafrost thaw if summer energy inputs are greater than losses in winter (Wright et al., 2022). With continued warming, sporadic to discontinuous permafrost could be substantially reduced or disappear by the end of this century (Carpino et al., 2021; Chasmer & Hopkinson, 2017; Quinton et al., 2011; Schuur & Mack, 2018).

Permafrost thaw features observed in lowland areas in the southern Taiga of western Canada include collapse scar peatlands (isolated bogs within permafrost plateaus), which formed as a result of permafrost plateau degradation, surface subsidence and water inundation (Quinton et al., 2009; Wright et al., 2008; Zoltai, 1993). Over time, progressive thawing of permafrost leads to the fragmentation and reduction of permafrost plateau area, isolated collapse scars expanding to interconnected wetlands (e.g. poor fens), and forest re-establishment in the absence of permafrost due to peatland drainage and hummock establishment (Carpino et al., 2021; Quinton et al., 2019a). Such forest re-establishment is

estimated to occur within half a century (Carpino et al., 2021). This differs to observations from a colder climatic period, where forest re-establishment occurred over multiple centuries and depended on the drying of soils due to the elevation of the ground surface in the process of permafrost aggradation (Carpino et al., 2021; Zoltai, 1993).

However, the timing and progression of this trajectory may vary across the region depending on regional climate gradients, climate change, surface elevation, soil material, and terrain and hydrological complexity (Sniderhan et al., 2023; Wright et al., 2022). For example, a recent study suggested contemporary permafrost aggradation occurred at higher latitudes in areas of higher terrain and hydrological complexity, which was associated with increased forest cover (Sniderhan et al., 2023). The challenge is therefore to understand which unmanaged ecosystems in which regions maintain ecosystem properties (e.g. vegetation structure, and ground elevation) and therefore, function, (in the absence of dramatic disturbance such as wildland fires and landslides) and which are sensitive to anthropogenic climate change, resulting in alteration.

1.2. Challenges for ecosystem change monitoring

Monitoring changes in short-to-tall vegetation structure as an indicator of changing ecosystems and altered ecosystem function is crucial, especially with regards to aboveground biomass changes, fuel continuity for wildland fires, and carbon storage/change in the southern Taiga of western Canada; an area comprising 10% of Canada's boreal land surface area (Natural Resources Canada, 2022). However, short funding cycles (often limited to ~5 years) and the need for resource intensive data collections over remote, vast, and inaccessible landscapes pose challenges for monitoring and change detection in this region. This is especially the case when quantifying vegetation

structural changes over longer periods (≥ a decade) across broad areas, and at spatial scales that enable changes to be observed (10s of meters, Camill & Clark, 2000).

Regionally, a relatively long history of remotely sensed data from passive optical Landsat imagery offers an opportunity to quantify longterm changes across the broader Taiga of Canada. However, these are not direct measures of ecosystem change. Rather they measure changes in the spectral reflectance of vegetation and the ground surface that are proxies for those changes. For example, using time-series of Landsat vegetation indices, a decline in the vegetation index observed in the central boreal biome was associated with a loss of forest aboveground biomass (AGB) and net primary productivity (Beck & Goetz, 2012; Goetz et al., 2005; Liu et al., 2023). However, trends in optical vegetation indices are also influenced by complex interactions between moisture availability and landscape position (Goetz et al., 2005), such that their relation to actual vegetation structural changes and maintenance on the ground is often highly uncertain.

Studies using airborne lidar data have been used to quantify 3D vegetation structure (Coops et al., 2021; Hopkinson et al., 2005; Næsset & Gobakken, 2008), and can supplement localized findings from field observations (Camill et al., 2001; Dearborn et al., 2021; Sniderhan & Baltzer, 2016), eddy covariance data (Chasmer et al., 2012; Flanagan & Syed, 2011; Helbig et al., 2022), in combination with historic aerial photography and select scenes of high-resolution satellite imagery (Chasmer et al., 2011; Jorgenson et al., 2022; Sniderhan et al., 2023).

1.3. Knowledge gaps

Spatially coincident airborne lidar data collected over multiple years for change detection analysis are limited in northern/remote environments as these systems require considerably

more logistical planning. In addition, airborne lidar applications evolved primarily out of commercial forestry needs and as such, products are predominantly produced for tall-stature upland forests (Næsset and Gobakken 2008; Wulder et al. 2012). Short-stature vegetation such as shrubs and juvenile and low-productive trees commonly found in peatland complexes and upland forest understory have been underrepresented in these studies. This is also due to a lack of allometric equations for short-stature vegetation per plant genus/species as well as their single plant components.

As a result, few studies have quantified longer-term (multi-year to decadal) short-to-tall stature vegetation structural changes across broad areas of northern Canada in high spatial resolution. This is however crucial, as changes in local vegetation structure are a key determinant of permafrost response to climate change (IPCC, 2023; Shur & Jorgenson, 2007), especially in the climatically sensitive sporadic to discontinuous permafrost zone.

1.4. Thesis aim and objectives

The aim of this thesis is to establish a framework for modelling, quantifying, and analyzing gradual short-to-tall stature vegetation structural changes due to progressive permafrost thaw at spatially coincident locations within the southern Taiga of western Canada. This includes the following objectives:

- To provide a means to improve modelling of aboveground biomass:
    - Develop regional allometric models using 1D, 2D, and 3D field measurements to predict aboveground biomass of shrubs and short-stature trees (herein “trees”).

    - Compare the utility of scaling using 1D, 2D, and 3D field-based models for all shrubs and all tree species combined (a general equation, which may be of utility for active remote sensing applications, such as lidar, in the future).
    - Provide allometric models for total AGB for each shrub and each tree species and genus examined as well as for the pooled data.
    - Recommend optimal methods of field data collection for prediction of shrub and small-stature tree AGB.
- To better understand the contributions of different plant components to the standing stocks of aboveground biomass and aboveground carbon:
    - Describe and discuss the proportion of plant component AGB for boreal shrub and short-stature tree species.
    - Provide allometric equations for estimating aboveground biomass of plant components of shrubs and short-stature trees.
- To enable the quantification of short-to-tall stature AGB change across varying vegetation structures in under-represented ecosystems:
    - Test the correspondence of airborne lidar-based height and cover metrics with field-based AGB across (a) the Taiga Plains and Shield ecozones in western Canada, and (b) forests growing within uplands and peat plateaus underlain by permafrost, peatlands, and forest to peatland ecotones.
    - Test model transferability from a low-density single channel to a high-density multi-channel lidar sensor.
    - Develop a single AGB model for shrubs, juvenile to mature trees, low productive trees, and a mix thereof.

- To improve understanding of vegetation structural changes in ecoregions and ecosystem types in the southern Taiga of western Canada:
    - extend the quantification of spatially explicit AGB and plant carbon changes beyond field sites and proximity to roads at subsampled locations where overlapping bi-temporal airborne lidar data are available.
    - determine the effects of gradual permafrost thaw on vegetation structures and whether certain vegetation functional types/structures were more sensitive than others.
    - identify which environmental and hydro-climatic drivers were relevant for explaining variability in aboveground biomass changes and what can be expect in the future as these play greater or lesser roles.
    - examine how these aboveground biomass changes are represented in regional and global aboveground biomass products and discuss the implications to current knowledge about the broader plant carbon balance in this region.

1.5. Study area

This study was conducted within the traditional lands of the Dene First Nations in the Northwest Territories, Canada, including the Łíídlıı̨ Kų́ę́, Dënësų̨linę́ Nëné, Acho Dene Koe, Dene Tha', Akaitcho Dene, Dehcho Dene, Tłı̨chǫ Ndè, Michif Piyii Métis, and NWT Métis Nation. The study area is underlain by sporadic to discontinuous permafrost and spans a latitudinal range of 300 km and a longitudinal range of 500 km within three ecoregions: the Taiga Plains Mid Boreal, Taiga Plains High Boreal, and Taiga Shield High Boreal (see study area figures 2.1, 3.1, 4.1, 5.2). The three ecoregions examined are

representative of a latitudinal and longitudinal gradient of climate, surficial geology and soils, and glacial history.

The climatology of the study area is generally cold and dry. The mildest climate is found in the Taiga Plains Mid Boreal and the coldest and driest climate in the Taiga Shield High Boreal (Environment and Natural Resources, 2024).

The terrain of the Taiga Plains Mid Boreal formed with the opening of the ice-free corridor at around 13.6 cal ka BP, during which melt water drained from the retreating Laurentide Ice Sheet in the east towards the west and sediment deposited in the interior Taiga Plains (Stoker et al., 2022) (Figure 1.1).

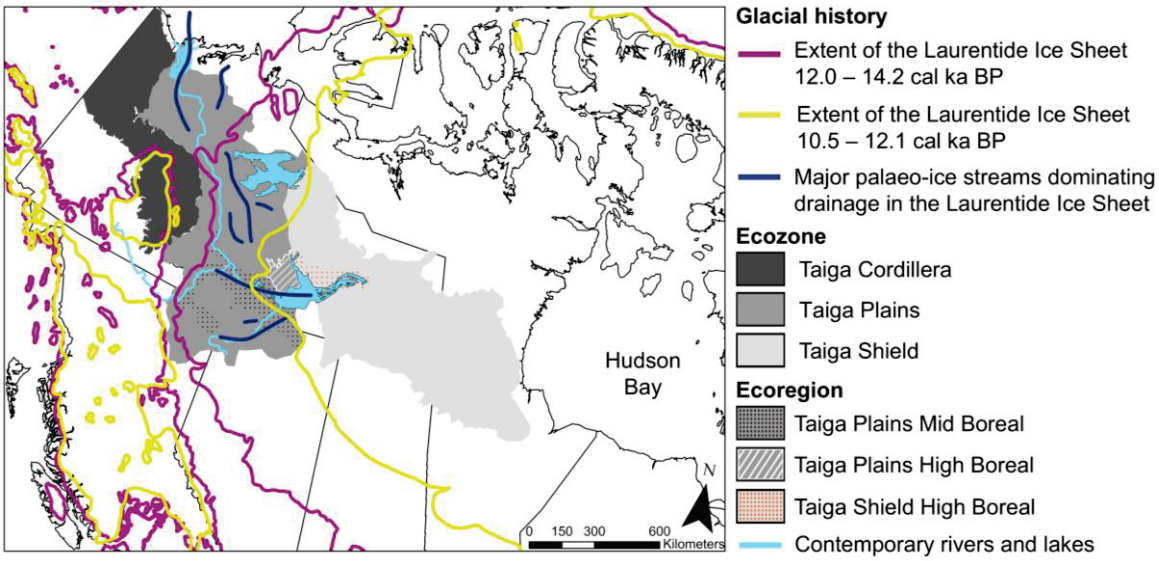

Figure 1.1. Study area within the Taiga Plains Mid Boreal, Taiga Plains High Boreal, and Taiga Shield High Boreal. The overlays of the extents of the Laurentide Ice Sheet at two stages during the last deglaciation (Dalton et al., 2020) illustrate the establishment of an ice-free corridor in the interior Taiga Plains. Palaeo-ice streams depict the dominant drainage channels of ice within the Laurentide Ice Sheet at some point after the last glacial maximum (Margold et al., 2015). Contemporary water bodies consist of the Liard River (west), Hay River (south), McKenzie River (centre to north), Great Slave Lake (south), and Great Bear Lake (north).

As such, the terrain is gently undulating to level and upland soils consist of fine to coarse lacustrine and till deposits with alluvial material, which was deposited along the Mackenzie and Liard rivers. Lower lying peatland complexes, which cover up to 71% of

the ecoregion (eastern Taiga Plains Mid Boreal), were shaped by former glacial lake McConnell and consist of fine-textured lacustrine plains.

In uplands, the moderate-to-well draining soils promote tall-stature mixed-wood (trembling aspen (*Populus tremuloides*), balsam poplar (*Poplar balsamifera*), white spruce (*Picea glauca*), jack pine (*Pinus banksiana*)), and pure coniferous (jack pine), and deciduous (trembling aspen) forests (Ecosystem Classification Group, 2009; Flade et al., 2020). Understory vegetation is diverse (e.g. low-bush cranberry (*Viburnum edule*), prickly wild rose (*Rosa acicularis*), alder (*Alnus* spp.), and herbaceous plants) (Ecosystem Classification Group, 2009; Flade et al., 2020). On permafrost plateaus, sparse and stunted black spruce trees (*Picea mariana*) are found with e.g. common labrador tea (*Rhododendron groenlandicum*), lichen (e.g. *Stereocaulon* spp., *Cladonia stygia, Cladonia mitis*) and moss (e.g. *Sphagnum fuscum, Sphagnum capillifolium*) ground cover (Garon-Labrecque et al., 2016). Peatlands range from moss (e.g. *Sphagnum balticum*, *Aulacomnium palustre*), sedge (e.g. *Carex* spp., *Trichophorum alpinum*) and shrub (e.g. dwarf birch (*Betula* spp.), willow (*Salix* spp.)) dominated (open) to treed (black spruce and tamarack (*Larix laricina*)) (Ecosystem Classification Group, 2009; Garon-Labrecque et al., 2016).

Within the Great Slave Plain in Taiga Plains High Boreal, glacial wave erosion and isostatic rebound after the last ice age formed a gentle dome shape topography (Ecosystem Classification Group, 2009). The coarse-textured and rapidly draining soil material in uplands (glacial till deposits above bedrock) promotes the establishment of pure jack pine stands in areas frequently disturbed by wildland fire. White spruce is also common near smaller streams and wetlands. Understory vegetation commonly consists of shrubby

cinquefoil (*Dasiphora fruticosa*), common bearberry (*Arctostaphylos uva-ursi*), and lichen ground cover (Ecosystem Classification Group, 2009; Flade et al., 2020). Half of the ecoregion is covered by shallow ponds, which are surrounded by extensive sedge-dominated floating fens. Permafrost plateaus are uncommon (Ecosystem Classification Group, 2009).

In the Taiga Shield High Boreal, the study area encompasses the Great Slave Lowland and Upland. These regions are characterized by low-relief, fractured granite bedrock outcrops dispersed with lakes and surrounding wetlands. The retreat of the Laurentide Ice Sheet and subsequent flooding left behind deposits of coarse-textured till and fine-textured lacustrine material in rock fractures and surrounding bedrock outcrops (Ecosystem Classification Group, 2008). In frequently-burned areas, young jack pine and paper birch forests are prevalent, while black spruce forests occur in areas of longer fire-return intervals (Ecosystem Classification Group, 2008). Permafrost plateaus are also common around shallow lakes and in low-lying areas (Ecosystem Classification Group, 2008). Bogs are found adjacent to permafrost plateaus and in wet depressions between bedrock outcrops. Extensive sedge and shrub dominated floating fens occur around lakes and ponds (Ecosystem Classification Group, 2008).

1.6. Thesis organization

Overall, this thesis uses field and bi-temporal airborne lidar data fusion and innovates in:

a) the establishment of short-stature allometric equations for shrub and juvenile/low productive tree genera/species (discussed in Chapter 2) and their aboveground biomass/carbon allocation to single plant components (discussed in Chapter 3); and

b) the modelling of shrub-to-tree aboveground biomass across changing relationships between airborne lidar point clouds and aboveground biomass magnitudes as ecosystems change form, ecosystem boundaries expand and recede, and airborne lidar technologies evolve (discussed in Chapter 4).

The approaches used enabled spatially explicit quantification of cumulative short-to-tall-stature vegetation structural changes (discussed in Chapter 5). In addition, uncertainties in carbon sink strength estimates associated with aboveground biomass in the southern Taiga of western Canada were reduced in comparison to regional to global aboveground biomass and carbon stock products derived using e.g. national forest inventory data, optical satellite imagery, and spaceborne lidar and radar data within machine learning environments (discussed in Chapter 5). The framework established in this thesis advances current understanding of gradual climate-mediated vegetation structural changes in a region identified as important climate regulator yet source of critical uncertainty (IPCC, 2023).

1.7. References

Baltzer, J., Veness, T., Chasmer, L., Sniderhan, A., & Quinton, W. (2014). Forests on thawing permafrost: fragmentation, edge effects, and net forest loss. *Global Change Biology*, *20*(3), 824–834. https://doi.org/10.1111/gcb.12349.

Beck, P. S. A., & Goetz, S. J. (2012). Corrigendum: Satellite observations of high northern latitude vegetation productivity changes between 1982 and 2008: ecological variability and regional differences. *Environmental Research Letters*, *7*(2), 029501. https://doi.org/10.1088/1748-9326/7/2/029501.

Camill, P. (1999). Peat accumulation and succession following permafrost thaw in the boreal peatlands of Manitoba, Canada. *Écoscience*, *6*(4), 592–602. https://doi.org/10.1080/11956860.1999.11682561.

Camill, P., & Clark, J. S. (2000). Long-term Perspectives on Lagged Ecosystem Responses to Climate Change: Permafrost in Boreal Peatlands and the Grassland/Woodland Boundary. *Ecosystems*, *3*(6), 534–544. https://doi.org/10.1007/s100210000047.

Camill, P., Lynch, J. A., Clark, J. S., Adams, J. B., & Jordan, B. (2001). Changes in Biomass, Aboveground Net Primary Production, and Peat Accumulation following Permafrost Thaw in the Boreal Peatlands of Manitoba, Canada. *Ecosystems*, *4*(5), 461–478. https://doi.org/10.1007/s10021-001-0022-3.

Carpino, O., Haynes, K., Connon, R., Craig, J., Devoie, É., & Quinton, W. (2021). Long-term climate-influenced land cover change in discontinuous permafrost peatland complexes. *Hydrology and Earth System Sciences*, *25*(6), 3301–3317. https://doi.org/10.5194/hess-25-3301-2021.

Chasmer, L., & Hopkinson, C. (2017). Threshold loss of discontinuous permafrost and landscape evolution. *Global Change Biology*, *23*(7), 2672–2686. https://doi.org/10.1111/gcb.13537.

Chasmer, L., Quinton, W. L., Hopkinson, C., Petrone, R., & Whittington, P. (2011). Vegetation Canopy and Radiation Controls on Permafrost Plateau Evolution within the Discontinuous Permafrost Zone, Northwest Territories, Canada: Vegetation and Radiation Controls on Permafrost Plateau Evolution. *Permafrost and Periglacial Processes*, n/a-n/a. https://doi.org/10.1002/ppp.724.

Chasmer, L., Kenward, A., Quinton, W., & Petrone, R. (2012). CO_2 Exchanges within Zones of Rapid Conversion from Permafrost Plateau to Bog and Fen Land Cover Types. *Arctic, Antarctic, and Alpine Research*, *44*(4), 399–411. https://doi.org/10.1657/1938-4246-44.4.399.

Connon, R., Quinton, W., Craig, J., & Hayashi, M. (2014). Changing hydrologic connectivity due to permafrost thaw in the lower Liard River valley, NWT, Canada. *Hydrological Processes*, *28*(14), 4163–4178. https://doi.org/10.1002/hyp.10206

Coops, N. C., Tompalski, P., Goodbody, T. R. H., Queinnec, M., Luther, J. E., Bolton, D. K., et al. (2021). Modelling lidar-derived estimates of forest attributes over space and time: A review of approaches and future trends. *Remote Sensing of Environment*, *260*, 112477. https://doi.org/10.1016/j.rse.2021.112477.

Dalton, A. S., Margold, M., Stokes, C. R., Tarasov, L., Dyke, A. S., Adams, R. S., et al. (2020). An updated radiocarbon-based ice margin chronology for the last deglaciation of the North American Ice Sheet Complex. *Quaternary Science Reviews*, *234*, 106223. https://doi.org/10.1016/j.quascirev.2020.106223.

Dearborn, K., Wallace, C., Patankar, R., & Baltzer, J. (2021). Permafrost thaw in boreal peatlands is rapidly altering forest community composition. *Journal of Ecology*, *109*(3), 1452–1467. https://doi.org/10.1111/1365-2745.13569.

Devoie, É. G., Craig, J. R., Dominico, M., Carpino, O., Connon, R. F., Rudy, A. C. A., & Quinton, W. L. (2021). Mechanisms of Discontinuous Permafrost Thaw in Peatlands. *Journal of Geophysical Research: Earth Surface*, *126*(11), e2021JF006204. https://doi.org/10.1029/2021JF006204.

Disher, B. S., Connon, R. F., Haynes, K. M., Hopkinson, C., & Quinton, W. L. (2021). The hydrology of treed wetlands in thawing discontinuous permafrost regions. Ecohydrology, 14(5), e2296. https://doi.org/10.1002/eco.2296.

Dulfer, H. E., Stoker, B. J., Margold, M., & Stokes, C. R. (2023). Glacial geomorphology of the northwest Laurentide Ice Sheet on the northern Interior Plains and western Canadian Shield, Canada. *Journal of Maps*, *19*(1), 2181714. https://doi.org/10.1080/17445647.2023.2181714.

Ecosystem Classification Group (Ed.). (2008). *Ecological regions of the Northwest Territories - Taiga Shield*. Yellowknife, NT, Canada: Department of Environment and Natural Resources, Government of the Northwest Territories.

Ecosystem Classification Group. (2009). *Ecological regions of the Northwest Territories - Taiga Plains* (Revised). Yellowknife, NT, Canada: Department of Environment and Natural Resources, Government of the Northwest Territories.

Enayetullah, H., Chasmer, L., Hopkinson, C., Thompson, D., & Cobbaert, D. (2023). Examining Drivers of Post-Fire Seismic Line Ecotone Regeneration in a Boreal Peatland Environment. *Forests*, *14*(10), 1979. https://doi.org/10.3390/f14101979

Environment and Natural Resources. (2024). Canadian Climate Normals: 1981-2010 [Data set]. Government of Canada,. Retrieved from https://climate.weather.gc.ca/climate_normals/station_select_1981_2010_e.html?searchType=stnProv&lstProvince=NT.

Flade, L., Hopkinson, C., & Chasmer, L. (2020). Allometric Equations for Shrub and Short-Stature Tree Aboveground Biomass within Boreal Ecosystems of Northwestern Canada. *Forests*, *11*(11), 1207. https://doi.org/10.3390/f11111207.

Flanagan, L. B., & Syed, K. H. (2011). Stimulation of both photosynthesis and respiration in response to warmer and drier conditions in a boreal peatland ecosystem: Peatland carbon dioxide exchange. *Global Change Biology*, *17*(7), 2271–2287. https://doi.org/10.1111/j.1365-2486.2010.02378.x.

Garon-Labrecque, M.-È., Léveillé-Bourret, É., Higgins, K., & Sonnentag, O. (2016). Additions to the boreal flora of the Northwest Territories with a preliminary vascular flora of Scotty Creek. *The Canadian Field-Naturalist*, *129*(4), 349. https://doi.org/10.22621/cfn.v129i4.1757.

Gibson, C., Chasmer, L., Thompson, D., Quinton, W., Flannigan, M., & Olefeldt, D. (2018). Wildfire as a major driver of recent permafrost thaw in boreal peatlands. *Nature Communications*, *9*(1), 3041. https://doi.org/10.1038/s41467-018-05457-1.

Goetz, S., Bunn, A. G., Fiske, G. J., & Houghton, R. A. (2005). Satellite-observed photosynthetic trends across boreal North America associated with climate and fire disturbance. *Proceedings of the National Academy of Sciences*, *102*(38), 13521–13525. https://doi.org/10.1073/pnas.0506179102.

Helbig, M., Živković, T., Alekseychik, P., Aurela, M., El-Madany, T. S., Euskirchen, E. S., et al. (2022). Warming response of peatland CO_2 sink is sensitive to seasonality in warming trends. *Nature Climate Change*, *12*(8), 743–749. https://doi.org/10.1038/s41558-022-01428-z.

Hopkinson, C., Chasmer, L., Sass, G., Creed, I., Sitar, M., Kalbfleisch, W., & Treitz, P. (2005). Vegetation class dependent errors in lidar ground elevation and canopy height estimates in a boreal wetland environment. *Canadian Journal of Remote Sensing*, *31*(2), 191–206. https://doi.org/10.5589/m05-007.

IPCC. (2023). *IPCC, 2023: Climate Change 2023: Synthesis Report. Contribution of Working Groups I, II and III to the Sixth Assessment Report of the Intergovernmental Panel on Climate Change [Core Writing Team, H. Lee and J. Romero (eds.)]. IPCC, Geneva, Switzerland.* (First) (p. 184). Geneva, Switzerland: Intergovernmental Panel on Climate Change (IPCC). https://doi.org/10.59327/IPCC/AR6-9789291691647.

Jorgenson, M., Kanevskiy, M., Roland, C., Hill, K., Schirokauer, D., Stehn, S., et al. (2022). Repeated Permafrost Formation and Degradation in Boreal Peatland Ecosystems in Relation to Climate Extremes, Fire, Ecological Shifts, and a Geomorphic Legacy. *Atmosphere*, *13*(8), 1170. https://doi.org/10.3390/atmos13081170.

Liu, Q., Peng, C., Schneider, R., Cyr, D., McDowell, N. G., & Kneeshaw, D. (2023). Drought-induced increase in tree mortality and corresponding decrease in the carbon sink capacity of Canada's boreal forests from 1970 to 2020. *Global Change Biology*, *29*(8), 2274–2285. https://doi.org/10.1111/gcb.16599.

Loudermilk, E. L., O'Brien, J. J., Goodrick, S. L., Linn, R. R., Skowronski, N. S., & Hiers, J. K. (2022). Vegetation's influence on fire behavior goes beyond just being fuel. *Fire Ecology*, *18*(1), 9, s42408-022-00132–9. https://doi.org/10.1186/s42408-022-00132-9.

Margold, M., Stokes, C. R., Clark, C. D., & Kleman, J. (2015). Ice streams in the Laurentide Ice Sheet: a new mapping inventory. *Journal of Maps*, *11*(3), 380–395. https://doi.org/10.1080/17445647.2014.912036.

Næsset, E., & Gobakken, T. (2008). Estimation of above- and below-ground biomass across regions of the boreal forest zone using airborne laser. *Remote Sensing of Environment*, *112*(6), 3079–3090. https://doi.org/10.1016/j.rse.2008.03.004.

Natural Resources Canada. (2022). Permaforst. Atlas of Canada (Version 5th Edition) [ESRI Shapefile]. Retrieved from https://maps-cartes.services.geo.ca/server_serveur/rest/services/NRCan/permafrost_atlas_of_canada_en/MapServer.

Quinton, W., Hayashi, M., & Chasmer, L. (2009). Peatland Hydrology of Discontinuous Permafrost in the Northwest Territories: Overview and Synthesis. *Canadian Water Resources Journal*, *34*(4), 311–328. https://doi.org/10.4296/cwrj3404311.

Quinton, W., Hayashi, M., & Chasmer, L. (2011). Permafrost-thaw-induced land-cover change in the Canadian subarctic: implications for water resources. *Hydrological Processes*, *25*(1), 152–158. https://doi.org/10.1002/hyp.7894.

Quinton, W., Berg, A., Braverman, M., Carpino, O., Chasmer, L., Connon, R., et al. (2019). A synthesis of three decades of hydrological research at Scotty Creek, NWT, Canada. *Hydrology and Earth System Sciences*, *23*(4), 2015–2039. https://doi.org/10.5194/hess-23-2015-2019.

Reisen, F., Duran, S. M., Flannigan, M., Elliott, C., & Rideout, K. (2015). Wildfire smoke and public health risk. *International Journal of Wildland Fire*, *24*(8), 1029. https://doi.org/10.1071/WF15034.

Schuur, E. A. G., & Mack, M. C. (2018). Ecological Response to Permafrost Thaw and Consequences for Local and Global Ecosystem Services. *Annual Review of Ecology, Evolution, and Systematics*, *49*(1), 279–301. https://doi.org/10.1146/annurev-ecolsys-121415-032349.

See, C. R., Virkkala, A.-M., Natali, S. M., Rogers, B. M., Mauritz, M., Biasi, C., et al. (2024). Decadal increases in carbon uptake offset by respiratory losses across northern permafrost ecosystems. *Nature Climate Change*. https://doi.org/10.1038/s41558-024-02057-4.

Shur, Y. L., & Jorgenson, M. T. (2007). Patterns of permafrost formation and degradation in relation to climate and ecosystems. *Permafrost and Periglacial Processes*, *18*(1), 7–19. https://doi.org/10.1002/ppp.582..

Sniderhan, A., & Baltzer, J. (2016). Growth dynamics of black spruce (*Picea mariana*) in a rapidly thawing discontinuous permafrost peatland. *Journal of Geophysical Research: Biogeosciences*, *121*(12), 2988–3000. https://doi.org/10.1002/2016JG003528.

Sniderhan, A., Spence, C., Kokelj, S., & Baltzer, J. (2023). Evidence for unexpected net permafrost aggradation driven by local hydrology and climatic triggers. *Environmental Research Letters*, *18*(11), 115001. https://doi.org/10.1088/1748-9326/acff0f.

Stoker, B. J., Margold, M., Gosse, J. C., Hidy, A. J., Monteath, A. J., Young, J. M., et al. (2022). The collapse of the Cordilleran–Laurentide ice saddle and early opening of the Mackenzie Valley, Northwest Territories, Canada, constrained by^{10} Be exposure dating. *The Cryosphere*, *16*(12), 4865–4886. https://doi.org/10.5194/tc-16-4865-2022.

Wilcox, E. J., Keim, D., De Jong, T., Walker, B., Sonnentag, O., Sniderhan, A. E., et al. (2019). Tundra shrub expansion may amplify permafrost thaw by advancing snowmelt timing. Arctic Science, 5(4), 202–217. https://doi.org/10.1139/as-2018-0028.

Wright, N., Quinton, W. L., & Hayashi, M. (2008). Hillslope runoff from an ice-cored peat plateau in a discontinuous permafrost basin, Northwest Territories, Canada. *Hydrological Processes*, *22*(15), 2816–2828. https://doi.org/10.1002/hyp.7005

Wright, S., Thompson, L., Olefeldt, D., Connon, R., Carpino, O., Beel, C., & Quinton, W. (2022). Thaw-induced impacts on land and water in discontinuous permafrost: A review of the Taiga Plains and Taiga Shield, northwestern Canada. *Earth-Science Reviews*, *232*, 104104. https://doi.org/10.1016/j.earscirev.2022.104104

Wulder, M. A., White, J. C., Bater, C. W., Coops, N. C., Hopkinson, C., & Chen, G. (2012). Lidar plots — a new large-area data collection option: context, concepts, and case

study. *Canadian Journal of Remote Sensing*, *38*(5), 600–618. https://doi.org/10.5589/m12-049.

Zoltai, S. C. (1993). Cyclic Development of Permafrost in the Peatlands of Northwestern Alberta, Canada. *Arctic and Alpine Research*, *25*(3), 240. https://doi.org/10.2307/1551820.

CHAPTER 2: ALLOMETRIC EQUATIONS FOR SHRUB AND SHORT-STATURE TREE ABOVEGROUND BIOMASS WITHIN BOREAL ECOSYSTEMS OF NORTHWESTERN CANADA

2.1. Abstract

Aboveground biomass (AGB) of short-stature shrubs and trees contain a substantial part of the total carbon pool within boreal ecosystems. These ecosystems, however, are changing rapidly due to climate-mediated atmospheric changes, with overall observed decline in woody plant AGB in boreal northwestern Canada. Allometric equations provide a means to quantify woody plant AGB and are useful to understand aboveground carbon stocks as well as changes through time in unmanaged boreal ecosystems. In this paper, we provide allometric equations, regression coefficients, and error statistics to quantify total AGB of shrubs and short-stature trees. We provide species- and genus-specific as well as multispecies allometric models for shrub and tree species commonly found in northwestern boreal forest and peatland ecosystems. We found that the three-dimensional field variable (volume) provided the most accurate prediction of shrub multispecies AGB ($R^2 = 0.79$, $p < 0.001$), as opposed to the commonly used one-dimensional variable (basal diameter) measured on the longest and thickest stem ($R^2 = 0.23$, $p < 0.001$). Short-stature tree AGB was most accurately predicted by stem diameter measured at 0.3 m along the stem length ($R^2 = 0.99$, $p < 0.001$) rather than stem length ($R^2 = 0.29$, $p < 0.001$). Via the two-dimensional variable cross-sectional area, small-stature shrub AGB was combined with small-stature tree AGB within one single allometric model ($R^2 = 0.78$, $p < 0.001$). The AGB models provided in this paper will improve our understanding of shrub and tree AGB within rapidly changing boreal environments.

2.2. Introduction

Ecosystems in northwestern Canada are changing rapidly due to a warming climate, drier conditions, extended growing season, and climate-mediated increases in frequency and intensity of disturbances, such as wildfire, permafrost thaw, insect and pathogen outbreaks, and anthropogenic natural resource extraction (e.g., (Flannigan et al., 2005; Gauthier et al., 2014; IPCC, 2014). One of the significant outcomes of climate-mediated change in these environments is the increased abundance of short-stature vegetation, such as shrubs (Myers-Smith et al., 2011) and low productive and juvenile trees, in particular where wildfire disturbance sets back ecosystems to an early successional stage post fire (Goetz et al., 2007) or in the rapidly changing transition zones between elevated forests and adjacent peatlands due to permafrost thaw (Chasmer & Hopkinson, 2017). Increased shrub cover influences important ecosystem functions, such as energy balance and hydrology (Goetz et al., 2007) at local to regional scales and greenhouse gas/carbon–climate cycle feedbacks at national to global scales (Goetz et al., 2007; Goulden et al., 2011), which could ultimately exacerbate these changes (Chasmer & Hopkinson, 2017; Helbig et al., 2016). Shrubs and short-stature trees contain a substantial part of the total aboveground carbon of unmanaged boreal forest and peatland ecosystems, although specific numbers remain uncertain (Kurz et al., 2013). For quantification of the complete carbon balance of Canada, aboveground biomass (AGB) of shrubs and short-stature trees need to be integrated into carbon accounting strategies in the future.

Although shrubification in permafrost environments has been reported (Berner et al., 2018; Chasmer & Hopkinson, 2017; Myers-Smith et al., 2011, 2020), spatially explicit quantities of shrub and short-stature tree AGB remain largely unknown for boreal

northwestern Canada for three reasons: (a) Existing allometric models for plant species were developed for larger tree individuals harvested in managed forests for merchantable volume (Lambert et al., 2005; Ung et al., 2008). As such, these models are not appropriate for quantification of the AGB of short-stature shrubs and trees growing in unmanaged ecosystems. (b) There is a lack of regionally applicable allometric models for shrub and short-stature tree species for unmanaged forests in boreal northwestern Canada. He et al. (2018) provide regression coefficients for allometric equations developed for three common shrub species and genera. However, these local models were developed for shrubs growing in two different peatland sites located in a different ecozone and as such may be less accurate when applied in a different study region within the discontinuous to sporadic permafrost zone and a different ecosystem type, such as transition zones between forest and peatlands. (c) The best predictor variable to model AGB of small-stature shrubs and trees remains unknown. Existing boreal shrub allometric equations typically use a 1D field variable, e.g., basal stem diameter (Berner et al., 2015; Chojnacky & Milton, 2008; He et al., 2018; Smith & Brand, 1983), to predict the mass of a 3D object (the shrub). However, the applicability of these models for scaling from a 1D variable to a 3D quantity has not been evaluated for shrubs and short-stature trees.

Here, we test the applicability of 1D, 2D, and 3D field measurements within allometric models to understand and improve the scaling relationships across shrub and short-stature tree species up to 4.5 m in height (herein “tree species”) in northern boreal regions. 1D field measurements describe shrub and tree structures based on a single-length observation, such as diameter or stem length. 2D field measurements, such as cross-

sectional area, represent two directions, while 3D measurements describe plant structures in three different directions (x, y, and z), such as volume.

The objectives of this study were as follows: (a) develop regional allometric models using 1D, 2D, and 3D field measurements to predict aboveground biomass of shrubs and short-stature trees (herein "trees"); (b) compare the utility of scaling using 1D, 2D, and 3D field-based models for all shrubs and all tree species combined (a general equation, which may be of utility for active remote sensing applications, such as lidar, in the future); (c) provide allometric models for total AGB for each shrub and each tree species and genus examined as well as for the pooled data; and (d) recommend optimal methods of field data collection for prediction of shrub and small-stature tree AGB. We hypothesized that 3D field variables would be best suited to predict shrub AGB because a 3D measurement considers the 3D properties of the plant structure. We also hypothesized that, by pooling data, the results would be less accurate; however, doing so would allow us to include these measures within a remote sensing-based structural model of biomass (e.g., using airborne lidar).

2.3. Materials and methods

2.3.1. Study area

Shrub and tree species examined in this study were destructively sampled across the southern margin of the sporadic to discontinuous permafrost zone of the Taiga Plains and Taiga Shield ecozones (Figure 2.1).

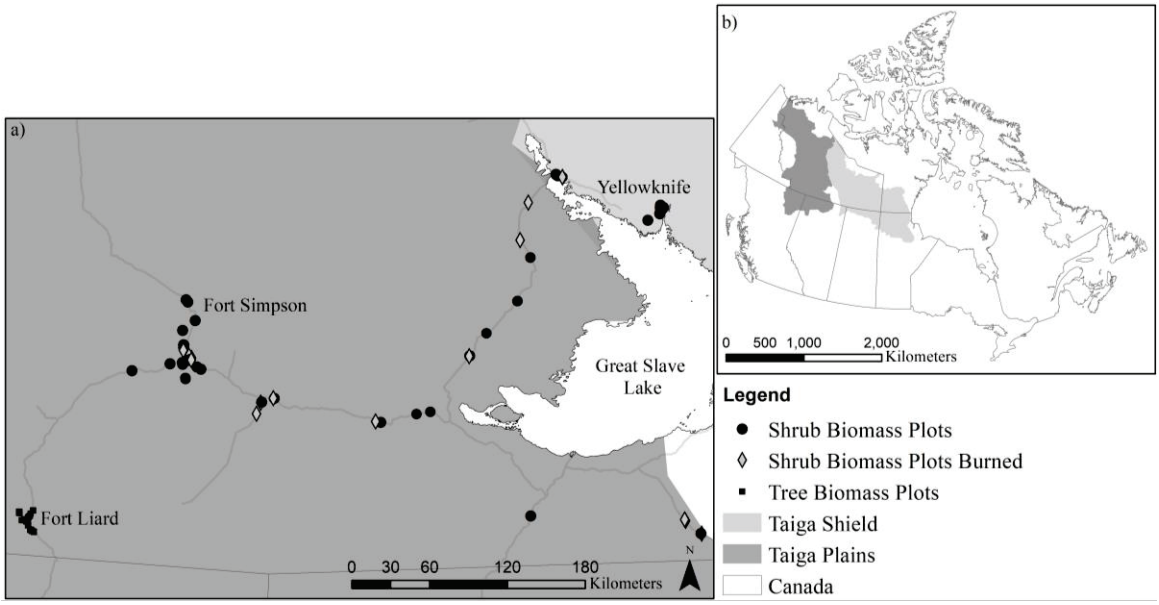

Figure 2.1. (a) Field locations of destructive sampling of shrub and short-stature tree AGB in peatlands and upland forest ecosystems. Field locations are distributed across the (b) mid-boreal Taiga Plains and high-boreal Taiga Shield ecoregions of the Northwest Territories, Canada.

The mean annual air temperature varies from −2.5 (Fort Simpson, Taiga Plains) to between −3 and −4 (Yellowknife, Taiga Shield) °C, while cumulative annual precipitation is 390 (Fort Simpson) and 360 (Yellowknife) mm, respectively (Ecosystem Classification Group, 2008, 2009). The geology is dominated by lacustrine plains overlain by peatlands with fine- to coarse-textured lacustrine and till in the mid-boreal Taiga Plains, which transitions towards the high boreal Taiga Shield into nearly level to rolling and hilly bedrock (Ecosystem Classification Group, 2008, 2009). In the Taiga Plains, approximately 25%–50% of the land surface area is covered by peatlands, consisting of peat plateaus underlain by permafrost, bogs, and fens (Ecosystem Classification Group, 2009). While shrubs dominantly grow in the transition zones between peat plateaus and bogs or fens, short-stature trees grow within upland forests or on elevated peat plateaus. In the high-boreal Taiga Shield, peatlands cover an area of less than 5% and occupy hollows within and between bedrock exposures (Ecosystem Classification Group, 2008). The dominant

vegetation in the mid-boreal Taiga Plains consists of black spruce (*Picea mariana*) and mixed hardwood and softwood forests containing similar species as found in the Taiga Shield ecozone. Taiga Shield ecosystems are dominated by black spruce and jack pine (*Pinus banksiana*) with abundance of paper birch (*Betula papyrifera*) and trembling aspen (*Populus tremuloides*) (Ecosystem Classification Group, 2008, 2009).

2.3.2. Shrub measurements, destructive sampling, and processing

To determine AGB of small-stature shrubs and trees growing in the mid-boreal Taiga Plains and high-boreal Taiga Shield ecoregions, we derived allometric models for five common shrub genera and species (*Alnus* spp., *Betula* spp., *Dasiphora fruticosa*, *Salix* spp., and *Shepherdia canadensis*) and four common tree genera and species (*Betula papyrifera*, *Picea* spp., *Populus balsamifera*, and *Populus tremuloides*). Plant individuals were measured and destructively sampled within 65 peatlands and upland forest ecosystems distributed across the two ecoregions in late July/early August 2018 and 2019. Field sample locations were situated in late successional sites and in sites disturbed by wildland fire within the last 50 years (Figure 2.1, Table 2.1) in order to represent the high variability of boreal ecosystem disturbance by wildfire and permafrost thaw in our allometric models.

Table 2.1. Overview of aboveground biomass (AGB) of shrub and tree samples harvested per ecoregion.

Ecozone	**Transects (Samples)**
Shrub Samples	
Taiga Plains	31 (127)
Taiga Shield	15 (79)
Tree Samples	
Taiga Plains	20 (105)
Total	66 (311)

Harvested plants were located within <10 m of field transects (Figure 2.2 a), which were set up randomly within each site. Between one to three transects were installed per site. Field transects were 25 m in length, starting in upland forests and traversing into peatlands and crossing the forest–peatland transition zone perpendicularly. This setup was chosen in order to capture the shrub abundance within the transition zones between peat plateaus and bogs/fens, where the largest and fastest ecosystem changes have been observed [6]. Shrubs were located along the transect with distance from the start of the transect. Shrubs were selected per transect within standing height ranges of 0.5 up to 3.5 m. A shrub individual was selected when it was alive and mostly free of leaf or stem disturbances. Up to five shrub individuals were sampled per transect.

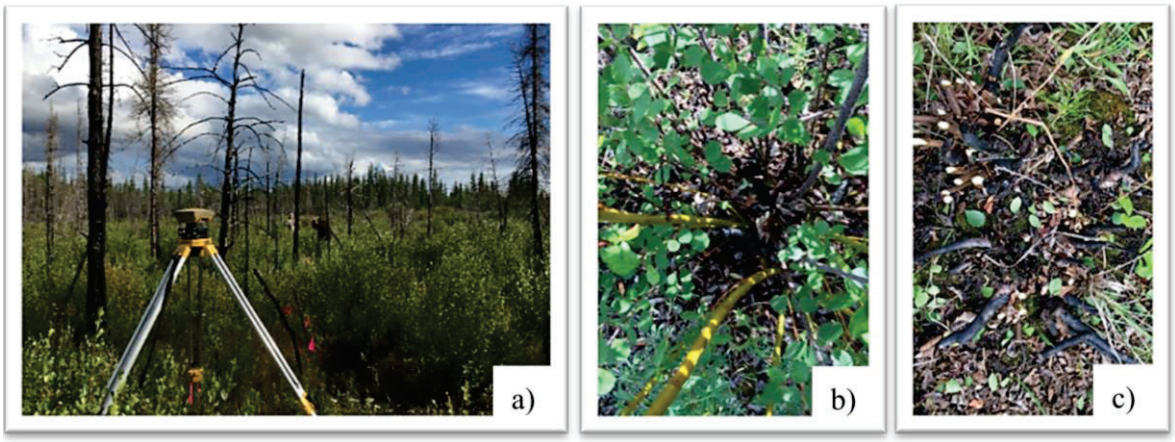

Figure 2.2. (a) Example of a transect traversing a burned upland forest into peatland (fire year 2015); (b,c) illustration of a *Betula glandulosa* shrub individual growing along the transect before and after destructive sampling, respectively.

Measured 1D variables for each individual shrub sample included maximum height (herein “max height” (m)), average maximum height (m), number of individual stems, and basal diameter of each stem (cm). Heights were measured using a tape measure, and

diameters were measured with a caliper. Previous studies have examined the relationship between the AGB of a single stem and the 1D independent variable measurement of the same stem (Berner et al., 2015; He et al., 2018). However, boreal shrubs are commonly multi-stemmed. In order to analyze how accurately 1D field-measured variables from a single stem can predict the AGB of the entire plant, we tested the basal diameter of the stem with the widest diameter (herein "max basal diameter" (cm)) and the length of the longest stem (herein "max stem length" (m)) within allometric relationships. To test a 2D variable, we transformed each basal diameter to cross-sectional area (cm^2) and summed this to total cross-sectional area per shrub individual. For the 3D variable, we measured the extent of the uppermost foliage layer perpendicular to the transect (herein "width" (m)) and parallel to the transect (herein "line-intercept cover" (m)) using a tape measure. The 3D shrub volume (m^3) (1) was then calculated as follows:

$$\text{Volume } (m^3) = \text{max height (m)} \times \text{line-intercept cover (m)} \times \text{width (m)}. \qquad (2.1)$$

Following measurements *in situ,* shrubs were clipped directly above the soil surface (Figure 2.2 c) and stored in paper bags for further processing. Dead stems were not harvested. In the laboratory, harvested samples were air dried for up to four months, separated into stem and leaf parts, and oven dried at 60 °C for a minimum of 48 h (Flanagan & Syed, 2011). Twigs and fruits were included as leaf parts. The total AGB was determined as dry weight (g) by weighing each shrub part (woody and leafy) and summing the dry weight of all parts per shrub individual.

2.3.3. Tree measurements, sampling, and processing

Small-stature tree AGB was collected in late July 2019 along 20 random transects adjacent to the permanent sample plots set up by the Canadian Forest Service, located near Fort Liard, Northwest Territories (NWT), Canada. Live trees were chosen from the understory and open areas across different height ranges determined in intervals of 0.5 m up to ≤4.5 m. In all cases, samples were mostly free of foliage disturbance/mortality and stem blemishes. *In situ* 1D tree measurements included stem length (m), and stem diameter (cm) measured at 0.03, 0.15, 0.30, and 1.3 m along the stem length starting from the average ground surface surrounding the tree. Stem diameters were transformed to cross-sectional area (cm^2) per tree individual to provide a 2D variable analogous to that for shrubs and thus offer the potential for a joint shrub and juvenile/low productive tree allometric equation. 3D volume was not measured for trees because tree AGB can best be predicted with diameter, stem length, or both variables combined (e.g., Lambert et al., 2005). Following measurements *in situ*, trees were cut as close to the ground surface as possible and packed into large paper bags to be transported back to the University of Lethbridge. In the laboratory, trees were separated into stem, branch, and leaf components after air drying of up to four months. Branches were cut off directly at the stem. Twigs and fruits were included as leaf parts, while bark was included as part of the stem. Dead branches were not included in the analysis. Oven drying and biomass derivation was completed using the methods described above for shrubs.

2.3.4. Derivation of aboveground biomass allometric equations

In situ structural measurements of harvested shrubs and trees were used to determine the most accurate 1D, 2D, or 3D independent variables to predict AGB. Three different forms of single variable regression analysis, which are most commonly used in biomass allometry (Baskerville, 1972; Berner et al., 2015; Bond-Lamberty et al., 2002; He et al., 2018; Mascaro et al., 2011; Smith & Brand, 1983) were tested for each 1D, 2D, and 3D independent variable per shrub and tree genus and species and for the pooled data. These were used to determine the most descriptive regression model of AGB for genus/species, multispecies shrubs, and multispecies trees as well as in general for all trees and shrubs combined. The first allometric biomass model (2.2) uses linear regression of the log-transformed dependent (y) and independent *in situ* (x) variables (herein "linear logarithmic regression (LLR)"):

$$\ln(y) = \ln(\beta) + \alpha * \ln(x) \quad (2.2)$$

where α and β are the regression coefficients. The back-transformation to an arithmetic scale was achieved using Equation (2.3):

$$y = \beta x^{\alpha} \quad (2.3)$$

However, the back-transformation resulted in a skewed distribution of $\hat{y}$ (Baskerville, 1972). Baskerville (1972) reported a general underestimation of 10%–20% when back-transforming the logarithmic regression estimates of AGB without correcting for skewness. To set this into context, we compared the results of LLR with the results of linear logarithmic regression with correction (herein "LLRC") (4–6):

$$ln(y) = ln(\beta) + \alpha * ln(x) + ln(\varepsilon) \quad (2.4)$$

$$y = \beta x^{\alpha} * \varepsilon \quad (2.5)$$

$$\varepsilon = e^{(\frac{\mathrm{MSE}}{2})} \quad (2.6)$$

where ε represents a multiplicative correction factor of the back-transformation with MSE as the mean square error of the regression (Baskerville, 1972; Mascaro et al., 2011). This correction removes the bias in Equation (2.3), which occurs following the back-transformation from a normal distribution of $\ln(\hat{y})$ for a given $\ln(x)$. LLR results are presented only to set LLRC model results into context, and usage is not recommended without the provided correction factor.

To avoid the problem of skewness, a majority of the research on biomass allometry have used the untransformed nonlinear relationship between dependent and independent variables to predict tree (Smith & Brand, 1983) and shrub (Berner et al., 2015; He et al., 2018; Smith & Brand, 1983) AGB. These models use iterative nonlinear least squares regression via a power function (herein "nonlinear least squares regression (NLS)") with an additive error term ε:

$$y = \beta x^{\alpha} + \varepsilon \quad (2.7)$$

The NLS function for biomass prediction is available in statistical software packages (e.g., "nls" function in the "stats" package in R (R Core Team, 2021)). The default nonlinear equation that is implemented in R assumes a homogeneous variance of regression residuals (Mascaro et al., 2011). However, trees and shrubs can be inherently heteroscedastic, such that the assumption of homogeneous residual variance across the range of the independent variable could lead to biased model predictions (Mascaro et al., 2011). Although weights can be specified in NLS functions, these should be applied when both arithmetic and logarithmic variances do not show uniformity (Baskerville, 1972). Our AGB data showed uniform variances on arithmetic scales for most species and on logarithmic scales for all

species. To understand the performance of using a non-weighted nonlinear model that does not address potential heteroscedasticity within the data, we compared NLS (2.7) with the results of the logarithmic-based models LLR (2.2–2.3) and LLRC (2.4–2.6).

The modeled biomass results of these three allometric models were evaluated using root mean square error (RMSE), coefficient of determination (R^2), and regression residual analysis. Residual analysis was performed using visual inspection of the relationships between dependent and independent variables as well as the total percentage error (%) derived via (2.8):

$$Total\ percentage\ error = \frac{\sum Modeled\ AGB - \sum Measured\ AGB}{\sum Measured\ AGB} * 100 \qquad (2.8)$$

Significance of the differences between the genus/species-specific AGB model means and the multispecies model means were evaluated with the *t*-test for equal variances and Welch's *t*-test for unequal variances. Equality of variances was tested with the *F*-test.

2.3.5. Biomass allometric models

In total, we used 1D, 2D, and 3D input variables and three different forms of regression (LLR, LLRC, and NLS) to predict shrub AGB. Regression coefficients and standard errors were calculated for (a) total shrub AGB per genus/species; (b) all shrubs combined per ecoregion; and (c) all shrubs within both ecoregions combined. Here, (c) represents a multispecies shrub allometric equation that can be applied to all shrubs across the southern half of the study region (NWT, Canada; Figure 2.1). For short-stature trees, we examined 1D and 2D predictor variables (3D tree volume predictors were not measured) and the three different regression equations described above (LLR, LLRC, and NLS). Similar to shrubs,

we have provided the allometric models that most accurately predict (a) total AGB for each tree species; (b) all tree species combined per ecoregion; and (c) for all trees within the two ecoregions combined (herein "multispecies trees"). In addition to individual "shrub" and "tree" models, we have provided a 2D input variable allometric model for total AGB prediction for small-stature shrubs and trees combined (herein "general shrubs and trees"). With the "general shrub and tree" model, we explored the utility of a single 1D (stem length) or 2D (cross-sectional area) variable for combined shrub and tree AGB prediction to understand whether these variables scale uniformly between shrubs and trees. Such combined approaches may have utility for rapid assessment in the field or using less invasive observation techniques (e.g., unmanned airborne vehicles or laser scanning) where plant species and type may be indeterminate.

2.4. Results and discussion

The ranges and averages (± standard deviation) of the predictor variables for 205 shrubs and 106 trees are provided in Appendix A (Supplementary Material Chapter 2, Tables S2.1 and S2.2, respectively). Regression coefficients, correction factors, and standard errors are presented in Tables S2.3–S2.5, and can be input into Equations (2.2)–(2.7). For all allometric models, regression coefficients were positive, indicating increasing biomass with increasing predictor variable for total AGB, as was found by Lambert et al. (2005).

The applicability of multispecies models to predict total AGB for single genus and species has been shown for shrubs by He et al. (2018). Similarly, the differences between our modeled means of total AGB via the multispecies equations and the genus/species-specific modeled means were not significant ($p > 0.05$). Furthermore, the difference between the modeled means of shrub and tree biomass in previously burned sites and the

unburned sites was not significant ($p > 0.05$). Species-specific coefficients for input into the allometric Equations (2.2)–(2.7) are provided in Table S2.3, using volume as the predictor and Table S2.4, using cross-sectional area as the predictor.

2.4.1. Comparison of 1D, 2D, and 3D variables for shrub total aboveground biomass prediction

For the genus/species-specific 1D-based models using max stem length or max basal diameter as input into each of the three allometric models (LLR, LLRC, and NLS), *Betula* spp., *Dasiphora fruticosa*, and *Salix* spp. had lower R^2 ($0.005 \leq R^2 \leq 0.325$) compared to *Shepherdia canadensis* ($0.433 \leq R^2 \leq 0.809$, Table S2.6). In addition, *Dasiphora fruticosa* was the only species where stem length was not significantly related ($p > 0.05$) to the dependent variable of measured total AGB. For the multispecies shrub models (pooled for all shrub genera and species), the use of 1D predictor variables yielded the lowest model fits (RMSE) ranging from 262 (NLS) to 318 (LLRC) g for max stem length and 252 (NLS) to 388 (LRC) g for max basal diameter (Table 2.2). These results are in contrast with previous allometric models for boreal (Berner et al., 2015; He et al., 2018; Smith & Brand, 1983) or subtropical (Ali et al., 2015) shrubs, where the 1D variable basal diameter of the longest stem had provided the most accurate prediction of total AGB. However, 1D field variables, although related to the dependent variable ($p < 0.001$) (with the exception of max stem length of *Dasiphora fruticosa*), did not explain total AGB variability when considering all stems of the entire plant ($0.228 \leq R^2 \leq 0.335$, Table 2.2, Figure 2.3 a,b). This was true for each genus/species model as well as the multispecies equation, with the exception of *Shepherdia canadensis*. For this species, max basal diameter was a similarly good predictor variable ($R^2 = 0.809$) to cross-sectional area ($R^2 = 0.738$) and volume ($R^2 =$

0.765, Table S2.6). The performance of total AGB models increased for all other genera and species as well as for all genera and species combined using the 3D predictor variable of volume, with R^2 ranging between 0.684 (*Betula* spp. and *Dasiphora fruticosa*) and 0.882 (*Alnus* spp.). The RMSEs for the multispecies models ranged from 141 (NLS) to 144 (LLR and LLRC) g with R^2 of ~0.790 using any of the three models (LLR, LLRC, and NLS; Table 2.2). Figure 2.3 a–d shows the relationship between the three models for 1D, 2D, and 3D variables for the multispecies shrub AGB.

Table 2.2. Model performances for multispecies shrub total ABG prediction (all p values < 0.001).

Model	Dimension	Input Variable	Total Percentage Error (%)	RMSE (g)	R^2
Linear logarithmic regression (LLR)	1D	Max stem length	−32	276.12	0.237
	1D	Max basal Diameter	−26	293.20	0.228
	2D	Cross-sectional Area basal	−4	233.46	0.534
	3D	Volume	−11	144.08	0.788
Linear logarithmic regression with correction (LLRC)	1D	Max stem length	23	317.95	0.237
	1D	Max basal Diameter	24	388.00	0.228
	2D	Cross-sectional Area basal	13	263.55	0.534
	3D	Volume	4	144.12	0.788
Nonlinear least squares regression (NLS)	1D	Max stem length	4	262.22	0.273
	1D	Max basal Diameter	8	251.68	0.335
	2D	Cross-sectional Area basal	10	190.75	0.621
	3D	Volume	1	141.04	0.790

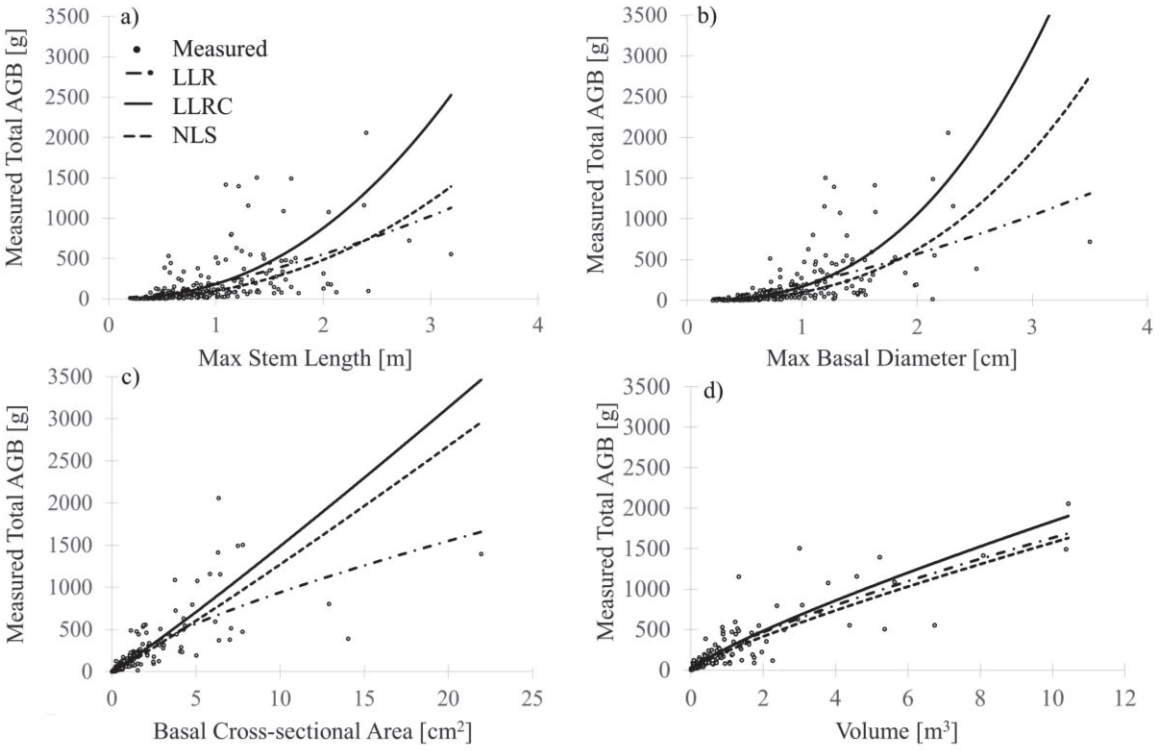

Figure 2.3. LLRC, LLR, and NLS model fits for each 1D (a,b), 2D (c), and 3D (d) predictor variable utilized to model total AGB for multispecies shrubs.

Of the three model forms tested, the 3D volume predictor produced the most consistent shrub AGB results (Figure 2.3, Table 2.3), suggesting the choice of model form is less critical when using a 3D predictor. As expected, the exponent α was greater for 1D models and close to unity for the 3D models. This suggests that a simple linear model would result in similar model fits compared to the LLRC or NLS models when using a 3D predictor. However, after testing this (results not shown), the model results achieved slightly less goodness of fit (R^2 = 0.769, RMSE 148.6 g) compared to LLRC or NLS (Table 2.2). Decreasing exponents (holding all else equal) can be explained by the nature of allometric scaling between 1D, 2D, and 3D measurements of a plant to its mass (a 3D attribute) via a power function. Assuming no change in the multiplier (β) (which might be

considered analogous to a density attribute), scaling from a 1D measurement to a 3D property requires a higher exponent (α) compared to scaling from a 2D or 3D measurement (Table 2.3). Therefore, predictions that are extrapolated from lower to higher dimensions contain more inherent model-based uncertainty than predictions requiring no dimensional extrapolation. However, field volume observations consisted of three single measurements and therefore might contain a high overall measurement uncertainty compared to a single 1D measurement. The exact quantity of model vs. field measurement error propagation is unknown, but the net outcome of the tests performed shows that 3D volume produced the highest AGB model accuracies, followed by 2D and then 1D models.

Table 2.3. Regression coefficients for each 1D, 2D, and 3D model to predict total AGB for multispecies shrubs with LLRC and NLS.

	Variable	LLRC β	NLS β	LLRC α	NLS α
Multi-species shrubs	Max stem length	100.988	192.186	2.262	1.530
	Max basal diameter	100.484	203.796	2.642	1.486
	Cross-sectional area	106.911	177.614	1.075	0.723
	Volume	233.224	272.116	0.829	0.778

Better model performance and linearity via the 3D predictor variable of volume may also be explained by the structural variability of multi-stemmed shrubs. For example, shrub stems can grow comparably long while being simultaneously thinner rather than being shorter but thicker, so the total dry weight of the shrub with the longer stems may be lower than the dry weight of a shrub that has shorter but thicker stems. This variability is represented in the scatterplots of Figure 2.3 a,b and illustrates that shrub structural variability cannot be sufficiently explained using a measurement from one single perspective alone. The structural heterogeneity of shrubs is a function of site conditions,

such as nutrient, water, and light availability. To capture structural heterogeneity, a measurement is needed that describes the shrub structure from three different perspectives. For example, a taller shrub with a single stem will be narrower in width and cover than a shrub with many stems extending in multiple directions. If we assume that the shrub with many stems has a larger width, then it is also likely that the shrub with many stems will have more biomass (dry weight). We demonstrated that neither max stem length nor max basal diameter could be used to predict the dry weight of multi-stemmed shrubs. Volume, however, captured the shrub extent and directional growth and therefore predicted total AGB with less total model uncertainty. The exception of better model performance using max basal diameter for *Shepherdia canadensis* can be explained by the comparably low number of stems for each harvested individual (<12 stems per plant) and the observed uniform growth of this species in the areas sampled.

A second alternative to volume is the measurement of basal diameters for all stems per plant, converted to cross-sectional area and summed. This is because (a) stem count is represented and (b) shrubs with larger stem counts usually have greater extents (width and line-intercept cover) and dry weight compared to shrubs with lower stem counts. To improve the accuracy of AGB predictions for northern boreal shrubs, measurements to determine volume (max height, line-intercept cover, and width) are recommended. These can be measured rapidly in the field. 1D measures may take slightly less time for shrub individuals that have developed a low number of stems. However, 1D measurements result in both over- and underestimation of AGB depending on the regression form used, especially for shrubs with a high number of stems. 2D cross-sectional area provides the second-best predictions of shrub AGB, although it is slightly more time intensive to

measure the basal diameter of each stem per shrub individual. Here, the time required increases with number of stems.

2.4.2. Comparison of regression models for shrub total aboveground biomass prediction

With regard to model comparisons (LLR, LLRC, and NLS), NLS produced the best model fits for each shrub genus and species (Table S2.6) as well as for the multispecies data (Table 2.2). Here, we found significant differences using 1D vs. 3D models. RMSE varied between 251.68 (NLS, using max basal diameter) and 317.95 (LLRC, using max stem length) g and were greatly reduced with volume as the input variable (RMSE between 141.04 (NLS) and 144.12 (LLRC) g). For the multispecies data, NLS and LLRC overestimated total AGB for all 1D, 2D, and 3D models, while LLR continuously underestimated total AGB (Table 2.2). NLS produced the best model fit, independent of the variable used, while the 3D models of all regression forms resulted in the best AGB predictions (RMSE = 141.04 g, R^2 = 0.790 (NLS), RMSE 144.08 g, R^2 = 0.788 (LLR), RMSE = 144.12 g, R^2 = 0.788 (LLRC); Table 2.2). However, although NLS produces slightly better model fits, nonlinear models require an even variance of errors across the domain of the predictor variable in order to perform valid comparisons of model uncertainties and regression coefficients amongst datasets (e.g., (Baskerville, 1972)). Residual analysis of our models showed that errors were free of heteroscedasticity. However, when models are transferred to different areas and data, we recommend using the LLRC-based models. This is because biomass data can contain natural heteroscedastic variation. Heteroscedasticity needs to be accounted for in the model development to ensure that model results do not contain bias (Mascaro et al., 2011). For example, Mascaro et al. (2011) reported a bias of ~100% overestimation when extending predicted small tree (diameter at breast height (DBH) range 2–12 cm) aboveground

biomass to stand level biomass using NLS. For model transfer purposes, we have provided regression coefficients and error statistics not only for our best models based on NLS but also for our LLRC models (Table S2.3).

2.4.3. Comparison of 1D and 2D Variables for Tree Total AGB Prediction

For the short-stature tree AGB equations, diameter measured at 0.3 m stem length resulted in better model fits compared to stem length for each genus and species (Table S2.7). For the multispecies data, total AGB prediction using stem length (1D variable) provided the lowest goodness of fit (highest RMSE and lowest R^2, Table 2.4, Figure 2.4), while inclusion of stem diameter at 0.3 m, alternatively cross-sectional area at 0.3 m, improved predictions by 87% using LLRC or NLS (Table 2.4).

Table 2.4. Model performance for multispecies tree total AGB prediction using 1D and 2D input parameters (all p values < 0.001).

Model	Dimension	Input Variable	Total Percentage Error (%)	RMSE (g)	R^2
LLR	1D	Stem length	−51	529.08	0.285
	1D	Diameter at 0.3 m	−20	188.71	0.987
	2D	Cross-sectional area at 0.3 m	−20	188.41	0.987
LLRC	1D	Stem length	−6	484.83	0.285
	1D	Diameter at 0.3 m	−10	134.00	0.987
	2D	Cross-sectional area at 0.3 m	−9	133.68	0.987
NLS	1D	Stem length	−1	482.77	0.286
	1D	Diameter at 0.3 m	2	62.25	0.988
	2D	Cross-sectional area at 0.3 m	2	62.25	0.988

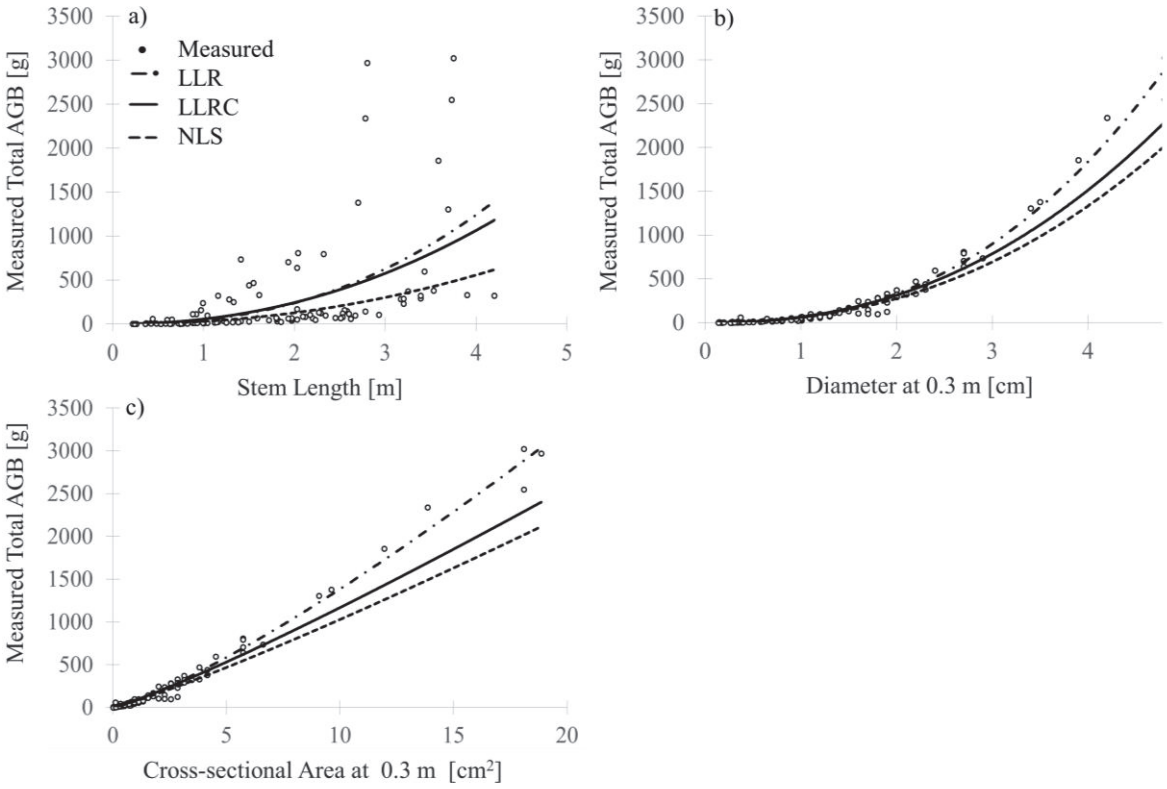

Figure 2.4. LLRC, LLR, and NLS model fits for each 1D (a,b), and 2D (c) predictor variable utilized to model total AGB for multispecies trees.

For multispecies tree total AGB prediction, the exponent α was greater for the 1D model based on stem length and close to unity for the 1D model diameter at 0.3 m, alternatively 2D model cross-sectional area at 0.3 m (Table 2.5). The 2D cross-sectional area model produced equivalent results compared to the 1D diameter model but allowed to effectively reconcile tree with shrub AGB predictions. The combined prediction of shrub and tree AGB has not been developed for this study region yet, but would allow the prediction of AGB for boreal short-stature shrubs and trees (<4.5 m) as well as tall-stature trees (>4.5 m) in just a few steps (see Section 2.3.5). When transferring these allometric models to different areas within the region, we recommend measuring the diameter at 0.3 m stem length.

Table 2.5. Regression coefficients to predict total AGB for multispecies trees with LLRC and NLS.

	Variable	LLRC β	NLS β	LLRC α	NLS α
Multispecies trees	Stem length	28.962	45.8224	2.132	2.380
	Diameter at 0.3 m	57.111	59.0721	2.272	2.479
	Cross-sectional area at 0.3 m	75.189	79.6818	1.136	1.240

2.4.4. Comparison of regression models for tree total aboveground biomass prediction

For the prediction of tree total AGB per genus/species and all genera/species combined, NLS achieved the lowest RMSE, highest R^2, and lowest total percentage error compared to measured biomass (<−5%–4%), while the dependent and independent variables were significantly related ($p < 0.001$, Table 2.4 and S2.7). LLR predictions resulted in the highest RMSE, similar R^2, and highest total percentage error relative to the measured biomass compared to LLRC and NLS for each genus/species and for all data combined. The single exception was for predicting total AGB for *Picea* spp. based on stem length (Table S2.7). Using LLR, the prediction based on stem length resulted in an underestimation of total AGB of −51% and an underestimation of −20% when using diameter or cross-sectional area, respectively, as input variable for the multispecies models. LLRC had comparably lower RMSE, similar R^2, and underestimated total multispecies AGB by −6% (stem length) to <−10% (diameter at 0.3 m, cross-sectional area at 0.3 m). In order to address potential heteroscedasticity effects, we have provided the regression coefficients for both NLS and LLRC models with cross-sectional area (measured at 0.3 m stem length) as predictor variable (Table S2.4).

2.4.5. Comparison of regression models for general shrub and tree total aboveground biomass prediction

The prediction of total AGB for shrubs and trees combined resulted in similar predictive capability to multispecies shrub and multispecies short-stature trees ($R^2 \geq 0.770, p < 0.001$). This was determined using the 2D independent variable of cross-sectional area, measured at the base for shrubs and at 0.3 m stem length for trees (Table 2.6, Figure 2.5). Relating modeled total AGB to measured total AGB showed no evident bias in the 2D-based prediction of combined shrub and tree AGB in comparison to 3D multispecies shrub and 2D multispecies tree AGB models. This is depicted in Figure 2.6, which shows modeled AGB in relation to measured AGB of the 2D general shrub and tree AGB model (Figure 2.6 e,f) in comparison to the 3D multispecies shrub (Figure 2.6 a,b) and 2D multispecies tree (Figure 2.6 b,c) AGB models. Similar to the multispecies shrub models, NLS achieved the lowest RMSE and highest R^2 (RMSE = 94.80 g, $R^2 = 0.776$). The RMSE of model LLR increased by 53% (RMSE = 202.17 g, $R^2 = 0.770$) and by 54% for the LLRC model (RMSE = 206.37 g, $R^2 = 0.770$). Compared to Ali et al. (2015), who derived best model fits for combined shrub and tree AGB prediction using diameter of the longest stem and total plant height combined, our model results show that AGB of boreal plants can be predicted with a simpler one-variable model using cross-sectional area. For our AGB models based on cross-sectional area, the exponent α was greater for the 1D model based on stem length and close to unity for the 2D model cross-sectional area at 0.3 m (Table 2.7). However, stem length of shrubs and trees was also weakly related to measured total AGB ($p < 0.001$, Table 2.6) and thus represents an alternative to cross-sectional area, which has potential for use in rapid field measurement or non-invasive observation situations (e.g., remote sensing via airborne lidar) where it may be acceptable to trade accuracy at the individual sample-level

for greater overall population representation. For model transfer purposes, we recommend the use of LLRC regression coefficients and correction factor in order to address heteroscedasticity.

Table 2.6. Model performances for combined general shrub and tree total AGB prediction (all p values < 0.001).

Model	Dimension	Input Variable	Total Percentage Error (%)	RMSE (g)	R^2
LLR	1D	Stem length	−44.15	378.72	0.249
	2D	Cross-sectional area	−11.17	202.17	0.770
LLRC	1D	Stem length	0.03	381.27	0.249
	2D	Cross-sectional area	0.02	206.37	0.770
NLS	1D	Stem length	22.53	292.51	0.500
	2D	Cross-sectional area	2.28	94.80	0.776

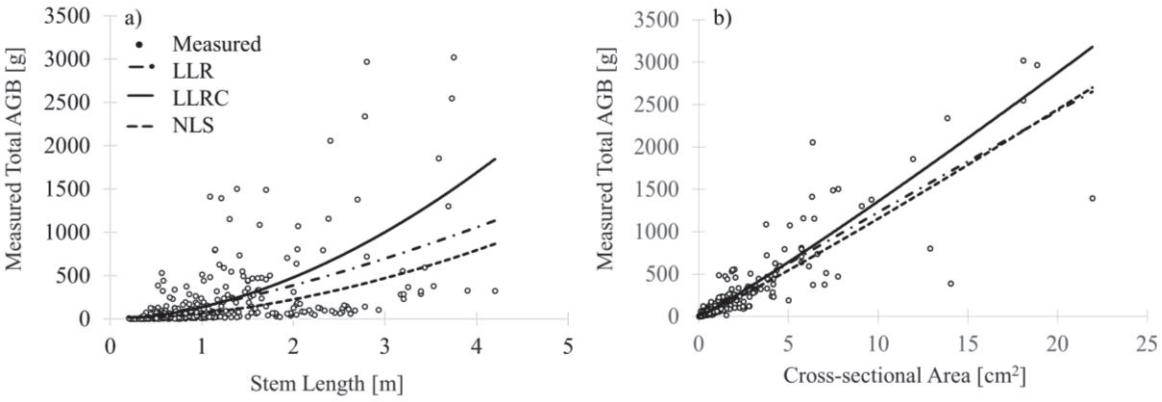

Figure 2.5. LLRC, LLR, and NLS model fits for the 2D predictor variable utilized to model total AGB for general shrubs and trees: (a) stem length and (b) cross-sectional area.

Table 2.7. Regression coefficients to predict total AGB for general shrubs and trees with LLRC and NLS.

	Variable	LLRC β	NLS β	LLRC α	NLS α
General shrubs and trees	Stem length	63.944	142.299	1.816	1.447
	Cross-sectional area	94.917	128.802	1.084	0.979

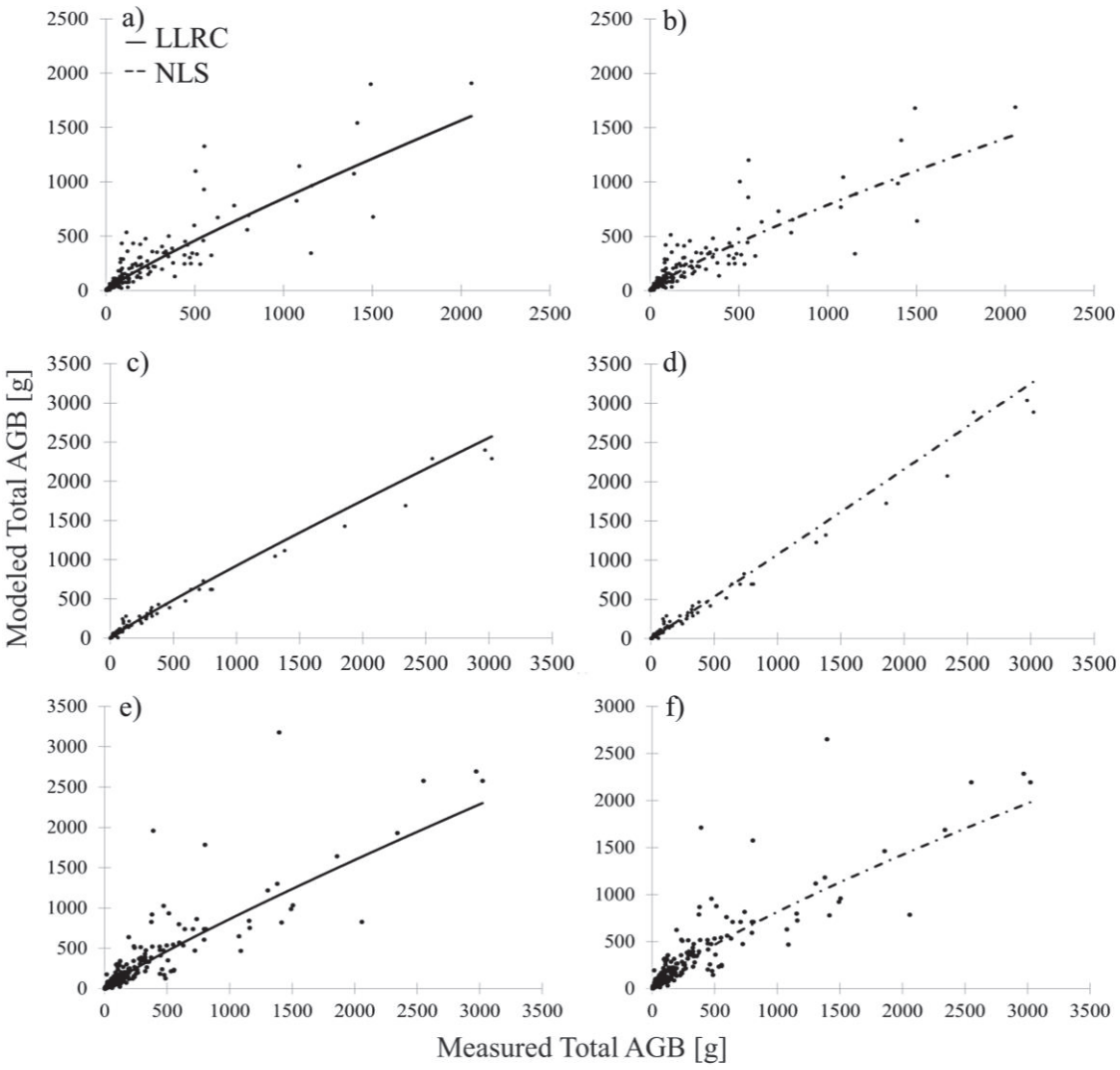

Figure 2.6. Measured total AGB related to modeled total AGB using LLRC and NLS for the 3D-based equations for multispecies shrubs (a,b) and the 2D-based equations for multispecies trees (c,d) as well as general shrubs and trees (e,f).

2.5. Conclusion

Our analysis has shown that AGB of shrubs can be modeled with higher accuracies when using a 3D field variable, such as volume. Small-stature tree AGB can be most accurately predicted with the stem diameter measured at 0.3 m stem length. In addition, we found that shrub AGB can be reconciled with small-stature tree AGB when using total stem cross-sectional area as the predictor variable. Based on the two best models, we have provided

regression coefficients and error statistics for the modelling of short-stature shrub and tree AGB for the region of sporadic to discontinuous permafrost in NWT, Canada. For model uncertainty propagation to total AGB predictions, we have provided the standard error of each model coefficient. We have provided species- and genus-specific as well as multispecies allometric models for shrubs and trees commonly found in boreal forest and peatland ecosystems. These equations are necessary for improving understanding and quantification of biomass change and the potential implications for carbon pools in northern environments, which are highly susceptible to climate change.

2.6. Overview supplementary material chapter 2

Table S2.1: Descriptive statistic by shrub species and genus by plant compartment (range of values in parentheses, followed by average ± standard deviation); Table S2.2: Descriptive statistic by tree species by plant compartment (range of values in parentheses, followed by average ± standard deviation); Table S2.3: Volume-based regression coefficient estimates with error statistics to be input into Equations (2.4)–(2.7) as appropriate to derive shrub AGB; Table S2.4: Cross-sectional area-based regression coefficient estimates with error statistic to be input into Equations (2.4)–(2.7) as appropriate to calculate tree AGB; Table S2.5: Cross-sectional area-based regression coefficients with error statistic to be input into Equations (2.4)–(2.7) as appropriate to calculate general shrub and tree AGB; Table S2.6: Model performances for shrub total ABG prediction per genus/species (all p values < 0.001); Table S2.7: Model performances for tree total ABG prediction per genus/species (all p values < 0.001).

2.7. Funding

This research was funded by the National Science and Engineering Research Council of Canada (NSERC)—Discovery Grants to Dr. Laura Chasmer and Dr. Christopher Hopkinson and a start-up grant provided to Dr. Laura Chasmer by the University of Lethbridge. Further funding was provided by the Canadian Foundation of Innovation Award to Dr. Christopher Hopkinson.

2.8. Acknowledgements

For support in field data collection and biomass processing, the authors would like to thank Tyler Rea and Ben Paulsen (Government of the NWT); Rachelle Shearing, Jesse Aspinall, Lavinia Haase, and Emily Jones (University of Lethbridge); and Garrett Isiah (Dehcho Guardian). For lab infrastructure, we would like to thank Larry Flanagan (University of Lethbridge). Finally, special thanks to William Quinton, the Aurora Research Institute, for support through the Dehcho Guardian program and the Dehcho Collaborative on Permafrost (DCoP).

2.9. References

Ali, A., Xu, M.-S., Zhao, Y.-T., Zhang, Q.-Q., Zhou, L.-L., Yang, X.-D., & Yan, E.-R. (2015). Allometric biomass equations for shrub and small tree species in subtropical China. *Silva Fennica*, *49*(4). https://doi.org/10.14214/sf.1275.

Baskerville, G. (1972). Use of Logarithmic Regression in the Estimation of Plant Biomass. *Canadian Journal of Forestry*, *2*, 49–53.

Berner, L. T., Alexander, H. D., Loranty, M. M., Ganzlin, P., Mack, M. C., Davydov, S. P., & Goetz, S. J. (2015). Biomass allometry for alder, dwarf birch, and willow in boreal forest and tundra ecosystems of far northeastern Siberia and north-central Alaska. *Forest Ecology and Management*, *337*, 110–118. https://doi.org/10.1016/j.foreco.2014.10.027.

Berner, L. T., Jantz, P., Tape, K. D., & Goetz, S. J. (2018). Tundra plant above-ground biomass and shrub dominance mapped across the North Slope of Alaska. *Environmental Research Letters*, *13*(3), 035002. https://doi.org/10.1088/1748-9326/aaaa9a.

Bond-Lamberty, B., Wang, C., & Gower, S. T. (2002). Aboveground and belowground biomass and sapwood area allometric equations for six boreal tree species of northern Manitoba. *Canadian Journal of Forest Research*, *32*(8), 1441–1450. https://doi.org/10.1139/x02-063.

Chasmer, L., & Hopkinson, C. (2017). Threshold loss of discontinuous permafrost and landscape evolution. *Global Change Biology*, *23*(7), 2672–2686. https://doi.org/10.1111/gcb.13537.

Chojnacky, D. C., & Milton, M. (2008). Measuring Carbon in Shrubs. In C. M. Hoover (Ed.), *Field Measurements for Forest Carbon Monitoring: A Landscape-Scale Approach* (pp. 45–72). Dordrecht: Springer Netherlands. https://doi.org/10.1007/978-1-4020-8506-2_5.

Ecosystem Classification Group (Ed.). (2008). *Ecological regions of the Northwest Territories - Taiga Shield*. Yellowknife, NT, Canada: Department of Environment and Natural Resources, Government of the Northwest Territories.

Ecosystem Classification Group. (2009). *Ecological regions of the Northwest Territories - Taiga Plains* (Revised). Yellowknife, NT, Canada: Department of Environment and Natural Resources, Government of the Northwest Territories.

Flanagan, L. B., & Syed, K. H. (2011). Stimulation of both photosynthesis and respiration in response to warmer and drier conditions in a boreal peatland ecosystem: PEATLAND CARBON DIOXIDE EXCHANGE. *Global Change Biology*, *17*(7), 2271–2287. https://doi.org/10.1111/j.1365-2486.2010.02378.x.

Flannigan, M. D., Logan, K. A., Amiro, B. D., Skinner, W. R., & Stocks, B. J. (2005). Future Area Burned in Canada. *Climatic Change*, *72*(1–2), 1–16. https://doi.org/10.1007/s10584-005-5935-y.

Gauthier, S., Bernier, P., Burton, P. J., Edwards, J., Isaac, K., Isabel, N., et al. (2014). Climate change vulnerability and adaptation in the managed Canadian boreal forest. *Environmental Reviews*, *22*(3), 256–285. https://doi.org/10.1139/er-2013-0064.

Goetz, S., Mack, M. C., Gurney, K. R., Randerson, J. T., & Houghton, R. A. (2007). Ecosystem responses to recent climate change and fire disturbance at northern high latitudes: observations and model results contrasting northern Eurasia and North America. *Environmental Research Letters*, *2*(4), 045031. https://doi.org/10.1088/1748-9326/2/4/045031.

Goulden, M. L., Mcmillan, A. M. S., Winston, G. C., Rocha, A. V., Manies, K. L., Harden, J. W., & Bond-Lamberty, B. P. (2011). Patterns of NPP, GPP, respiration, and NEP during boreal forest succession: CARBON DYNAMICS DURING BOREAL SUCCESSION. *Global Change Biology*, *17*(2), 855–871. https://doi.org/10.1111/j.1365-2486.2010.02274.x.

He, A., McDermid, G. J., Rahman, M. M., Strack, M., Saraswati, S., & Xu, B. (2018). Developing Allometric Equations for Estimating Shrub Biomass in a Boreal Fen. *Forests*, *9*(9), 569. https://doi.org/10.3390/f9090569.

Helbig, M., Chasmer, L., Kljun, N., Quinton, W., Treat, C., & Sonnentag, O. (2016). The positive net radiative greenhouse gas forcing of increasing methane emissions from

a thawing boreal forest-wetland landscape. *Global Change Biology*, *23*(6), 2413–2427. https://doi.org/10.1111/gcb.13520.

IPCC. (2014). *Climate Change 2014: Synthesis Report. Contributions of Working Groups I, II, and III to the Fifth Assessment Report of the Intergovernmental Panel on Climate Change* (p. 151). Geneva, Switzerland. Retrieved from https://archive.ipcc.ch/pdf/assessment-report/ar5/syr/SYR_AR5_FINAL_full_wcover.pdf.

Kurz, W. A., Shaw, C. H., Boisvenue, C., Stinson, G., Metsaranta, J., Leckie, D., et al. (2013). Carbon in Canada's boreal forest — A synthesis. *Environmental Reviews*, *21*(4), 260–292. https://doi.org/10.1139/er-2013-0041.

Lambert, M.-C., Ung, C.-H., & Raulier, F. (2005). Canadian national tree aboveground biomass equations. *Canadian Journal of Forest Research*, *35*(8), 1996–2018. https://doi.org/10.1139/x05-112.

Mascaro, J., Litton, C. M., Hughes, R. F., Uowolo, A., & Schnitzer, S. A. (2011). Minimizing Bias in Biomass Allometry: Model Selection and Log-Transformation of Data. *Biotropica*, *43*(6), 649–653. https://doi.org/10.1111/j.1744-7429.2011.00798.x.

Myers-Smith, I. H., Forbes, B. C., Wilmking, M., Hallinger, M., Lantz, T., Blok, D., et al. (2011). Shrub expansion in tundra ecosystems: dynamics, impacts and research priorities. *Environmental Research Letters*, *6*(4), 045509. https://doi.org/10.1088/1748-9326/6/4/045509.

Myers-Smith, I. H., Kerby, J. T., Phoenix, G. K., Bjerke, J. W., Epstein, H. E., Assmann, J. J., et al. (2020). Complexity revealed in the greening of the Arctic. *Nature Climate Change*, *10*(2), 106–117. https://doi.org/10.1038/s41558-019-0688-1.

R Core Team. (2021). R: A language and environment for statistical computing. Vienna, Austria: R Foundation for Statistical Computing. Retrieved from https://www.R-project.org/.

Smith, W. B., & Brand, G. J. (1983). *Allometric Biomass Equations for 98 Species of Herbs, Shrubs, and Small Trees* (Vol. 299). Washington, DC, USA: U.S. Department of Agriculture, Forest Service, North Central Forest Experiment Station. https://doi.org/10.2737/nc-rn-299.

Ung, C.-H., Bernier, P., & Guo, X.-J. (2008). Canadian national biomass equations: new parameter estimates that include British Columbia data. *Canadian Journal of Forest Research*, *38*(5), 1123–1132. https://doi.org/10.1139/X07-224.

CHAPTER 3: ABOVEGROUND BIOMASS ALLOCATION OF BOREAL SHRUBS AND SHORT-STATURE TREES IN NORTHWESTERN CANADA

3.1. Abstract

In this follow-on study on aboveground biomass of shrubs and short-stature trees, we provide plant component aboveground biomass (herein 'AGB') as well as plant component AGB allometric models for five common boreal shrub and four common boreal short-stature tree genera/species. The analyzed plant components consist of stem, branch, and leaf organs. We found similar ratios of component biomass to total AGB for stems, branches, and leaves amongst shrubs and deciduous tree genera/species across the southern Northwest Territories, while the evergreen *Picea* genus differed in the biomass allocation to aboveground plant organs compared to the deciduous genera/species. Shrub component AGB allometric models were derived using the three-dimensional variable volume as predictor, determined as the sum of line-intercept cover, upper foliage width, and maximum height above ground. Tree component AGB was modeled using the cross-sectional area of the stem diameter as predictor variable, measured at 0.30 m along the stem length. For shrub component AGB, we achieved better model fits for stem biomass (60.33 g ≤ RMSE ≤ 163.59 g; 0.651 ≤ R^2 ≤ 0.885) compared to leaf biomass (12.62 g ≤ RMSE ≤ 35.04 g; 0.380 ≤ R^2 ≤ 0.735), as has been reported by others. For short-stature trees, leaf biomass predictions resulted in similar model fits (18.21 g ≤ RMSE ≤ 70.0 g; 0.702 ≤ R^2 ≤ 0.882) compared to branch biomass (6.88 g ≤ RMSE ≤ 45.08 g; 0.736 ≤ R^2 ≤ 0.923) and only slightly better model fits for stem biomass (30.87 g ≤ RMSE ≤ 11.72 g; 0.887 ≤ R^2 ≤ 0.960), which suggests that leaf AGB of short-stature trees (< 4.5 m) can be more accurately

predicted using cross-sectional area as opposed to diameter at breast height for tall-stature trees. Our multi-species shrub and short-stature tree allometric models showed promising results for predicting plant component AGB, which can be utilized for remote sensing applications where plant functional types cannot always be distinguished. This study provides critical information on plant AGB allocation as well as component AGB modelling, required for understanding boreal AGB and aboveground carbon pools within the dynamic and rapidly changing Taiga Plains and Taiga Shield ecozones. In addition, the structural information and component AGB equations are important for integrating shrubs and short-stature tree AGB into carbon accounting strategies in order to improve our understanding of the rapidly changing boreal ecosystem function.

3.2. Introduction

Boreal ecosystems of northwestern Canada store approximately 2.1% of the global terrestrial carbon (C) on 0.3% of the global land surface area (Vitt et al., 2000). Therefore, the global atmospheric climate-C cycle is tightly coupled to the changing C dynamics of northern boreal ecosystems (Kurz et al., 2013). For effective emissions targets and mitigation strategies, it is essential to reduce the high uncertainties of the C balance of unmanaged boreal ecosystems (Bernier et al., 2012; Kurz et al., 2013). However, C accounting of unmanaged boreal ecosystems is challenging because these ecosystems are changing at unknown rates due to (1) the cumulative impacts of interacting climate-mediated and anthropogenic disturbances (Baltzer et al., 2014; Chasmer & Hopkinson, 2017; Dale et al., 2001; Quinton et al., 2009) and (2) the enhanced frequency, intensity, duration, and timing of these disturbances. For example, in boreal ecosystems of northwestern Canada the vegetation structure and composition has changed significantly

towards increased abundance of shrubs (Myers-Smith et al., 2011, 2020) and short-stature low productive or juvenile trees. This is in particular the case where ecosystems were set back to an early successional stage post wildland fire disturbance (Goetz et al., 2007) or in the rapidly changing transition zones between elevated forests and adjacent peatlands due to permafrost thaw (Chasmer & Hopkinson, 2017). This in turn has significant effects on ecosystem function and ecosystem-atmosphere interactions at local to regional scales (Chasmer & Hopkinson, 2017; Helbig et al., 2016) as well as at national to global scales (Goetz et al., 2007; Goulden et al., 2011). For example, prominent shrub and broadleaf tree growth in, e.g., post-fire vegetation succession is likely the explaining factor for returning production levels to an annual net C uptake within 10 to 15 years post burn (e.g., (Amiro et al., 2006; Beck & Goetz, 2012; Goulden et al., 2011). However, boreal shrubs and short-stature trees are not integrated into C accounting strategies. This is because of a lack of available spatially explicit structural and quantitative information on boreal shrub and short-stature tree species, as discussed in our related study (Flade et al., 2020). Therefore, aboveground biomass (AGB) allocation data for shrubs and short-stature trees are necessary to better understand the contributions of different plant components to the standing stocks of AGB and aboveground C in this region, while plant component AGB allometric equations for shrubs and short-stature trees provide a means to improve modelling of AGB and aboveground C pools.

Consequently, the first objective of this paper was to describe and discuss the proportion of plant component AGB for boreal shrub and short-stature tree species. Plant components were separated into stems, branches, and leaves. The second objective was to provide allometric equations for estimating aboveground biomass of plant components of

shrubs and short-stature trees. This paper is a follow-on study on shrub and short-stature tree total AGB allometric equations (Flade et al., 2020). While in the previous study (Flade et al., 2020) we focused on total AGB allometric equations using 1D, 2D, and 3D predictor variables, in this study we analyze the AGB allocation to different plant components and provide plant component-specific allometric equations leveraging the same field data as described by Flade et al. (2020). The plant component data provided in this study is a crucial next step towards improved C pool partitioning required for improved C accounting strategies for unmanaged boreal ecosystems of northwestern Canada (Bernier et al., 2012).

3.3. Materials and methods

3.3.1. Study area

Plant component AGB was derived from shrubs and short-stature trees growing in the mid-boreal Taiga Plains and high-boreal Taiga Shield ecoregions of the Northwest Territories (Figure 3.1). The climate in this region is characterized by cold mean annual air temperatures, ranging from −2.5 °C near Fort Simpson (Taiga Plains) to −3/−4 °C near Yellowknife (Taiga Shield). The area receives between 360 mm (Yellowknife) and 390 mm (Fort Simpson) cumulative annual precipitation. The genera and species sampled are *Alnus* spp., *Betula* spp., *Dasiphora fruticosa*, *Salix* spp., and *Shepherdia canadensis*, which represent common boreal shrub genera/species in this study area. Common boreal tree genera/species sampled are *Betula papyrifera*, *Picea glauca* and *mariana* (combined to *Picea* spp.), *Populus balsamifera*, and *Populus tremuloides* (Ecosystem Classification Group, 2008, 2009).

3.3.2. Plant destructive sampling

A total of 206 shrub and 105 tree individuals were measured and destructively sampled at 65 different peatland and forest sites. In order to capture the various stages of boreal ecosystem succession in our field data, field sampling locations were situated in late successional sites and in sites disturbed by wildland fire within the last 50 years. For a detailed field sampling plan, we refer to our previous study (Flade et al., 2020). Trees were sampled within the last two weeks in July 2019, while shrubs were harvested during the late July/early August period of 2018 and 2019. Therefore, shrub foliage might show higher variability compared to tree foliage due to the potential influences of changes in phenology. Shrubs and short-stature trees were destructively sampled from the understory and open areas across different height ranges determined in intervals of 0.5 m up to ≤ 4.5 m. A plant individual was selected for harvest when it was alive and mostly free of foliage disturbance/mortality and stem blemishes. Following measurements *in situ* (Flade et al., 2020), plants were clipped directly above the soil surface and stored in paper bags for further processing. Dead stems were not harvested. In the laboratory, harvested plants were air dried for up to 4 months and separated into stems, branches, and leaves. All plant components were oven dried at 60 °C for a minimum of 48 hrs. Constant mass was confirmed by weighing the largest plant individuals at multiple times post drying. Twigs and fruits were counted to the leaf component, while bark was included as part of the stem. For trees, branches were cut off directly at the stem. Shrubs did not develop distinctive branches and were separated into leaf and stem components only. The total AGB for shrubs and trees was determined as dry weight (g) by weighing each plant component and

summing the dry weight of all components per individual plant. In this study, we present measured plant component AGB as a percentage of the total AGB per plant genus/species.

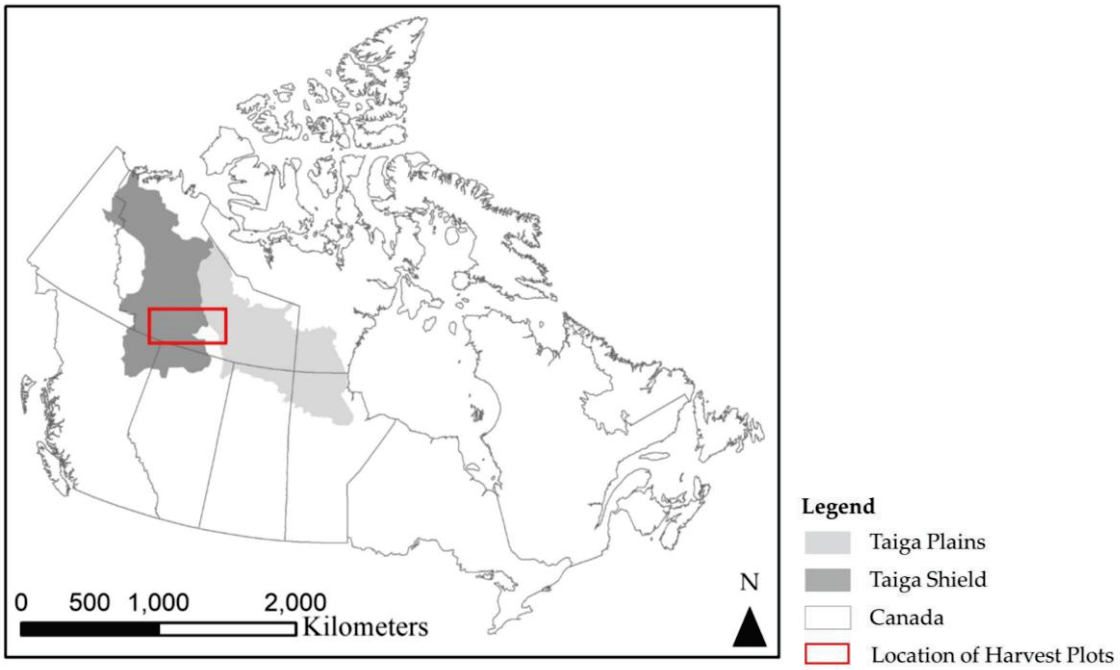

Figure 3. 1. Area of harvested aboveground biomass of shrubs and trees, distributed across the sporadic to discontinuous permafrost zone of the Taiga Plains and Taiga Shield ecozones of boreal northwestern Canada.

3.3.3. *In situ* measurements and plant component aboveground biomass allometric equations

We derived AGB allometric equations for each plant component per plant genus/species as well as all shrub genera/species (multi-species shrubs) and tree genera/species (multi-species trees) combined. The methods follow the same procedures used to determine total AGB in (Flade et al., 2020). The *in situ* structural measurements of harvested shrubs and trees used to determine the most accurate AGB predictions were volume for shrubs and cross-sectional area for trees (Flade et al., 2020). Volume was derived by measuring the extent of the upper-most foliage layer perpendicular to the transect (herein 'width' (m)) and parallel to

the transect (herein 'line-intercept cover' (m)) using a tape measure. The 3D shrub volume (m^3) was then calculated as:

$$\text{Volume } (m^3) = \text{max height (m)} \times \text{line-intercept cover (m)} \times \text{width (m)}. \quad (3.1)$$

For short-stature trees, cross-sectional area (cm^2) was derived from the measured stem diameters. Stem diameters were measured at 0.30 m along the stem length starting from the average ground surface surrounding the tree (Flade et al., 2020).

Highest model fits were derived using iterative non-linear least squares regression (herein 'NLS') via a power function:

$$y = \beta x^{\alpha} + \varepsilon \quad (3.2)$$

where y is the dependent variable, x is the independent *in situ* variable (volume for shrubs and cross-sectional area for trees), α and β are the regression coefficients, and ε is an additive error term, as discussed by Flade et al. (2020). Because our AGB data showed uniform variances on arithmetic scales for most species as well as on logarithmic scales for all species, we did not apply weights to our models. In order to address potential heteroscedasticity in shrub and short-stature AGB data, we also developed ABG allometric equations using linear logarithmic regression with correction (herein 'LLRC'):

$$ln(y) = ln(\beta) + \alpha * ln(x) + ln(\varepsilon) \quad (3.3)$$

$$y = \beta x^{\alpha} * \varepsilon \quad (3.4)$$

$$\varepsilon = e^{(\frac{MSE}{2})} \quad (3.5)$$

where ε represents a multiplicative correction factor (CF) of the back-transformed arithmetic values, derived with MSE as the mean square error of the regression [16,19,20].

The modeled biomass results were evaluated using root mean square error (RMSE), coefficient of determination (R^2), and regression residual analysis. Residual analysis was

performed using visual inspection of the relationships between dependent and independent variables. Regression coefficients are reported with standard errors.

3.4. Results and discussion

3.4.1. Measured plant component aboveground biomass

The amounts of harvested individual plants per genus/species and descriptive statistics of measured plant component AGB are provided in Table 3.1. The percentages of the measured AGB per plant component is provided in Figure 3.2. We found similar plant AGB for leaves and stems for all five shrub genera/species, ranging from 15% (*Alnus* spp.) to 19% (*Betula* spp.) for leaves, and from 81% (*Betula* spp.) to 85% (*Alnus* spp.) for stems, respectively (Figure 3.2 a). Similarly uniform was the measured plant component AGB for deciduous tree species, ranging from 10% (*Betula papyrifera*) to 16% (*Populus tremuloides*) leaf biomass, 12% (*Populus tremuloides*) to 17% (*Betula papyrifera*) branch biomass, and 72% (*Populus tremuloides*) to 77% (*Populus balsamifera*) stem biomass (Figure 2b). The measured plant component AGB of the evergreen *Picea* genus had lower stem biomass (49%) and higher branch (27%) and leaf (25%) biomass compared to the deciduous tree and shrub genera/species. This finding can be explained by the thick and often longer branches of the sampled *Picea* plants in comparison to the branches of short-stature deciduous tree species. We further found that the biomass of leaves and branches combined (52%) was approximately equal to the stem biomass (49%) of the *Picea* genus. Although biomass allocation changes with tree size and age (e.g. Konôpka et al., 2010; Petersson et al., 2012), Petersson et al. (2012) reported approximately 45% combined leave and branch biomass and 40% stem biomass (including bark) for 11 to 20 year old *Pinus sylvestris* stands in Sweden, while Johansson (1999) derived a mean stem biomass

proportion of 56% for 17 to 54 year old *Picea abies* stands growing on abandoned farmland in Sweden. In addition, we found that all five shrub genera/species had similar AGB allocations comparable to the three deciduous tree species.

Table 3.1. Descriptive statistic per plant genus/species and plant component (minimum and maximum values in parentheses, average ± standard deviation).

Plant Genus/Species	No. of Samples	Maximum Height [m]	Total AGB [g]	AGB Stems [g]	AGB Branches [g]	AGB Leaves/Needles [g]
Alnus spp.	33	[0.2; 3.2] 1.3 ± 0.7	[1.3; 2057.1] 311.4 ± 470.9	[0.6; 1856] 264.8 ± 401.8	-	[0.4; 289.7] 46.7 ± 68.0
Betula spp.	46	[0.2; 2.1] 1.1 ± 0.4	[4.0; 1154.1] 232.7 ± 261.1	[2.2; 1057.2] 188.2 ± 228.4	-	[1.3; 154.7] 44.5 ± 42.3
Dasiphora fruticosa	20	[0.2; 0.9] 0.6 ± 0.4	[5.1; 530.8] 117.6 ± 127.9	[3.6; 434.6] 96.2 ± 105.8	-	[1.5; 96.2] 21.4 ± 22.7
Salix spp.	79	[0.3; 2.8] 0.9 ± 0.5	[0.8; 1503.7] 143.3 ± 302.5	[0.4; 1381.4] 118.4 ± 261.1	-	[0.4; 284.8] 24.9 ± 47.0
Shepherdia canadensis	28	[0.3; 1.7] 0.8 ± 0.4	[7.1; 552.0] 121.5 ± 158.9	[5.7; 484.0] 99.5 ± 134.9	-	[1.1; 127.0] 22.0 ± 28.6
Betula papyrifera	15	[0.7, 3.4] 2.0 ± 0.8	[4.2; 596.2] 127.7 ± 162.2	[2.6; 444.9] 93.0 ± 122.4	[0.8; 95.7] 22.0 ± 26.1	[0.8; 55.6] 12.7 ± 14.8
Picea glauca	14	[0.4; 3.8] 1.8 ± 1.2	[10.5; 3021.8] 865.0 ± 992.4	[3.4; 1789.6] 426.1 ± 545.6	[1.2; 739.4] 212.5 ± 247.8	[5.9; 947.8] 226.4 ± 270.5
Picea mariana	15	[0.4; 3.6] 1.6 ± 0.9	[12.5; 2968.9] 668.5 ± 801.2	[4.3; 1269.6] 326.0 ± 412.2	[3.1; 1103.6] 195.2 ± 270.4	[5.1; 595.7] 157.1 ± 152.2
Populus balsamifera	31	[0.2; 4.2] 1.7 ± 1.1	[1.0; 380.9] 85.7 ± 103.3	[0.7; 294.9] 65.7 ± 81.3	[0.3; 53.1] 11.3 ± 13.7	[0.04; 47.0] 10.1 ± 11.1
Populus tremuloides	30	[0.4; 3.9] 1.8 ± 0.9	[1.1; 329.2] 67.8 ± 84.3	[0.5; 233.7] 50.2 ± 58.7	[0.04; 52.4] 8.6 ± 13.2	[0.2; 58.1] 10.9 ± 14.0

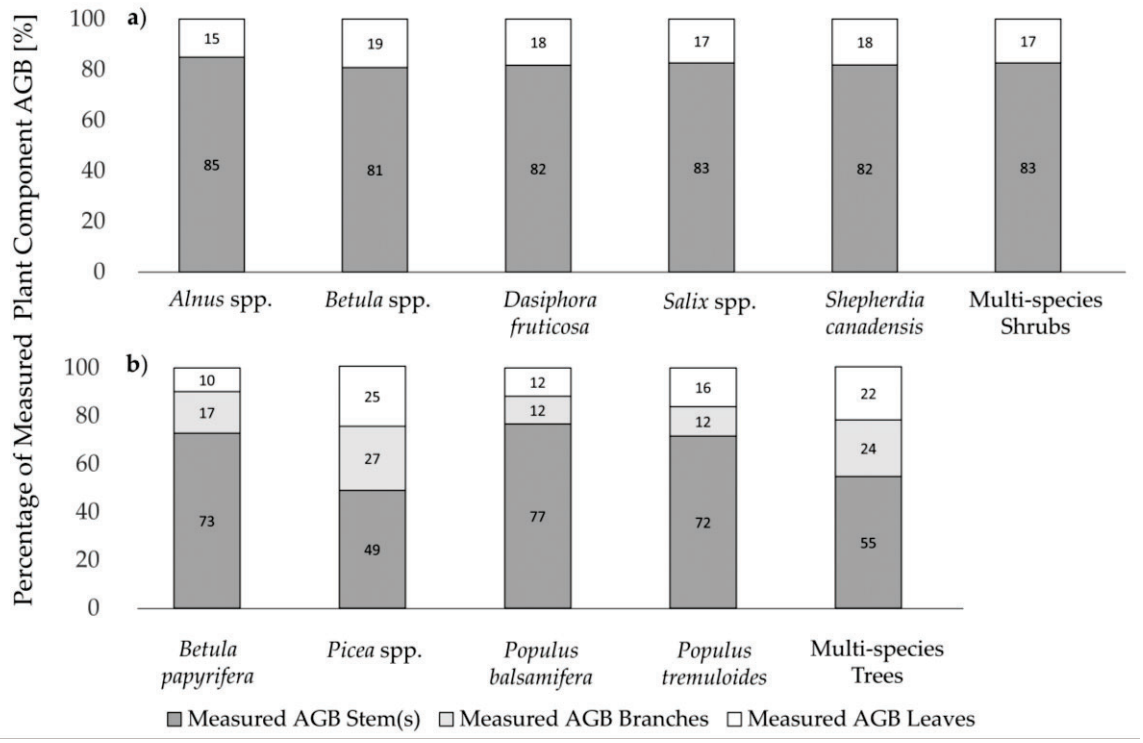

Figure 3.2. Measured aboveground biomass [%] per plant component for common boreal (a) shrub and (b) short-stature tree genera/species.

The variability of measured plant component AGB per shrub and short-stature tree genus/species is depicted in Figure 3.3a–g, respectively. From the five shrub genera/species sampled, *Alnus* spp. and *Betula* spp. were similar and showed greater variation compared to *Dasiphora fruticosa*, *Salix* spp., and *Shepherdia canadensis*. This differs from the findings of, e.g. He et al. (2018), who found greatest structural differences between *Alnus* spp. and *Betula* spp. However, in our study *Betula* spp. showed greater differences in leaf biomass compared to all other genera/species, which is similar to the reported differences in total AGB of the *Betula* genus by the same authors (He et al., 2018). In addition, we found similar structural growth forms of *Alnus* spp. and *Betula* spp. as reported by Lantz et al. (2013) and Moffat et al. (2016) for Arctic environments. *Alnus* spp. had stems growing

in an outward radiating form, while both *Alnus* spp. and *Betula* spp. developed long shoots. However, *Salix* spp. was the dominant species in our study area compared to *Betula nana* dominance on lichen plots found in the Tuktoyaktuk coastland tundra (Moffat et al., 2016). Our study results showed further that *Salix* spp. had a lower median of stem biomass and more outliers compared to the other four genera/species. This might not only be due to greater structural variability of this genus, but also due to the larger sample amount (n = 79, Table 3.1), which increases the sampling of a greater range of structural variation. However, *Salix* spp. was the dominant genus at our field locations, and therefore, the larger sample amount represents the naturally dominant occurrence of *Salix* spp. in our study area. For deciduous short-stature tree genera/species, stem, branch, and leaf biomass (Figure 3.3 d–g) showed similar variation, while *Picea* spp. had greater ranges, outliers, and medians for stem, branch, and leaf biomass, as previously described (Figure 3.2 b). In addition, it needs to be mentioned that influences of phenological changes could be the reason for slightly greater shrub foliage AGB variation compared to deciduous tree foliage AGB variation, due to the measuring period of shrubs extending into early August (Figure 3.3 c,g).

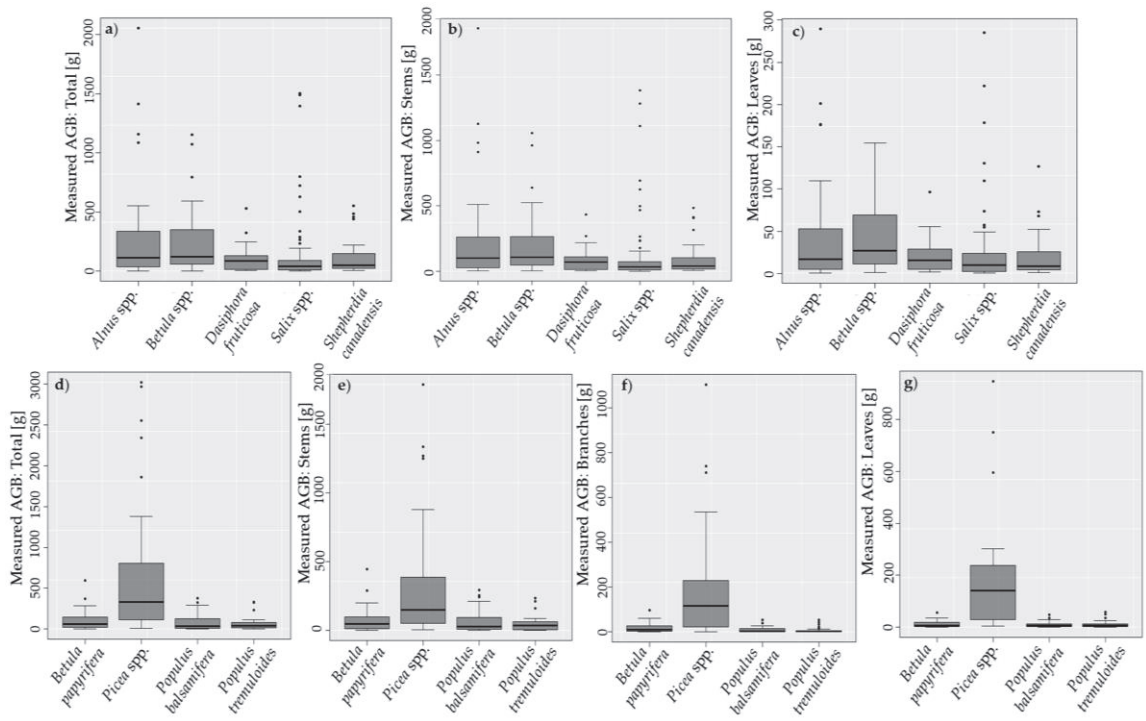

Figure 3.3. Boxplots of measured aboveground biomass [g] per plant component (total, stem, branch, and leaf aboveground biomass (AGB)) for common boreal (a–c) shrub and (d–g) short-stature tree genera/species. Points represent outliers of the distribution.

These findings suggest that short-stature deciduous tree genera/species may be combined with shrub genera/species as input into C allocation or terrestrial primary production models. However, model results might be improved when short-stature evergreen tree genera/species are analyzed separately, as already suggested by, e.g. Gower et al. (Gower et al., 1997), because these plant types differ in C budget processes, such as net primary production and C allocation (Baldocchi & Vogel, 1996; Bonan, 2015; Gower et al., 1997), as well as percentage of plant component AGB. In addition, variations in plant traits, such as dry matter of leaves, adult plant height, leaf area, seed mass, leaf mass per area, and leaf nitrogen, vary among species as well as within species, in particular at local scales and in areas of low species richness (e.g., Thomas et al., 2020)). This suggests a need to additionally incorporate plant trait information in earth system models to improve

understanding of the responses of plant communities, e.g., in ecosystem function and community assembly, to climate-mediated changes of environmental conditions (Thomas et al., 2020). The data used in this paper, does not provide the complete list of plant trait information, however, the plant component information might be useful as a first step towards improved earth system models in northern boreal environments.

3.4.2. Modeled plant component aboveground biomass and allometric equations

Regression coefficients and error statistics for the modelling of plant component AGB are provided for each genus/species as well as for multi-species shrubs (Table 3.2) and short-stature trees (Table 3.3). Because we found different AGB allocation of *Picea* spp., we also provided one combined component model for all deciduous tree species excluding *Picea* spp. (herein 'reduced hardwood tree model') (Table 3.3).

Modeled total AGB that was derived by the sum of the single component AGB models was on average 0.13 g ± 1.67 g standard deviation (0.03% of modeled mean total AGB) higher for shrubs, and 1.88 g ± 1.09 g standard deviation (0.67%) higher for trees respectively, compared to the total AGB model results.

For shrub component AGB, we achieved better model fits for stem biomass (60.33 g ≤ RMSE ≤ 163.59 g; $0.651 \leq R^2 \leq 0.885$) compared to leaf biomass (12.62 g ≤ RMSE ≤ 35.04 g; $0.380 \leq R^2 \leq 0.735$) for each genus/species as well as for the general multi-species shrub model using the three-dimensional predictor variable volume. Higher prediction errors of leaf and branch biomass models vs. stem biomass models have been found as well by Lambert et al. (2005). However, except for *Shepherdia canadensis*, R^2 are above 0.5 for all other genera/species and multi-species shrubs (Table 3.2).

Table 3.2. Volume-based regression coefficient estimates with error statistics to be input into Equation (3.2)–(3.5) as appropriate to derive shrub component AGB

		Model	LN(β)	β	SE (β)	α	SE (α)	CF	RMSE [g]	R^2
Alnus spp.	Stems	LLRC	5.104	164.6793		0.9474		1.2166	163.59	0.882
		NLS		146.3720	30.0176	1.0210	0.1021		137.23	0.885
	Leaves	LLRC	3.418	30.5083		0.7862		1.1792	35.04	0.735
		NLS		37.0392	8.5131	0.7805	0.1213		35.01	0.735
Betula spp.	Stems	LLRC	5.415	224.7525	.	0.8135		1.1766	137.05	0.651
		NLS		275.7010	28.2444	0.8980	0.1222		134.39	0.654
	Leaves	LLRC	3.977	53.3567		0.6370		1.2068	27.51	0.578
		NLS		64.8446	5.1663	0.6047	0.1019		27.48	0.579
Dasiphora fruticosa	Stems	LLRC	5.350	210.6083		0.7564		1.1608	60.72	0.672
		NLS		255.6900	31.3893	0.8490	0.2042		60.33	0.675
	Leaves	LLRC	3.714	41.0175		0.6228		1.1800	13.20	0.676
		ILS		55.9038	6.56778	0.8269	0.1911		12.62	0.691
Salix spp.	Stems	LLRC	5.161	174.3387		0.8857		1.1364	112.78	0.814
		NLS		210.9940	22.3109	0.8320	0.0588		111.90	0.817
	Leaves	LLRC	3.664	39.0171		0.7380		1.1767	33.75	0.519
		ILS		48.6847	5.6819	0.5734	0.0728		31.76	0.546
Shepherdia canadensis	Stems	LLRC	5.073	159.6526		0.7601		1.1018	62.16	0.789
		NLS		192.057	18.0495	0.6690	0.0849		60.68	0.801
	Leaves	LLRC	3.504	33.2482		0.6807		1.2342	23.74	0.380
		NLS		38.9539	5.84277	0.4535	0.1263		21.77	0.427
Multi-species Shrubs	Stems	LLRC	5.240	188.6701		0.8642		1.1842	123.31	0.795
		NLS		220.1460	12.7277	0.8170	0.0337		120.10	0.796
	Leaves	LLRC	3.692	40.1250		0.7151		1.2335	31.52	0.586
		NLS		50.4742	2.9920	0.5945	0.0393		30.12	0.600

Table 3.3. Regression coefficient estimates with error statistics based on cross-sectional area to be input into Equation (3.2)–(3.5) as appropriate to derive short-stature tree component AGB.

		Model	LN(β)	β	SE (β)	α	SE (α)	CF	RMSE [g]	R^2
Betula papyrifera	Stems	LLRC	3.970	52.9845		1.2370		1.0660	40.88	0.898
		NLS		41.4994	11.9728	1.5494	0.2193		36.63	0.913
	Branches	LLRC	2.634	13.9294		1.1440		1.0542	8.33	0.900
		NLS		12.7152	2.95996	1.2921	0.1826		8.08	0.905
	Leaves	LLRC	2.124	8.3645		1.0140		8.6012	70.00	0.882
		NLS		7.8627	2.1302	1.2143	0.2150		5.70	0.853
Picea spp.	Stems	LLRC	3.894	49.1069		1.0670		1.0782	170.97	0.928
		NLS		42.8437	11.9427	1.2201	0.1030		129.29	0.929
	Branches	LLRC	3.430	30.8766		1.0230		1.1129	94.07	0.892
		NLS		19.1842	6.6497	1.2866	0.1272		80.78	0.904
	Leaves	LLRC	3.821	45.6498		0.8059		1.1088	123.21	0.702
		NLS		42.2998	17.9815	0.9148	0.1635		119.89	0.704
Populus balsamifera	Stems	LLRC	3.805	44.9253		1.1320		1.1648	25.46	0.919
		NLS		47.3512	5.5776	1.3235	0.1053		22.43	0.924
	Branches	LLRC	1.773	5.8885		1.1140		1.4758	6.88	0.736
		NLS		7.6872	1.8698	1.2340	0.2211		6.83	0.737
	Leaves	LLRC	2.028	7.5989		1.0370		1.4577	5.81	0.832
		ILS		8.31954	1.1695	1.1007	0.1313		4.53	0.834
Populus tremuloides	Stems	LLRC	3.770	43.3801		1.0670		1.1627	13.64	0.950
		NLS		41.7058	3.0681	1.2658	0.0680		11.72	0.960
	Branches	LLRC	1.682	5.3763		1.0910		1.5380	6.18	0.816
		NLS		4.5910	1.0036	1.8127	0.1858		4.42	0.888
	Leaves	LLRC	2.255	9.5353		0.8919		1.1365	6.50	0.854
		NLS		8.07253	1.0364	1.4362	0.1149		4.11	0.917

(Table 3.3 continued)

		Model	LN(β)	β	SE (β)	α	SE (α)	CF	RMSE [g]	R^2
Hardwood Trees	Stems	LLRC	3.830	46.0625		1.1220		1.1482	30.87	0.887
		NLS		41.4212	3.9694	1.4431	0.0807		26.48	0.904
	Branches	LLRC	1.927	6.8689		1.1270		1.4893	8.7	0.760
		NLS		6.4825	1.1607	1.5966	0.1475		8.00	0.789
	Leaves	LLRC	2.138	8.4825		0.9655		1.2434	5.57	0.826
		NLS		8.28683	0.8242	1.2225	0.0872		4.44	0.841
Multi-species Trees	Stems	LLRC	3.833	46.2009		1.1090		1.1296	80.19	0.939
		NLS		49.1790	5.0772	1.1712	0.0393		73.17	0.940
	Branches	LLRC	2.336	10.3398		1.2690		1.6568	51.61	0.919
		NLS		12.7920	2.2283	1.4315	0.0639		45.08	0.923
	Leaves	LLRC	2.584	13.2500		1.1070		1.5055	73.11	0.768
		NLS		20.2891	4.6584	1.1807	0.0872		67.96	0.767

For short-stature trees, leaf biomass predictions using cross-sectional area as the independent variable resulted in similar model fits (18.21 g ≤ RMSE ≤ 70.0 g; 0.702 ≤ R^2 ≤ 0.882) compared to branch biomass (6.88 g ≤ RMSE ≤ 45.08 g; 0.736 ≤ R^2 ≤ 0.923) and only slightly better model fits for stem biomass (30.87 g ≤ RMSE ≤ 11.72 g; 0.887 ≤ R^2 ≤ 0.960) for each genus/species as well as the general hardwood and multi-species tree models (Table 3.3). This suggests that leaf biomass can be predicted using cross-sectional area as an independent variable for short-stature trees, leading to better results as the prediction of leaf biomass of tall-stature trees (diameter at breast height (DBH) > 9 cm) using DBH as an independent variable (e.g., Lambert et al., 2005; Ung et al., 2008)). Due to the different AGB allocation of *Picea* spp., we derived a reduced hardwood tree model including only the remaining hardwood tree species, as explained above. For this reduced hardwood tree model however, we did not receive better overall model fits (0.760 ≤ R^2 ≤ 0.887) compared to the full model that includes all tree genera/species (0.767 ≤ R^2 ≤ 0.940). In fact, model fits for stem and branch biomass were better for the full multi-species tree model. However, model fits for leaf biomass improved using the reduced hardwood tree model (Table 3.3).

The inspection of dependent vs. independent variable for the multi-species shrub and tree component models (Figure 3.4 a,b) as well as the standardized residuals (Figure 3.4 c,d) showed higher residuals of modeled leaf biomass compared to stem biomass for shrubs, while residuals were relatively homogeneous across all three modeled plant components for trees, as indicated by the goodness-of-fit metrics discussed above.

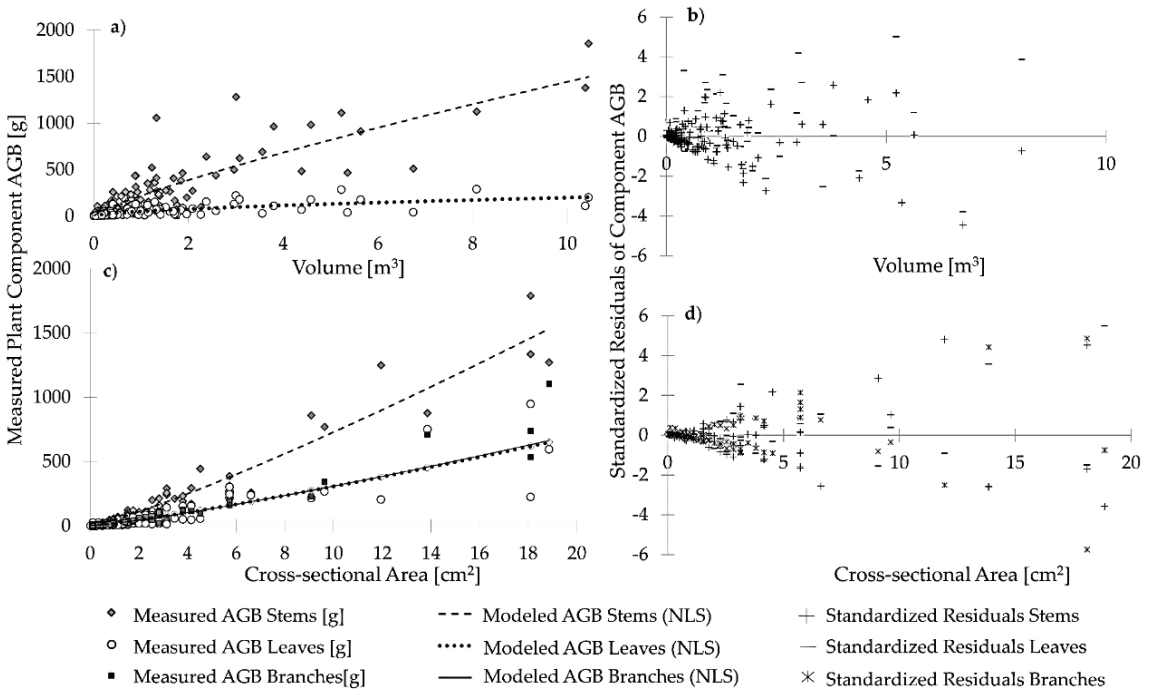

Figure 3.4. Model fits and standardized residuals per plant component for multi-species (a,b) shrub and (c,d) short-stature tree AGB. Shrub and tree component AGB was modeled via iterative nonlinear least-squares regression, using volume and cross-sectional area as the predictor variable, respectively.

For shrubs, the highest residuals were attributed to four shrub genera/species excluding *Shepherdia canadensis*, while the highest tree residuals corresponded to *Picea glauca* as well as *mariana*. Although this might imply that the multi-species tree component AGB models were mainly fit to *Picea* spp., we did not find higher residuals for smaller tree species in the multi-species component models. We achieved similar results with LLRC (not shown). This suggests that our multi-species models may have utility for using less invasive observation techniques (e.g., unmanned airborne vehicles or laser scanning) where plant species and type may be indeterminate. Furthermore, our genus/species-specific as well as multi-species models for predicting single plant component AGB may be well suited for scaling plant component and total AGB of shrubs and short-stature trees to the sporadic

to discontinuous permafrost zones of the Taiga Plains and Taiga Shield ecozones of boreal northwestern Canada.

3.5. Conclusions

In this study we describe plant AGB allocation to leaf, branch, and stem components as well as plant component AGB allometric models for common boreal shrub and short-stature tree genera/species (< 4.5 m height above ground) found in boreal northwestern Canada. We found similar AGB allocation to stems, branches, and leaves of shrubs and deciduous tree genera/species across our study region, while the sampled evergreen *Picea* genus differed in the AGB allocation to the aboveground plant components. Our plant component AGB allometric models showed better model fits for stem biomass compared to leaf biomass for shrubs. For short-stature trees, leaf biomass predictions resulted in similar model fits compared to branch biomass predictions with slightly better model fits for stem biomass predictions. In addition, our multi-species allometric models for shrubs and short-stature trees might be utilized for remote sensing techniques that do not allow to distinguish between plant functional types. This dataset and equations are a useful next step for integrating shrubs and short-stature tree AGB into C accounting strategies in order to improve our understanding of the rapidly changing boreal ecosystem function of forest and peatland ecosystems within the sporadic to discontinuous permafrost region. This provides an improved ability to develop full ecosystem models in the most climatically vulnerable and changing ecosystems found in the northern hemisphere.

3.6. Funding

This research was funded by the National Science and Engineering Research Council of Canada (NSERC)—Discovery Grants to Dr. Laura Chasmer and Dr. Christopher

Hopkinson. Funding for field work has been provided by a start-up grant to Dr. Laura Chasmer from the University of Lethbridge. Further funding was provided by the Canadian Foundation of Innovation Award to Dr. Christopher Hopkinson.

3.7. Acknowledgements

Fieldwork was supported by the Government of the Northwest Territories—Tyler Rea and Ben Paulsen and the Dehcho Guardians program supported by William Quinton, Wilfrid Laurier University. For support in field data collection and biomass processing, the authors would like to thank Rachelle Shearing, Jesse Aspinall, Emily Jones, and Lavinia Haase from the University of Lethbridge, as well as Garrett Isiah with the Dehcho Guardian program. For provision of lab infrastructure (ovens) and expertise, we would like to thank Larry Flanagan from the University of Lethbridge. We also thank three anonymous reviewers for their careful reviews.

3.8. References

Amiro, B. D., Orchansky, A. L., Barr, A. G., Black, T. A., Chambers, S. D., Chapin Iii, F. S., et al. (2006). The effect of post-fire stand age on the boreal forest energy balance. *Agricultural and Forest Meteorology*, *140*(1–4), 41–50. https://doi.org/10.1016/j.agrformet.2006.02.014.

Baldocchi, D. D., & Vogel, C. A. (1996). Energy and CO_2 flux densities above and below a temperate broad-leaved forest and a boreal pine forest. *Tree Physiology*, *16*(1–2), 5–16. https://doi.org/10.1093/treephys/16.1-2.5.

Baltzer, J., Veness, T., Chasmer, L., Sniderhan, A., & Quinton, W. (2014). Forests on thawing permafrost: fragmentation, edge effects, and net forest loss. *Global Change Biology*, *20*(3), 824–834. https://doi.org/10.1111/gcb.12349.

Beck, P. S. A., & Goetz, S. J. (2012). Corrigendum: Satellite observations of high northern latitude vegetation productivity changes between 1982 and 2008: ecological variability and regional differences. *Environmental Research Letters*, *7*(2), 029501. https://doi.org/10.1088/1748-9326/7/2/029501.

Bernier, P., Kurz, W. A., Lemprière, T., & Ste-Marie, C. (2012). *A Blueprint for Forest Carbon Science in Canada 2012–2020* (p. 52). Ottawa: Natural Resources Canada. Canadian Forest Service. Retrieved from

https://publications.gc.ca/collections/collection_2013/rncan-nrcan/Fo4-43-2012-eng.pdf.

Bonan, G. (2015). *Ecological Climatology: Concepts and Applications* (3rd ed.). Cambridge: Cambridge University Press. https://doi.org/10.1017/CBO9781107339200.

Chasmer, L., & Hopkinson, C. (2017). Threshold loss of discontinuous permafrost and landscape evolution. *Global Change Biology*, *23*(7), 2672–2686. https://doi.org/10.1111/gcb.13537.

Dale, V. H., Joyce, L. A., Mcnulty, S., Neilson, R. P., Ayres, M. P., Flannigan, M. D., et al. (2001). Climate Change and Forest Disturbances. *BioScience*, *51*(9), 723. https://doi.org/10.1641/0006-3568(2001)051[0723:CCAFD]2.0.CO;2.

Ecosystem Classification Group (Ed.). (2008). *Ecological regions of the Northwest Territories - Taiga Shield*. Yellowknife, NT, Canada: Department of Environment and Natural Resources, Government of the Northwest Territories.

Ecosystem Classification Group. (2009). *Ecological regions of the Northwest Territories - Taiga Plains* (Revised). Yellowknife, NT, Canada: Department of Environment and Natural Resources, Government of the Northwest Territories.

Flade, L., Hopkinson, C., & Chasmer, L. (2020). Allometric Equations for Shrub and Short-Stature Tree Aboveground Biomass within Boreal Ecosystems of Northwestern Canada. *Forests*, *11*(11), 1207. https://doi.org/10.3390/f11111207.

Goetz, S., Mack, M. C., Gurney, K. R., Randerson, J. T., & Houghton, R. A. (2007). Ecosystem responses to recent climate change and fire disturbance at northern high latitudes: observations and model results contrasting northern Eurasia and North America. *Environmental Research Letters*, *2*(4), 045031. https://doi.org/10.1088/1748-9326/2/4/045031.

Goulden, M. L., Mcmillan, A. M. S., Winston, G. C., Rocha, A. V., Manies, K. L., Harden, J. W., & Bond-Lamberty, B. P. (2011). Patterns of NPP, GPP, respiration, and NEP during boreal forest succession: CARBON DYNAMICS DURING BOREAL SUCCESSION. *Global Change Biology*, *17*(2), 855–871. https://doi.org/10.1111/j.1365-2486.2010.02274.x.

Gower, S. T., Vogel, J. G., Norman, J. M., Kucharik, C. J., Steele, S. J., & Stow, T. K. (1997). Carbon distribution and aboveground net primary production in aspen, jack pine, and black spruce stands in Saskatchewan and Manitoba, Canada. *Journal of Geophysical Research: Atmospheres*, *102*(D24), 29029–29041. https://doi.org/10.1029/97JD02317.

He, A., McDermid, G. J., Rahman, M. M., Strack, M., Saraswati, S., & Xu, B. (2018). Developing Allometric Equations for Estimating Shrub Biomass in a Boreal Fen. *Forests*, *9*(9), 569. https://doi.org/10.3390/f9090569.

Helbig, M., Chasmer, L., Kljun, N., Quinton, W., Treat, C., & Sonnentag, O. (2016). The positive net radiative greenhouse gas forcing of increasing methane emissions from a thawing boreal forest-wetland landscape. *Global Change Biology*, *23*(6), 2413–2427. https://doi.org/10.1111/gcb.13520.

Johansson, T. (1999). Biomass production of Norway spruce (Picea abies (L.) Karst.) growing on abandoned farmland. *Silva Fennica*, *33*(4). https://doi.org/10.14214/sf.649.

Konôpka, B., Pajtík, J., Moravčík, M., & Lukac, M. (2010). Biomass partitioning and growth efficiency in four naturally regenerated forest tree species. *Basic and Applied Ecology*, *11*(3), 234–243. https://doi.org/10.1016/j.baae.2010.02.004.

Kurz, W. A., Shaw, C. H., Boisvenue, C., Stinson, G., Metsaranta, J., Leckie, D., et al. (2013). Carbon in Canada's boreal forest — A synthesis. *Environmental Reviews*, *21*(4), 260–292. https://doi.org/10.1139/er-2013-0041.

Lambert, M.-C., Ung, C.-H., & Raulier, F. (2005). Canadian national tree aboveground biomass equations. *Canadian Journal of Forest Research*, *35*(8), 1996–2018. https://doi.org/10.1139/x05-112.

Lantz, T. C., Marsh, P., & Kokelj, S. V. (2013). Recent Shrub Proliferation in the Mackenzie Delta Uplands and Microclimatic Implications. *Ecosystems*, *16*(1), 47–59. https://doi.org/10.1007/s10021-012-9595-2.

Moffat, N. D., Lantz, T. C., Fraser, R. H., & Olthof, I. (2016). Recent Vegetation Change (1980–2013) in the Tundra Ecosystems of the Tuktoyaktuk Coastlands, NWT, Canada. *Arctic, Antarctic, and Alpine Research*, *48*(3), 581–597. https://doi.org/10.1657/AAAR0015-063.

Myers-Smith, I. H., Forbes, B. C., Wilmking, M., Hallinger, M., Lantz, T., Blok, D., et al. (2011). Shrub expansion in tundra ecosystems: dynamics, impacts and research priorities. *Environmental Research Letters*, *6*(4), 045509. https://doi.org/10.1088/1748-9326/6/4/045509.

Myers-Smith, I. H., Kerby, J. T., Phoenix, G. K., Bjerke, J. W., Epstein, H. E., Assmann, J. J., et al. (2020). Complexity revealed in the greening of the Arctic. *Nature Climate Change*, *10*(2), 106–117. https://doi.org/10.1038/s41558-019-0688-1.

Petersson, H., Holm, S., Ståhl, G., Alger, D., Fridman, J., Lehtonen, A., et al. (2012). Individual tree biomass equations or biomass expansion factors for assessment of carbon stock changes in living biomass – A comparative study. *Forest Ecology and Management*, *270*, 78–84. https://doi.org/10.1016/j.foreco.2012.01.004.

Quinton, W., Hayashi, M., & Chasmer, L. (2009). Peatland Hydrology of Discontinuous Permafrost in the Northwest Territories: Overview and Synthesis. *Canadian Water Resources Journal*, *34*(4), 311–328. https://doi.org/10.4296/cwrj3404311.

Thomas, H. J. D., Bjorkman, A. D., Myers-Smith, I. H., Elmendorf, S. C., Kattge, J., Diaz, S., et al. (2020). Global plant trait relationships extend to the climatic extremes of the tundra biome. *Nature Communications*, *11*(1), 1351. https://doi.org/10.1038/s41467-020-15014-4.

Ung, C.-H., Bernier, P., & Guo, X.-J. (2008). Canadian national biomass equations: new parameter estimates that include British Columbia data. *Canadian Journal of Forest Research*, *38*(5), 1123–1132. https://doi.org/10.1139/X07-224.

Vitt, D. H., Halsey, L. A., Bauer, I. E., & Campbell, C. (2000). Spatial and temporal trends in carbon storage of peatlands of continental western Canada through the Holocene, *37*.

CHAPTER 4: A BI-TEMPORAL AIRBORNE LIDAR SHRUB-TO-TREE ABOVEGROUND BIOMASS MODEL FOR THE TAIGA OF WESTERN CANADA

4.1. Abstract

Monitoring aboveground biomass (AGB) is critical for carbon reporting and quantifying ecosystem change. AGB from field data can be scaled to the region using airborne lidar. However, lidar-based AGB products emphasize upland forests, which may not represent the conditions in rapidly changing peatland complexes in the southern Taiga of western Canada. In addition, to ensure that modelled AGB changes do not incorporate systematic error due to differences between older and newer lidar technologies, model transfer tests are required. The aim of this study was to develop one bi-temporal lidar-based AGB model applicable to (1) vegetation structure at varying vertical and horizontal continuity in this region and to (2) data collected with an earlier generation lidar system for which Canada-wide aerial coverage is available. Goodness-of-fit metrics show that AGB can be modelled with moderate (R^2 = 48-58% Taiga Shield, peatlands) to high accuracies (R^2 = 83-89% Taiga Plains, upland/ permafrost plateau forests including ecotones) by using the point clouds average height and 90th height percentile within a weighted approach as function of modelled AGB and calibrating the earlier lidar data. These results are important for quantifying climate change effects on forest to peatland ecotones.

4.2. Introduction

Aboveground biomass (AGB) is commonly defined as the dry weight of live terrestrial vegetation above the soil surface, of which ~50% is sequestered as carbon in plant material.

As such, AGB is an essential constituent of net primary production (NPP) (Chapin et al., 2006) providing a means to quantify components of the carbon cycle of terrestrial ecosystems as well as short- and long-term changes to this store when measured over time. AGB is therefore an Essential Climate Variable (ECV), critical for improving understanding of Earth system cycles (Duncanson et al., 2019; GCOS, 2010; Herold et al., 2019) and a necessary part of international carbon reporting frameworks (Hopkinson et al., 2016a). For example, the total global carbon uptake of forests between 1990 and 2007 was equivalent to 60% of the cumulative anthropogenic carbon emissions. This was driven by temperate and boreal forests due to carbon sink offsets in tropical forests (Pan et al., 2011). However, changes in climate and disturbance regimes negatively impact the potential of forests to function as carbon sinks (Bonan, 2015), especially in the boreal biome (Gauthier et al., 2014; Price et al., 2013). Changes in the boreal forest carbon balance directly affect global mitigation and adaption strategies to climate change (IPCC, 2023; Kurz et al., 2013). To fulfil carbon reporting obligations, repeat national field inventory measurements (e.g. Gillis et al., 2005) are integrated with remote sensing data (Coops et al., 2021; Wulder et al., 2012) or statistical and process models (Pan et al., 2011) to derive local to regional information on increased (vegetation growth) and decreased (mortality) plant carbon stocks over time. Light detection and ranging (lidar) sensors on ground-based or aerial platforms have produced accurate vegetation structural and AGB estimates in forests (Coops et al., 2021; Hopkinson et al., 2004, 2006; Wulder et al., 2012; Xi et al., 2020). Furthermore, airborne lidar-based vegetation structure and AGB integrated with field plots, allometry, aerial photographs (Chasmer et al., 2011), eddy covariance (Chasmer et al., 2008; Hopkinson et al., 2016a), and satellite imagery (Luther et al., 2019; Matasci et al., 2018)

reduce spatial uncertainties in AGB accumulation across broader regions. A detailed review of the evolution and application of lidar within forestry contexts in Canada can be found in Wulder et al. (2012) and Coops et al. (2021).

Within the next decade, multiple spaceborne platforms will be launched for scaling AGB from forest inventory plots to the globe (Herold et al., 2019), such as the Biomass mission (European Space Agency (ESA)) and the Multi-footprint Observation LIDAR and Imager mission (MOLI, Japan Aerospace Exploration Agency). These are in addition to currently available Global Ecosystem Dynamics Instrument (GEDI, National Aeronautics and Space Administration (NASA) and University of Maryland) and Ice, Cloud, and Land Elevation Satellite 2 (ICESat-2, NASA) data. Examples of such scaling efforts within boreal forests are presented in Castilla et al. (2022) and Mahoney et al. (2018). The consistent validation of these global wall-to-wall AGB products will be a challenge due to limited high-quality reference data with well-reported uncertainties (available to the public), and error propagation of allometric equations (Duncanson et al., 2019). AGB maps derived from airborne or terrestrial lidar have been proposed as a means for consistent validation of spaceborne products (Duncanson et al., 2019; Wulder et al., 2012). However, lidar AGB products evolved primarily out of commercial forestry needs and as such, are predominantly produced for upland forest ecosystems (Næsset and Gobakken, 2008; Wulder et al., 2012). Typically these under-represent vegetation attributes in dynamic peatland complexes dominated by short-stature vegetation (shrubs and juvenile/low productive trees) and in upland forest understories, although considered in some studies (e.g. Poley et al., 2020; Wagers et al., 2021). Yet, to achieve a holistic understanding of, and to accurately quantify changing boreal ecosystem carbon stocks, short-stature

vegetation should be accounted for in AGB products and in carbon reporting obligations for the following reasons:

1. Although the largest standing AGB stocks are found in trees (Bonan 2015; Kristensen et al. 2015), short-stature vegetation, such as shrubs growing in the forest understory, reach >50% of the net primary productivity levels of trees due to rapid turnover rates (Nilsson and Wardle, 2005).
2. The high contribution to litterfall as a pathway for nutrient input strongly influences surrounding tree establishment and growth (Bonan, 2015; Nilsson and Wardle, 2005).
3. With increasing wildland fire frequency, severity, and area burned in Canada (Flannigan et al., 2005; Kasischke and Turetsky, 2006; Price et al., 2013), a growing proportion of boreal ecosystems are at early successional stages dominated by short-stature vegetation.
4. Due to permafrost thaw and subsequent changes in hydrological drainage patterns in discontinuous to sporadic permafrost environments in northwestern Canada (Carpino et al., 2018, 2021; Connon et al., 2014, 2015; Quinton et al., 2019), the most rapid ecosystem changes occur within peatland complexes, such as low productive forests on permafrost plateaus, peatlands, and ecotonal areas (e.g. Chasmer and Hopkinson, 2017).

Furthermore, the use of airborne lidar AGB products for consistent spaceborne AGB validation will require repeat lidar surveys across multiple vegetation growth years to quantify uncertainties of plant growth/ mortality as a function of time (e.g. Hopkinson et al., 2008) and to reduce uncertainties in vegetation dynamics that could support sustainable

forest management (Tompalski et al., 2018). Such dynamics are often monitored by coincident comparisons over time (e.g. using bi-temporal and multi-temporal data) or by space-for-time approaches, which can be useful to determine rates of vegetation change following disturbance. In the latter case, changes with different years since disturbance (Enayetullah et al., 2023) represent rates of growth and mortality related to early; mid; and later successional phases. However, this assumes that changes in environmental conditions are negligible across post-disturbance vegetation change regimes, as illustrated in numerous studies. For example, Auestad et al. (2023) showed that environmental variables contribute greatly to rates of change and vary between sites, thus confounding comparisons using space-for-time approaches. Wu et al. (2022) found that local environmental influences on white spruce growth rates were sometimes greater than the temporal rate of change associated with age. This can contribute to over- or under-estimation of response to climate change.

Coincident temporal comparisons between datasets remove the limitations of space-for-time transferability of growth/mortality rates associated with differences in environmental drivers between sites, though are more costly to collect and may introduce systematic error in point cloud distribution when using less temporally stable metrics (e.g. described in Hopkinson et al., 2016b). With regards to airborne lidar data collected in this study (described below), bi-temporal data are useful, especially when longer time periods between lidar data collections are available. These are required to quantify both changes in slower rates of growth/mortality of conifer and deciduous trees, and more rapid rates of shrubs and juvenile trees, especially in relatively low productivity northern forests and peatlands over broad areas and with varying environmental influences on plant

growth/mortality. However, multi-year airborne lidar data are often collected by different sensors due to ongoing advances in commercial lidar technology (Hopkinson et al., 2016b). When used for the quantification of subtle ecosystem changes, like canopy height through time, each generation of lidar sensor will display unique observation characteristics, leading to variable levels of measurement uncertainty and potential systematic errors (Hopkinson et al., 2016b). Such errors can result from differences in laser pulse energy and footprint differences (Hopkinson, 2007), point cloud density (Lim et al., 2008) or canopy penetration and pulse timing efficiencies (Chasmer et al., 2006; Hopkinson, 2007; Næsset, 2009). Further systematic errors due to differences in lidar survey parameters (e.g. flying altitude and speed) and sensor calibration can be addressed at the mission planning stage, and differences in geospatial point cloud locations can be registered during post-processing (Hopkinson et al., 2008).

While studies investigated the effects of different lidar sensors on forest canopy metrics (Hopkinson et al., 2016b; Lim et al., 2008; Næsset, 2009), AGB model transfer across sensors is less explored and is not considered in AGB models for short-stature vegetation that are often characterised by less stable metrics (e.g. height percentiles < 75).

The objectives of this study were two-fold: (1) To facilitate short- to tall-stature AGB mapping in under-represented ecosystems within the global climate system, we tested airborne lidar height and cover metrics across (a) the Taiga Plains and Shield ecozones in western Canada, and (b) forests growing within uplands and peat plateaus underlain by permafrost, peatlands, and forest to peatland ecotones. (2) To better understand the effects of technological differences between two lidar sensors on observed vegetation height and modelled AGB, we tested model transferability from a low-density single channel to a high-

density multi-channel lidar sensor. To enable the quantification of AGB change across varying vegetation structure from different lidar sensors, the aim of this study was to develop a single AGB model for shrubs, juvenile to mature trees, low productive trees, and a mix thereof (herein referred to as 'bi-temporal shrub-to-tree AGB model'). Addressing these goals will further enable research into the magnitudes and rates of ecotonal AGB and plant carbon increases and decreases that occur at the boundaries of advancing or receding landcovers, which are responding most rapidly to climatic- or disturbance-based changes. The AGB model transfer tests employed in this study can be used as examples for future studies aiming to compare AGB products across different generation lidar systems, such as systems with higher pulse repetition frequencies, and multi-channel or photon counting capabilities.

4.3. Methods

4.3.1. Study area

The study was conducted in the southern Taiga, Northwest Territories, Canada, underlain by sporadic to discontinuous permafrost (Figure 4.1) across a latitudinal range of 300 km and a longitudinal range of 500 km. The terrain of the study region is gently undulating to level. In the Taiga Plains Mid Boreal, mean elevation decreases from 350 m above sea level in the west (Liard Upland) to 175 m above sea level in the east (Great Slave Lowland). Elevation increases in the Taiga Sield High Boreal from west to east from 100 m to 300 m above sea level. The proportional area per ecosystem type varies across this region along a west to east gradient, whereby up to 71% of the Taiga Plains Mid Boreal ecoregion are covered by peatland complexes and up to 53% and 30% of the Taiga Plains and Taiga Shield High Boreal are covered by extensive shoreline fens around shallow ponds (Ecosystem

Classification Group, 2008; 2009). Upland mixed-wood, deciduous, and coniferous forests are most productive in the Liard Plain (western Taiga Plains Mid Boreal) and transition to dominantly jack pine (*Pinus banksiana)* or white spruce (*Picea glauca)* stands in the fire prone Taiga Plains High Boreal, and jack pine, black spruce (*Picea mariana)*, and paper birch (*Betula papyrifera)* stands on and between bedrock outcrops in the Taiga Shield High Boreal. Within the extensive peatland complexes in the Taiga Plains Mid Boreal, peat plateaus underlain by permafrost (herein 'permafrost plateaus') occur adjacent to lower-lying permafrost-free peatlands. These consist of sparse and stunted black spruce trees with lichen ground cover. The dominant vegetation in peatlands ranges from moss, sedge, and shrub (e.g. dwarf birch (*Betula* spp.), willow (*Salix* spp.)) dominated (open) to treed (black spruce and tamarack (*Larix laricina*)) (Ecosystem Classification Group, 2009).

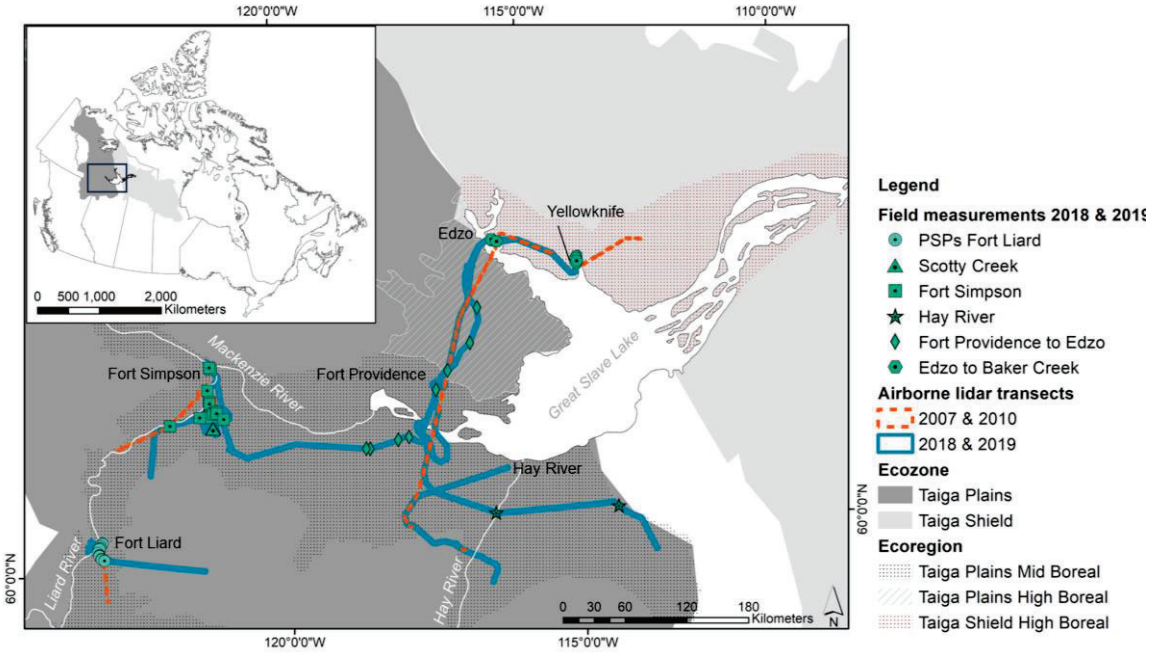

Figure 4.1. Study area of 2018, 2019 field measurements and airborne lidar transects in the Taiga Plains and Taiga Shield ecozones, Northwest Territories, Canada. Field measurements were used to develop aboveground biomass models based on the coincident 2018, 2019 Titan lidar data. Models were then transferred to the 2007, 2010 ALTM 3100 lidar data. (Ecozone and ecoregion boundaries were derived from the National Ecological Framework for Canada dataset).

4.3.2. Field measurements

Field data were collected from mid-July to mid-August in 2018 and 2019 within 53 transects of approximately 25 m in length (Flade et al., 2020; 2021). Transects were sampled in unmanaged ecosystems undisturbed by insect infestation with some in areas burned by wildland fire (<70 years). Transects started in forested uplands or permafrost plateaus and traversed into adjacent peatlands perpendicular to the outer transition boundary at ~10 m along each transect. Outer transition boundaries were visually determined where forests noticeably reduced in plant height and changed in species composition from trees mixed with shrubs and herbaceous vegetation into moss, grass, sedge, and shrub dominated "open peatlands" or sparsely forested "treed peatlands".

Measurements were made within circular forest mensuration plots (5 m radius, 78.5 m^2; n = 36) installed at the start of the transect and included genus/species identification, tree density, tree height (Vertex 5 Haglöf Sweden) and stem diameter at the base (tree height <1.5 m) and at breast height for every live tree. Typical forest mensuration plots span a 400 m^2 area. However, due to prioritizing the amount of transects across the region over the size of forest mensuration plots, we reduced the area to encompass a 5 m radius around the centre point of the transect start. Plots included between 14 and 76 individual trees (average 40), representing a range of structural characteristics. Transect start and end points were located using Global Navigation Satellite System (GNSS) Hiper SRII base station and rover (Topcon Corp., Japan). Surface level measurements of ground elevation were collected at 1 m intervals along the transect to ensure accurate registration with airborne lidar data. Plant structural data were collected within 1 m^2 plots (herein 'micro plots') along the transect (n = 1250). Measurements included two-dimensional cover and height for live

woody short-stature (≤4.5 m) to tall-stature (>4.5 m) plants per genus/species (Flade et al., 2020; 2021).

In addition to transects, field data from 20 permanent sampling plots (PSPs) in upland forests near Fort Liard were used to increase the representation of the upper range of tall-stature tree AGB in our study area (Figure 4.1). Precise Point Positioning (PPP) GNSS measurements were used to geolocate two diagonal corners of each of the 400 m^2 rectangular plots, operated for ~ 45 minutes at each corner to converge to centimetre-grade accuracy. Measurements consisted of tree height and diameter at breast height (DBH) for short-stature (DBH <9 cm) and tall-stature trees (DBH ≥9 cm). Species-level shrub cover and 1 out of 3 height categories were also collected. Shrub species were assigned the average height value of the respective height category. For ground covering shrub species, we determined height based on the average height of the respective species as measured in proximal transect vegetation plots. The selection of PSPs limited to Fort Liard (where upland forests are most productive) was due to the availability of highly accurate geo-located field data coincident to Titan lidar data (described below), which was not available at other PSP locations within the NWT. In addition, these sites were visited in person enabling a better understanding and documentation of vegetation structure and composition as well as site condition.

4.3.3. Field-based aboveground biomass derivation

To determine short-stature (≤4.5 m height) plant AGB within each plot, the product of cover and height per shrub genus/species resulted in a three-dimensional volume derivative, which was used as input into genus/species-specific shrub allometric equations based on

iterative nonlinear least squares regression (Flade et al., 2020). Short-stature tree stem length served as input into genus/species-specific tree allometric equations using iterative nonlinear least squares regression (Table 4.1, Flade et al., 2020). For shrub and short-stature tree genera/species without a dedicated allometric equation, the pooled allometric equations for shrubs, soft, and hardwood trees were used (Flade et al., 2020). For tall-stature tree species, tree height and diameter at breast height (DBH) were used in allometric AGB equations provided by Lambert et al. (2005).

Table 4.1. Stem length-based regression coefficient estimates with error statistics to be input into Equation 4 – 7 (Flade et al., 2020) for linear logarithmic regression with correction (LLRC) and iterative nonlinear least squares regression (NLS) as appropriate to derive short-stature tree AGB (≤4.5 m height).

		Coefficients							
		LN(β)	**β**	**SE (β)**	**α**	**SE (α)**	**CF**	**R^2 [%]**	**RMSE (g)**
Betula papyrifera	LLRC	2.485	12.0010		2.7300		1.0764	89.8	65.41
	NLS		3.9337	2.5136	3.9470	0.5440		92.5	44.93
Picea glauca	LLRC	4.938	139.4910		2.2640		1.0405	81.0	471.04
	NLS		242.6640	117.9150	1.7489	0.3940		82.7	414.62
Picea mariana	LLRC	5.131	169.1862		2.1910		1.1047	70.7	464.89
	NLS		282.5400	118.1550	1.6753	0.3920		73.7	413.48
Populus balsamifera	LLRC	2.897	18.1197		2.0780		1.0722	91.4	31.02
	NLS		20.8387	4.2502	2.0616	0.1698		91.4	30.33
Populus tremuloides	LLRC	2.429	11.3475		2.2790		1.0824	88.4	32.01
	NLS		6.1033	1.6867	2.9998	0.2316		91.0	25.42
Softwood (*Picea* spp.)	LLRC	5.041	154.6246		2.2240		1.0775	76.6	488.66
	NLS		268.9470	79.7794	1.6831	0.2526		79.1	415.77
Hardwood	LLRC	2.691	14.7464		2.1960		1.1054	79.3	54.92
	NLS		13.2239	3.1752	2.4982	0.2020		79.5	51.31
Multi-species Trees	LLRC	3.366	28.9624		2.1320		1.9117	28.5	484.83
	NLS		45.8224	28.8121	2.3799	0.5261		28.6	482.77

Standard error (SE); correction factor (CF)

Finally, AGB for each plant was summed within forest mensuration and micro plots for comparison with airborne lidar data. Further aggregation of field-based AGB was conducted to ensure adequate numbers of lidar returns per plot required for lidar return metric comparisons with field-based AGB. Micro plots along transects were aggregated separately within forested areas including transition zones and peatlands, and summed AGB in forests (including transition zone) and peatlands were scaled to 2 m widths. For circular forest mensuration plots that overlapped with the micro plots, we scaled the summed shrub AGB (forests including transition zone) to the same area as the forest mensuration plots and added the two AGB amounts together. Total AGB was converted to Mg ha^{-1}, resulting in 59 forest (including transition zones) and 44 peatland AGB values which were compared in a regression analysis with airborne lidar return metrics.

4.3.4. Airborne lidar data collection and processing

Airborne lidar surveys were conducted between July 30th to August 3rd, 2007, and 2010 and again during July and August of 2018 and 2019 coincident with field data collection. Lidar systems used were small-footprint multiple-discrete return Teledyne Optech Inc. (Ontario, Canada) Airborne Laser Terrain Mappers (ALTM). In 2007 and 2010, an ALTM 3100 system (manufactured in 2004) was used operating at 1064nm wavelength, while in 2018 and 2019 surveys were conducted with an ALTM Titan multi-channel system (manufactured in 2015) operating in three wavelengths (532 nm, 1064 nm and 1550 nm). Both were operated with similar flight and sensor settings, but the newer Titan sensor produced two to three times the return density of the older system (Table 4.2).

Table 4.2. Lidar survey settings and configuration of the single channel ALTM 3100 and multi-channel Titan sensors.

Sensor model	**ALTM 3100**	**Titan**
Dates of surveys	Jul/Aug 2007, 2010	Jul/Aug 2018 & 2019
Wavelength (nm)	1064	532, 1064, 1550
Pulse repetition frequency (kHz)	50-70	75-100 (225-300 total)
Field of view (deg)	30-40	30
Flying altitude (m agl)	~900-1500	~900-1200
Nominal point density (pts/m^2)	~3	~8
Approximal horizontal (x, y) and vertical (z) offsets to ground control (Titan) and between data sets	<1m (x, y) and <0.3m (z)	

Following pre-processing, the 3D lidar point clouds were quality controlled and filtered using TerraScan (Terrasolid Ltd., Finland). Low, air points, and isolated returns (noise) were deleted for quality control purposes, and remaining single and last returns were classified into ground points. All returns within -0.1m to 0m vertical distance to ground points were added to the ground class. All remaining non-ground returns were normalized relative to height above ground using 'LASheight' within the LAStools suite (rapidlasso GmbH, Germany).

To mitigate long GNSS baseline trajectory errors and facilitate accurate comparisons between the Titan lidar data and coincident field plot and transect data, lidar point clouds were manually block adjusted (per lidar flight strip) in x, y, and z direction to match ground control. Where necessary, adjustments in x, y, and z were made for each surveyed transect by overlapping the Titan lidar point clouds in Quick Terrain Modeler (version 8.3.1, Applied Imagery, USA) with ground control points (Profile Analysis Tool) and visually adjusting the Titan lidar data until systematic differences were reduced to zero. Control points and other visual reference data consisted of 1m interval ground surface

elevations (GNSS and surface levelling measurements) and localised maximum short-stature and tall-stature vegetation heights. For all field transects and lidar flight strips the required adjustments were <1m in x and y and <0.3m in z (Table 4.2). Ground classified lidar data from 2007 and 2010 ALTM 3100 surveys were then registered to the aligned Titan lidar data by again overlapping the point clouds and shifting the ALTM 3100 data. Offsets were within the range mentioned above (Table 4.2).

Registered and height normalized returns were then clipped to coincident field transects (forests including transition zone, and peatlands) and forest-mensuration plots for regression and model development. Common lidar metrics were derived for each clipped area using LAStools and the "lidR" package (Roussel et al., 2020; Roussel and Auty, 2022) (R Core Team 2021, Austria). These included height percentiles (from the 5^{th} to the 99^{th} percentile), interquartile range of return heights (25^{th} to 75^{th} height percentile), minimum, maximum, average, and standard deviation of all heights, kurtosis, skewness, and average square height using all lidar returns above ground level (hagl). Cover and density metrics were derived for all lidar returns above 0.5 m hagl. Lidar metrics per sensor were also gridded at 5 m x 5 m grid cell resolution for the complete region ("lidR" and "raster" packages in R) to apply the final AGB model. This cell size was chosen to ensure sufficient numbers of points per Titan and ALTM 3100 grid cell (needed to distinguish between lidar height percentiles), while also maintaining relatively high spatial resolution. This is especially important in ecotones that may be changing horizontally but are within a Landsat grid cell. 5 m cells can also be aggregated to the scale of forest inventory plots (typically 20 m x 20 m or 11.28 m radius, National Forest Inventory) and Landsat imagery (30 m x

30 m grid cell). A canopy height model was derived at the same grid cell resolution based on the maximum height of each cell.

4.3.5. Lidar-based aboveground biomass model development

Correspondence between coincident field-derived AGB and lidar metrics per clipped area was evaluated within a pre-selection process using the Pearson correlation coefficient, retaining those metrics that had the highest or second highest correlations in a minimum of two strata. Furthermore, lidar metrics were retained when assumptions of parametric regression were met, as tested by the Anderson Darling test to determine deviation of residuals from normality, as well as residual plots to determine heteroscedasticity. Each of the remaining lidar metrics was used as the predictor variable within single variable iterative nonlinear least squares regression via a power function (Equation 4.1), which is commonly used to infer AGB from field and lidar data. The model form was:

$$AGB_{lidar\ sensor} = b * lidar\ metric^{\,a} \quad (4.1)$$

where b and a are model coefficients. To better understand magnitudes of model errors of nonlinear least squares regression, model fits were compared to linear regression with forced y-intercept. Forcing the intercept through the origin ensured that AGB equalled zero for zero lidar points above the terrain surface. Model performance per lidar metric was analysed to determine the optimal lidar metric for (1) each stratum (ecozone, ecosystem type) and (2) all strata combined using leave-one-out cross validation during model development. Goodness-of-fit statistics included the coefficient of determination (R^2), root mean squared error (RMSE), and absolute model bias (Bias) which are most commonly used in AGB regression analysis (Coops et al., 2021). To compare RMSEs across strata that

deviate in their group means, the root mean squared error and bias relative to the mean (RMSE% and Bias% respectively) were derived.

To determine whether a single lidar metric could be used to model AGB with moderate to high accuracy across the region, a general AGB model was developed for each lidar metric using data of all strata combined (herein called 'general AGB model'). To evaluate model accuracies, the general AGB models (one for each lidar metric) were applied to each stratum and compared to respective stratum-specific AGB model fits.

The criteria for the selection of the optimal lidar metric as predictor of bi-temporal shrub-to-tree AGB required: (1) high goodness-of-fit statistics of the general AGB model for each stratum, and (2) minimal difference in the lidar metric when compared between sensors (see below).

4.3.6. Lidar metric comparison across sensors

When transferring an AGB model trained for Titan to the older ALTM 3100 data, systematic errors might occur due to differences in point cloud density (Lim et al., 2008) or canopy penetration characteristics (Chasmer et al., 2006; Hopkinson, 2007) even when flight settings and sensor calibration are the same between flights and point clouds are geo-registered. To test for deviations between the sensors' characterisations of height without available corresponding field data, deviations had to be isolated from signals stemming from successional vegetation changes. Therefore, gridded lidar metrics were compared between sensors in late-successional upland forests in which canopy characteristics between the two survey periods (8-12 years) were assumed to be minimal due to slow successional changes in the study region (Castilla et al., 2022). This assumption was

corroborated by observed negligible changes in the ALTM 3100 and Titan 5m x 5m Canopy Height Models combined with qualitative comparisons at matching locations in Google Earth Pro where multi-year imagery was available. Hereby, general areas of stable maximum canopy height in uplands were visually identified for sample locations across the entire study region. Within these, a total of 558 grid cells were randomly selected at which values of lidar metrics were extracted for further model transfer analysis. To confirm negligible change in these grid cells, differences in mean canopy height and standard deviation were quantified. Differences in the first quartile (based on the distribution of extracted canopy heights) were also determined to test for negligible changes in short-stature vegetation as found in the forest understory or in open upland sites. Subsequently, to quantify deviations between the sensors' characterisations of height, the covariance of each corresponding Titan (observed) and ALTM 3100 (predicted) lidar metric was derived for sampled grid cells by comparing the slope against the 1:1 line of correspondence between observed and predicted values (Piñeiro et al. 2008). Lidar metrics retained as candidates for the final bi-temporal shrub-to-tree AGB model development were selected based on demonstrating ≤±2% deviation from unity (1:1) in slope and ≥95% in explained variance (R^2).

4.3.7. Lidar metric calibration and selection for bi-temporal shrub-to-tree aboveground biomass modelling

Based on the two criteria of high goodness-of-fit statistics across strata for the general AGB models and high covariance between corresponding Titan and ALTM 3100 lidar metrics, the retained ALTM 3100 lidar metrics were calibrated using the slope (determined above)

as calibration coefficient (c, Equation 4.2). General ALTM 3100 AGB was subsequently modelled for each grid cell per lidar metric as:

$$AGB_{ALTM\ 3100,calibrated} = b * (c * lidar\ metric\ )^a \qquad (4.2)$$

General Titan AGB per grid cell was derived without the application of a calibration coefficient (Equation 4.1).

Finally, for the selection of the optimal predictor of bi-temporal shrub-to-tree AGB, deviations in modelled general Titan and calibrated ALTM 3100 AGB were analysed across lidar metrics to identify AGB ranges for which lidar metrics deviated in their predictions. This comparison was based on 1381 sampled grid cells distributed randomly across the study region, which covered AGB values from 0 to 400 Mg ha^{-1}. A recommendation for the optimal lidar metric was made relative to a specific AGB range. The final bi-temporal shrub-to-tree AGB model was then a combination of metrics applied to specific AGB ranges using a weighted approach. Hereby, modelled AGB per lidar metric (herein called exemplarily 'model output 1' and 'model output 2') was multiplied by a weighting factor (0%-100%), which increased for model output 1 and decreased inversely for model output 2 as a certain AGB range was approached for which model output 1 was deemed more reliable (i.e. lower variance in AGB compared between sensors).

4.4. Results

4.4.1. Aboveground biomass model comparison

A comparison of the field-based AGB across strata is illustrated in Table 4.3 to provide geographic context for the distribution across ecozones and ecosystem types. Field data indicated that the Taiga Plains contained more than three times the average AGB as found

in the Taiga Shield. However, some data were collected in highly productive forests near Fort Liard (Figure 4.1), resulting in a shift in the third quartile. Within ecosystem types, forests in uplands and permafrost plateaus also contained greater average biomass relative to peatlands, which are commonly dominated by 'open' moss and graminoid forms.

Table 4.3. Descriptive statistics of field-derived AGB (Mg ha^{-1}) for the complete field data and stratified into ecozone and ecosystem type.

Strata	**n**	**Mean (SD)**	**1st Quartile**	**3rd Quartile**	**Max**
All ecosystem types and ecozones	103	49.9 (75.2)	2.3	54.1	330.4
Ecozone					
Taiga Plains	79	65.7 (85.3)	4.0	118.4	330.4
Taiga Shield	24	17.0 (18.6)	0.8	30.9	56.6
Ecosystem type					
Upland/permafrost plateau forests	59	96.0 (85.2)	29.5	143.6	330.4
Peatlands	44	3.9 (5.4)	0.7	4.1	21.8

SD: Standard deviation.

The lidar metrics retained in the pre-selection process were characteristic of the height distributions of lidar returns consisting of the average height, interquartile range of heights, and 75th and 90th height percentiles of all lidar returns within each plot (Table 4.4). In addition, we included the 95th height percentile, which is a common predictor of canopy height (Mahoney et al., 2018; Popescu et al., 2002; Riggins et al., 2009) and growth in forests (Hopkinson et al., 2008).

Table 4.4. Pearson correlation coefficient of linear relationships between Titan lidar metrics and field-based AGB within corresponding plots used to refine the selection of lidar metrics for lidar-based stratum specific and general AGB model development.

	Taiga Plains	Taiga Shield	Upland/Permafrost Plateau Forest	Peatlands	All data
Percentile 5	-0.23	0.00	-0.18	0.55	-0.14
Percentile 10	-0.13	0.00	-0.07	0.55	-0.03
Percentile 25	0.59	0.12	0.56	0.55	0.66
Percentile 50	0.90	0.33	0.89	0.61	0.93
Percentile 75	0.95	0.74	0.92	0.78	0.97
Percentile 90	0.94	0.79	0.90	0.57	0.95
Percentile 95	0.93	0.72	0.89	0.43	0.94
Percentile 99	0.91	0.71	0.87	0.40	0.92
Interquartile range	0.94	0.74	0.91	0.76	0.96
Average height	0.95	0.76	0.92	0.69	0.97
Average square height	0.89	0.68	0.86	0.43	0.92
Minimum	-0.23	0.00	-0.18	0.55	-0.15
Maximum	0.89	0.68	0.85	0.33	0.90
Standard deviation	0.94	0.74	0.90	0.43	0.95
Cover (> 0.5 m agl)	0.80	0.66	0.75	0.71	0.78
Density (> 0.5 m agl)	0.83	0.71	0.79	0.66	0.81
Kurtosis	-0.39	-0.50	-0.45	-0.24	-0.38
Skewness	-0.60	-0.52	-0.68	-0.22	-0.57

Highest Pearson correlation coefficient per stratum coloured in grey, second highest coloured in yellow.

Using each of these lidar height metrics (m hagl) as input variable within nonlinear least squares regression via a power function resulted in moderate to high correspondence to field-derived AGB (Mg ha^{-1}) for stratum specific models (R^2 = 61% to 90% reported for the best lidar height metric per stratum) (Table 4.5). Model errors were moderate overall for highest R^2 predictors (RMSE < 34 Mg ha^{-1}; Bias < 26 Mg ha^{-1}) but were greater in peatlands and the Taiga Shield ecozone. Model errors increased for all strata and lidar metrics using the linear model form (difference in RMSE% = 0 to 21; difference in Bias% = -4 to 7) (Table 4.5).

Table 4.5. Titan lidar height metrics after pre-selection, regression coefficients and leave-one-out cross validated model fits for stratum-specific and general AGB models using single variable nonlinear least squares regression via a power function.

	Coefficients								
Lidar metric	b	SE (b)	a	SE (a)	R^2 (%)	RMSE (Mg ha^{-1})	%RMSE (%)	Bias (Mg ha^{-1})	%Bias (%)
General model									
Average height	21.974	1.951	0.966	0.038	93.7	18.9 (+0.8)	38.0 (+1.5)	12.8 (-0.1)	25.7 (-0.1)
IQR	14.969	1.822	0.939	0.440	92.0	21.4 (+1.0)	42.8 (+2.1)	13.6 (0)	27.4 (0)
Percentile 75	12.979	1.510	0.966	0.041	93.7	19.0 (+0.7)	38.2 (+1.3)	12.7 (0)	25.4 (0)
Percentile 90	5.393	0.950	1.187	0.058	91.4	22.0 (+1.9)	44.1 (+3.8)	13.9 (+1.2)	27.8 (+2.4)
Percentile 95	3.346	0.724	1.306	0.070	72.9	24.0 (+3.6)	48.2 (+7.1)	14.8 (+3.4)	29.6 (+6.8)
Taiga Plains model									
Average height	27.084	3.170	0.890	0.051	90.0	27.0 (+1.5)	41.2 (+2.2)	18.4 (-0.8)	28.0 (-1.2)
IQR	19.493	2.986	0.856	0.056	88.7	27.4 (+3.3)	41.7 (+5.0)	18.8 (+0.1)	28.6 (+0.2)
Percentile 75	17.214	2.655	0.878	0.055	89.8	28.7 (0)	43.7 (0)	18.1 (-0.2)	27.5 (-0.2)
Percentile 90	7.644	1.636	1.083	0.071	88.5	28.9 (+0.9)	44.0 (+1.4)	19.3 (+0.2)	29.4 (+0.3)
Percentile 95	5.088	1.285	1.183	0.082	87.2	30.6 (+1.9)	46.5 (+2.8)	20.6 (+2.0)	31.4 (+3.0)
Taiga Shield model									
Average height	23.524	3.094	0.706	0.183	61.2	11.6 (+1.1)	68.4 (+6.2)	8.3 (-0.3)	48.6 (-1.6)
IQR	21.315	3.020	0.493	0.112	64.9	11.1 (+3.0)	65.0 (+17.8)	8.6 (-0.7)	50.7 (-3.8)
Percentile 75	21.067	3.049	0.495	0.114	64.3	11.2 (+2.9)	65.6 (+17.2)	8.7 (-0.7)	51.0 (-4.3)
Percentile 90	10.629	3.512	0.718	0.207	64.0	11.2 (+0.9)	65.6 (+5.2)	7.2 (+0.2)	42.5 (+1.0)
Percentile 95	9.008	3.874	0.673	0.238	55.4	12.5 (+1.4)	73.2 (+8.4)	7.7 (-0.6)	45.2 (-3.5)

(Table 4.5 continued)

	Coefficients								
Lidar metric	b	SE (b)	a	SE (a)	R^2 (%)	RMSE (Mg ha^{-1})	%RMSE (%)	Bias (Mg ha^{-1})	%Bias (%)
Upland/Permafrost plateau forest model (including ecotones)									
Average height	32.744	4.203	0.811	0.058	84.5	33.5 (+3.2)	34.9 (+3.3)	25.8 (+0.1)	26.8 (+0.1)
IQR	22.037	3.770	0.813	0.064	82.3	36.0 (+2.9)	37.5 (+3.1)	28.2 (+0.7)	29.4 (+0.7)
Percentile 75	20.578	3.542	0.817	0.062	83.5	34.7 (+2.6)	36.2 (+2.7)	27.2 (+0.3)	28.4 (+0.3)
Percentile 90	10.069	2.371	0.995	0.080	81.8	36.4 (+0.6)	37.9 (+0.6)	28.2 (0)	29.4 (0)
Percentile 95	7.432	2.044	1.064	0.091	79.8	38.3 (+0.8)	39.9 (+0.8)	29.3 (+0.3)	30.5 (+0.4)
Peatland model									
Average height	11.492	1.260	1.410	0.270	51.0	3.8 (+0.3)	98.3 (+8.0)	2.5 (+0.1)	65.0 (+2.8)
IQR	11.136	1.090	0.776	0.116	56.3	3.6 (+0.3)	92.3 (+8.7)	2.4 (0)	61.1 (-1.0)
Percentile 75	9.803	0.911	0.865	0.122	61.1	3.4 (+0.2)	87.0 (+6.3)	2.4 (-0.1)	60.9 (-1.8)
Percentile 90	4.229	0.931	0.703	0.218	31.9	4.5 (+0.3)	115.1 (+9.0)	2.9 (0)	75.4 (-1.0)
Percentile 95	3.573	0.897	0.503	0.190	23.7	4.7 (+0.8)	122.0 (+20.5)	3.0 (0)	78.8 (-1.0)

Comparison to increased (+) and decreased (-) model errors of linear regression with forced y-intercept in brackets.

SE: Standard error; IQR: interquartile range. Highest goodness-of-fit metrics per stratum coloured in grey.

Comparisons of goodness-of-fit statistics across lidar height metrics showed that average height was the best predictor of field-derived AGB for the Taiga Plains and upland/permafrost plateau forests (R^2 = 90% and 85%; RMSE = 27 Mg ha^{-1} and 34 Mg ha^{-1} respectively). For the remaining strata, model fits improved using the interquartile range as predictor variable within the Taiga Shield model (R^2 = 65%; RMSE = 11 Mg ha^{-1}), and the 75th height percentile within the peatland model (R^2 = 61%; RMSE = 3 Mg ha^{-1}).

Model performance improved when modelling AGB for all strata combined using the general AGB model (R^2 = 73% to 94%, RMSE = 19 Mg ha^{-1} to 24 Mg ha^{-1}, Bias = 13 Mg ha^{-1} to 15 Mg ha^{-1}) (Table 4.5). Highest correspondence to field-based AGB and lowest model errors were hereby achieved using the average height or the 75th height percentile as predictor variable (R^2 = 94%; RMSE = 19 Mg ha^{-1}; Bias =13 Mg ha^{-1}) (Figure 4.2).

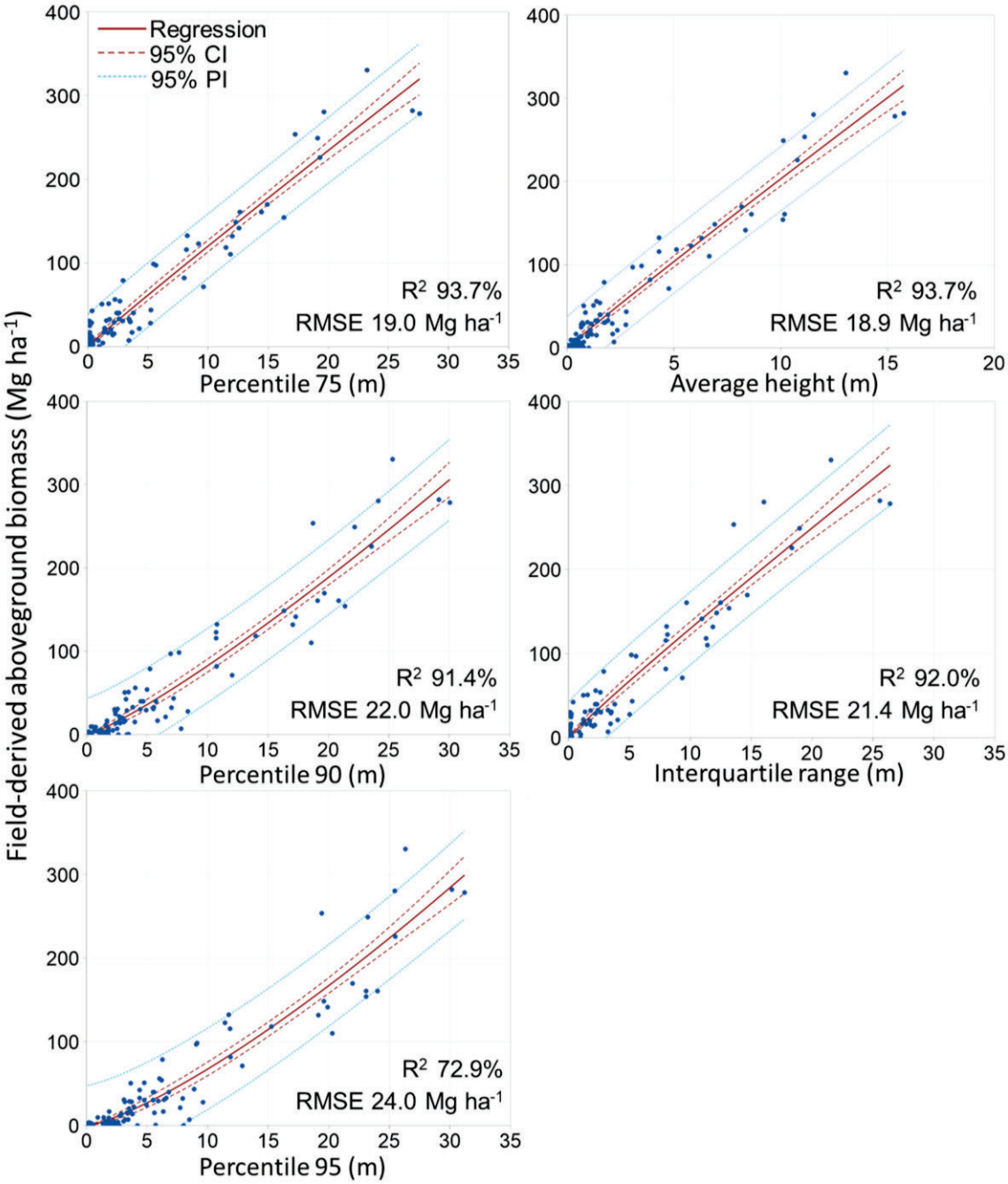

Figure 4.2. Field-derived aboveground biomass (AGB) related to lidar height metrics (m) for all strata combined using iterative nonlinear least squares regression via a power function illustrated within the 95th confidence interval (CI) and 95th prediction interval (PI).

Evaluating the performance of the general AGB models (developed per lidar height metric) within each stratum (Table 4.6) showed a mean reduction in explained model

variability by -2% and a mean increase in RMSE by 1 Mg ha^{-1}, while Bias remained stable in average at 0.3 Mg ha^{-1}. Magnitudes of decreased model performance varied per ecosystem type and lidar metric used. In the Taiga Plains and upland/permafrost plateau forests, the predictor average height produced highest model fits (R^2 = 90% and 84%; RMSE = 28 Mg ha^{-1} and 36 Mg ha^{-1} respectively). In the Taiga Shield, explained model variance was highest for the 90th height percentile (R^2 = 59%), while model errors were lowest for the average height (RMSE = 12 Mg ha^{-1}; Bias = 8 Mg ha^{-1}). In peatlands, the 75th height percentile explained the highest model variance (R^2 = 61%) and had lowest model errors (RMSE = 4.0 Mg ha^{-1}; Bias = 2.6 Mg ha^{-1}). However, relative to the measured mean, AGB model errors where high (RMSE% = 103; Bias% = 67).

Table 4.6. General AGB model fits per Titan lidar height metric evaluated for stratum-specific Taiga ecoregions and ecosystem types.

Lidar metric	R^2 (%)	RMSE (Mg ha^{-1})	%RMSE (%)	Bias (Mg ha^{-1})	Bias (%)
Taiga Plains					
Average height	89.7	27.7 (+0.3)	42.2 (+0.5)	17.7 (+0.1)	27.0 (+0.1)
IQR	88.6	29.3 (+0.6)	44.6 (+1.0)	18.4 (+0.3)	28.1 (+0.4)
Percentile 75	89.7	28.0 (+0.3)	42.6 (+0.5)	17.6 (+0.1)	26.8 (+0.2)
Percentile 90	86.9	29.5 (0)	45.0 (0)	19.8 (-0.4)	30.2 (-0.6)
Percentile 95	86.9	31.2 (+1.0)	47.6 (+1.5)	19.8 (+2.6)	30.2 (+3.9)
Taiga Shield					
Average height	57.9	12.3 (0)	72.0 (+0.1)	8.2 (-0.2)	48.0 (-1.0)
IQR	56.6	14.0 (+0.2)	82.2 (-1.1)	9.1 (-0.6)	53.4 (-3.3)
Percentile 75	55.8	13.6 (0)	79.7 (+0.2)	8.5 (-0.4)	50.1 (-2.1)
Percentile 90	59.4	12.4 (+2.1)	72.7 (+12.4)	8.2 (+2.1)	48.2 (+12.3)
Percentile 95	47.5	14.8 (+5.2)	87.1 (+30.4)	8.5 (+4.0)	49.7 (+23.7)
Upland/Permafrost plateau forest (including ecotones)					
Average height	84.1	35.9 (+0.7)	37.4 (+0.7)	25.6 (+0.6)	26.7 (+0.6)
IQR	82.5	37.4 (+1.1)	39.0 (+1.1)	28.0 (+0.5)	29.1 (+0.5)
Percentile 75	83.8	36.6 (+0.6)	38.1 (+0.6)	27.0 (+0.3)	28.1 (+0.3)
Percentile 90	81.6	38.3 (-1.3)	39.9 (-1.3)	28.0 (-0.5)	29.2 (-0.5)
Percentile 95	79.5	40.7 (-1.3)	42.3 (-1.3)	29.2 (0.4)	30.4 (+0.4)
Peatland					
Average height	47.5	7.1 (-0.8)	183.3 (-19.9)	5.0 (-0.7)	129.3 (-17.1)
IQR	57.0	4.2 (-0.4)	108.4 (-10.0)	2.6 (-0.2)	66.3 (-4.7)
Percentile 75	61.4	4.0 (-0.3)	102.5 (-7.1)	2.6 (-0.1)	66.6 (-3.4)
Percentile 90	32.5	6.8 (+3.6)	175.4 (+92.2)	3.9 (+2.3)	101.8 (+60.4)
Percentile 95	14.2	10.7 (+6.4)	278.0 (+165.6)	5.2 (+5.2)	135.2 (+134.2)

Comparison to increased (+) and decreased (-) model errors of linear regression with forced y-intercept in brackets.
IQR: Interquartile range. Highest goodness-of-fit metrics per stratum coloured in grey.

4.4.2. Lidar metric comparison across sensors

To identify the optimal lidar height metric candidates for predicting bi-temporal shrub-to-tree AGB, the second criteria (besides high goodness-of-fit statistics for each stratum) required negligible, calibratable systematic error when transferring the model trained for the Titan data to older ALTM 3100 data. To isolate sensor differences from signals

stemming from successional vegetation changes, 558 grid cells in late-successional upland forests were randomly selected and analysed. Here, differences in the mean canopy height were within ± 0.5m and differences in the standard deviation ranged from 0 to 0.4m for the retained lidar metrics. Differences in the first quartile were within ± 0.1m (except for the 95th height percentile and the interquartile range ± 0.5m) representative of short-stature vegetation found in the understory and in open upland sites. Evaluation of covariance between Titan and ALTM 3100 lidar height metrics in these late-successional upland sites showed lowest overall explained variance and highest deviations from a 1:1 linear relationship for the interquartile range and the 95th height percentile, which in addition to lowest goodness-of-fit statistics excluded them from subsequent bi-temporal shrub-to-tree AGB model development (Table 4.7).

Table 4.7. Covariances between corresponding multi-channel Titan (observed) and single channel ALTM 3100 (predicted) lidar height metrics.

Lidar metric	Calibration coefficient *c*	SE of calibration coefficient *c*	R^2
General AGB Model			
Average height	1.0149	0.0086	96.1
IQR	0.9405	0.0106	93.4
Percentile 75	0.9969	0.0079	96.6
Percentile 90	1.0200	0.0051	98.6
Percentile 95	1.0253	0.0046	98.9

Calibration coefficients *c* represent the slope of the linear relationship between observed and predicted lidar height metrics. These were used to correct the respective ALTM 3100 height grids for subsequent use in the bi-temporal shrub-to-tree AGB model (Equation 4.2).

SE: Standard error, IQR; interquartile range.

The lowest deviations across sensors were achieved for the 75th height percentile (difference in slope compared to 100% = -0.3%) (Table 4.7). However, correspondence between the Titan and ALTM 3100 75th height percentiles showed increased variance towards higher Titan values below 3 m (Figure 4.3). For vegetation heights below 5 m, lowest variances were achieved by the average height (Figure 4.3). The 1.5% difference in slope (relative to 100%) for the complete average height range is driven by increased variances for average heights above 10 m. Here, the 90th height percentile showed lower variance (Figure 4.3) resulting in the highest overall correspondence between sensors (R^2 = 99%) albeit deviations from a 1:1 slope by 2%. For further development of the bi-temporal shrub-to-tree AGB model, ALTM 3100 lidar metrics were calibrated using the slope (Table 4.7) as calibration coefficient (Equation 4.2).

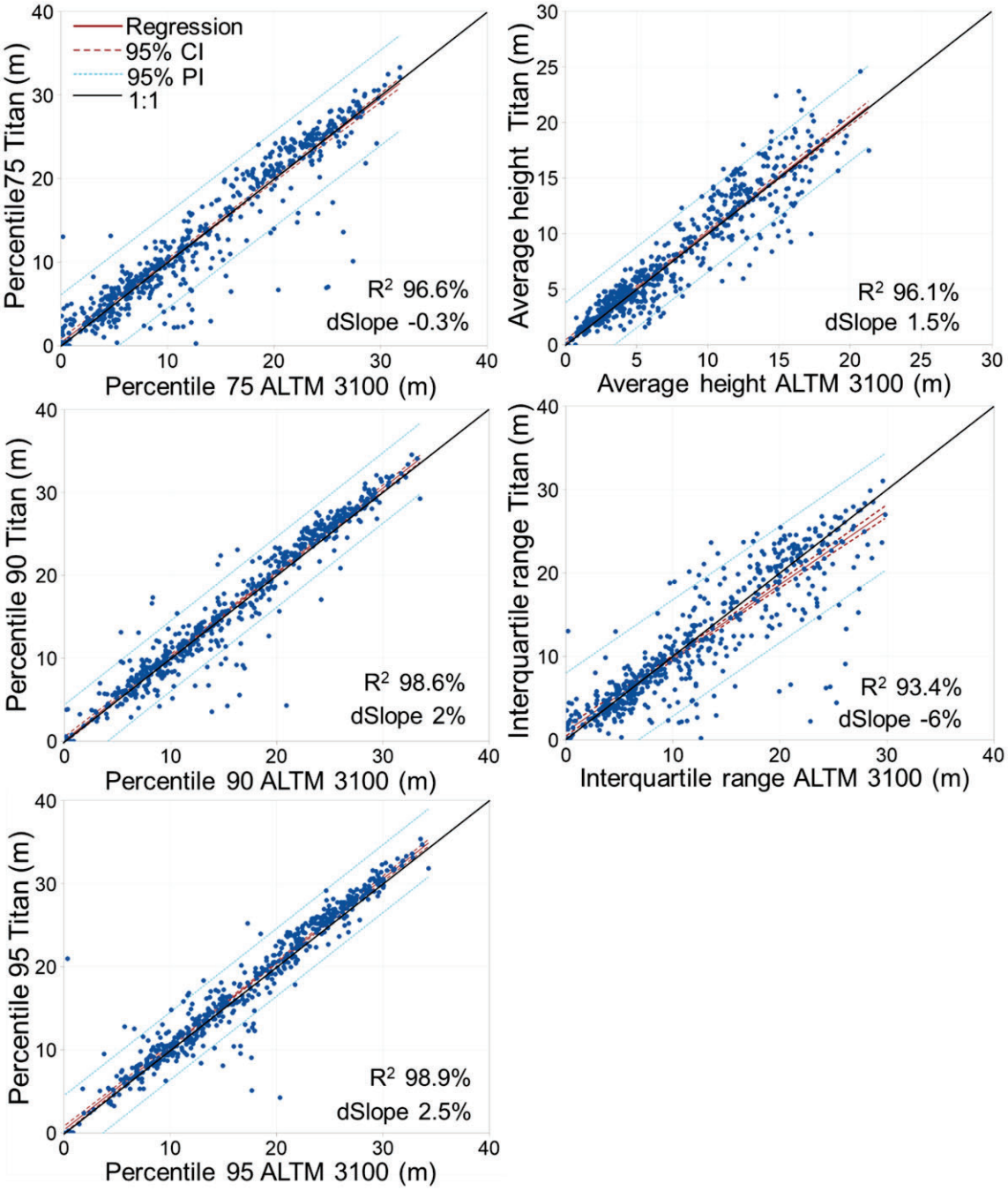

Figure 4.3. Covariance of Titan (observed) and ALTM 3100 (predicted) lidar height metrics to evaluate potential for systematic error during aboveground biomass model transfer based on 558 randomly selected grid cells in late successional upland forests. Slopes are represented as percent deviation of a 1:1 relationship (dSlope).

4.4.3. Lidar metric selection for bi-temporal shrub-to-tree aboveground biomass model development

For selecting the optimal lidar height metric as predictor of bi-temporal shrub-to-tree aboveground biomass, both goodness-of-fit statistics of modelled AGB (general AGB model per height metric) (Table 4.6) and covariance of corresponding lidar metrics between sensors (Table 4.7, Figure 4.3) revealed the average height, 75th height percentile, and 90th height percentile as the top three candidates. Using the 75th height percentile as predictor, highest goodness-of-fit statistics were achieved for all strata combined (same as average height) and for peatlands while overall deviation in 75th height percentiles between sensors was negligible. However, the increased variance between sensors for vegetation heights below 3 m (noted above) was critical because this threshold is representative of vegetation heights found dominantly in peatland complexes, potentially overestimating increases in peatland AGB between 2018, 2019 Titan and 2007, 2010 ALTM 3100 lidar surveys. In comparison, the average height metric demonstrated lower variances across sensors for short-stature vegetation and lowest model errors for all strata except peatlands when used as predictor within the general AGB model. In peatlands, model errors exceeded those of the 75th height percentile-based general AGB model, but these were likewise high at RMSE% >100 and Bias% >60. Increased variances in the upper height range across sensors suggested however, that the average height was not the single optimal predictor for the complete AGB range. For upper vegetation heights, the 90th height percentile showed lower variance between sensors and 90th height percentile-based general AGB model results achieved high goodness-of-fit statistics in uplands/permafrost plateaus (R^2 = 82%; RMSE = 38 Mg ha^{-1}; Bias = 28 Mg ha^{-1}) (Table 4.6). This indicated that the optimal lidar metric for modelling bi-temporal shrub-to-tree AGB was a function of the respective AGB

range, representative of differences in vegetation structure and canopy heights. Calibration of ALTM 3100 lidar metrics (Equation 4.2) was therefore necessary to further evaluate variances of modelled AGB (between sensors) compared for the retained lidar metrics for certain AGB ranges. Corresponding to variances in lidar height metrics across sensors in late-successional upland sites, analysis of general Titan AGB and calibrated ALTM 3100 AGB across the complete study region emphasized lower variance below 100 Mg ha^{-1} when using average height as predictor, and above 100 Mg ha^{-1} when using the 90^{th} percentile (Figure 4.4).

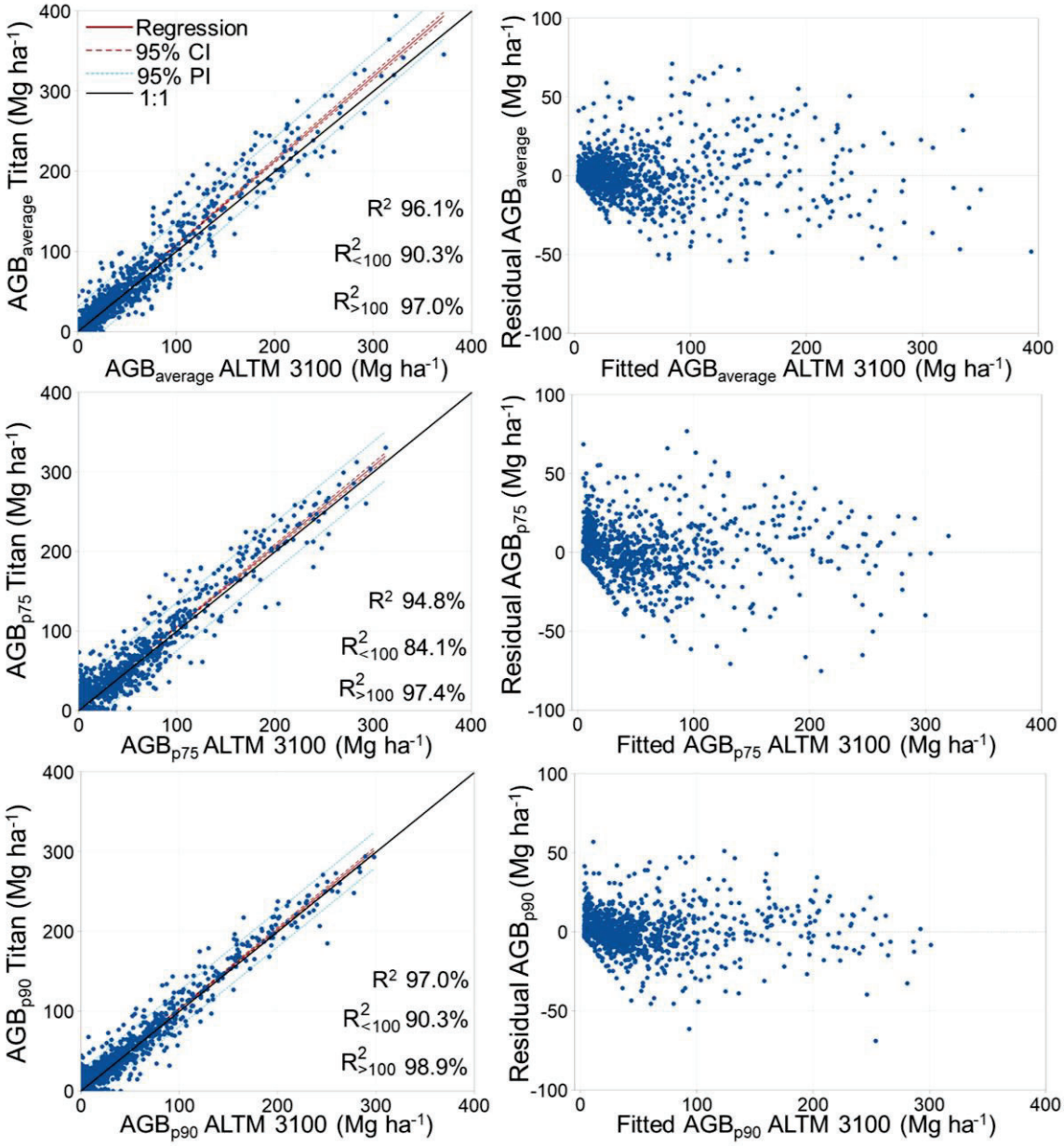

Figure 4.4. Covariance of Titan (observed) and ALTM 3100 (predicted) aboveground biomass (AGB) to evaluate the optimal lidar height metric as predictor of bi-temporal shrub-to-tree AGB across different ecozones, ecosystem types, and ALTM sensors based on 1381 randomly selected grid cells. Residuals of modelled AGB (ALTM 3100) per lidar height metric (average height (average), 75th and 90th height percentile (p75 and p90)) are presented on the right column.

The final bi-temporal shrub-to-tree AGB model combined the average height-based general AGB model and the 90th height percentile-based general AGB model within a weighted

approach as a function of modelled AGB (average height-based general AGB model). Final AGB per grid cell was then derived as (Equation 4.3):

$$AGB_{(Titan;\ calibrated\ ALTM\ 3100)} = x * AGB_{average\ height} + y * AGB_{90th\ height\ percentile} \quad (4.3)$$

whereby x=100%; y=0% for AGB ≤ 75 Mg ha^{-1}, and x=0%; y=100% for AGB ≥125 Mg ha^{-1}. To avoid artifacts at the 100 Mg ha^{-1} threshold, a sliding scale was applied between 75 Mg ha^{-1} and 125 Mg ha^{-1}, which decreased successively for increasing average height based AGB (x, Equation 4.3) and inversely increased successively for increasing 90th height percentile based AGB (y, Equation 4.3) using a step size of 2% for each 1 Mg ha^{-1}.

4.4.4. Bi-temporal shrub-to-tree aboveground biomass model evaluation

To evaluate the bi-temporal shrub-to-tree AGB model, correspondence between modelled (Titan) and measured AGB as well as model error were analysed and compared to the general Titan AGB models based on the average height and the 90th height percentile. Here, goodness-of-fit statistics were equal to average height-based model fits for the Taiga Shield and peatland strata. This was because maximum AGB values remained below 75 Mg ha^{-1} (Table 4.8). For the Taiga Plains and upland/permafrost plateau strata, model fits improved compared to the 90th height percentile-based model and decreased compared to the average height-based model (R^2 = 89% and 83%; RMSE = 29 Mg ha^{-1}and 37 Mg ha^{-1} respectively). Across all strata, reduced correspondence was negligible at -1.5% (R^2 = 92%) in comparison to the average height-based model. Increases in RMSE% and Bias% remained low at 4% and 2% respectively (RMSE = 21 Mg ha^{-1}; Bias = 14 Mg ha^{-1}) (Table 4.8).

Table 4.8. Final bi-temporal shrub-to-tree AGB model evaluated for all strata combined and for stratum-specific Taiga ecoregions and ecosystem types.

	R^2 (%)	RMSE (Mg ha^{-1})	%RMSE (%)	Bias (Mg ha^{-1})	%Bias (%)
All strata					
	92.2	21.03	42.2	13.7	27.5
Taiga Plains					
	89.0	28.6	43.6	18.6	28.3
Taiga Shield*					
	57.9	12.3	72.0	8.2	48.0
Upland/Permafrost plateau forest (including ecotones)					
	82.7	37.3	38.9	27.0	28.1
Peatland*					
	47.5	7.1	183.3	5.0	129.3

AGB was derived combining the modelled Titan average height-based AGB and 90th height percentile-based AGB within a weighted approach as a function of AGB (Equation 4.3).

*Same as average height based general AGB model per respective stratum (Table 4.6)

4.5. Discussion

The airborne lidar-based AGB models presented here are the first of their kind that were developed across a range of vegetation structures at varying degrees of vertical and horizontal continuity for the northwestern boreal underlain by sporadic to discontinuous permafrost. To address AGB changes in rapidly changing ecosystems such as forest to peatland ecotones, the final bi-temporal shrub-to-tree AGB model had to accommodate conditions of variable vegetation heights, and understory to overstory canopy covers. As such, model errors were expected to be higher in this region compared to models developed for commercial forests with continuous tall-stature tree canopies. However, albeit at the upper limit, model errors were within the range of errors reported in other studies, while correspondence of lidar-based and field-based AGB was often improved. In boreal Canada for example, Margolis et al. (2015) reported model errors ranging from 30 Mg ha^{-1} to 33 Mg ha^{-1} (RMSE) and model correspondence from 50% to 65% (R^2) for airborne lidar-based

AGB in managed upland mixed wood, conifer, and hardwood stands. Their model fits improved for an ecoregion specific model for the central Canadian Shield for conifer stands (R^2 = 80%; RMSE = 22 Mg ha^{-1}). However, for mixed wood forests in western Canada, model error increased to 35 Mg ha^{-1} (Margolis et al., 2015). These results are comparable to our best-fitting stratum specific and general AGB models for the Taiga Shield ecozone (R^2 = 65% and 58%; RMSE = 11 Mg ha^{-1} and 12 Mg ha^{-1}) and unmanaged upland/permafrost plateau forests distributed across the complete study region (R^2 = 85% and 84%; RMSE = 34 Mg ha^{-1} and 36 Mg ha^{-1}) (Table 4.5). Model fits based on the final bi-temporal shrub-to-tree AGB model were also within the range of Margolis et al. (2015) (R^2 = 58% and 83%; RMSE = 12 Mg ha^{-1} and 37 Mg ha^{-1} for the Taiga Shield and upland/permafrost plateau forests respectively) (Table 4.8). For managed forest stands in the eastern Canadian boreal, Luther et al. (2019) reported validated airborne lidar-based AGB regression accuracies of 83% (R^2) and 24 Mg ha^{-1} (RMSE). The RMSE% differed from their measured mean by 18%, which is ~half of the RMSE% derived in our study when applying the final bi-temporal shrub-to-tree AGB model in unmanaged upland/permafrost plateau forests (Table 4.8). However, their field-based mean AGB was 1.3 times greater compared to our study and understory vegetation (<2m) was not included in their modelling approach. AGB model accuracies could not be compared in Canadian peatland ecosystems due to a lack of comparable studies. Reported model errors of treed wetland AGB across all of Canada (RMSE = 22.2 Mg ha^{-1}) in Margolis et al. (2015) for example, were at the upper limit of our field-based AGB (21.8 Mg ha^{-1}, Table 4.3). However, Räsänen et al. (2020) derived between 45% to 53% explained model variabilities for deciduous shrubs within a fen peatland in northern Finland using multi-source input

data within random forest regression. The average height-based stratum specific and general AGB models as well as the final bi-temporal shrub-to-tree AGB model presented in our study were at the upper end of the reported range in peatlands (R^2 = 51% and 48% respectively) (Table 4.5, 4.6, and 4.8).

Overall, AGB model accuracies were higher in the Taiga Plains and in upland/permafrost plateau forests compared to the Taiga Shield and peatlands using either stratum-specific models (Table 4.5) or a generalized AGB model (Table 4.6, 4.8) independent of the lidar metric used as predictor. These strata are characteristic of short-stature plant dominance and sparse to absent tree cover and as such are closer to the noise level inherent in airborne lidar data. This is because plant canopies close to the ground surface can often not be accurately positioned in height or distinguished from ground points. Sparse, discontinuous vegetation cover has a higher chance of remaining undetected between single laser scan lines. This is increased where lidar campaigns are flown as single strips across the landscape missing additional lidar returns from side overlaps and resulting overall in lower point densities per m^2. In addition, the decreased travel distance of laser pulses through a short-stature plant canopy in comparison to a tall-stature canopy reduces the possibility of pulse reflections from plant material at varying heights. This reduces the range of vertical height distributions and lidar return densities, with fewer multiple returns (Hopkinson et al., 2005). Differences between lidar height metrics are therefore less pronounced, increasing the uncertainty of height-based lidar metrics in shorter vegetation (Hopkinson et al., 2005).

The choice of the optimal lidar height metric to be used as predictor within the final bi-temporal shrub-to-tree AGB model depended equally on goodness-of-fit statistics and

minimal, calibratable offsets between sensors of different lidar point cloud characteristics (point density and canopy penetration). A previous study by Lim et al. (2008) analysed the effect of lidar point density on canopy heights. The authors suggested that, analogous to statistical sampling, an increase in point density should not lead to a different canopy height sampling distribution because both (low and high return densities) represent a sample of the complete population (canopy). However, a comparison of vertical height profiles between the Titan and a Gemini ALTM (similar to the ALTM 3100) in upland forests by Hopkinson et al. (2016b) showed that the Titan sensor preferentially sampled upper canopy regions due to reflections from 532 nm and 1550 nm channels. Channel-dependent differences in the canopy height sampling distribution were most pronounced between the 25^{th} and 75^{th} height percentiles and decreased for percentiles > 75%. For the upper percentiles (>90%) differences in lidar height profiles were also lowest between the three Titan channels (Hopkinson et al., 2016b). Here, the use of upper percentiles for deriving AGB tends to be relatively stable within the vertical noise and in the case of multi-channel lidar, deeper than average returns from the canopy at 532 nm and 1550 nm tend to balance higher than average returns from the 1064nm channel (Hopkinson et al., 2016b). This emphasized the use of the 90^{th} height percentile (calibrated for the ALTM 3100 data) for higher AGB ranges within the bi-temporal shrub-to-tree AGB model. For lower AGB ranges, our results suggest that differences across sensors reduced using an average as opposed to a percentile approach. The average height represents the central tendency (analogous to centre of mass) of a vertical profile from the ground to the top of canopy, equally weighing all datapoints in the distribution. As such, this metric is equally sensitive to the tails at the low (ground) or high (top of canopy) end of the overall distribution and is

therefore more influenced by open vs. closed canopy conditions. The implicit integration of vegetation height and cover attributes at the grid cell level made this variable a robust predictor across variable vegetation structures and canopy continuity, and therefore an optimal predictor for stratum-specific AGB models and the bi-temporal shrub-to-tree AGB model. The height calibration of the ALTM 3100 dataset (Equation 4.2) however was necessary as increased heights in the multi-channel 2018, 2019 Titan dataset compared to the single channel 2007, 2010 ALTM 3100 dataset could overestimate vegetation growth in an AGB change detection analysis.

These results will be relevant in future studies aiming to compare different generation lidar systems and for the validation of spaceborne AGB change products. The ALTM 3100 sensor was state-of-the-art technology circa 2005. Therefore, wide area coverage is available for many parts of Canada, USA, Europe, etc. which contributed to the use of this sensor for many baseline vegetation studies. Since circa 2010, there has been a proliferation of new lidar sensor technologies, including the use of multiple single and variable wavelength lidar systems, which produce high pulse repetition frequencies, high sample point densities, and multi-wavelength capability, especially since 2014. Therefore, the need to compare and calibrate between lidar systems for vegetation change from older to newer technologies to understand and quantify change is becoming increasingly important.

Lastly, the bi-temporal shrub-to-tree AGB model was applied using a weighted approach of the gridded Titan and calibrated ALTM 3100 average height and 90^{th} height percentile-based AGB models. This approach was chosen over the use of stratum-specific AGB models. Model performance increased when the model was developed for the

respective dominant vegetation structure and canopy openness, ranging from +1% (-1.6 Mg ha^{-1}) in the Taiga Plains to +7% (-1.2 Mg ha^{-1}) in the Taiga Shield and from +2% (-3.8 Mg ha^{-1}) in upland/permafrost plateau forests to +14% (-3.7 Mg ha^{-1}) in peatlands (reported as difference in R^2 (RMSE) for the best fitting model per stratum). However, the low n in stratum-specific models (Table 4.3) reduced confidence in model coefficients, which is reflected in larger model coefficient standard errors in comparison to the general AGB models (Table 4.5). In addition, for application of stratum-specific AGB models, high confidence is required over which grid cells certain models are applied, which requires the use of an external landcover classification. The total error of modelled AGB will then be the combination of errors of (1) the respective AGB model and (2) the landcover classification. Overall accuracies of an external landcover classification in this region range from 73% to 94% (Bourgeau-Chavez et al., 2019) depending on the landcover type, while western parts of our study area were not included. In addition, classification accuracies are often unknown for specific areas where validation data were not available (e.g. Chasmer et al., 2020, Bourgeau-Chavez et al., 2022) or were developed at an earlier/later date resulting in further discrepancies. The compound errors of a combined use of stratum specific AGB models and a static landcover classification are therefore expected to exceed the error of a generalized AGB model. Edge effects at class boundaries will especially be minimized using the bi-temporal shrub-to-tree AGB model enabling investigation of ecotonal changes, which are changing most rapidly with climate change (Chasmer and Hopkinson, 2017).

4.6. Conclusion

This study developed and examined the accuracy of airborne lidar-based AGB models across a range of vegetation structures at varying degrees of vertical and horizontal

continuity to advance timely research into forest to peatland ecotonal changes. Ecosystem types included productive upland forests, stunted forests on permafrost plateaus, open and treed peatlands, and forest to peatland ecotones within the southern Taiga of the Northwest Territories. The objectives were to test and evaluate (1) airborne lidar height and cover metrics, and (2) model transferability between a lower density single channel (ALTM 3100) and a higher density multi-channel (Titan) lidar sensor with the aim to develop a single bi-temporal shrub-to-tree AGB model to be used across all examined strata without the need for landcover classifications. AGB models were developed using lidar height and cover return metrics (refined in a pre-selection process) and coincident field-based AGB within single variable nonlinear least squares regression. Leave-one-out cross validated model goodness-of-fits were high in the Taiga Plains and forested uplands/permafrost plateaus, and moderate in the Taiga Shield and peatlands. AGB model errors and explained model variance were within the range reported in other studies. Model accuracies and confidence in model coefficients improved when predicting AGB across all strata within a general AGB model using either the average height or the 75th height percentile of all lidar returns as predictors. However, tests for covariance between lidar height metrics of the Titan and ALTM 3100 sensors showed (a) high explained variance, (b) minimal correctable systematic error, and (c) negligible residual error at the low height range (where AGB changes are expected to be most pronounced) for the average height and 90th height percentile. Both lidar height metrics were calibrated for offsets between sensors (ALTM 3100 dataset) and used as general predictor of AGB across the study region. Comparisons of modelled AGB between sensors per metric showed lower variances in modelled AGB

using average height (below 100 Mg ha^{-1}) and the 90^{th} height percentile (above 100 Mg ha^{-1}) as predictor variable.

The final bi-temporal shrub-to-tree AGB model was therefore developed using a weighted approach as a function of modelled AGB. Evaluation of the bi-temporal shrub-to-tree AGB model showed moderate model fits in the Taiga Shield and peatlands and high goodness-of-fit statistics in the Taiga Plains and upland/permafrost plateau forests. Model performance reduced compared to stratum-specific AGB models, which were developed for the respective dominant vegetation structure and canopy openness. However, lower confidence of model coefficients of stratum-specific AGB models and added uncertainties of an external land cover classification are expected to exceed uncertainties of the bi-temporal shrub-to-tree AGB model especially at rapidly changing forest to peatland ecotones. The ability to transfer the bi-temporal shrub-to-tree AGB model between sensors enables future research of spatially explicit changes of AGB and provides an example for future studies aiming to compare AGB products amongst different generations of lidar systems. The results of this study are therefore important for research of the cumulative effects of climate change on boreal ecosystems in the Taiga of western Canada, identified as a critical area of uncertainty (IPCC 2023). Lastly, the results could aid in the consistent validation of spaceborne AGB and quantification of wildland fire fuel dynamics with further potential to improve accuracy of reported carbon stocks, broadening of the scope in carbon reporting obligations to unmanaged forest areas, and better understanding and predicting fire behaviour and carbon losses/pollution associated with wildland fire in these under-represented yet critical ecosystems.

4.7. Funding

This project was funded in part by NSERC Discovery Grants to L. Chasmer [Grant number: (2017-04492)] and C. Hopkinson [Grant number: (2017-04362)], a University of Lethbridge start up grant to L. Chasmer, the NSERC Canada Wildfire Network (Chasmer) [Grant number: RES0049086], a CFI grant for field survey equipment to C. Hopkinson [Grant number: (32436)], and a grant to purchase the Titan lidar system through Western Economic Diversification Canada [Grant number: (000015316)].

4.8. Acknowledgments

We would like to acknowledge the help of various field assistants: Emily Jones, Kailyn Nelson, Dr. Craig Mahoney, Rachelle Shearing, Jesse Aspinall, Garrett Isiah, and Lavinia Haase and field assistance from the Government of the Northwest Territories (Tyler Rea, Ben Paulsen), the Dehcho Guardian Program, and the Dehcho Collaborative on Permafrost. Lidar surveys and data pre-processing were conducted by Maxim Okhrimenko. We would also like to thank Dr. William Quinton for useful early discussion and the Liidlii Kue First Nation and Dr. William Quinton for research support within the Scotty Creek Research Station, NWT.

4.9. References

Auestad, I., Rydgren, K., Halvorsen, R., Avdem, I., Berge, R., Bollingberg, I., & Lima, O. (2023). Use climatic space-for-time substitutions with care: Not only climate, but also local environment affect performance of the key forest species bilberry along elevation gradient. *Ecology and Evolution*, *13*(8), e10401. https://doi.org/10.1002/ece3.10401.

Bonan, G. (2015). *Ecological Climatology: Concepts and Applications* (3rd ed.). Cambridge: Cambridge University Press. https://doi.org/10.1017/CBO9781107339200.

Bourgeau-Chavez, L., Graham, J. A., Endres, S., French, N. H. F., Battaglia, M., Hansen, D., & Tanzer, D. (2019). Arctic-Boreal Vulnerability Experiment (ABoVE): Ecosystem Map, Great Slave Lake Area, Northwest Territories, Canada, 1997-2011

(Version 1) [ESRI Shapefile,GTiff], 181.195416 MB. https://doi.org/10.3334/ORNLDAAC/1695.

Bourgeau-Chavez, L., Graham, J. A., Vander Bilt, D. J. L., & Battaglia, M. J. (2022). Assessing the broadscale effects of wildfire under extreme drought conditions to boreal peatlands. *Frontiers in Forests and Global Change*, *5*, 965605. https://doi.org/10.3389/ffgc.2022.965605.

Carpino, O., Berg, A. A., Quinton, W., & Adams, J. (2018). Climate change and permafrost thaw-induced boreal forest loss in northwestern Canada. *Environmental Research Letters*, *13*(8), 084018. https://doi.org/10.1088/1748-9326/aad74e.

Carpino, O., Haynes, K., Connon, R., Craig, J., Devoie, É., & Quinton, W. (2021). Long-term climate-influenced land cover change in discontinuous permafrost peatland complexes. *Hydrology and Earth System Sciences*, *25*(6), 3301–3317. https://doi.org/10.5194/hess-25-3301-2021.

Castilla, G., Hall, R. J., Skakun, R., Filiatrault, M., Beaudoin, A., Gartrell, M., et al. (2022). *The Multisource Vegetation Inventory (MVI): A Satellite-Based Forest Inventory for the Northwest Territories Taiga Plains* (p. 1108). Retrieved from https://www.mdpi.com/2072-4292/14/5/1108.

Chapin, F. S., Woodwell, G. M., Randerson, J. T., Rastetter, E. B., Lovett, G. M., Baldocchi, D. D., et al. (2006). Reconciling Carbon-cycle Concepts, Terminology, and Methods. *Ecosystems*, *9*(7), 1041–1050. https://doi.org/10.1007/s10021-005-0105-7.

Chasmer, L., & Hopkinson, C. (2017). Threshold loss of discontinuous permafrost and landscape evolution. *Global Change Biology*, *23*(7), 2672–2686. https://doi.org/10.1111/gcb.13537.

Chasmer, L., Hopkinson, C., & Treitz, P. (2006). Investigating laser pulse penetration through a conifer canopy by integrating airborne and terrestrial lidar. *Canadian Journal of Remote Sensing*, *32*(2), 116–125. https://doi.org/10.5589/m06-011.

Chasmer, L., Kljun, N., Barr, A., Black, A., Hopkinson, C., McCaughey, H., & Treitz, P. (2008). Influences of vegetation structure and elevation on CO_2 uptake in a mature jack pine forest in Saskatchewan, Canada. *Canadian Journal of Forest Research*, *38*(11), 2746–2761. https://doi.org/10.1139/X08-121.

Chasmer, L., Quinton, W. L., Hopkinson, C., Petrone, R., & Whittington, P. (2011). Vegetation Canopy and Radiation Controls on Permafrost Plateau Evolution within the Discontinuous Permafrost Zone, Northwest Territories, Canada: Vegetation and Radiation Controls on Permafrost Plateau Evolution. *Permafrost and Periglacial Processes*, n/a-n/a. https://doi.org/10.1002/ppp.724

Connon, R., Quinton, W., Craig, J., & Hayashi, M. (2014). Changing hydrologic connectivity due to permafrost thaw in the lower Liard River valley, NWT, Canada. *Hydrological Processes*, *28*(14), 4163–4178. https://doi.org/10.1002/hyp.10206.

Connon, R., Quinton, W., Craig, J. R., Hanisch, J., & Sonnentag, O. (2015). The hydrology of interconnected bog complexes in discontinuous permafrost terrains. *Hydrological Processes*, *29*(18), 3831–3847. https://doi.org/10.1002/hyp.10604.

Coops, N. C., Tompalski, P., Goodbody, T. R. H., Queinnec, M., Luther, J. E., Bolton, D. K., et al. (2021). Modelling lidar-derived estimates of forest attributes over space and time: A review of approaches and future trends. *Remote Sensing of Environment*, *260*, 112477. https://doi.org/10.1016/j.rse.2021.112477.

Duncanson, L., Armston, J., Disney, M., Avitabile, V., Barbier, N., Calders, K., et al. (2019). The Importance of Consistent Global Forest Aboveground Biomass Product Validation. *Surveys in Geophysics*, *40*(4), 979–999. https://doi.org/10.1007/s10712-019-09538-8.

Ecosystem Classification Group (Ed.). (2008). *Ecological regions of the Northwest Territories - Taiga Shield*. Yellowknife, NT, Canada: Department of Environment and Natural Resources, Government of the Northwest Territories.

Ecosystem Classification Group. (2009). *Ecological regions of the Northwest Territories - Taiga Plains* (Revised). Yellowknife, NT, Canada: Department of Environment and Natural Resources, Government of the Northwest Territories.

Enayetullah, H., Chasmer, L., Hopkinson, C., Thompson, D., & Cobbaert, D. (2023). Examining Drivers of Post-Fire Seismic Line Ecotone Regeneration in a Boreal Peatland Environment. *Forests*, *14*(10), 1979. https://doi.org/10.3390/f14101979.

Flade, L., Hopkinson, C., & Chasmer, L. (2020). Allometric Equations for Shrub and Short-Stature Tree Aboveground Biomass within Boreal Ecosystems of Northwestern Canada. *Forests*, *11*(11), 1207. https://doi.org/10.3390/f11111207.

Flannigan, M. D., Logan, K. A., Amiro, B. D., Skinner, W. R., & Stocks, B. J. (2005). Future Area Burned in Canada. *Climatic Change*, *72*(1–2), 1–16. https://doi.org/10.1007/s10584-005-5935-y.

Gauthier, S., Bernier, P., Burton, P. J., Edwards, J., Isaac, K., Isabel, N., et al. (2014). Climate change vulnerability and adaptation in the managed Canadian boreal forest. *Environmental Reviews*, *22*(3), 256–285. https://doi.org/10.1139/er-2013-0064.

GCOS. (2010). *Implementation plan for the global observing system for climate change in support of the UNFCCC* (GCOS-138 No. WMO/TD-No. 1523) (p. 186). Geneva, Switzerland: WMO, UNESCO, UNEP, ICSU. Retrieved from https://library.wmo.int/records/item/58703-implementation-plan-for-the-global-observing-system-for-climate-in-support-of-the-unfccc.

Gillis, M. D., Omule, A. Y., & Brierley, T. (2005). Monitoring Canada's forests: The National Forest Inventory. *The Forestry Chronicle*, *81*(2), 214–221. https://doi.org/10.5558/tfc81214-2.

Herold, M., Carter, S., Avitabile, V., Espejo, A. B., Jonckheere, I., Lucas, R., et al. (2019). The Role and Need for Space-Based Forest Biomass-Related Measurements in Environmental Management and Policy. *Surveys in Geophysics*, *40*(4), 757–778. https://doi.org/10.1007/s10712-019-09510-6.

Hopkinson, C. (2007). The influence of flying altitude, beam divergence, and pulse repetition frequency on laser pulse return intensity and canopy frequency distribution. *Canadian Journal of Remote Sensing*, *33*(4), 312–324. https://doi.org/10.5589/m07-029.

Hopkinson, C., Chasmer, L., Young-Pow, C., & Treitz, P. (2004). Assessing forest metrics with a ground-based scanning lidar. *Canadian Journal of Forest Research*, *34*(3), 573–583. https://doi.org/10.1139/x03-225.

Hopkinson, C., Chasmer, L., Lim, K., Treitz, P., & Creed, I. (2006). Towards a universal lidar canopy height indicator. *Canadian Journal of Remote Sensing*, *32*(2), 139–152. https://doi.org/10.5589/m06-006.

Hopkinson, C., Chasmer, L., & Hall, R. (2008). The uncertainty in conifer plantation growth prediction from multi-temporal lidar datasets. *Remote Sensing of Environment*, *112*(3), 1168–1180. https://doi.org/10.1016/j.rse.2007.07.020.

Hopkinson, C., Chasmer, L., Barr, A. G., Kljun, N., Black, T. A., & McCaughey, J. H. (2016). Monitoring boreal forest biomass and carbon storage change by integrating airborne laser scanning, biometry and eddy covariance data. *Remote Sensing of Environment*, *181*, 82–95. https://doi.org/10.1016/j.rse.2016.04.010.

Hopkinson, C., Chasmer, L., Gynan, C., Mahoney, C., & Sitar, M. (2016). Multisensor and Multispectral LiDAR Characterization and Classification of a Forest Environment. *Canadian Journal of Remote Sensing*, *42*(5), 501–520. https://doi.org/10.1080/07038992.2016.1196584.

IPCC. (2023). *IPCC, 2023: Climate Change 2023: Synthesis Report. Contribution of Working Groups I, II and III to the Sixth Assessment Report of the Intergovernmental Panel on Climate Change [Core Writing Team, H. Lee and J. Romero (eds.)]. IPCC, Geneva, Switzerland.* (First) (p. 184). Geneva, Switzerland: Intergovernmental Panel on Climate Change (IPCC). https://doi.org/10.59327/IPCC/AR6-9789291691647.

Kasischke, E. S., & Turetsky, M. R. (2006). Recent changes in the fire regime across the North American boreal region—Spatial and temporal patterns of burning across Canada and Alaska. *Geophysical Research Letters*, *33*(9), 2006GL025677. https://doi.org/10.1029/2006GL025677.

Kristensen, T., Næsset, E., Ohlson, M., Bolstad, P. V., & Kolka, R. (2015). Mapping Above- and Below-Ground Carbon Pools in Boreal Forests: The Case for Airborne Lidar. *PLOS ONE*, *10*(10), e0138450. https://doi.org/10.1371/journal.pone.0138450.

Kurz, W. A., Shaw, C. H., Boisvenue, C., Stinson, G., Metsaranta, J., Leckie, D., et al. (2013). Carbon in Canada's boreal forest — A synthesis. *Environmental Reviews*, *21*(4), 260–292. https://doi.org/10.1139/er-2013-0041.

Lambert, M.-C., Ung, C.-H., & Raulier, F. (2005). Canadian national tree aboveground biomass equations. *Canadian Journal of Forest Research*, *35*(8), 1996–2018. https://doi.org/10.1139/x05-112.

Lim, K., Hopkinson, C., & Treitz, P. (2008). Examining the effects of sampling point densities on laser canopy height and density metrics. *The Forestry Chronicle*, *84*(6), 876–885. https://doi.org/10.5558/tfc84876-6.

Luther, J. E., Fournier, R. A., Van Lier, O. R., & Bujold, M. (2019). Extending ALS-Based Mapping of Forest Attributes with Medium Resolution Satellite and Environmental Data. *Remote Sensing*, *11*(9), 1092. https://doi.org/10.3390/rs11091092.

Mahoney, C., Hall, R., Hopkinson, C., Filiatrault, M., Beaudoin, A., & Chen, Q. (2018). A Forest Attribute Mapping Framework: A Pilot Study in a Northern Boreal Forest, Northwest Territories, Canada. *Remote Sensing*, *10*(9), 1338. https://doi.org/10.3390/rs10091338.

Margolis, H. A., Nelson, R. F., Montesano, P. M., Beaudoin, A., Sun, G., Andersen, H.-E., & Wulder, M. A. (2015). Combining satellite lidar, airborne lidar, and ground plots to estimate the amount and distribution of aboveground biomass in the boreal forest of North America. *Canadian Journal of Forest Research*, *45*(7), 838–855. https://doi.org/10.1139/cjfr-2015-0006.

Matasci, G., Hermosilla, T., Wulder, M. A., White, J. C., Coops, N. C., Hobart, G. W., & Zald, H. S. J. (2018). Large-area mapping of Canadian boreal forest cover, height, biomass and other structural attributes using Landsat composites and lidar plots. *Remote Sensing of Environment*, *209*, 90–106. https://doi.org/10.1016/j.rse.2017.12.020.

Næsset, E. (2009). Effects of different sensors, flying altitudes, and pulse repetition frequencies on forest canopy metrics and biophysical stand properties derived from small-footprint airborne laser data. *Remote Sensing of Environment*, *113*(1), 148–159. https://doi.org/10.1016/j.rse.2008.09.001.

Næsset, E., & Gobakken, T. (2008). Estimation of above- and below-ground biomass across regions of the boreal forest zone using airborne laser. *Remote Sensing of Environment*, *112*(6), 3079–3090. https://doi.org/10.1016/j.rse.2008.03.004.

Nilsson, M.-C., & Wardle, D. A. (2005). Understory vegetation as a forest ecosystem driver: evidence from the northern Swedish boreal forest. *Frontiers in Ecology and the Environment*, *3*(8), 421–428. https://doi.org/10.1890/1540-9295(2005)003[0421:UVAAFE]2.0.CO;2.

Pan, Y., Birdsey, R. A., Fang, J., Houghton, R., Kauppi, P. E., Kurz, W. A., et al. (2011). A Large and Persistent Carbon Sink in the World's Forests. *Science*, *333*(6045), 988–993. https://doi.org/10.1126/science.1201609.

Piñeiro, G., Perelman, S., Guerschman, J. P., & Paruelo, J. M. (2008). How to evaluate models: Observed vs. predicted or predicted vs. observed? *Ecological Modelling*, *216*(3–4), 316–322. https://doi.org/10.1016/j.ecolmodel.2008.05.006.

Poley, L. G., Laskin, D. N., & McDermid, G. J. (2020). Quantifying Aboveground Biomass of Shrubs Using Spectral and Structural Metrics Derived from UAS Imagery. *Remote Sensing*, *12*(14), 2199. https://doi.org/10.3390/rs12142199

Popescu, S. C., Wynne, R. H., & Nelson, R. F. (2002). Estimating plot-level tree heights with lidar: local filtering with a canopy-height based variable window size. *Computers and Electronics in Agriculture*, *37*(1–3), 71–95. https://doi.org/10.1016/S0168-1699(02)00121-7.

Price, D. T., Alfaro, R. I., Brown, K. J., Flannigan, M. D., Fleming, R. A., Hogg, E. H., et al. (2013). Anticipating the consequences of climate change for Canada's boreal forest ecosystems. *Environmental Reviews*, *21*(4), 322–365. https://doi.org/10.1139/er-2013-0042.

Quinton, W., Berg, A., Braverman, M., Carpino, O., Chasmer, L., Connon, R., et al. (2019). A synthesis of three decades of hydrological research at Scotty Creek, NWT, Canada. *Hydrology and Earth System Sciences*, *23*(4), 2015–2039. https://doi.org/10.5194/hess-23-2015-2019.

Räsänen, A., Juutinen, S., Kalacska, M., Aurela, M., Heikkinen, P., Mäenpää, K., et al. (2020). Peatland leaf-area index and biomass estimation with ultra-high resolution remote sensing. *GIScience & Remote Sensing*, *57*(7), 943–964. https://doi.org/10.1080/15481603.2020.1829377.

Riggins, J. J., Tullis, J. A., & Stephen, F. M. (2009). Per-segment Aboveground Forest Biomass Estimation Using LIDAR-Derived Height Percentile Statistics. *GIScience & Remote Sensing*, *46*(2), 232–248. https://doi.org/10.2747/1548-1603.46.2.232.

Roussel, J.-R., & Auty, D. (2022). *Airborne LiDAR Data Manipulation and Visualization for Forestry Applications* (No. R package version 4.0.1). Retrieved from https://cran.r-project.org/package=lidR.

Roussel, J.-R., Auty, D., Coops, N. C., Tompalski, P., Goodbody, T. R. H., Meador, A. S., et al. (2020). lidR: An R package for analysis of Airborne Laser Scanning (ALS) data. *Remote Sensing of Environment*, *251*, 112061. https://doi.org/10.1016/j.rse.2020.112061.

Tompalski, P., Coops, N., Marshall, P., White, J., Wulder, M., & Bailey, T. (2018). Combining Multi-Date Airborne Laser Scanning and Digital Aerial Photogrammetric Data for Forest Growth and Yield Modelling. *Remote Sensing*, *10*(3), 347. https://doi.org/10.3390/rs10020347.

Wagers, S., Castilla, G., Filiatrault, M., & Sanchez-Azofeifa, G. A. (2021). Using TLS-Measured Tree Attributes to Estimate Aboveground Biomass in Small Black Spruce Trees. *Forests*, *12*(11), 1521. https://doi.org/10.3390/f12111521.

Wu, F., Jiang, Y., Zhao, S., Wen, Y., Li, W., & Kang, M. (2022). Applying space-for-time substitution to infer the growth response to climate may lead to overestimation of tree maladaptation: Evidence from the North American White Spruce Network. *Global Change Biology*, *28*(17), 5172–5184. https://doi.org/10.1111/gcb.16304.

Wulder, M. A., White, J. C., Bater, C. W., Coops, N. C., Hopkinson, C., & Chen, G. (2012). Lidar plots — a new large-area data collection option: context, concepts, and case study. *Canadian Journal of Remote Sensing*, *38*(5), 600–618. https://doi.org/10.5589/m12-049.

Xi, Z., Hopkinson, C., Rood, S. B., & Peddle, D. R. (2020). See the forest and the trees: Effective machine and deep learning algorithms for wood filtering and tree species classification from terrestrial laser scanning. ISPRS Journal of Photogrammetry and Remote Sensing, 168, 1–16. https://doi.org/10.1016/j.isprsjprs.2020.08.001.

CHAPTER 5: HYDROCLIMATIC SHIFTS IN ECOSYSTEMS IN THE SOUTHERN TAIGA OF WESTERN CANADA: WOODY ABOVEGROUND BIOMASS GAINS EXCEEDING LOSSES DUE TO MORTALITY

5.1. Abstract

Complex land cover change processes occurring since the retreat of the Laurentide Ice Sheet and anthropogenic climate change are altering successional states of ecosystems and distribution of vegetation structure across the southern Taiga of northwestern Canada, a region identified as an important yet uncertain climate regulator. In this study we a) quantify short-to-tall-stature vegetation structural changes at the plot level over vast areas and across environmental gradients, and b) examine these changes across the range of variability of local to regional environmental and hydroclimatic drivers. We use bi-temporal airborne lidar data over a decade with coincident field data, shrub and short-stature tree allometric equations, and a bi-temporal shrub-to-tree aboveground biomass model to reduce uncertainty in the magnitudes and directions of short-to-tall-stature vegetation trajectories. Results show that peatland complexes in the Taiga Plains Mid Boreal and Taiga Shield High Boreal shifted in their vegetation structure towards increased abundance of woody vegetation, whereby increases in short-stature vegetation (≤ 4.5 m in height) outweighed losses from tall-statured vegetation (> 4.5 m in height). Across the ecoregions, these shifts were most pronounced in permafrost plateaus (58% of the areas sampled), ecotones from permafrost plateau to peatland (43%), and fens (25%). Shifts were partially driven by increasing mean annual air temperature and decreasing total annual

precipitation, which increased drying conditions over the last 9 years. This was emphasized by topographical drivers related to plant available water at a given location. Overall, the fusion of field data, allometric equations, and transect-wide bi-temporal airborne lidar data enabled the quantification of vegetation trajectories of both short- and tall-stature vegetation and elevation changes beyond past areas of intense research and over longer periods of time compared to commonly short-term funding initiatives (typically 5-6 years). In addition, we increased accuracy in carbon sink strength estimates associated with aboveground biomass in the southern Taiga of western Canada. The results provide a critical baseline from which to compare future vegetation structural and elevation changes associated with sporadic and discontinuous permafrost evolution and could be used to develop maps of wildland fire fuels over climatically sensitive parts of northwestern Canada in the future.

5.2. Introduction

Climate change alters rates of successional changes of ecosystems and distribution of vegetation structure across the Taiga of western Canada (Schuur & Mack, 2018). This is in addition to dynamic land cover changes occurring since the onset of the deglaciation of the Laurentide Ice Sheet after the last glacial maximum (~22.1 cal ka BP) and the subsequent establishment of an ice-free corridor in the interior Taiga Plains (Dulfer et al., 2023). Changes in local vegetation structure are a key determinant of permafrost response to climate change (IPCC, 2023; Shur & Jorgenson, 2007), especially in climatically sensitive areas where soil temperatures are close to 0°C, such as in the sporadic to discontinuous permafrost zone. Here, relict permafrost can persist despite being in disequilibrium with the current climate, for as long as the ecosystem maintains ecological properties and

processes related to energy and mass exchanges (e.g. vegetation structure, organic layer depth) (Shur & Jorgenson, 2007). However, once initiated, permafrost thaw triggers positive feedbacks that enhance thaw (Camill & Clark, 2000; Shur & Jorgenson, 2007). Such feedbacks function through alterations to vegetation structure (e.g. vegetation growth, and densification, mortality) (Baltzer et al., 2014; Camill, 1999a; Jorgenson et al., 2022) due to changes in local hydrology (Balliston & Price, 2022; Connon et al., 2014; Mack et al., 2021; Mäkiranta et al., 2018; Wright et al., 2008) and nutrient cycling (Mekonnen et al., 2021) as permafrost thaws. For example, vegetation structural changes in the form of increased abundance of short-stature vegetation (e.g. shrubs and juvenile trees) or tree mortality accelerate thaw due to changes in the surface energy balance (Chasmer et al., 2011b; Quinton et al., 2011; Schuur & Mack, 2018; Wilcox et al., 2019), thus dramatically altering ecosystems on and in proximity to permafrost at unprecedented rates (Gauthier et al., 2014; Price et al., 2013). The implications of these changes occur over broad areas, affecting carbon sink potential (Helbig et al., 2022; Price et al., 2013; See et al., 2024), and rates of wildland fire spread (Loudermilk et al., 2022; Thompson et al., 2019) and smoke emissions (Reisen et al., 2015). A regional loss of sporadic to discontinuous permafrost is expected by the end of this century (Carpino et al., 2021; Chasmer & Hopkinson, 2017; Quinton et al., 2011; Schuur & Mack, 2018), which will have multiple impacts to Indigenous communities (Wright et al., 2022) and flora/fauna habitats (Price et al., 2013), among other important ecological services.

Monitoring changes in vegetation structure as an indicator of altered ecosystem function and wildland fire fuels/emissions is therefore crucial. However, quantification of vegetation structural changes over longer periods (≥ a decade) across broad regions, and at

spatial scales that enable changes to be observed, is challenging. This is due in part to short funding cycles, which often limit observations to approximately 5 years and the requirement for resource intensive data collections over remote, vast, and inaccessible landscapes. As a result, few studies have quantified longer-term (multi-year to decadal) vegetation structural changes across broad areas of northern Canada.

Current knowledge of vegetation structural changes and underlying processes are understood at a few sites using long-term field observations, such as plot measurements (Camill et al., 2001; Dearborn et al., 2021; Sniderhan & Baltzer, 2016) and eddy covariance data (Chasmer et al., 2012; Flanagan & Syed, 2011; Helbig et al., 2022), in combination with historic aerial photography and high-resolution satellite imagery (Chasmer et al., 2011b; Jorgenson et al., 2022; Sniderhan et al., 2023). Studies using airborne lidar data have been used to quantify 3D vegetation structure (Hopkinson et al., 2005; Hopkinson et al., 2006; Næsset & Gobakken, 2008), but these data have not been widely available until recently and require considerably more logistical planning. The following is understood using both field and remotely sensed data/methods within this region.

Local ecosystem properties that emphasize maintenance of vegetation structure on/near sporadic to discontinuous permafrost, function such that permafrost is 1) buffered against incident solar radiation and warm air temperatures during the growing season (amount of tree foliage and canopy closure, thick, unsaturated organic layer), and 2) exposed to cold air temperatures in the winter season (snow interception by evergreen tree canopy, saturated organic soils) (Camill, 1999b; Jenness, 1949). North to east facing slopes also showed vegetation densification and reduced permafrost thaw rates (Chasmer & Hopkinson, 2017). In areas underlain by Precambrian shield, fill-and-spill mechanisms

between upland bedrock, valleys, and lakes hydrologically connect ecosystems by spilling into lower lying ecosystems after an ecosystem-specific threshold is exceeded (Spence & Woo, 2003). The hydrological connectivity may buffer vegetation structure from impacts related to prolonged dry conditions.

In contrast, vegetation structural changes are caused by feedbacks between the soil layer and the atmosphere (Disher et al., 2021). For example, tree mortality is caused by 1) increased drying in the soil column above a deepening active layer, and 2) waterlogging of soils (enhanced on south to west facing slopes (Chasmer & Hopkinson, 2017)) as permafrost thaws (Baltzer et al., 2014; Patankar et al., 2015; Sniderhan & Baltzer, 2016). In later stages of permafrost thaw, increased drainage of peatlands occurs due to a reduction of permafrost plateau areas, which function as barriers to peatland hydrological connectivity and an increase in runoff contributing area (Connon et al., 2014, 2015; K. M. Haynes et al., 2018; Quinton et al., 2019b). This enhances shifts in vegetation structure towards increased abundance of short-stature shrubs (Chasmer & Hopkinson, 2017) and deciduous trees (Dearborn et al., 2021), observed in some peatlands. In areas underlain by shield, changes in vegetation structure may occur when hydrological network channels remain disconnected over multiple years (Spence & Woo, 2003) and may also be related to lowering of lake water levels (Kokelj et al., 2023) and subsequent infilling (Kokelj & Jorgenson, 2013).

These diverse ecological changes are significant. Climate change and increased magnitudes and frequencies of pulse disturbance events (Schuur & Mack, 2018) (e.g. wildland fire) may push ecosystems in the sporadic to discontinuous permafrost zone beyond ranges of variability/thresholds into new successional states (Bathiany et al., 2024;

Holling, 1973; Lenton et al., 2008). The challenge is to understand which ecosystems maintain current vegetation structure and therefore, function, and which are sensitive to anthropogenic climate change, resulting in alteration. In addition, identifying the environmental and hydroclimatic drivers that promote maintenance and change are not well understood.

This study examined changes in vegetation structure over the past decade (2010 to 2019) at sampled locations in upland forests, forests on permafrost plateau middles (herein permafrost plateaus'), bogs and fens (herein 'peatlands'), and in upland forest and permafrost plateau to peatland ecotones (forest margins) in three ecoregions (Taiga Plains Mid Boreal, Taiga Plains High Boreal, Taiga Shield High Boreal). In addition to the changes examined in ecoregion-specific ecosystem types (listed above), sampled changes were also aggregated and estimated for the broader region; i.e. a) for pooled ecosystem types per ecoregion, and b) ecosystem types pooled across ecoregions. By using field and overlapping bi-temporal airborne lidar data fusion the study aims to answer the following questions for the above listed ecosystem types per ecoregion (questions 1 and 3) and the broader region (questions 1, 2 and 3)

1. What were the effects of gradual permafrost thaw on vegetation structure? And were certain plant functional groups/structures more sensitive than others?
2. What were the environmental and climatic drivers of these changes? And what can we expect in the future as these play greater or lesser roles?
3. How are these changes represented in regional and global aboveground biomass products and what are the implications to current knowledge about the broader plant carbon balance in this region?

Vegetation structural changes were quantified using overlapping airborne lidar data in 2007/2010 and 2018/2019 (Figure 5.1) and are assessed through: aboveground biomass (AGB); carbon stored in aboveground woody plant components (stems including bark and branches, which represents a fraction of total biomass, herein 'plant C'); and vegetation height. Combined, these represent vertical and lateral changes and were used as an indicator of the cumulative impacts of multiple, interacting feedbacks occurring within the system.

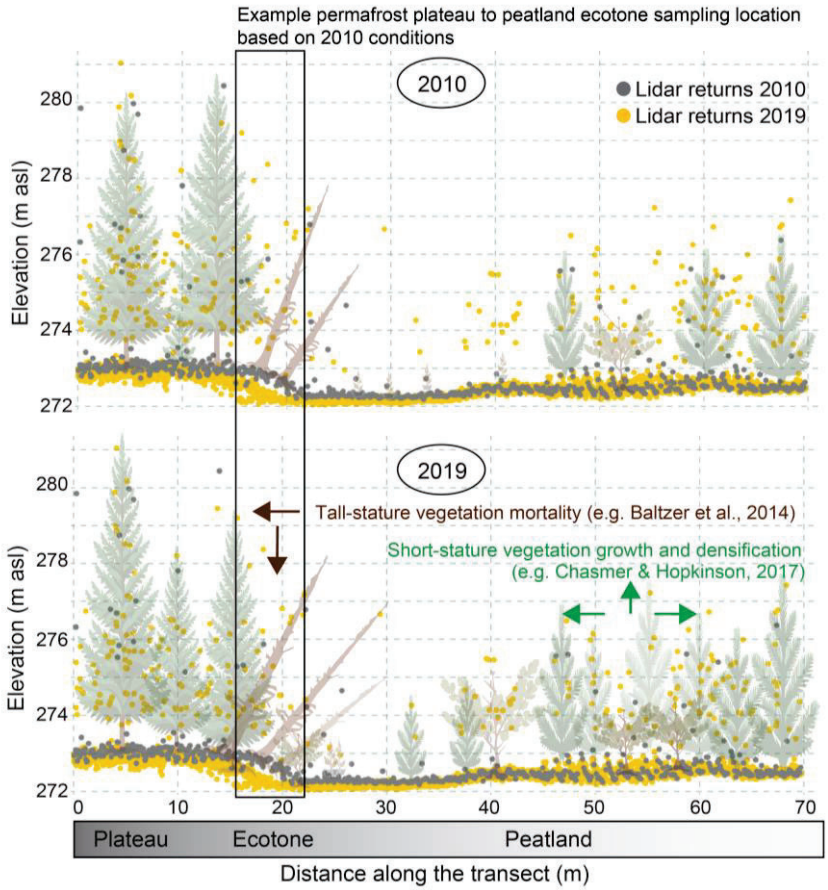

Figure 5.1. Conceptualization of changes in vegetation structure determined from overlapping lidar point clouds in 2007/2010 (grey) and 2018/2019 (yellow) along a cross-section from a higher elevated permafrost plateau (left) to a lower lying permafrost free peatland (right). Woody vegetation growth, densification, and expansion exceeding mortality was conceptualized based on changes in the lidar points. Sample locations in ecotones shown as black box.

AGB is a constituent of net primary production (NPP) (Chapin et al., 2006), i.e. the standing AGB stock of over- and under-story vegetation, of which 50% is stored as carbon in stem,

branches, and leaf components. In contrast to NPP, however, AGB change is the net increase (plant growth, densification) or decrease (mortality, thinning) in AGB excluding tissue turnover from litterfall (Chapin et al., 2006; Hopkinson et al., 2016). To reconcile terminology used in the carbon flux context, NPP is the remaining C content from gross primary production (GPP) after subtraction of the C lost due to autotrophic respiration (Ra), while GPP minus ecosystem respiration (autotrophic and heterotrophic) results in net ecosystem production (NEP) (Chapin et al., 2006). Neither NPP nor NEP are equivalent to change in AGB carbon over time, as the tissue turnover from leaves, twigs, branches and entire stems that fall to the ground as dead organic material can be a large source of difference at both the plant and ecosystem scale.

This study is important for advancing the research into the cumulative effects of gradual permafrost thaw on ecosystems in the southern Taiga of western Canada. Improved quantification of the changes in these systems over larger areas will be critically important for understanding accelerating ecosystem succession, feedbacks to the global carbon-climate system, and the implications of changing aboveground biomass and wildland fire fuels to northern communities.

5.3. Materials and methods

5.3.1. Study area

This study was conducted within the traditional lands of the Dene First Nations in the southern Northwest Territories, Canada (Figure 5.2). Vegetation structural changes and drivers were analysed at subsampled locations within a 150,000 km^2 area from the Taiga Plains Mid and High Boreal to the Taiga Shield High Boreal in areas were overlapping airborne lidar data was available and was not recently disturbed by wildland fire (since

~1965). The sampled areas examined cover a longitudinal and latitudinal gradient of climate, surficial geology, and glacial history but are not a complete representation of the heterogeneity occurring in this region. Permafrost extent varied from sporadic in the west and south to discontinuous in the east and north.

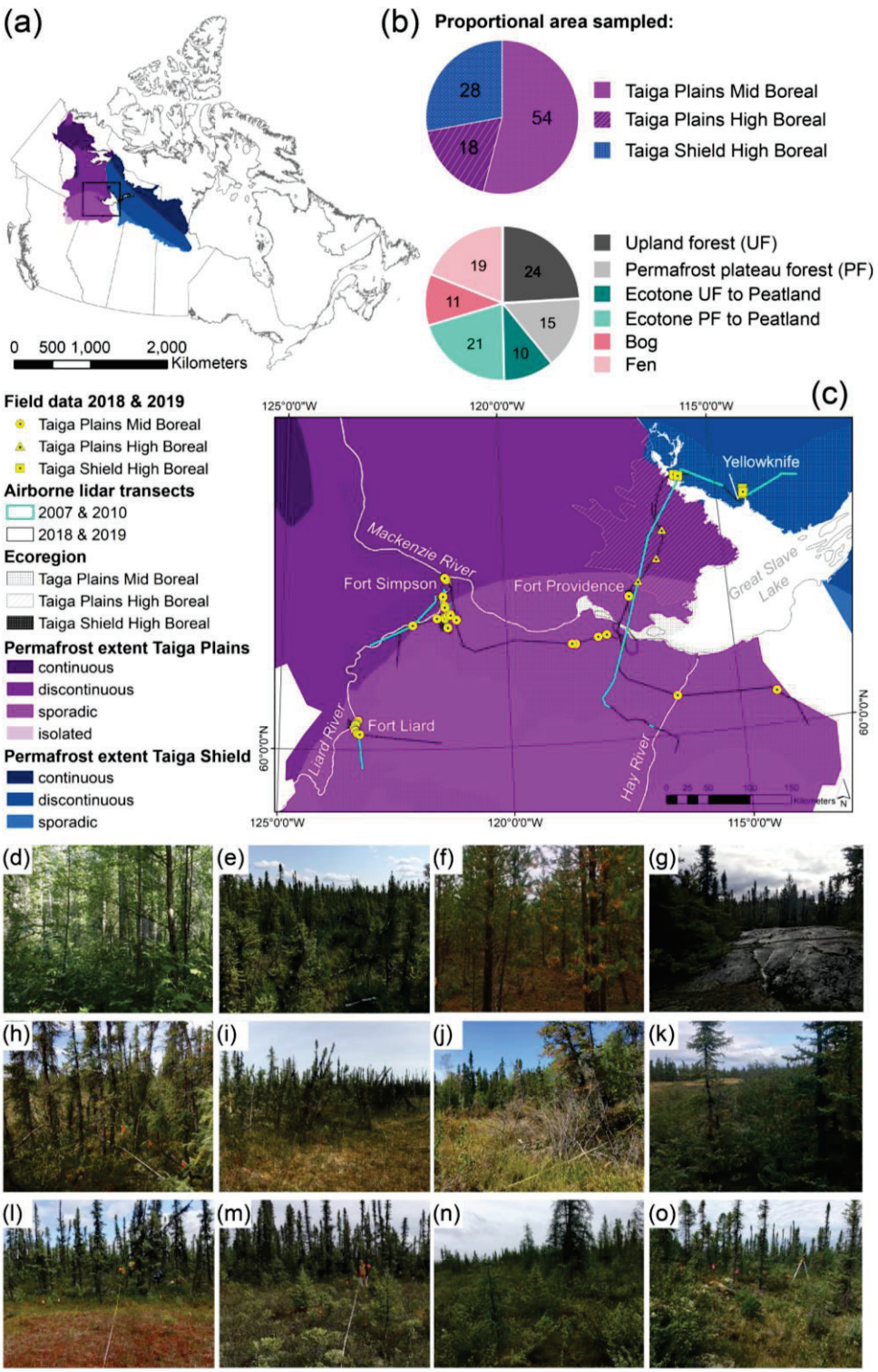

Figure 5.2. (a) Study area in the southern Taiga of western Canada; (b) proportion of sampled ecoregions and ecosystem types; (c) field sampling locations with coincident airborne lidar; and photographs of most common ecosystem types ranging from (d) upland mixed-wood and (e) coniferous forest in the Taiga Plains Mid Boreal, (f) Taiga Plains High Boreal, and (g) Taiga Shield High Boreal to peatland complexes. Within peatland complexes, ecosystem types investigated were (h) permafrost plateaus and (i) ecotones between

permafrost plateaus and peatlands (upland ecotones not shown) in the Taiga Plains Mid Boreal, (j) Taiga Plains High Boreal, and (k) Taiga Shield High Boreal. Peatlands ranged from open and shrubby ((l, m) Taiga Plains Mid Boreal, (n) Taiga Plains High Boreal) to treed (o) Taiga Shield High Boreal) bogs and fens.

The climatology of the study area consists of cold, relatively dry climates. The mildest climate is found in the western Taiga Plains Mid Boreal (Fort Liard) and the coldest and driest climate in the Taiga Shield High Boreal. Mean annual air temperatures in the period between 1981 to 2010 ranged from -4.3°C (Yellowknife) to -2.8°C (Fort Simpson) and -1.0°C (Fort Liard). Total average precipitation ranged from 451.7 mm (Fort Liard) to 387.6 mm (Fort Simpson) and 288.6 mm (Yellowknife) (Environment and Natural Resources, 2024).

Plant species composition varies with the underlying substrate and drainage properties. In the Taiga Plains Mid Boreal, moderate-to-well draining fine to coarse textured lacustrine and till deposits on uplands support tall mixed-wood stands (trembling aspen (*Populus tremuloides*), balsam poplar (*Populus balsamifera*), white spruce (*Picea glauca*), jack pine (*Pinus banksiana*)), and stands of jack pine and trembling aspen (Ecosystem Classification Group, 2009). Within the Taiga Plains High Boreal, upland soils consist of rapidly draining coarse textured glacial till deposits above bedrock, which promote the establishment of extensive jack pine stands frequently disturbed by wildland fire. White spruce and trembling aspen are also common (Ecosystem Classification Group, 2009). In the Taiga Shield High Boreal (Great Slave Lowland and Upland), coarse-textured till and fine-textured lacustrine material in bedrock fractures and around bedrock outcrops support plant communities that range from jack pine, black spruce, and paper birch combined with shrubs and lichen (thin soils) to black spruce or mixed-wood forests with

shrubs and mosses (on deeper soils and higher soil moisture availability). Wildland fire is common (Ecosystem Classification Group, 2008).

Peatland complexes also vary across the region. In the Taiga Plains Mid Boreal, these cover up to 71% of the area and consist of slightly elevated forested peat plateaus underlain by permafrost (herein 'permafrost plateaus') adjacent to permafrost-free peatlands. Forests on permafrost plateaus consist of sparse and stunted black spruce trees (*Picea mariana*) (2 m to 12 m, Chasmer et al., 2014) with e.g. common labrador tea (*Rhododendron groenlandicum*), and various lichens and mosses (Garon-Labrecque et al., 2016). Peatland forms include open, shrubby, and treed (including black spruce and tamarack (*Larix laricina*) (Ecosystem Classification Group, 2009; Garon-Labrecque et al., 2016). In the Taiga Plains High Boreal, 50% of the ecoregion is covered by shallow ponds that dot the ecoregion and which are surrounded by extensive sedge-dominated fens (herein "floating fens"). Permafrost plateaus are uncommon (Ecosystem Classification Group, 2009). In the Taiga Shield High Boreal, permafrost plateaus occur around shallow lakes and in low-lying areas (Ecosystem Classification Group, 2008). Floating fens are extensive (up to 30% spatial coverage) and dominated by sedges and shrubs (Ecosystem Classification Group, 2008).

5.3.2. Field data collection and aboveground biomass

Decadal bi-temporal AGB was used as one component to quantify structural changes of short- to tall-stature vegetation. This required the scaling from field measurements to field-based AGB using allometric equations, and scaling from field-based AGB to spatially overlapping bi-temporal airborne lidar.

Field data collection is described in Flade et al. (2020, 2021, 2024). Briefly, this included 20 permanent sampling plots in Fort Liard (Government of the Northwest Territories, 2019), 36 circular forest mensuration plots (5 m radius), and 53 transects (from upland and permafrost plateau forests to peatlands) with 1250 microplots ($1m^2$) to measure vegetation characteristics (genus/species, height, cover, stem diameter at the base and at breast height) across ecotonal boundaries (Figure 5.1, 5.2). All plots were located using a Global Navigation Satellite System (GNSS) (Topcon Corp., Japan) (Flade et al., 2024).

AGB was calculated using the product of height and cover for shrubs, stem length for trees ≤ 4.5 m height (Flade et al., 2020), and height with diameter at breast height for trees > 4.5 m height (Lambert et al., 2005) as input into genus/species-specific and general allometric equations. Field-derived AGB was summed per plant within each plot. Plots were scaled and aggregated into forests (including forest to peatland transition zones) and peatlands and converted to Mg ha^{-1} (Flade et al., 2024).

5.3.3. Airborne lidar data and bi-temporal shrub-to-tree AGB model implementation

Airborne lidar data were collected as scanning lidar transects over large distances between July and August in 2007, 2010 using an ALTM 3100 (1064 nm, Optech Inc. Toronto, Canada) and again in 2018, 2019 using an ALTM Titan (three-wavelengths, Teledyne Optech Inc.). The systems were operated with similar flight and sensor settings described in Flade et al. (2024). Lidar data were classified into ground (single and last returns) and all returns, height normalized, and geo-registered (Flade et al., 2024). Transect locations were chosen to sample a wide range of ecosystem types occurring in the study region, which are characteristic of the heterogeneous environmental conditions (e.g. surficial geology,

topography, and glacial history). However, transects represent a sample of the general study region and do not cover the full variety of ecosystem types and environmental conditions. Using these transects for quantification of spatially explicit vegetation structural changes at further subsampled locations within overlapping airborne lidar is therefore a limitation when changes are aggregated and reported for the complete region (see below).

The lidar-based AGB model development was described in Flade et al. (2024). Briefly, field-based AGB was compared with lidar height and cover metrics using iterative nonlinear least squares regression. The optimal predictor (lidar metric) was chosen based on high goodness-of-fit statistics and minimal, calibratable offsets between sensors (Flade et al., 2024). The final bi-temporal shrub-to-tree AGB model uses the average height and the 90^{th} height percentile of all lidar returns per plot within a weighted approach as a function of modelled AGB. To apply this model, both metrics were gridded for spatially overlapping temporal lidar data using a grid cell size of 5 m x 5 m. This cell size was chosen to capture a sufficient number of points per grid cell, maintain relatively high spatial resolution, and enable scaling to national forest inventory plots and Landsat imagery (Flade et al., 2024). The earlier ALTM 3100 grids were calibrated to minimize offsets between sensors (Flade et al., 2024). AGB per grid cell was initially derived using the general average height and 90^{th} percentile AGB models. Final bi-temporal shrub-to-tree AGB was then derived using the average height based AGB values (for grid cells with average height based AGB $\leq$ 75 Mg ha^{-1}) and the 90^{th} height percentile based AGB values (for grid cells with average height based AGB $\geq$ 125 Mg ha^{-1}). For grid cells with average height based AGB values between 75 Mg ha^{-1} and 125 Mg ha^{-1}, a sliding scale from 0% to 100% was applied, which decreased and inversely increased for increasing average height based AGB

and 90th height percentile based AGB, respectively, using a step size of 2% for each 1 Mg ha^{-1} (Flade et al., 2024).

To examine AGB changes relative to changes in canopy height, an average maximum CHM was created by resampling a 1 m x 1 m localized-maxima CHM to 5 m x 5 m grid cell size. To analyze AGB change in relation to topographical ecosystem properties, triangulated irregular network (TIN) elevation models (DEMs), and localized-maxima digital surface models (DSMs) were produced at 2 m x 2 m, and 5 m x 5 m grid cell resolution.

5.3.4. Change detection analysis

To quantify AGB and canopy height changes, the 5m x 5m 2007/2010 AGB and CHM grids were subtracted from the 2018/2019 AGB and CHM grids, so that increases were 'positive', and decreases 'negative'. Changes were further normalized to the 2010 to 2019 period by first dividing changes by the number of years to derive annual change and second, multiplying annual change by nine years. Grids were then subsampled using a stratified sampling approach (Cochran, 1977), sampling a partial range of ecosystem types and environmental conditions within each strata. The total number of sample points were determined following methods described in Hermosilla et al. (2018). Choosing a 99% confidence limit, and a 60% estimated areal coverage available for sampling (based on overlapping airborne lidar transects in the Taiga Plains Mid Boreal, Taiga Plains High Boreal, and Taiga Shield High Boreal, excluding water bodies, unvegetated bedrock, areas disturbed by wildland fire, anthropogenic infrastructure, and flight strip edges) resulted in a total of 3600 points. These were distributed across uplands and peatland complexes (permafrost plateau, peatland (bog, fen), upland and permafrost plateau to peatland

ecotones). This resulted in three broader strata per ecoregion (upland and permafrost plateau, peatland, ecotones from upland and permafrost plateaus to peatlands). The minimum sampling size per stratum was estimated by allocating half of the total sample points equally across the strata and the remainder proportionally to the relative areal coverage per stratum. Approximate proportional areal coverage was estimated by adapting the 2019 landcover classification of Hermosilla et al. (2022) and identifying corresponding landcover classes based on spatial overlap with those of Chasmer et al. (2014) in the Scotty Creek watershed.

Sampling points were placed manually in locations of continuous canopy cover using moderate resolution Landsat imagery within Google Earth Pro based on 2007/2010 snow free conditions. Lidar-based AGB, CHM, and AGB and CHM change were extracted per 5 m x 5 m cell containing a sample point and used in the subsequent analysis. Sample points were labelled as “Upland forest (UF)” and “Peatland complex”. Peatland complex strata included “Permafrost plateau forest (PF)”, “Peatland” and “Ecotone from UF/PF to peatland”. Peatland strata included “Bog” and “Fen”. Peatland form ranged from “open (including shrubby)” to “treed”. This refinement of the stratification was based on expert interpretation of landcover characteristics aided by various reports (Ecosystem Classification Group, 2008, 2009; Gibson et al., 2020; Wright et al., 2022). A CHM, a lidar-Worldview-based classification from the same period (Chasmer et al., 2011), and a landcover classification by Bourgeau-Chavez (2019) for the 1997 to 2011 period, available for a subset of the area, also aided the interpretation. Sampling points at ecotones from UF and PF to peatland were placed at the outer edges of forests based on visual changes in color and texture of vegetation in 2007/2010 Google Earth imagery and reduced plant

heights in the CHM, which is indicative of changes in species composition from trees mixed with shrubs and herbaceous vegetation in forests to moss, grass, sedge, and shrub dominated "open peatlands" or sparsely forested "treed peatlands" found in the field (Flade et al., 2024). Distances between sample points were ≥ 30 m to minimize spatial autocorrelation, and > 100 m from lidar flightline edges. The total sampled areal coverage (based on a 5 m x 5 m grid cell resolution) comprised 2% of the area within overlapping airborne lidar data used in this study, which covered unmanaged uplands and peatland complexes not recently (since ~1965) disturbed by wildland fire.

5.3.5. Quantifying aboveground biomass changes and plant carbon stocks

Findings were reported as the mean ± standard deviation of AGB change and change in canopy height in each stratum. Mean changes were also derived for aggregated strata to estimate changes for the broader area. Overall, strata were organized into a) ecoregion-specific ecosystem types, b) pooled ecosystem types per ecoregion, and c) ecosystem types pooled across ecoregions. Tables 5.1 and S5.1 list the number of sampling points in each stratum per level of organization. Statistically significant differences between cumulative 2010 and 2019 AGB distributions were determined in each stratum and between strata based on two-sample Kolmogorov-Smirnov tests and a significance level of 0.05, as the 2010 and 2019 AGB data (not the AGB change data) were nonparametric (Anderson-Darling normality test).

Plant C was derived in two steps. First, total plant C was estimated as 50% of the total AGB (all aboveground plant components). From this estimate, woody C was estimated as the average between the lowest (*Picea* spp., 76%) and highest (*Betula papyrifera*, 90%)

proportions of carbon allocation to woody plant components (stem including bark, branches), as measured across the study region (Flade et al., 2021).

Table 5.1. Random sample points (n) per ecoregion (pooled ecosystem types) and ecosystem type (pooled across ecoregions) and equivalent area sampled (ha) based on a 5 m x 5 m grid cell resolution.

Ecoregion	n	Area sampled	Pooled ecosystem type	n	Area sampled
Taiga Plains Mid Boreal	1998	5.0	Upland (UF)	892	2.2
Taiga Plains High Boreal	673	1.7	Peatland complex	2814	7.0
Taiga Shield High Boreal	1035	2.6	Permafrost plateau (PF)	560	1.4
Total	3706	9.3	Ecotone UF to Peatland	387	1.0
			Ecotone PF to Peatland	770	1.9
			Peatland	1097	2.7
			Bog	396	1.0
			Fen	701	1.8

5.3.6. Determining antecedent vegetation structure and plant functional groups

To better understand the antecedent vegetation structural conditions which were maintained/altered, 2010 starting conditions of vegetation heights (Figure 5.3a) were examined. These were derived from the average maximum 5 m x 5 m CHM.

To determine AGB changes based on antecedent vegetation structural conditions, the AGB change distribution (mean, median, interquartile range) was examined for each 2010 canopy height bin per stratum. Bin sizes were determined manually and required explorative analysis of distinct break points in the frequency distribution of sampled 2010 CHM per stratum. For the final bins used in this analysis, height thresholds a) were the same in all strata (to enable across strata comparison), and b) showed reasonable (compared to what was reported in the literature for this region e.g. Chasmer & Hopkinson, 2017)

AGB gains, losses, and maintenance in the corresponding lidar grids. Height bins were placed in a stepwise fashion, whereby an additional bin was created when the minimum requirements for n were met in each bin, which were four (ecoregion-specific ecosystem types), seven (pooled ecosystem types per ecoregion), and 30 (ecosystem types pooled across ecoregions). If requirements were not met, sample points were aggregated with the previous bin.

The resulting height bins were associated with broader plant functional groups based on heights measured *in situ* within the study region (Flade et al., 2020, 2021) and commonly reported heights per plant functional group (Alberta Wetland Classification System, 2015; Alberta Wetland Classification System, 2021; The Canadian Wetland Classification System, 1987). Under the assumptions of a continuous canopy cover within the 5 m x 5 m grid cells, height thresholds represented areas dominated by non-woody vegetation (bryophytes, lichen, grasses, sedges), short-stature vegetation (shrubs, juvenile and low productive mature trees), and tall-stature vegetation (high productive juvenile to mature trees) in 2010 (Figure 5.3a).

Extracted 2010 and 2019 AGB values were aggregated within the corresponding plant functional group and gains and losses between 2010 and 2019 were analyzed to understand counterbalancing of AGB and plant C across broader plant functional groups.

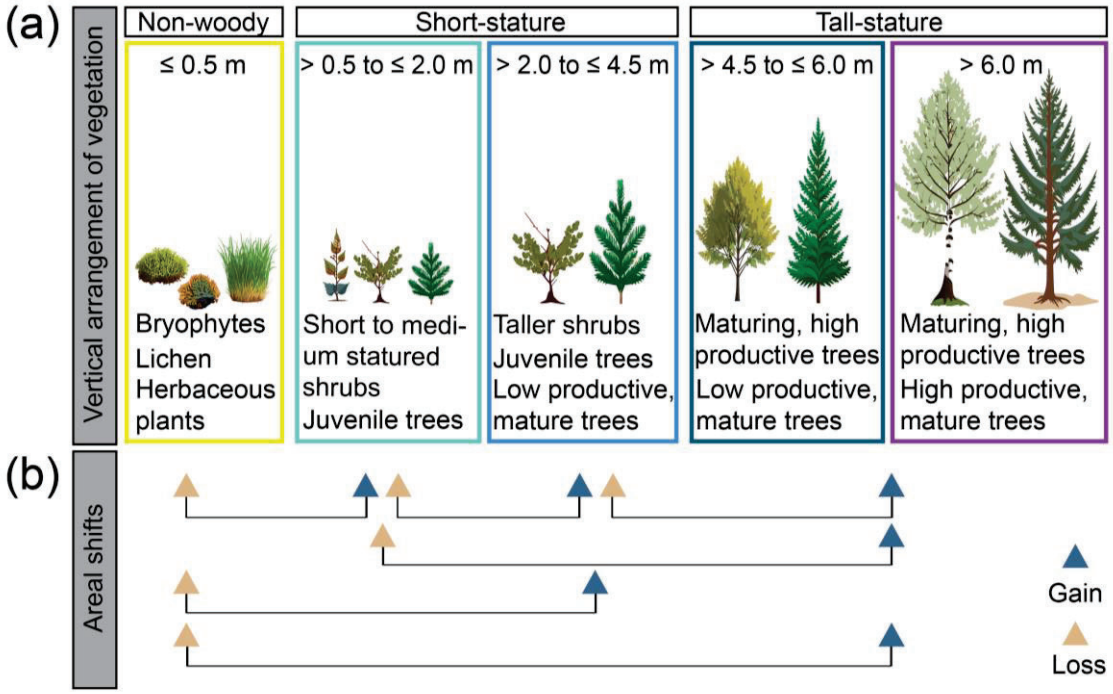

Figure 5.3. (a) Conceptualization of vertical height bins and associated dominant plant functional groups using growth form as distinguishing trait based on a 5 m x 5 m area under the assumptions of a continuous canopy cover; and (b) shifts in dominance of plant functional groups indicating shifts in successional stages. Shifts leading to more aboveground biomass and plant C across the landscape are considered a gain, the reverse a loss (Schematics of vegetation were created in Adobe Illustrator (v 2000) using the AI based "Text to Vector Graphic" tool).

5.3.7. Evaluating regional shifts in dominant vegetation structure

To better understand shifts in dominant vegetation structure from 2010 to 2019, shifts in the relative proportion of the number of samples per plant functional group were analyzed (Figure 5.3b). Grid cells within the two tall-stature vegetation groups (Figure 5.3a) were combined to allow for across strata comparison. Shifts in dominance of plant functional groups (increased/decreased number of samples relative to the total number of samples (%)) were used to indicate shifts in successional stages for pooled ecosystem types per ecoregion and ecosystem types pooled across ecoregions.

Shifts in sample proportions per plant functional group were further segmented into gains and losses (Figure 5.3b). Shifts leading to increased aboveground biomass and plant C in the landscape due to growth, densification, and woody plant expansion were considered a gain. Shifts leading to lesser amounts of AGB and plant C in the landscape (e.g. mortality followed by revegetation of a lower plant functional group) were considered a loss.

5.3.8. Determination of drivers of aboveground biomass change and maintenance using random forest

To better understand the range of important drivers of AGB changes and maintenance, predictive variables at the start of the observation period were used to parameterize a random forest regression tree model (ArcGIS Pro, ESRI, USA). Variables were extracted from 5 m x 5 m grids at the same sampling points. To reduce bias in the model towards non-changing environments (dominant trend in the data), the number of sample points per stratum were normalized using an equal area histogram approach.

Regional climatic variables consisted of the slope of a 30-year trend in mean annual air temperature (MAAT) and total annual precipitation (TAP) change. MAAT and TAP were derived from downscaled and gridded Climate NA data (Wang et al., 2016) from 1989 to 2019, including the last 10 years of the field/lidar-based change detection analysis. The slopes of the trends through annual deviations from the preceding 1961 to 1990 baseline period were derived for each sampled point. Trends in MAAT and TAP represented changes in energy and water inputs, respectively, into the system. Further energy inputs consisted of the total amount of incident solar radiation hours reaching the upper canopy (herein “incident radiation”). This was computed using GRASS GIS (r.sunmask.datetime

tool) within QGIS (Version 3.30.2). For each day, a raster layer of total hours was produced using the 2 m x 2 m 2010 DSM as input. Daily sunshine hours were summed on a per grid cell basis for the period March 1st (to ensure the start of the growing season was included) to December 21st (winter solstice). Latitude and longitude represented the position along the climatic and surface geological gradient (herein "gradient position").

Local to proximal environmental properties consisted of the following topographical variables derived from the 2010 lidar DEMs: surface elevation, aspect, slope, topographical position index (TPI), and topographical wetness index (TWI). The latter was considered to indicate the topographical potential for wetness of an area and was therefore considered as water input. Ground subsidence due to e.g., permafrost thaw was also included by subtracting the 2010 from the 2019 DEMs (herein "elevation change"). Lastly, because AGB change was a function of starting AGB conditions, 2010 AGB values were included to initialize starting values.

To determine relevant scales of environmental drivers, variables were also extracted as mean values within square windows around each sample point. Window sizes started with the 4 neighboring cells and grew incrementally until a maximum extent was reached at which each variable was correlated to the cell based AGB change. Range of correlation was determined using semi-variograms. For the computation of the TWI, we constrained the analysis to 90 m around the sampled cell to avoid artifacts of flow accumulation at lidar flight strip edges.

Regression-based random forest was executed as 100 independent model runs, retaining 20% of the data randomly for model validation. Driver variables were reduced by a stepwise backward selection until a) the most important scale was found per variable and

b) the most important variables were found per ecoregion (pooled ecosystem types) and per ecosystem type (pooled across ecoregions). The number of trees (initialized with 500) was gradually increased until model fits and ranking of driver importance were relatively stable (change in ranking order of 1 or 2 variables as opposed to all variables determined from 10 independent model runs). The final models were run 10 times (each run 100 times) to determine ranking stability (Millard & Richardson, 2015). Random forest model results were compared to univariate correspondence between AGB change and driver variable (Pearson correlation coefficient, reported for the best scale) to understand the utility of the machine learning approach, which allows for interaction between drivers and scales.

5.3.9. Comparison to regional and global aboveground biomass products

The 2010 AGB and annual AGB change (period 2019-2010) results in this study were compared to a) regional shrub and tree 2010 AGB and annual AGB change (2014-2010) derived within the NASA Arctic-Boreal Vulnerability Experiment (ABoVE) (Wang et al., 2021a), and b) global tree 2010 AGB and annual AGB change (period 2019-2010) derived by the ESA Biomass Climate Change Initiative (CCI) (Santoro & Cartus, 2024; Santoro et al., 2021). Data in a) were derived using Landsat-5 and -7 surface reflectance imagery and full-waveform lidar returns from the Geoscience Laser Altimeter System (GLAS) with machine learning (Wang et al., 2021a; Wang et al., 2021b), and data in b) were derived using SAR C-band and L-band data with semi-empirical models (Santoro & Cartus, 2024; Santoro et al., 2021). The results of this study were resampled to the same grid cell resolution as data from a (30 m x 30 m) and b (70 m x 70 m) and were compared at the same sampling points. We restricted the comparison to the ESA Biomass CCI data to the

pooled datasets due to the coarse grid cell resolution of these global products, which were produced for large-scale climate and carbon modelling objectives.

5.4. Results

5.4.1. Aboveground biomass and plant carbon changes

5.4.1.1. Ecoregion-specific ecosystem types

Between 2010 and 2019, mean AGB increased in all ecosystem types sampled in the Taiga Shield High Boreal (Table 5.2, Figure 5.4), especially in upland forests at an annual rate of 0.4 Mg ha^{-1} a^{-1} (9-year total 5.7 ± 7.3 Mg ha^{-1}, $p = 0.02$) and in ecotones from upland forest to open fen at an annual rate of 0.6 Mg ha^{-1} a^{-1} (9-year total 5.8 ± 7.8 Mg ha^{-1}, $p < 0.01$). These gained in average 2.4 Mg C ha^{-1} over the 9-year period (Table 5.2, Table S5.2). Mean AGB also increased in ecotones from permafrost plateau to open fen at an annual rate of 0.4 Mg ha^{-1} a^{-1} (9-year total 4.0 ± 4.0 Mg ha^{-1}, $p < 0.05$, 1.7 Mg C ha^{-1}), but increases were not significant in ecotones from upland forest and permafrost plateau to open bog ($p > 0.4$) (Figure 5.4, Table S5.2). Permafrost plateaus had greater increases in AGB (0.6 Mg ha^{-1} a^{-1}, 9-year total 5.2 ± 6.7 Mg ha^{-1}, $p = 0.02$) compared to peatlands, gaining in total 2.2 Mg C ha^{-1}. Open fens adjacent to lakes and open bogs in bedrock depressions also shifted to greater AGB and plant C at an annual rate of 0.1 Mg ha^{-1} a^{-1} (9-year total 1.0 ± 2.3 Mg ha^{-1}, $p < 0.01$, 0.4 Mg C ha^{-1}, and 0.5 ± 1.5 Mg ha^{-1}, $p < 0.001$, 0.2 Mg C ha^{-1}, respectively) (Table S5.2, Figure 5.4). The mean relative increase in open fens (46%) was the highest sampled within the ecoregion. Spatially explicit changes (Figure 5.5) also showed AGB increases occurring mainly within and around bedrock outcrops and in open fens.

Table 5.2. Distribution of sampled aboveground biomass change (ΔAGB) per ecoregion-specific ecosystem type, pooled ecosystem types per ecoregion, and ecosystem types pooled across ecoregions.

	ΔAGB (Mg ha^{-1} a^{-1})	ΔAGB (Mg ha^{-1})			ΔAGB relative to 2010 (%)		Δ plant C (Mg C ha^{-1})	
Stratum	Mean	Mean	SD	IQR	Mean	IQR	Mean	SD
Ecoregion and ecoregion-specific ecosystem types								
Taiga Plains Mid Boreal	*0.22*	*2.0*	*14.9*	*-0.9*	*7.0*	*-4.0*	*0.8*	*6.2*
Upland (UF)	-0.19	-1.7	25.5	-3.1	-2.0	-5.0	-0.7	10.6
Peatland complex	0.34	3.1	9.6	2.8	24.0	19.0	1.3	4.0
Permafrost plateau (PF)	0.73	**6.6**	11.5	3.0	35.0	19.0	**2.8**	4.8
Ecotone UF to Peatland	0.03	0.3	14.5	-0.1	1.0	0.0	0.1	6.0
Ecotone PF to Peatland	0.28	2.5	8.6	1.0	20.0	7.0	1.0	3.6
Peatland	0.23	2.1	5.3	2.9	47.0	80.0	0.9	2.2
Bog	0.19	1.7	4.0	2.5	38.0	60.0	0.7	1.6
Fen	0.27	2.4	6.3	**3.4**	**57.0**	**123.0**	1.0	2.6
Taiga Plains High Boreal	*-0.10*	*-0.9*	*13.5*	*-0.2*	*-2.0*	*0.0*	*-0.4*	*5.6*
Upland (UF)	-0.01	-0.1	17.6	3.2	0.0	8.0	-0.05	7.3
Peatland complex	-0.14	-1.3	10.8	-3.5	-6.0	-13.0	-0.5	4.5
Ecotone UF to Peatland	-0.29	**-2.6**	14.0	**-8.1**	-6.0	**-19.0**	-1.1	5.8
Peatland	-0.08	-0.7	9.1	-1.2	-6.0	-8.0	-0.3	3.8
Bog	-0.02	-0.2	9.5	1.4	-2.0	9.0	-0.1	4.0
Fen	-0.11	-1.0	8.9	-1.0	**-8.0**	-8.0	-0.4	3.7
Taiga Shield High Boreal	*0.44*	*4.0*	*6.9*	*3.9*	*20.0*	*14.0*	*1.7*	*2.9*
Upland (UF)	0.63	**5.7**	7.3	4.2	14.5	16.0	**2.4**	3.1
Peatland complex	0.41	3.7	6.8	5.5	22.8	25.1	1.5	2.8
Permafrost plateau (PF)	0.58	5.2	6.7	1.6	19.7	7.8	2.2	2.8
Ecotone UF to Peatland	0.51	4.6	7.3	**8.6**	**31.9**	**63.7**	1.9	3.0
Ecotone PF to Peatland	0.43	3.9	7.0	2.0	25.2	11.1	1.6	2.9
Peatland	0.23	2.1	6.2	3.7	21.7	46.5	0.9	2.6
Bog	0.06	0.5	1.5	0.1	31.6	17.7	0.2	0.6
Fen	0.28	2.5	6.8	5.6	21.4	44.3	1.1	2.8
Ecosystem types pooled across ecoregions								
Upland (UF)	0.04	0.4	20.8	-0.3	1.0	0.0	0.2	8.7
Peatland complex	0.29	2.6	9.2	3.2	17.0	16.0	1.1	3.8
Permafrost plateau (PF)	0.68	**6.1**	10.0	**1.4**	**28.0**	7.0	**2.5**	4.2
Ecotone UF to Peatland	0.04	0.4	13.2	-2.9	1.0	-4.0	0.1	5.5
Ecotone PF to Peatland	0.32	2.9	8.2	0.9	22.0	8.0	1.2	3.4

Peatland	0.14	1.3	6.9	1.0	16.0	12.0	0.5	2.9
Bog	0.12	1.1	5.7	1.2	17.0	**18.0**	0.5	2.4
Fen	0.16	1.4	7.5	0.9	15.0	9.0	0.6	3.1

IQR: Interquartile range (3rd quartile – 1st quartile); change derived as IQR 2019 – IQR 2010; increases are shown in blue, decreases in brown, greatest increases/decreases per ecosystem type in bold

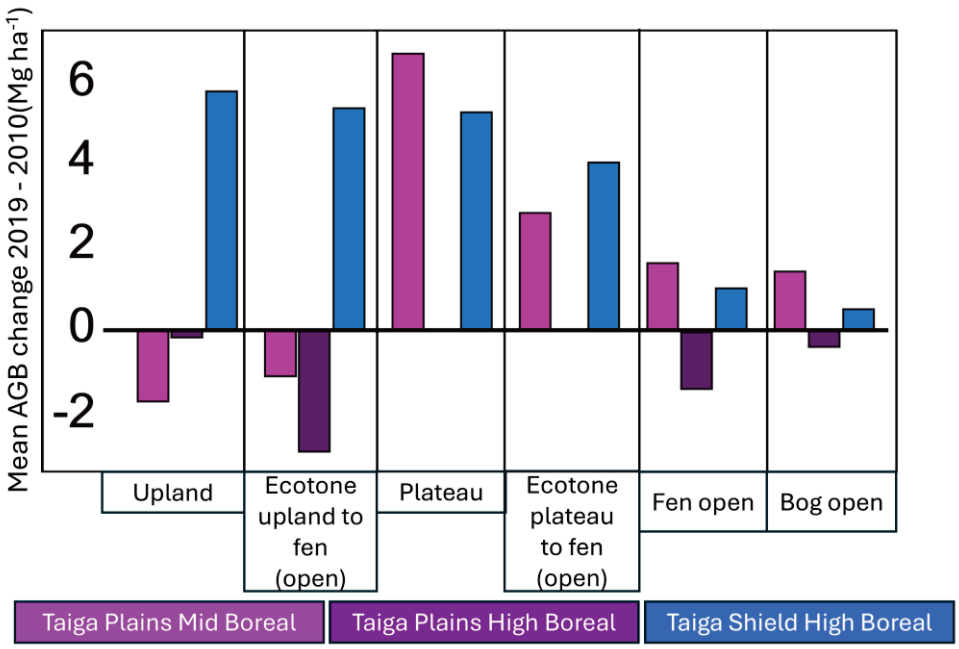

Figure 5.4. Most important mean AGB changes (Mg ha^{-1}) for ecoregion-specific ecosystem types from 2010 to 2019.

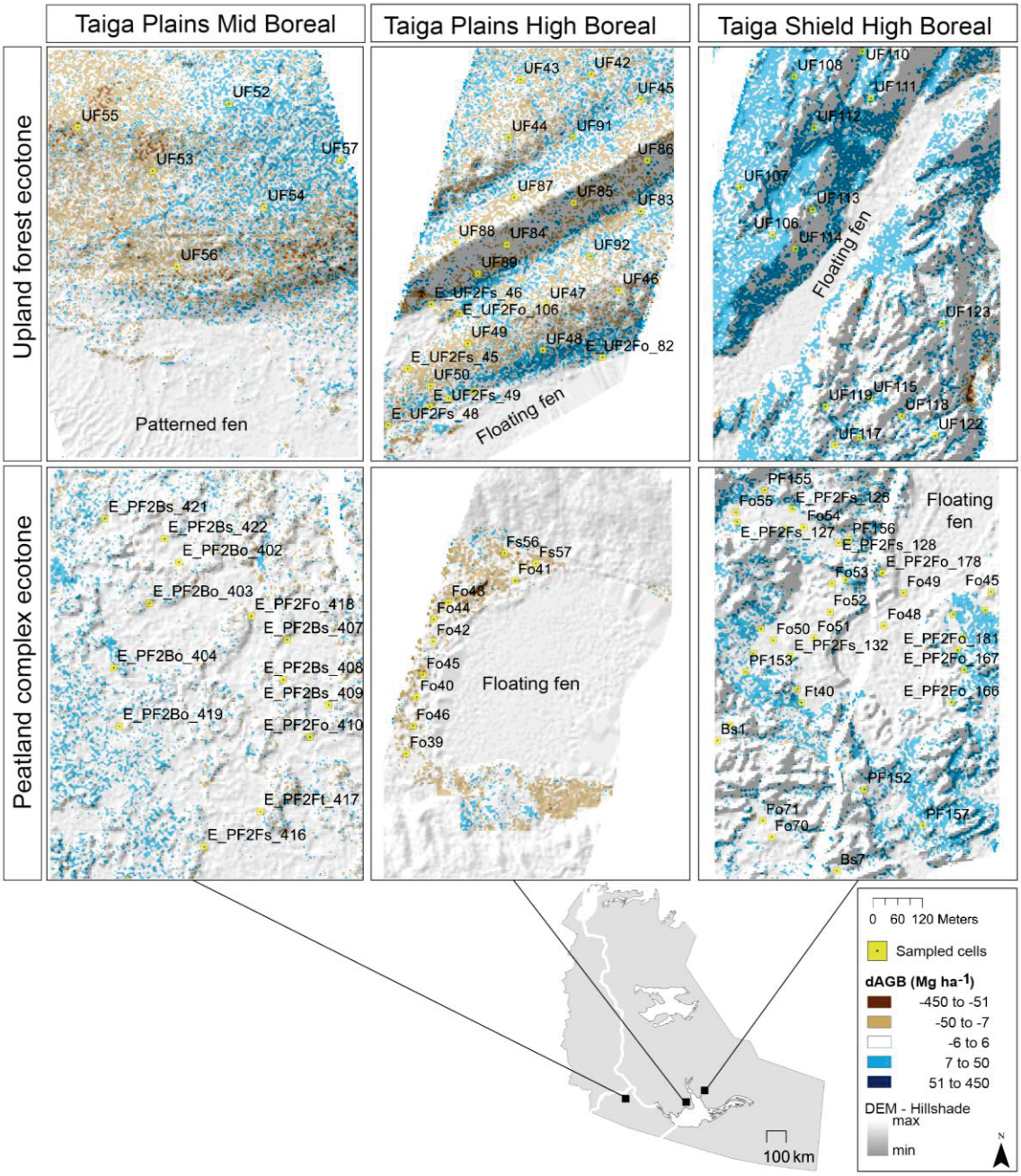

Figure 5.5. Aboveground biomass change (dAGB) per ecoregion in upland forests and peatland complexes and their ecotones. A lidar DEM-based hillshade model indicates terrain variation. Sampled grid cells are labelled based on 2010 conditions as upland forest (UF), forest on permafrost plateau (PF), Bog (B), Fen (F). Peatland form indicated as open (o), shrubby (s), treed (t). Ecotones (E) are labelled starting from UF/PF to (2) peatland class and form. A majority filter was applied to emphasize the main changes.

A mean decrease in AGB and plant C over the 9-year period was observed in all ecosystem types sampled within the Taiga Plains High Boreal (Figure 5.4), except in ecotones from upland forest to open bog (5.3% mean relative increase) (Table 5.2, Table S5.2). Mean relative decreases ranged from -0.2% in upland forests (-0.1 Mg ha^{-1} a^{-1}, 9-year total -0.1 ± 17.6 Mg ha^{-1}, -0.05 Mg C ha^{-1}) to -20.4% in open fens (-0.2 Mg ha^{-1} a^{-1}, 9-year total -1.4 ± 9.2 Mg ha^{-1}, -0.6 Mg C ha^{-1}). However, decreases were statistically not significant in all ecosystem types ($p > 0.4$) and some grid cells in upland forests and ecotones from upland forest to fen increased in AGB (Figure 5.5).

A mean decrease was also observed in upland forests in the Taiga Plains Mid Boreal at an annual rate of -0.2 Mg ha^{-1} a^{-1} (-1.7 ± 25.5 Mg ha^{-1}, $p = 0.9$, -0.7 Mg C ha^{-1}), while AGB in peatland complexes increased at a mean annual rate of 0.3 Mg ha^{-1} a^{-1} (9-year total 3.1 ± 9.6 Mg ha^{-1}, $p < 0.0001$, 1.3 Mg C ha^{-1}) (Table 5.2, Figure 5.4). This was due to large mean increases in permafrost plateaus at an annual rate of 0.7 Mg ha^{-1} a^{-1} (9-year total 6.6 ± 11.5 Mg ha^{-1}, $p < 0.0001$, 2.8 Mg C ha^{-1}) (Table 5.2, Figure 5.4) and in ecotones from permafrost plateau to open bog and fen at an annual rate of 0.3 Mg ha^{-1} a^{-1} (9-year total 2.4 ± 7.5 Mg ha^{-1}, $p < 0.0001$, 1.0 Mg C ha^{-1}, and 2.8 ± 9.5 Mg ha^{-1}, $p < 0.001$, 1.2 Mg C ha^{-1}, respectively) (Table S5.2). Mean AGB also increased in ecotones from upland forest to open and treed bog but decreased in ecotones from upland forest into open and treed fen, but were not significant ($p > 0.1$) and increases seemed to balance decreases (Figure 5.5). Increases at an annual rate of 0.2 Mg ha^{-1} a^{-1} in both open fens (9-year total 1.6 ± 2.7, $p < 0.0001$, 0.7 Mg C ha^{-1}) and open bogs (9-year total 1.4 ± 2.1 Mg ha^{-1}, $p < 0.0001$, 0.6 Mg C ha^{-1}) exceeded those found in the Taiga Shield High Boreal. These were the largest

relative mean increases sampled in the study region (123% and 154 %, respectively) (Figure 5.4, Table S5.2).

5.4.1.2. Pooled ecosystem types per ecoregion

Aggregating sampled AGB and plant C changes across ecosystem types per ecoregion showed that overall, mean AGB increases were two times greater in the Taiga Shield High Boreal (0.4 Mg ha^{-1} a^{-1}, 9-year total 4.0 ± 6.9 Mg ha^{-1}, $p < 0.001$, 1.7 Mg C ha^{-1}) than in the Taiga Plains Mid Boreal (0.2 Mg ha^{-1} a^{-1}, 9-year total 2.0 ± 14.9 Mg ha^{-1}, $p < 0.001$, 0.8 Mg C ha^{-1}) (Table 5.2). Aggregated mean AGB slightly decreased in the Taiga Plains High Boreal at an annual rate of -0.1 Mg ha^{-1} a^{-1} (9-year total -0.9 ± 13.5 Mg ha^{-1}, $p = 0.9$, -0.4 Mg C ha^{-1}) (Table 5.2).

5.4.1.3. Ecosystem types pooled across ecoregions

Across the southern NWT, mean AGB increases from 2010 to 2019 were 6.5 times greater in peatland complexes (0.3 Mg ha^{-1} a^{-1}, 9-year total 2.6 ± 9.2 Mg ha^{-1}, $p < 0.00001$) compared to upland forests (0.04 Mg ha^{-1} a^{-1}, 9-year total 0.4 ± 20.8 Mg ha^{-1}, $p = 0.5$, Table 5.2) when sampled ecosystem types were pooled across all three ecoregions. Increases in plant C over the 9-year period were equivalent to 1.1 Mg C ha^{-1} and 0.2 Mg C ha^{-1}, respectively. Within peatland complexes, an overall mean relative increase of 28% on permafrost plateaus resulted in a gain that was ~15 times greater than in sampled upland forests over the 9-year period (Table 5.2). This increase was the highest sampled in the region (0.7 Mg ha^{-1} a^{-1}, 9-year total 6.1 ± 10.0 Mg ha^{-1}, $p < 0.00001$, 2.5 Mg plant C ha^{-1}). In permafrost plateau to peatland ecotones, mean AGB increases were the second highest (0.3 Mg ha^{-1} a^{-1}, 9-year total 2.9 ± 8.2 Mg ha^{-1}, $p < 0.001$, 1.2 Mg C ha^{-1}). Here, ecotones from permafrost plateau to open fen and bog were significant ($p < 0.0001$), while those to

treed fen and bog were not ($p > 0.1$). Ecotones from upland forest to treed fen were the only sampled ecosystem type within the region that in average lost AGB and plant C within the decade at an annual rate of -0.4 Mg ha^{-1} a^{-1} (9-year total -3.3 ± 20.3 Mg ha^{-1}, $p = 0.7$, -1.4 Mg C ha^{-1}). Within peatlands, sampled mean AGB increases were ~2 times greater in treed fens (0.4 Mg ha^{-1} a^{-1}, 9-year total 3.2 ± 10.0 Mg ha^{-1}, $p = 0.1$, 1.3 Mg C ha^{-1}) compared to treed bogs (0.2 Mg ha^{-1} a^{-1}, 9-year total 1.5 ± 8.6 Mg ha^{-1}, $p < 0.05$, 0.6 Mg C ha^{-1}), while this was reversed in open bogs (0.1 Mg ha^{-1} a^{-1}, 9-year total 0.9 ± 2.6 Mg ha^{-1}, $p < 0.0001$, 0.4 Mg C ha^{-1}) compared to open fens (0.06 Mg ha^{-1} a^{-1}, 9-year total 0.5 ± 5.6 Mg ha^{-1}, $p < 0.0001$, 0.2 Mg C ha^{-1}). Across the study region, relative increases were also greatest in open bogs (39%). These regionally high increases in open bogs caused a shift in the vegetation structure towards increased variability that has more than doubled (113% dIQR, Table S5.3). As a result of the greater structural heterogeneity in open bogs, general bog and fen ecosystems (significantly different in 2010 ($p < 0.0001$)) moved towards more similar structural distribution in 2019 ($p = 0.02$).

5.4.2. Antecedent vegetation structural conditions

In areas within upland forests and permafrost plateaus in the Taiga Plains Mid Boreal that were dominated by short-stature vegetation (≤ 4.5 m) in 2010, AGB and plant C was in average gained. Losses occurred in areas dominated by tall-stature vegetation (> 4.5 m in 2010) (Figure 5.6b). In all other ecosystem types this height threshold occurred at 2.0 m, whereby AGB was gained in areas below and lost above. The AGB and plant C gains from short-stature vegetation outweighed the losses from tall-stature vegetation, resulting in the net AGB and plant C gain in each ecosystem type, except in upland forests and in upland forest to fen ecotones (Table 5.2, Table S5.2).

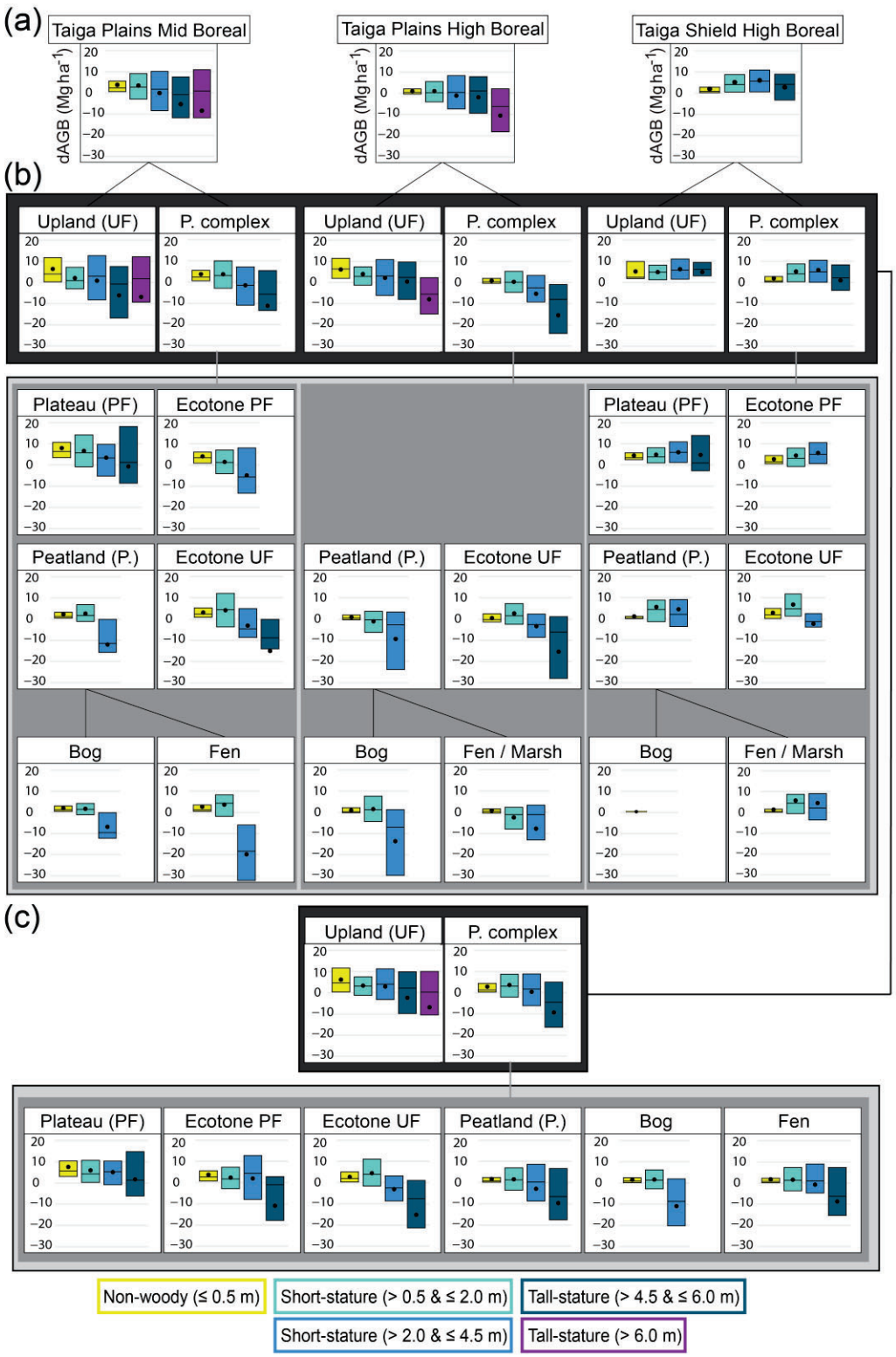

Figure 5.6. Boxplots of aboveground biomass change (dAGB, Mg ha^{-1}) per plant functional group evaluated for: a) pooled ecosystem types per ecoregion, b) ecoregion-specific ecosystem types, and c) ecosystem types pooled across ecoregions. Mean change represented as black points, median change as black lines, and 1st to 3rd quartiles as colored box.

In these ecosystem types however, AGB gains greatly reduced losses. The large gains in vegetation ≤ 2.0 m in the ecoregion resulted in an overall net AGB and plant C gain when changes in sampled ecosystem types were pooled across the ecoregion (Table 5.2, Figure 5.6a).

In the Taiga Plains High Boreal, upland forests gained AGB and plant C on average in sampled areas that were dominated by vegetation growing up to 6 m in height, while mean losses occurred above this threshold (Figure 5.6b). Gains and losses on either side of the threshold were approximately equal in magnitude, resulting in a mean change close to zero (Figure 5.6b). In all other ecosystem types, AGB and plant C gains found in vegetation growing ≤ 2.0 m did not outweigh losses from vegetation above this threshold (Figure 5.6b), resulting in a net loss for the complete sampled ecoregion (Table 5.2, Figure 5.6a).

In the Taiga Shield High Boreal, AGB and plant C was gained in all vegetation height bins in all sampled ecosystem types, except in ecotones from upland forest to peatland (bog and fen) in areas dominated by vegetation growing > 2.0 m and ≤ 4.5 m (Figure 5.6b). However, in this height range, greatest gains were found in upland forests, permafrost plateaus, and ecotones from permafrost plateau into fen, which outweighed those losses. In general, the gains in short-stature vegetation in combination with gains in tall-stature vegetation (upland forests and permafrost plateaus) resulted in the sampled net gain in the ecoregion that was greater than in the Taiga Plains Mid Boreal (Table 5.2, Figure 5.6a) (described above).

5.4.3. Regional shifts in dominant vegetation structure

To better understand whether ecosystems shifted in dominant vegetation structure, shifts in the relative proportions of the number of sampled areas dominated by a plant functional group were analyzed (herein 'samples') (Figure 5.7). In 2010 most samples were categorized as non-woody vegetation (≤ 0.5 m: 31.3 % Taiga Plains High Boreal to 46.1% Taiga Plains Mid Boreal) (Figure 5.7a). Within a decade, this shifted to a dominance in short-stature vegetation (≤ 2.0 m: 36.7 % Taiga Plains Mid Boreal; ≤ 4.5 m: 33.3% Taiga Shield High Boreal), and tall-stature vegetation (> 4.5m: 27.6 % Taiga Plains High Boreal).

The greatest shifts leading to AGB and plant carbon gains in the landscape were also from non-woody to short-stature vegetation in the Taiga Plains Mid Boreal (19.6%) and occurred within short-stature vegetation (from ≤ 2 m to ≤ 4.5 m) in the Taiga Shield High Boreal (20.4%) (Table 5.3, Figure 5.7a). Samples in the Taiga Plains High Boreal shifted in even proportions from non-woody to tall-stature vegetation (9.8% to 10.5%). Greatest shifts leading to losses in AGB and plant carbon occurred in the Taiga Plains High Boreal across all plant functional groups (Table 5.3). However, losses were comparatively low (≤ 1.9%). A replacement of tall-stature with non-woody vegetation was not observed (Figure 5.7a).

Table 5.3. Dominant shifts in vegetation structure based on proportional change in numbers of samples (%) per plant functional group between 2010 and 2019 for ecoregions.

Main forms of structural shifts	Taiga Plains Mid Boreal	Taiga Plains High Boreal	Taiga Shield High Boreal
Gain in AGB and plant C			
non-woody to short-stature	**19.6**	9.8	12.8
within short-stature	11.9	10.5	**20.4**
short-stature to tall-stature	5.5	**10.1**	9.3
Loss of AGB and plant C			
short-stature to non-woody	0.8	**1.9**	0.5
within short-stature	0.5	**1.0**	0.0
tall-stature to short-stature	0.6	**1.3**	0.2
Net gains			
non-woody to short-stature	**18.8**	7.9	12.3
within short-stature	11.4	9.5	**20.4**
short-stature to tall-stature	4.9	8.8	**9.1**

Gains are shown in blue, losses in brown, greatest shifts per plant functional group in bold

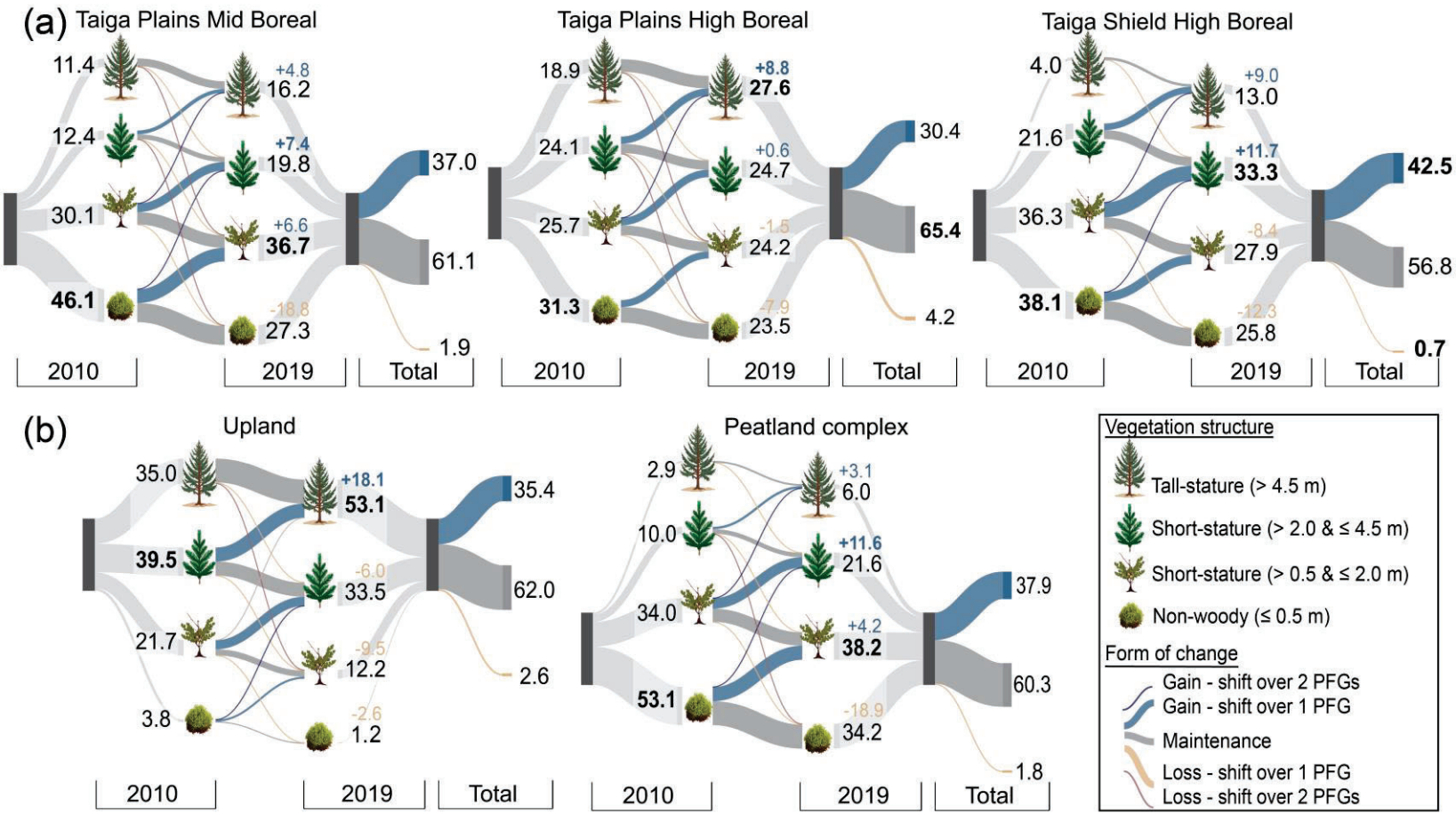
(a) Taiga Plains Mid Boreal
11.4
12.4
30.1
46.1
+4.8
16.2
+7.4
19.8
+6.6
36.7
-18.8
27.3
37.0
61.1
1.9
2010
2019
Total
Taiga Plains High Boreal
18.9
24.1
25.7
31.3
+8.8
27.6
+0.6
24.7
-1.5
24.2
-7.9
23.5
30.4
65.4
4.2
2010
2019
Total
Taiga Shield High Boreal
4.0
21.6
36.3
38.1
+9.0
13.0
+11.7
33.3
-8.4
27.9
-12.3
25.8
42.5
56.8
0.7
2010
2019
Total
(b) Upland
35.0
39.5
21.7
3.8
+18.1
53.1
-6.0
33.5
-9.5
12.2
-2.6
1.2
35.4
62.0
2.6
2010
2019
Total
Peatland complex
2.9
10.0
34.0
53.1
+3.1
6.0
+11.6
21.6
+4.2
38.2
-18.9
34.2
37.9
60.3
1.8
2010
2019
Total
Vegetation structure
Tall-stature (> 4.5 m)
Short-stature (> 2.0 & ≤ 4.5 m)
Short-stature (> 0.5 & ≤ 2.0 m)
Non-woody (≤ 0.5 m)
Form of change
Gain - shift over 2 PFGs
Gain - shift over 1 PFG
Maintenance
Loss - shift over 1 PFG
Loss - shift over 2 PFGs

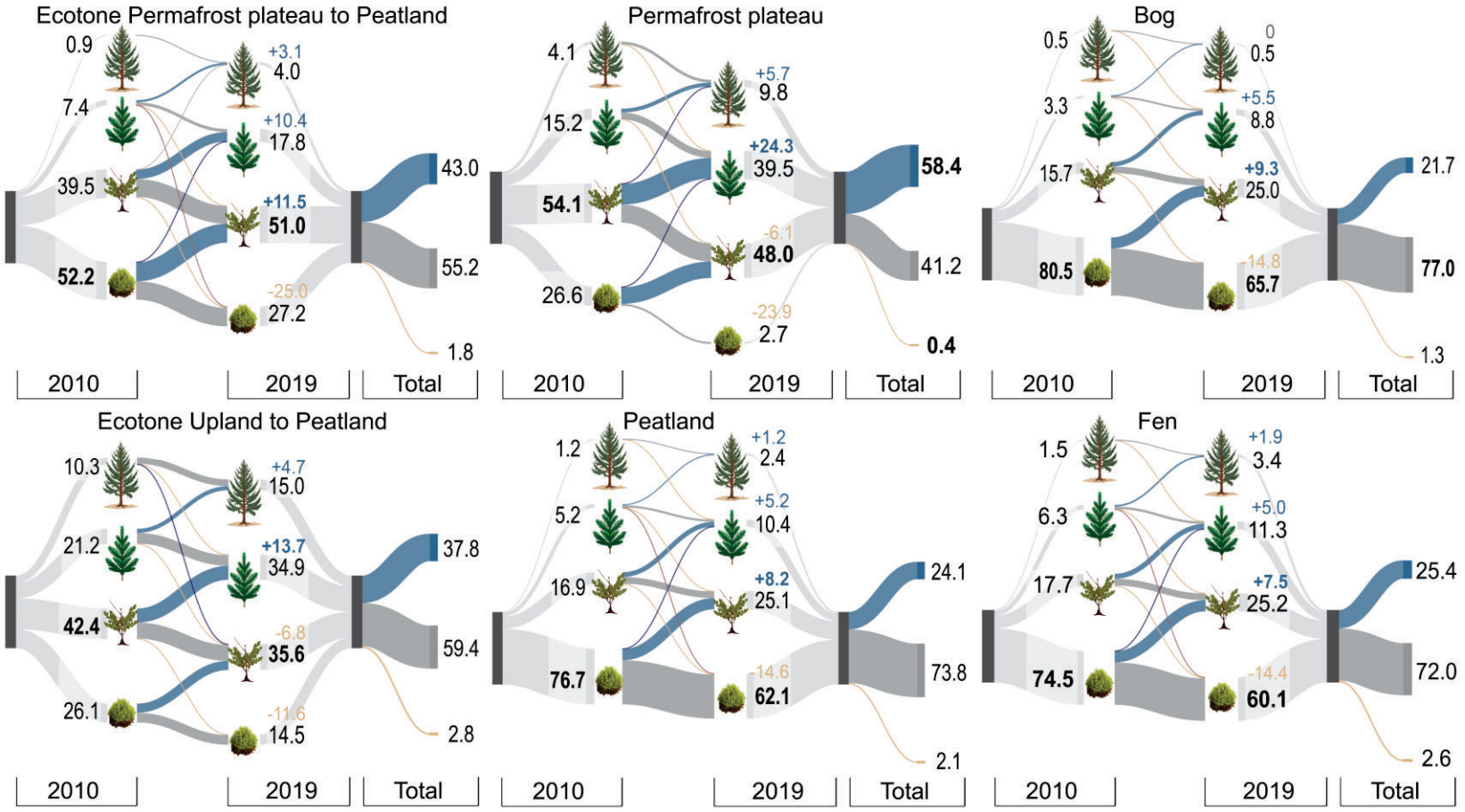

Figure 5.7. Sankey diagrams showing shifts in the relative proportions of the number of sampled areas dominated by a plant functional group (PFG) from 2010 to 2019 (%) for a) pooled ecosystem types per ecoregion, and b) ecosystem types pooled across ecoregions. Gains/losses (in blue/brown) (%) refer to increases/decreases of AGB and plant C.

In total, the greatest (lowest) proportions of samples gaining (losing) AGB and plant C, were found in the Taiga Shield High Boreal (42.5% (0.7%)). Within the Taiga Plains, proportions of samples that gained AGB and plant C were greater in the Mid Boreal (37%), while those that lost AGB and plant C were greater in the High Boreal (4.2%). The Taiga Plains High Boreal however had the greatest proportion of samples that maintained dominant vegetation structure (65.4%) (Figure 5.7a).

Comparing ecosystem types pooled across ecoregions, sampled upland forests shifted from a dominance in short-stature (≤ 4.5 m: 39.5%) to tall-stature vegetation (53.1%) (Figure 5.7b). Within peatland complexes, shifts in dominant vegetation structure were observed only in permafrost plateau to peatland ecotones from non-woody (52.2%) to short-stature vegetation (≤ 2.0 m: 51.0%). All other sampled ecosystem types within peatland complexes maintained their dominant vegetation structure (non-woody: bogs and fens, short-stature vegetation: permafrost plateaus and upland to peatland ecotones) (Figure 5.7b). However, the number of samples in the non-woody plant functional group reduced by ~ 20% in bogs and fens and by ~50% - 100% in upland to peatland ecotones and permafrost plateaus, respectively (Figure 5.7b). Simultaneously, the number of samples increased by up to 160% in the short-stature plant functional group (permafrost plateaus).

Greatest shifts leading to AGB and plant carbon gains in the landscape were found in permafrost plateau to peatland ecotones (non-woody to short-stature vegetation, 26.8%), in permafrost plateaus (within short-stature vegetation, 28.6%), and in upland forests (short- to tall-stature vegetation, 19.8%) (Table 5.4). Shifts leading to AGB and plant C losses were greatest in fens (short-stature to non-woody vegetation), upland forest to

peatland ecotones (within short-stature vegetation), and in upland forests (tall- to short-stature vegetation). However, losses occurred in less than 2% of the samples.

In total, the greatest (lowest) proportions of samples gaining (losing) AGB and plant C, respectively, were found in permafrost plateaus (58.4% (0.4%)) (Figure 5.7b). Bogs had the greatest proportion of samples that maintained vegetation structure (77%).

Table 5.4. Dominant shifts in vegetation structure based on proportional change in numbers of samples (%) per plant functional group between 2010 and 2019 for pooled ecosystem types.

Main forms of structural shifts	Up-land	Peatland complex	Permafrost plateau	Ecotone UF	Ecotone PF	Peat-land	Bog	Fen
Gain in AGB and plant C								
Non-woody to short-stature	3.0	20.0	23.9	12.7	**26.8**	15.9	15.4	16.1
Within short-stature	12.6	14.5	**28.6**	19.4	13.1	6.7	6.1	7.0
Short- to tall-stature	**19.8**	3.4	5.9	5.7	3.1	1.5	0.2	2.3
Loss of AGB and plant C								
Short-stature to non-woody	0.3	1.1	0.0	1.0	1.7	1.3	0.5	**1.8**
Within short-stature	0.6	0.4	0.2	**0.8**	0.1	0.4	0.5	0.4
Tall- to short-stature	**1.7**	0.3	0.2	1.0	0.0	0.4	0.3	0.4
Net gains								
Non-woody to short-stature	2.7	18.9	23.9	11.7	**25.1**	14.6	14.9	14.3
Within short-stature	12	14.1	**28.4**	18.6	13	6.3	5.6	6.6
Short- to tall-stature	**18.1**	3.1	5.7	4.7	3.1	1.1	-0.1	1.9

Gains are shown in blue, losses in brown, greatest shifts per plant functional group in bold

5.4.4. Environmental and climatic drivers of aboveground biomass change and maintenance

To better understand the range of variability of drivers that promote AGB changes and maintenance, important regional climatic and local to proximal environmental variables were identified. Univariate correspondence between AGB change and driver variable was weak for all strata examined (Pearson correlation coefficient $\geq$ -0.2 and $\leq$ 0.2), except for

the correspondence between AGB change and elevation change (5 m x 5 m) in permafrost plateaus (Pearson correlation coefficient = -0.5, Table 5.5). In comparison, the interaction between drivers and scales using random forest improved regression results such that models were significant ($p < 0.001$) for all strata examined. Explained model variance was higher when importance of drivers was determined per ecosystem type (pooled across ecoregions, 22% - 41%) than per ecoregion (pooled ecosystem types, 16% - 24%) (Table 5.6). Using 2010 AGB values as calibration variable was critical, as the magnitudes and mechanisms of change were dependent on vegetation structure at starting conditions (previously described).

Table 5.5. Pearson correlation coefficients for the univariate correspondence between aboveground biomass change (2019-2010, Mg ha^{-1}) and driver variable (reported for the scale (m x m) at which correspondence was highest) for ecosystem types pooled per ecoregion and ecosystem types pooled across ecoregions.

Stratum	Elevation		Elevation change		Aspect		Slope		TPI		TWI	
Ecoregion												
Taiga Plains Mid Boreal	-0.1	(90 x 90)	-0.2	(10 x 10)	0.1	(20 x 20)	0.0	(90 x 90)	0.1	(90 x 90)	-0.1	(10 x 10)
Taiga Plains High Boreal	0.1	(10 x 10)	0.1	(60 x 60)	0.1	(15 x 15)	0.1	(90 x 90)	0.1	(90 x 90)	-0.1	(60 x 60)
Taiga Shield High Boreal	0.0	(90 x 90)	0.0	(30 x 30)	0.0	(10 x 10)	0.1	(30 x 30)	0.0	(90 x 90)	-0.2	(20 x 20)
Ecosystem type												
Upland (UF)	-0.2	(5 x 5)	0.0	(90 x 90)	0.1	(20 x 20)	0.1	(90 x 90)	-0.1	(60 x 60)	-0.1	(10 x 10)
Peatland complex	0.0	(5 x 5)	-0.3	(5 x 5)	0.0	(10 x 10)	0.1	(90 x 90)	0.1	(60 x 60)	-0.1	(30 x 30)
Permafrost plateau (PF)	0.1	(5 x 5)	-0.5	(5 x 5)	-0.1	(30 x 30)	0.1	(60 x 60)	0.2	(90 x 90)	-0.1	(60 x 60)
Ecotone UF to Peatland	0.0	(90 x 90)	-0.2	(15 x 15)	0.1	(15 x 15)	0.2	(90 x 90)	-0.1	(90 x 90)	-0.2	(90 x 90)
Ecotone PF to Peatland	-0.1	(90 x 90)	-0.1	(90 x 90)	0.0	(5 x 5)	0.0	(90 x 90)	0.1	(15 x 15)	-0.1	(20 x 20)
Peatland	0.0	(90 x 90)	-0.2	(15 x 15)	-0.1	(60 x 60)	0.0	(5 x 5)	0.0	(30 x 30)	-0.1	(20 x 20)
Bog	0.1	(5 x 5)	-0.3	(15 x 15)	-0.1	(90 x 90)	-0.1	(5 x 5)	0.1	(10 x 10)	0.1	(5 x 5)
Fen	0.0	(90 x 90)	-0.1	(15 x 15)	-0.1	(60 x 60)	0.0	(5 x 5)	0.0	(30 x 30)	-0.1	(15 x 15)

Elevation change (2019-2010), topographical position index (TPI), topographical wetness index (TWI).

Table 5.5. continued

Stratum	Incident radiation		Trend MAAT	Trend TAP	Latitude	Longitude
Ecoregion						
Taiga Plains Mid Boreal	0.1	(90 x 90 m)	-0.2	-0.2	-0.1	0.2
Taiga Plains High Boreal	-0.1	(5 x 5 m)	0.2	0.2	0.2	0.2
Taiga Shield High Boreal	-0.2	(30 x 30 m)	0.0	0.0	0.0	0.0
Ecosystem type						
Upland (UF)	-0.1	(5 x 5 m)	-0.1	-0.2	0.1	0.2
Peatland complex	-0.1	(5 x 5 m)	0.0	-0.1	-0.1	0.1
Permafrost plateau (PF)	-0.1	(5 x 5 m)	-0.4	-0.3	-0.2	0.2
Ecotone UF to Peatland	0.1	(90 x 90 m)	0.2	0.0	0.0	0.0
Ecotone PF to Peatland	-0.2	(90 x 90 m)	-0.1	-0.2	0.1	0.2
Peatland	0.0	(5 x 5 m)	0.1	0.1	0.0	0.0
Bog	0.1	(15 x 15 m)	-0.1	0.0	-0.2	0.0
Fen	-0.1	(90 x 90 m)	0.2	0.1	0.0	0.0

Total incident radiation hours (incident radiation), trends in mean annual air temperature (MAAT) and total annual precipitation (TAP) deviations from climate normals.

Table 5.6. Random forest regression model performance and parameter settings.

Stratum	R^2 mean (%)	R^2 max (%)	R^2 OOB (%)	Ranking stability (%)	Nr. of trees	Mean tree depth	Nr. of sampled parameters
Ecoregion							
Taiga Plains Mid Boreal	24	43	19	40	1000	23	1
Taiga Plains High Boreal	22	46	17	100	1500	17	1
Taiga Shield High Boreal	16	32	11	20	1000	19	1
Ecosystem type							
Upland (UF)	26	63	23	60	1000	19	5
Peatland complex	31	44	25	80	500	23	2
Permafrost plateau (PF)	37	60	27	70	1000	16	1
Ecotone UF to Peatland	33	63	26	100	1000	14	2
Ecotone PF to Peatland	22	41	11	80	500	17	4
Peatland	34	62	25	100	2000	19	1
Bog	41	78	39	50	1000	13	1
Fen	28	59	19	70	2000	17	2

R^2 derived through independent validation datasets (random selection of 20% of the input data) representing the mean and the max of 100 individual model runs. Out-of-bag (OOB) explained model variability was internally computed through bagging. Ranking stability derived as number of times (%) the same ranking was achieved in 10 independent model runs, each run 100 times. Number of randomly sampled parameters used at each split in node.

In general, local to proximal topographical drivers, which relate to the distribution of plant available water in the landscape, were more important than drivers related to regional climatic energy inputs (incident radiation, trend in MAAT) into the system (Figure 5.8). For example, an important topographical driver in ecoregions and ecosystem types containing permafrost was elevation change (Taiga Plains Mid Boreal, Taiga Shield High Boreal, upland forests, permafrost plateaus). In ecosystem types, where changes in vegetation structure were previously observed to be dependent on topographical position relative to the surrounding area (waterlogging in submerged positions, increased woody vegetation on locally raised terrain (Chasmer & Hopkinson, 2017; Dearborn et al., 2021; Kristine M. Haynes et al., 2021), elevation and topographical position were indeed

important drivers of AGB change (ecotones from upland forest and permafrost plateau to peatland, fens). In bogs, elevation was also an important driver. Aspect was an important driver in ecoregions of greater terrain complexity (Taiga Shield High Boreal) and in permafrost plateau to peatland ecotones. For the latter, greater vegetation densification were previously observed in north-west compared to south-east facing slopes (in some peatland complexes) associated with lesser rates of areal permafrost plateau loss and fragmentation (Chasmer & Hopkinson, 2017).

Water inputs into the system (trend in TAP, topographical potential for wetness (TWI)) were important in ecosystem types and ecoregions that are mainly comprised of rapidly draining mineral soils (Taiga Plains High Boreal, upland forests, ecotones form upland forest to peatland). In addition, AGB changes in permafrost plateaus were also driven by trends in TAP. Due to the large area comprised by upland forest and permafrost plateaus in the Taiga Plains Mid Boreal, the trend in TAP was consequently also an important driver when samples were pooled within this ecoregion. In comparison, AGB changes in the Taiga Shield High Boreal, bogs, and in ecotones from permafrost plateau to peatland were driven by trends in MAAT, not TAP. AGB changes in permafrost plateaus, however, were driven by both. Landscape position along the latitudinal climate gradient was only relevant in peatlands (bogs and fens) and in the Taiga Plains High Boreal. In peatlands, magnitudes and mechanisms of vegetation structural changes differed in lower compared to higher latitudes, where peatlands transitioned from extensive areal coverage and deep peat soils (collapse scar bogs, channel fens, Taiga Plains Mid Boreal) to lesser areal coverage and lower peat depths (bogs in bedrock depressions and floating fens around ponds/lakes, Taiga Plains High Boreal, Taiga Shield High Boreal). This transition was

directly captured within the Taiga Plains High Boreal, where samples were distributed across a greater latitudinal gradient (Figure 5.2).

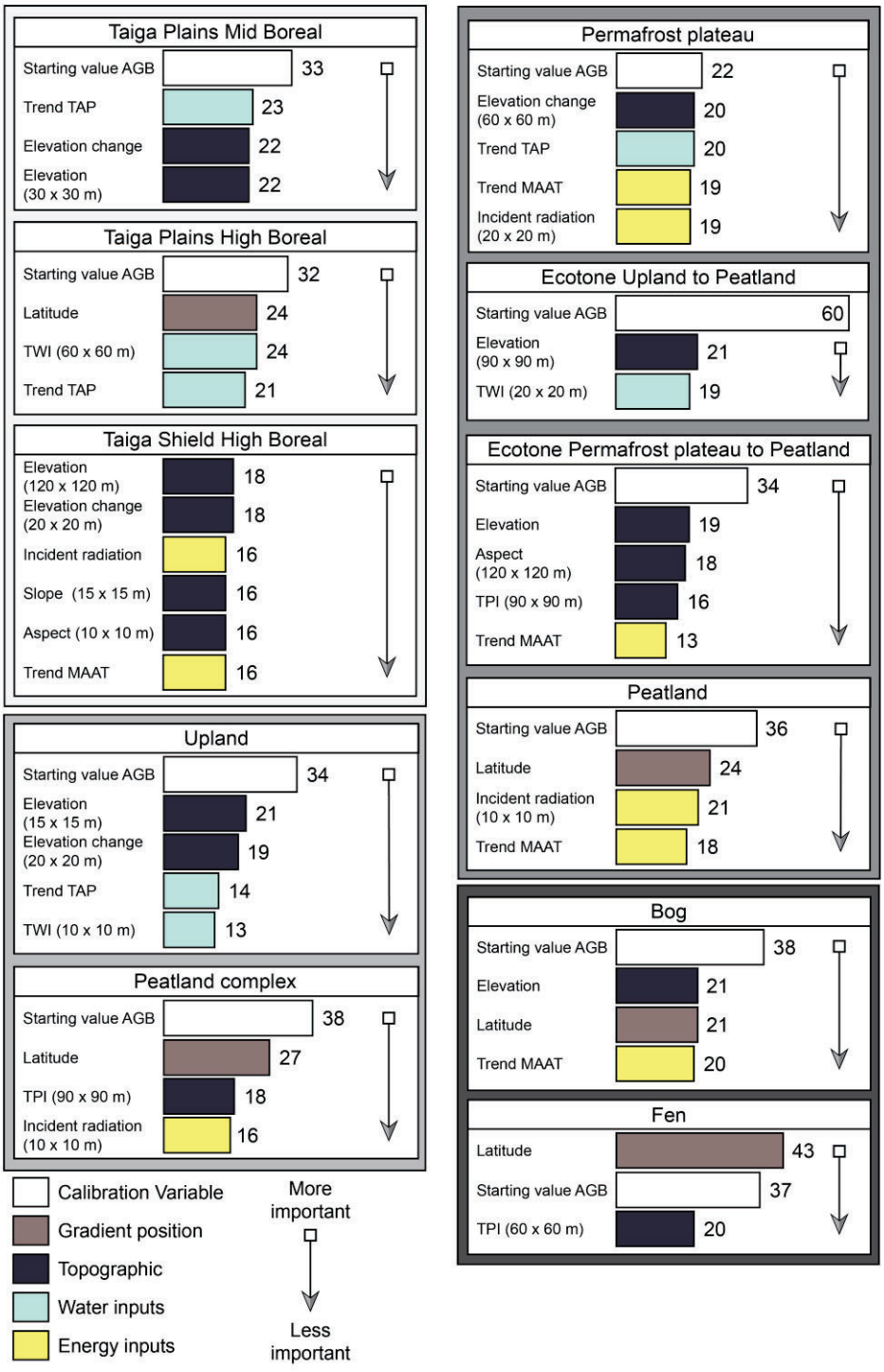

Figure 5.8. Important drivers (%) of AGB change (2019-2010) at relevant scales for sampled ecosystem types pooled per ecoregion and ecosystem types pooled across ecoregions. Drivers represent regional climatic (trends in mean annual air temperature (MAAT) and total annual precipitation (TAP) deviations from climate normals, total incident radiation hours, gradient position) and local to proximal environmental variables (elevation, elevation change (2019-2010), aspect, slope, topographical position index (TPI), and topographical wetness index (TWI)).

5.4.5. Comparison to regional and global aboveground biomass products

A comparison of the results in this study with regional shrub and tree AGB derived within the NASA ABoVE at the same sampling points showed the following: Landsat- and GLAS-based AGB estimates in 2010 were consistently higher compared to this study for ecosystem types dominated by short-stature vegetation and lower for ecosystem types dominated by tall-stature vegetation (Figure 5.9). Largest differences occurred in permafrost plateaus and permafrost plateau to peatland ecotones (up to 24.9 Mg ha^{-1}, 216%), and in upland forests (up to -20.0 Mg ha^{-1}, -23%) (Figure 5.9). The closest correspondence in 2010 AGB was found in ecotones from upland forest to peatland in all three ecoregions (Figure 5.9), specifically to open fen (range in AGB_{2010} difference from -1.2 to 4.2 Mg ha^{-1}, -3% to 100%). This suggests that for a certain mix of short- and tall-stature vegetation structures and variable soil moisture conditions within the grid cell, over- and underestimated AGB balanced to converge to quantities similar to this study. This was also observed in the Taiga Plains High Boreal, where 2010 AGB prediction errors counterbalanced across ecosystem types (Figure 5.9) (difference in mean AGB_{2010} 1.3 Mg ha^{-1}, 4%).

Nevertheless, AGB quantities were assigned incorrectly across strata, as previously suggested by Neigh et al. (2013). In addition, contrary to the assumption that regional inaccuracies would be minimal due to counterbalancing of prediction errors across strata (Neigh et al., 2013; Wang et al., 2021b), 2010 AGB was predicted 27% (Taiga Shield High Boreal) and 39% (Taiga Plains Mid Boreal) higher compared to this study. As a result, carbon stock estimates were inflated in regions where large areal proportions are comprised by ecosystem types dominated by short-stature vegetation (e.g. shrubs, sparse and stunted

trees on shield and within peatland complexes). We assume this is evident in each year of the time series.

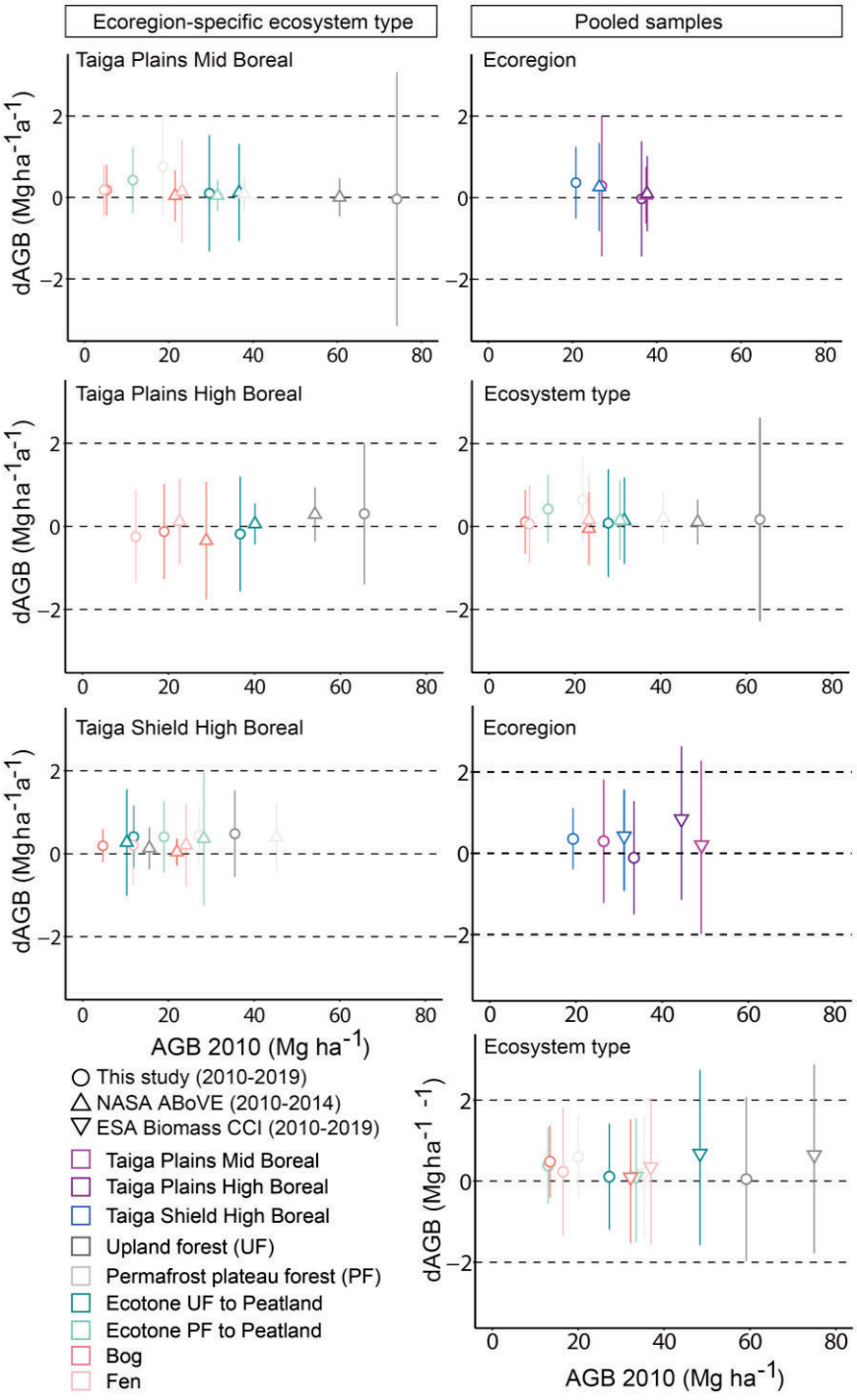

Figure 5.9. Comparison of aboveground biomass change per year (y-axis) relative to starting conditions (2010, x-axis) between this study, boreal-wide NASA ABoVE annual shrub and tree aboveground biomass

maps (Wang et al., 2021), and global ESA Biomass Climate Change Incentive tree aboveground biomass maps (Santoro & Cartus, 2024). Depicted are the mean ± standard deviation of all samples within each stratum.

Annual rates of NASA ABoVE AGB change also differed to those reported in this study and differences were less consistent across vegetation structures (Figure 5.9). Overall, the homogeneous rates of annual AGB change across ecosystem types suggest that subtle differences related to ecosystem-type specific processes were not discernable with the data and methods used (Wang & Friedl, 2019). However, the annual rates of AGB change were derived for a shorter time period (2010 – 2014) and the combination of increases in MAAT and decreases in TAP since 2014 (Figure S5.1) could have increased annual rates in short-stature woody vegetation growth and expansion as observed in this study.

We therefore compared our results to those obtained by the ESA Biomass Climate Change Initiative (Santoro & Cartus, 2024; Santoro et al., 2021) at the same sampling points. We found that 2010 AGB was estimated higher compared to this study in all ecoregions and ecosystem types (Figure 5.9), surpassing recommended deviations of < 20% (for AGB > 50 Mg ha^{-1}) and < 10 Mg ha^{-1} (for AGB < 50 Mg ha^{-1}) by the Global Climate Observing System (GCOS). Deviations were on average 15 Mg ha^{-1} (60%) across ecoregions and 20 Mg ha^{-1} (130%) across ecosystem types, ranging from 11 Mg ha^{-1} in the Taiga Plains High Boreal to 23 Mg ha^{-1} in the Taiga Plains Mid Boreal (33% to 86%) and from 14 Mg ha^{-1} in treed fens to 31 Mg ha^{-1} in ecotones from upland forest to treed fen (27% to 285%). AGB in upland forests and permafrost plateaus was estimated higher by 16 Mg ha^{-1} (27%) and 15 Mg ha^{-1} (77%), respectively.

Annual rates of change were estimated lower for the Taiga Plains Mid Boreal (-0.2 Mg ha^{-1} a^{-1}) and higher for the Taiga Plains High Boreal (0.9 Mg ha^{-1} a^{-1} difference), for which the direction of change was also incorrectly estimated (Figure 5.9), similar to Wang et al. (2021). In the Taiga Shield High Boreal however, AGB was found to increase in similar rates (-0.03 Mg ha^{-1} a^{-1} difference), even though 2010 and 2019 AGB estimates were higher compared to this study. With regards to ecosystem types, differences ranged from -0.5 Mg ha^{-1} a^{-1} in permafrost plateaus to 0.5 Mg ha^{-1} a^{-1} in upland forests and 0.7 Mg ha^{-1} a^{-1} in ecotones from permafrost plateau to treed bog. Higher estimations in ecotones from upland forest to open fen were counterbalanced by lower estimations in ecotones from upland forests to treed fen, resulting in the lowest deviance in annual AGB change (0.005 Mg ha^{-1} a^{-1}).

5.5. Discussion

This study is the first of its kind to quantify decadal short-to-tall-stature vegetation structural and plant C changes at the plot level for a range of ecosystem types distributed across sensitive and rapidly changing environmental and climatic gradients from the Taiga Plains to the Shield of northwestern Canada. We leveraged extensive field data (~1306 forest and micro plots including mensuration information from bryophytes and lichen to tall-stature trees) and shrub and short-stature tree allometric equations (Flade et al., 2020, 2021) with coincident airborne lidar data and a bi-temporal shrub-to-tree AGB model (Flade et al., 2024). The innovation to model shrub-to-tree AGB across changing relationships between lidar point clouds and AGB magnitudes as a) ecosystems change form, b) ecosystem boundaries expand and recede, and c) airborne lidar technologies develope, enabled us to advance understanding of gradual climate-mediated vegetation

structural changes in a region identified as important climate regulator yet source of critical uncertainty (IPCC, 2023).

5.5.1. Vegetation mortality

Analogous to other studies, we found decreases in mean AGB and plant C in areas dominated by tall-stature vegetation (> 4.5 m, upland forests, permafrost plateaus) and vegetation > 2.0 m (ecotones from upland forest and permafrost plateau to peatland, peatlands) in the broader Taiga Plains Mid and High Boreal (Figure 5.6). For example, on a local scale, previous studies found black spruce mortality outweighed recruitment in permafrost plateaus and at ecotones from permafrost plateau to peatland in the western part of the Taiga Plains Mid Boreal at the boundary of sporadic and discontinuous permafrost (Baltzer et al., 2014; Carpino et al., 2018; Chasmer & Hopkinson, 2017; Dearborn et al., 2021). This was associated with both increased drying in the soil column above a deepening frost table (permafrost plateaus), and waterlogging of soils due to lateral runoff (ecotones from permafrost plateau to peatland) as permafrost thawed (Baltzer et al., 2014; Dearborn et al., 2021; Patankar et al., 2015; Sniderhan & Baltzer, 2016).

On a regional scale, a decline in MODIS-derived percent tree cover (250 m x 250 m grid cells) between 2000 and 2014 was also observed in poorly draining areas associated with waterlogging due to permafrost thaw at the southern margin of the Taiga Plains Mid Boreal (Helbig, Pappas, et al., 2016). In well-draining areas, mean decreases were small, similar to our results in the Taiga Plains High Boreal (Helbig, Pappas, et al., 2016). Using optical remote sensing vegetation indices (30 m x 30 m grid cells) and tree mortality simulations, Liu et al. (2023) estimated an annual above and below ground biomass loss of

3.0 ± 0.6 Mg ha^{-1} a^{-1} (between 1970 and 2020) in boreal forests in Canada associated with drought-induced tree mortality. However, rates of tree regeneration and short-stature vegetation dynamics were not included in the modelling workflow, and changes in upland forests were not separate from those in lowlands.

5.5.2. Including short-stature vegetation in AGB and plant C accounting

Results here also show that between 2010 and 2019, AGB and plant C gains in short-stature vegetation (≤ 4.5 m in upland forests and permafrost plateaus, ≤ 2.0 m in ecotones and peatlands) were significant (Figure 5.6) and partially reduced (upland forests, ecotones from upland forest to fen) or outweighed (all other ecosystem types) losses in all sampled ecosystem types in the Taiga Plains Mid Boreal (Table 5.2). The dominant shift was from non-woody to short-stature vegetation (≤ 2.0 m, Figure 5.7). In addition, in the Taiga Shield High Boreal, where increases in short-stature vegetation occurred in tandem with increases in tall-stature vegetation (most pronounced in and around bedrock outcrops and fens, Figure 5.5), mean AGB and plant C gains were twice as high as in the Taiga Plains Mid Boreal (Table 5.2). Most of the areas sampled shifted from non-woody to short-stature vegetation (≤ 4.5 m, Figure 5.7). Across the study region, permafrost plateaus gained 15 times as much AGB and plant C than upland forests. This is confounding given that some of the most productive upland forests are located within the Taiga Plains Mid Boreal (milder climate and rich soils), while a harsher climate and confinement of tree expansion to depressions in and around bedrock outcrops were known to be limiting factors for upland forest productivity levels in the Taiga Shield High Boreal in the past (Ecosystem Classification Group, 2009). In addition, in peatland complexes, accelerated rates of permafrost thaw since 1997/1998 (Chasmer & Hopkinson, 2017) resulted in widespread permafrost plateau

forest loss exceeding recruitment in the prior decade (Taiga Plains Mid Boreal, Baltzer et al., 2014). This suggests that the increasing trend in MAAT and decreasing trend in TAP since 2010 (Figure S5.1), may have altered conditions in both ecoregions in favor of woody vegetation establishment, growth, and expansion, especially in low-lying areas.

Increases in short-stature vegetation cover in the Taiga Plains Mid Boreal, and tree cover in the Taiga Shield High Boreal were observed in other studies in localized areas (Chasmer and Hopkinson 2017 (Scotty Creek watershed 2008 – 2015), and Sniderhan et al., 2023 (Baker Creek watershed, 1976 – 2016), respectively). Both vegetation structural changes were associated with increased drying conditions. However, analogous to these studies and given the variable driver importance results, we argue that the underlying mechanisms driving these changes differed between the two ecoregions.

5.5.3. Environmental and hydro-climatic drivers of aboveground biomass changes and maintenance

For the Taiga Plains Mid Boreal, Chasmer and Hopkinson (2017), predicted that, with continued acceleration of permafrost thaw driven drainage of peatland complexes (Connon et al., 2015; Haynes et al., 2018; Kokelj et al., 2023; Quinton et al., 2019b), woody AGB gains would exceed losses in the future. This is because the subsequent hummock establishment supports the establishment and expansion of woody vegetation, which preferably grows on well-draining soils (Chasmer & Hopkinson, 2017; Haynes et al., 2021). In the Taiga Shield High, conditions suitable for woody vegetation may have been created by the disconnection of hydrological network channels between upland bedrock, valleys, and lakes over multiple years (Spence & Woo, 2003). The lowering of lake water levels in the decade preceding this analysis (Kokelj et al., 2023) may have also emphasized

woody vegetation growth. It is assumed that the increased tree canopy cover may have led to permafrost aggradation in some areas (Sniderhan et al., 2023).

This study is the first to find evidence of these differing climate-mediated mechanistic changes over large areas within the Taiga Plains Mid Boreal and Taiga Shield High Boreal. As a consequence, our results suggest that rates of climate-mediated permafrost thaw and landscape evolution in the Taiga Plains Mid Boreal may be faster than expected (~half a century, Carpino et al., 2021). Shifts from the intermediate stages of collapse scar wetland expansion to the later stages of expedited drainage, hummock formation, and forest growth (absence of permafrost) occurred within a decade in the areas sampled. In addition, expedited stages of permafrost thaw also show as subsidence of a larger permafrost plateau area, rather than at localized spots within and along edges. This was indicated by the relevant scale at which elevation change was an important control (60 m x 60 m, Figure 5.8). Given that AGB and plant C gains were the highest amongst ecosystem types, this is an important and necessary addition to the conceptual framework by Carpino et al. (2021).

In the Taiga Shield High Boreal, woody vegetation grew in even faster rates (Table 5.2). In addition to the ecoregion-specific findings above, we suggest that the increasing trend in MAAT (Figure S5.1), may have increased soil temperatures and thereby nutrient mineralization (Mekonnen et al., 2021), which is largely a limiting control on woody vegetation growth in the Taiga Shield High Boreal (Ecosystem Classification Group, 2008). This is supported by the finding that aspect, slope, and solar incident radiation hours were also relevant drivers of AGB change (Figure 5.8). Further research needs to investigate the evolution of permafrost in this ecoregion.

Finally, the decreasing trend in TAP since 2010 was a limiting control on upland forest productivity levels in the Taiga Plains High Boreal (Figure S5.1). With further climate change and evaporative demand exceeding precipitation (Price et al., 2013), these ecosystems might become increasingly vulnerable to further drying conditions.

5.5.4. Implications

Vegetation structural changes occurred not only within the grid cell, but as advancing and receding of ecosystem boundaries (Figure 5.10). This is evident when mapping 2010 and 2019 plant functional groups across ecotones from upland forest and permafrost plateau to peatland (Figure 5.10). The large and widespread proportional increases in woody vegetation across the study region remained unquantified in previous studies due to the limitations in detecting these changes with optical, coarse resolution satellite remote sensing (Baltzer et al., 2014; Carpino et al., 2021; Sniderhan et al., 2023). While decreases and receding of tall-stature vegetation from peatlands towards upland forest and permafrost plateau did occur (Figure 5.5, Table 5.2), increases and expansion of short-stature vegetation from upland forest and permafrost plateau towards peatlands occurred simultaneously and over larger areas in the Taiga Plains Mid Boreal and Taiga Shield High Boreal (Figure 5.10).

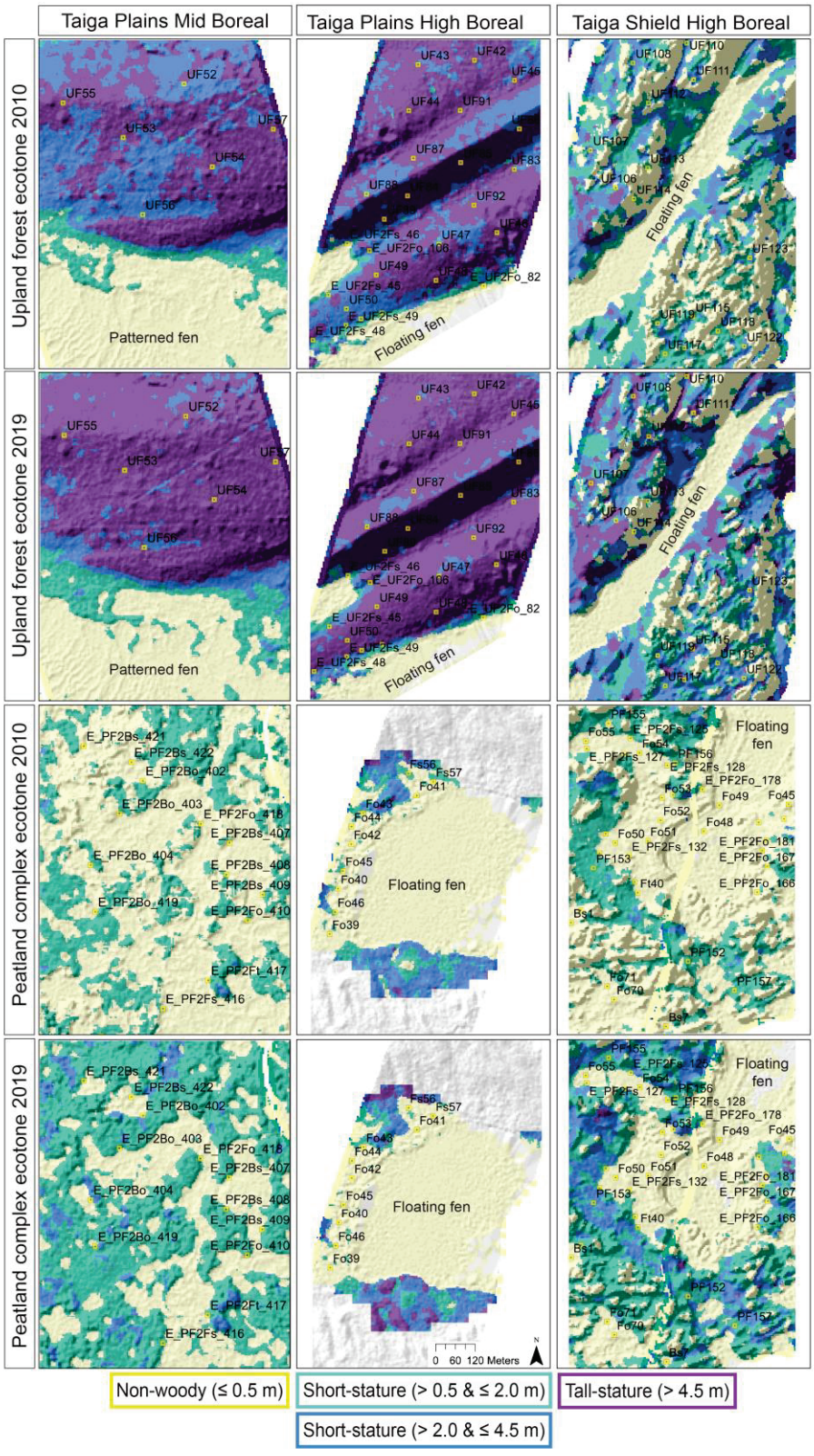

Figure 5.10. Distribution of plant functional groups in 2010 and 2019 per ecoregion in upland forests and peatland complexes and their ecotones in example areas. A lidar DEM-based hillshade model indicates terrain variation. A majority filter was applied to emphasize the main changes.

The expansion of short-stature vegetation into areas previously dominated by non-woody vegetation in both ecoregions increased the connectivity of ecosystems by vegetation that could become fuel for wildland fire, given the appropriate warming and drying conditions (Figure 5.10). The expansion of woody vegetation may have locally increased drying conditions in a perpetuating cycle due to feedbacks related to evaporation, transpiration, and interception (reviewed in Waddington et al., 2015). The increased vegetation and potential wildland fire connectivity may have contributed to the burning of the Scotty Creek basin in Fall 2022 and the record-breaking rates of wildland fire spread in 2023 in this region (Jain et al., 2024; Ritter et al., 2023). This was previously observed in the Boreal Plains and Taiga Shield High Boreal, where drought induced wetland connectivity caused some of the largest areas burned in modern times (Bourgeau-Chavez et al., 2022; Thompson et al., 2019). The return to managing northern landscapes through indigenous-led cultural burning practices (Christianson et al., 2022) and FireSmart activities around communities is an increasingly critical need.

In the Taiga Plains High Boreal, where large upland forest areas were already affected by wildland fire between 2010 and 2015 (Bourgeau-Chavez et al., 2022), increased vegetation fuel connectivity was not a concern. In neighbouring unburned areas, AGB and plant C decreased in higher and increased in lower elevations. In floating fens around ponds/lakes, the proportional area covered by short-stature vegetation reduced (Figure 5.10). This suggests that available plant water may have been an important control in these systems and could be an area of future research. Although AGB and plant C losses were counterbalanced resulting in average in a minor loss, further atmospheric warming and drying (Price et al., 2013) could enhance losses in the future. Given that water inputs into

these systems were among the most important drivers (Figure 5.8), successional trajectories of these ecosystems after wildland fire disturbance may be of concern and need further investigation.

5.5.5. Limitations

The overall net AGB and plant C gains due to growth and densification of woody vegetation were determined by the increase in the average height and the height of the 90th percentile of all lidar returns in a 5 m x 5m grid cell. Uncertainties in AGB and AGB change are greater for short-stature vegetation compared to tall-stature vegetation (Flade et al. 2024, Hopkinson et al., 2005). In addition, lidar returns reflecting from dead branches of fallen trees might have falsely been attributed as an increase in short-stature vegetation (Figure 5.1), overestimating AGB and plant C gains. Changes in short-stature vegetation can occur rapidly and may fluctuate from year to year and within the growing season (Rodrigues et al., 2024). Furthermore, the differentiation of short- and tall-stature vegetation (used to quantify rates of expansion) was based on the average maximum canopy height within a 5 m x 5 m grid cell. At this grid cell level various combinations of short- and tall-stature vegetation can occur. The differentiation is therefore limited to the assumption of vertical and horizontal canopy continuity within the grid cell. However, this was considered in the placement of the sample points. Specific locations, where short-stature vegetation increased, also overlapped with those reported in other studies for similar time periods (Chasmer & Hopkinson, 2017; Haynes et al., 2021). Field measurements (Flade et al., 2020) and photographs (Figure 5.2) also showed widespread abundance of short-stature vegetation across the Taiga Plains Mid Boreal and Taiga Shield High Boreal in 2018 and 2019 as opposed to tree mortality, raising confidence in our results. Lastly, by

focusing on the July/August conditions, we were able to quantify the maximum rates of vegetation structural changes occurring in these systems before the start of senescence.

With regards to the driver importance, random forest models could only partially explain AGB change variability. Although this might be attributed to the highly variable and counterbalancing of changes, other variables such as water table depths, distance to ephemeral water bodies and permafrost plateau fragmentation need to be investigated in the future, which were found important in other studies (Baltzer et al., 2014; Haynes et al., 2018). Lag effects between atmospheric warming, permafrost thaw, and vegetation structural changes also need to be considered.

The basis of such analysis will be an improved, regularly updated land surface classification over the complete study region, including also peatland class and form and improved outlines of historical wildland fire boundaries. For example, Helbig et al. (2016) elaborate that reliable knowledge about an area's wildland fire history does not date back for more than ~60 years, while the growth period of upland trees may exceed 100 years. Although woody vegetation increases were attributed to climate-mediated hydroclimatic changes, upland forests in the Taiga Shield High Boreal may not have reached their final successional stage.

Lastly, our results were derived from a stratified sample of overlapping airborne lidar data, which were also a sample of the broader region, to avoid additional error from an external land cover classification, which are largest at ecotones (Flade et al., 2024). As such, the mean changes occurring in the region depended on the number of samples that went into the overall calculation. Future efforts need to be directed towards improving

regional and multi-temporal wall-to-wall AGB maps, to investigate potential bias in the regional mean AGB and plant C changes determined from sampled areas in this study.

5.5.6. Future research needs

Despite these limitations, with our approach we reduced key sources of unquantifiable error (Neigh et al., 2013) inherent in regional to global AGB and carbon stock products that are commonly derived using e.g. national forest inventory data, optical satellite imagery (≥ 30m x 30m grid cells), and spaceborne lidar and radar data within machine learning environments. Such products lack the necessary field data and allometric equations including short-stature vegetation and independence of static land cover classifications. These are in addition to limited sensitivity of spaceborne lidar sensors to short-stature/sparse vegetation (e.g. Geoscience Laser Altimeter (Neigh et al., 2013) and Global Ecosystem Dynamics Investigation (Campbell et al., 2024) systems) and tall-stature/dense vegetation (L-Band synthetic aperture radar backscatter (Santoro et al., 2021). In contrast, our approach enabled the detection and quantification of vegetation structures that are changing rapidly, including transitions from non-woody to short- and tall-stature woody vegetation associated with changes in canopy heights that were, to date, hidden within the large uncertainties of regional to global products.

Given the differences compared with our results, the carbon sink strength in boreal regions (Pan et al., 2011) may be estimated optimistic across the circumboreal. This might also explain the higher land carbon sink estimate in bottom-up compared to top-down approaches for European boreal forests (Lauerwald et al., 2024). Future research needs to integrate short-stature vegetation in bottom-up modelling frameworks, from field data and

allometric equations to the final models used to infer AGB and plant C, though this is difficult with global products, such as Landsat, which provides an important long-term record of environmental change. This study provides an example of such a framework, which could be expanded to include regional satellite imagery with the overall purpose to reduce uncertainty in regional estimates of AGB and carbon sink strength of ecosystems in the southern Taiga of western Canada.

5.6. Conclusion

Climate change is rapidly changing ecosystems in the southern Taiga of northwestern Canada, a region that is highly dynamic due to landcover change processes related to the retreat of former ice sheets. This study is the first to a) quantify decadal short-to-tall-stature vegetation structural and plant C changes at the plot level for a wide range of sampled ecosystem types and b) examine these changes across the range of variability of local/proximal environmental to regional climatic drivers.

Between 2010 and 2019, AGB and plant C losses due to tree mortality were partially reduced or compensated by gains in short-stature vegetation (≤ 2.0 m in height) in all sampled ecosystem types in the Taiga Plains Mid Boreal. In the Taiga Shield High Boreal, ecosystem types gained AGB and plant C across all vegetation structures. While ~60% of the areas sampled in these ecoregions remained unchanged, up to 20% shifted from non-woody (open) to short-stature vegetation (≤ 4.5 m in height). These shifts occurred most dominantly as short-stature vegetation densification within permafrost plateaus (Taiga Plains Mid Boreal), and along bedrock outcrops and in floating fens ponds/lakes (Taiga Shield). Gains in short-stature vegetation also outweighed losses in tall-stature vegetation in ecotones from permafrost plateau to peatland (Taiga Plains Mid Boreal, Taiga Shield

High Boreal) and upland forest to peatland (Taiga Shield High Boreal). In the Taiga Plains High Boreal, vegetation heights increased between 2010 and 2019. However, AGB and plant C gains in lower lying areas were offset by losses in higher elevated areas, resulting overall in statistically non-significant changes in all ecosystem types sampled in this ecoregion. Across the study region, permafrost plateaus gained 15 times as much AGB and plant C compared to upland forests. Bogs and fens moved towards similar vegetation structure in 2019, having increased similarly in short-stature vegetation in areas previously dominated by non-woody vegetation.

The large AGB and plant C changes and successional shifts towards woody vegetation in the Taiga Plains Mid Boreal and Taiga Shield High Boreal were both associated with increased drying conditions due to increasing trends in MAAT and decreasing trends in TAP. However, the underlying mechanisms of these changes differed, such that climate change exerted an indirect control through permafrost evolution (reduction of permafrost plateau area, hydrological connection of ecosystems, peatland drainage) in the former and changes in hydrological storage terms (disconnection of hydrological network channels, lowering of lake levels (Kokelj et al., 2023)) and potentially increased nutrient mineralization due to warmer soils in the latter. Based on our results, we also suggest that shifts from the intermediate stages of collapse scar wetland expansion to the later stages of expedited drainage, hummock formation, and forest growth (absence of permafrost) in the Taiga Plains Mid Boreal occurred faster than expected (within a decade as opposed to half a century). In the Taiga Shield High Boreal, permafrost aggradation was found to be unlikely across the broader region of the Taiga Shield High Boreal and needs to be further investigated. The increased connectivity due to fuels and increased drying

conditions in both ecoregions could increase the area consumed during wildland fires in the future. Here, community-based management and Indigenous-led fire practices will be critical for remote communities in the future.

In the Taiga Plains High Boreal, a lack of knowledge about changes in water table positions and lake levels prevents understanding of the causes of these changes. However, the decreasing trend in TAP was an important driver in this ecoregion, which consists dominantly of areas underlain by coarse-textured, well-draining soils. These ecosystems might be increasingly vulnerable to continued drying conditions and should be considered in future monitoring programs.

Overall, uncertainties in structural vegetation changes are higher for short-stature compared to tall-stature vegetation (Flade et al., 2024). In addition, knowledge of the directions and magnitudes of the mean changes occurring in the region is based on stratified, randomly sampled grid cells. However, by integrating short-stature vegetation, we have provided a framework that will reduce uncertainty in regional to global estimates of AGB and carbon sink strength of ecosystems in the southern Taiga of western Canada. The framework could be expanded to include regional satellite imagery and could be valuable for analyzing the record breaking 2023 year of wildland fire (and other high fire years from 2014 to now) as well as future wildland fire susceptibility. Finally, our results will provide a baseline from which to compare future vegetation structural changes and successional shifts due to continued pressures on these systems by climate change.

5.7. Overview supplementary material Chapter 5

Figure S5.1: Trends in downscaled and gridded ClimateNA data of a) mean annual air temperatures (MAAT) and b) total annual precipitation (TAP) from 1998 to 2019 for

ecoregions within the southern Northwest Territories on sporadic to discontinuous permafrost. Trends derived as slopes of linear trendlines plotted through annual climate variable deviations from climate normals (1961 to 1990) on a per grid-cell basis. Mean trends (± standard deviations) derived as averages of sampled grid cells per ecoregion; Table S5.1: Random sample points (n) per ecoregion-specific ecosystem types; Table S5.2: Distribution of sampled aboveground biomass change (dAGB) for ecoregion-specific ecotones and peatland class and form; Table S5.3: Distribution of sampled aboveground biomass change (dAGB) for ecotones and peatland class and form (pooled for all ecoregions).

5.8. Funding

This project was funded in part by NSERC Discovery Grants to L. Chasmer [Grant number: (2017-04492)] and C. Hopkinson [Grant number: (2017-04362)], a University of Lethbridge start up grant to L. Chasmer, the NSERC Canada Wildfire Network (Chasmer) [Grant number: RES0049086], a CFI grant for field survey equipment to C. Hopkinson [Grant number: (32436)], and a grant to purchase the Titan lidar system through Western Economic Diversification Canada [Grant number: (000015316)].

5.9. Acknowledgements

We would like to acknowledge the help of various field assistants: Emily Jones, Kailyn Nelson, Rachelle Shearing, Jesse Aspinall, and Lavinia Haase and field assistance from the Government of the Northwest Territories (Tyler Rea, Ben Paulsen), the Dehcho Guardian Program (Garreth Isiah), and the Dehcho Collaborative on Permafrost. Lidar surveys and data pre-processing were conducted by Maxim Okhrimenko. We would also like to thank Dr. William Quinton for useful discussion and the Liidlii Kue First Nation and Dr. Quinton

for research support within the Scotty Creek Research Basin, NWT.

5.10. References

Alberta Wetland Classification System. (2015). Edmonton, Alberta: Alberta Environment and Sustainable Resource Development.

Alberta Wetland Classification System. (2021). *Field guide*. Edmonton, AB: Ducks Unlimited Canada.

Balliston, N., & Price, J. S. (2022). Beyond fill and spill: Hydrological connectivity in a sub-arctic bog-fen-tributary complex in the Hudson Bay Lowlands, Canada. *Hydrological Processes*, *36*(4), e14575. https://doi.org/10.1002/hyp.14575.

Baltzer, J., Veness, T., Chasmer, L., Sniderhan, A., & Quinton, W. (2014). Forests on thawing permafrost: fragmentation, edge effects, and net forest loss. *Global Change Biology*, *20*(3), 824–834. https://doi.org/10.1111/gcb.12349.

Bathiany, S., Bastiaansen, R., Bastos, A., Blaschke, L., Lever, J., Loriani, S., et al. (2024). Ecosystem Resilience Monitoring and Early Warning Using Earth Observation Data: Challenges and Outlook. *Surveys in Geophysics*. https://doi.org/10.1007/s10712-024-09833-z.

Bourgeau-Chavez, L., Graham, J. A., Endres, S., French, N. H. F., Battaglia, M., Hansen, D., & Tanzer, D. (2019). Arctic-Boreal Vulnerability Experiment (ABoVE)ABoVE: Ecosystem Map, Great Slave Lake Area, Northwest Territories, Canada, 1997-2011 (Version 1) [ESRI Shapefile,GTiff], https://doi.org/10.3334/ORNLDAAC/1695.

Bourgeau-Chavez, L., Graham, J. A., Vander Bilt, D. J. L., & Battaglia, M. J. (2022). Assessing the broadscale effects of wildfire under extreme drought conditions to boreal peatlands. *Frontiers in Forests and Global Change*, *5*, 965605. https://doi.org/10.3389/ffgc.2022.965605.

Camill, P. (1999a). Patterns of boreal permafrost peatland vegetation across environmental gradients sensitive to climate warming. *Canadian Journal of Botany*, *77*(5), 721–733.

Camill, P. (1999b). Peat accumulation and succession following permafrost thaw in the boreal peatlands of Manitoba, Canada. *Écoscience*, *6*(4), 592–602. https://doi.org/10.1080/11956860.1999.11682561.

Camill, P., & Clark, J. S. (2000). Long-term Perspectives on Lagged Ecosystem Responses to Climate Change: Permafrost in Boreal Peatlands and the Grassland/Woodland Boundary. *Ecosystems*, *3*(6), 534–544. https://doi.org/10.1007/s100210000047.

Camill, P., Lynch, J. A., Clark, J. S., Adams, J. B., & Jordan, B. (2001). Changes in Biomass, Aboveground Net Primary Production, and Peat Accumulation following Permafrost Thaw in the Boreal Peatlands of Manitoba, Canada. *Ecosystems*, *4*(5), 461–478. https://doi.org/10.1007/s10021-001-0022-3.

Campbell, M. J., Eastburn, J. F., Dennison, P. E., Vogeler, J. C., & Stovall, A. E. L. (2024). Evaluating the performance of airborne and spaceborne lidar for mapping biomass

in the United States' largest dry woodland ecosystem. *Remote Sensing of Environment*, *308*, 114196. https://doi.org/10.1016/j.rse.2024.114196.

Carpino, O., Berg, A. A., Quinton, W., & Adams, J. (2018). Climate change and permafrost thaw-induced boreal forest loss in northwestern Canada. *Environmental Research Letters*, *13*(8), 084018. https://doi.org/10.1088/1748-9326/aad74e.

Carpino, O., Haynes, K., Connon, R., Craig, J., Devoie, É., & Quinton, W. (2021). Long-term climate-influenced land cover change in discontinuous permafrost peatland complexes. *Hydrology and Earth System Sciences*, *25*(6), 3301–3317. https://doi.org/10.5194/hess-25-3301-2021.

Chapin, F. S., Woodwell, G. M., Randerson, J. T., Rastetter, E. B., Lovett, G. M., Baldocchi, D. D., et al. (2006). Reconciling Carbon-cycle Concepts, Terminology, and Methods. *Ecosystems*, *9*(7), 1041–1050. https://doi.org/10.1007/s10021-005-0105-7.

Chasmer, L., & Hopkinson, C. (2017). Threshold loss of discontinuous permafrost and landscape evolution. *Global Change Biology*, *23*(7), 2672–2686. https://doi.org/10.1111/gcb.13537.

Chasmer, L., Hopkinson, C., Veness, T., Quinton, W., & Baltzer, J. (2014). A decision-tree classification for low-lying complex land cover types within the zone of discontinuous permafrost. *Remote Sensing of Environment*, *143*, 73–84. https://doi.org/10.1016/j.rse.2013.12.016.

Chasmer, L., Quinton, W. L., Hopkinson, C., Petrone, R., & Whittington, P. (2011). Vegetation Canopy and Radiation Controls on Permafrost Plateau Evolution within the Discontinuous Permafrost Zone, Northwest Territories, Canada: Vegetation and Radiation Controls on Permafrost Plateau Evolution. *Permafrost and Periglacial Processes*, n/a-n/a. https://doi.org/10.1002/ppp.724.

Chasmer, L., Kenward, A., Quinton, W., & Petrone, R. (2012). CO_2 Exchanges within Zones of Rapid Conversion from Permafrost Plateau to Bog and Fen Land Cover Types. *Arctic, Antarctic, and Alpine Research*, *44*(4), 399–411. https://doi.org/10.1657/1938-4246-44.4.399.

Christianson, A. C., Sutherland, C. R., Moola, F., Gonzalez Bautista, N., Young, D., & MacDonald, H. (2022). Centering Indigenous Voices: The Role of Fire in the Boreal Forest of North America. *Current Forestry Reports*, *8*(3), 257–276. https://doi.org/10.1007/s40725-022-00168-9.

Cochran, W. G. (1977). *Sampling techniques* (3rd ed). New York: Wiley.

Connon, R., Quinton, W., Craig, J., & Hayashi, M. (2014). Changing hydrologic connectivity due to permafrost thaw in the lower Liard River valley, NWT, Canada. *Hydrological Processes*, *28*(14), 4163–4178. https://doi.org/10.1002/hyp.10206.

Connon, R., Quinton, W., Craig, J. R., Hanisch, J., & Sonnentag, O. (2015). The hydrology of interconnected bog complexes in discontinuous permafrost terrains. *Hydrological Processes*, *29*(18), 3831–3847. https://doi.org/10.1002/hyp.10604.

Dearborn, K., Wallace, C., Patankar, R., & Baltzer, J. (2021). Permafrost thaw in boreal peatlands is rapidly altering forest community composition. *Journal of Ecology*, *109*(3), 1452–1467. https://doi.org/10.1111/1365-2745.13569.

Disher, B. S., Connon, R. F., Haynes, K. M., Hopkinson, C., & Quinton, W. L. (2021). The hydrology of treed wetlands in thawing discontinuous permafrost regions. *Ecohydrology*, *14*(5), e2296. https://doi.org/10.1002/eco.2296.

Dulfer, H. E., Stoker, B. J., Margold, M., & Stokes, C. R. (2023). Glacial geomorphology of the northwest Laurentide Ice Sheet on the northern Interior Plains and western Canadian Shield, Canada. Journal of Maps, 19(1), 2181714. https://doi.org/10.1080/17445647.2023.2181714.

Ecosystem Classification Group (Ed.). (2008). *Ecological regions of the Northwest Territories - Taiga Shield*. Yellowknife, NT, Canada: Department of Environment and Natural Resources, Government of the Northwest Territories.

Ecosystem Classification Group. (2009). *Ecological regions of the Northwest Territories - Taiga Plains* (Revised). Yellowknife, NT, Canada: Department of Environment and Natural Resources, Government of the Northwest Territories.

Environment and Natural Resources. (2024). Canadian Climate Normals: 1981-2010 [Data set]. Government of Canada. Retrieved from https://climate.weather.gc.ca/climate_normals/station_select_1981_2010_e.html?searchType=stnProv&lstProvince=NT.

Flade, L., Hopkinson, C., & Chasmer, L. (2020). Allometric Equations for Shrub and Short-Stature Tree Aboveground Biomass within Boreal Ecosystems of Northwestern Canada. *Forests*, *11*(11), 1207. https://doi.org/10.3390/f11111207.

Flade, L., Hopkinson, C., & Chasmer, L. (2021). Aboveground Biomass Allocation of Boreal Shrubs and Short-Stature Trees in Northwestern Canada. *Forests*, *12*(2), 234. https://doi.org/10.3390/f12020234.

Flade, L., Hopkinson, C., & Chasmer, L. (2024). A Bi-Temporal Airborne Lidar Shrub-to-Tree Aboveground Biomass Model for the Taiga of Western Canada: Un Modèle Bitemporal de Biomasse Aérienne D'arbuste à D'arbre Pour le Lidar Aéroporté Pour la Taïga du L'ouest du Canada. *Canadian Journal of* Remote *Sensing*, *50*(1), 2379915. https://doi.org/10.1080/07038992.2024.2379915.

Flanagan, L. B., & Syed, K. H. (2011). Stimulation of both photosynthesis and respiration in response to warmer and drier conditions in a boreal peatland ecosystem: Peatland carbon dioxide exchange. *Global Change Biology*, *17*(7), 2271–2287. https://doi.org/10.1111/j.1365-2486.2010.02378.x.

Garon-Labrecque, M.-È., Léveillé-Bourret, É., Higgins, K., & Sonnentag, O. (2016). Additions to the boreal flora of the Northwest Territories with a preliminary vascular flora of Scotty Creek. *The Canadian Field-Naturalist*, *129*(4), 349. https://doi.org/10.22621/cfn.v129i4.1757.

Gibson, C., Morse, P., Kelly, M., Turetsky, M., Baltzer, J., Gringas-Hill, T., & Kokelj, S. (2020). *Thermokarst Mapping Collective: Protocol for organic permafrost terrain and preliminary inventory from the Taiga Plains test area, Northwest Territories*

(No. NWT Open Report 2020-10) (p. 24). Northwest Territories Geological Survey. Government of the Northwest Territories. Retrieved from https://ostrnrcan-dostrncan.canada.ca/handle/1845/138870.

Haynes, K. M., Connon, R. F., & Quinton, W. (2018). Permafrost thaw induced drying of wetlands at Scotty Creek, NWT, Canada. *Environmental Research Letters*, *13*(11), 114001. https://doi.org/10.1088/1748-9326/aae46c.

Haynes, K. M., Smart, J., Disher, B., Carpino, O., & Quinton, W. L. (2021). The role of hummocks in re-establishing black spruce forest following permafrost thaw. *Ecohydrology*, *14*(3), e2273. https://doi.org/10.1002/eco.2273.

Helbig, M., Pappas, C., & Sonnentag, O. (2016). Permafrost thaw and wildfire: Equally important drivers of boreal tree cover changes in the Taiga Plains, Canada. *Geophysical Research Letters*, *43*(4), 1598–1606. https://doi.org/10.1002/2015GL067193.

Helbig, M., Živković, T., Alekseychik, P., Aurela, M., El-Madany, T. S., Euskirchen, E. S., et al. (2022). Warming response of peatland CO_2 sink is sensitive to seasonality in warming trends. *Nature Climate Change*, *12*(8), 743–749. https://doi.org/10.1038/s41558-022-01428-z.

Holling, C. S. (1973). Resilience and Stability of Ecological Systems. *Annual Review of Ecology and Systematics*, *4*, 1–23. https://www.jstor.org/stable/2096802.

Hopkinson, C., Chasmer, L., Barr, A. G., Kljun, N., Black, T. A., & McCaughey, J. H. (2016). Monitoring boreal forest biomass and carbon storage change by integrating airborne laser scanning, biometry and eddy covariance data. *Remote Sensing of Environment*, *181*, 82–95. https://doi.org/10.1016/j.rse.2016.04.010.

Hopkinson, C., Chasmer, L., Lim, K., Treitz, P., & Creed, I. (2006). Towards a universal lidar canopy height indicator. *Canadian Journal of Remote Sensing*, *32*(2), 139–152. https://doi.org/10.5589/m06-006.

Hopkinson, C., Chasmer, L., Sass, G., Creed, I., Sitar, M., Kalbfleisch, W., & Treitz, P. (2005). Vegetation class dependent errors in lidar ground elevation and canopy height estimates in a boreal wetland environment. Canadian Journal of Remote Sensing, 31(2), 191–206. https://doi.org/10.5589/m05-007.

IPCC. (2023). *IPCC, 2023: Climate Change 2023: Synthesis Report. Contribution of Working Groups I, II and III to the Sixth Assessment Report of the Intergovernmental Panel on Climate Change [Core Writing Team, H. Lee and J. Romero (eds.)]. IPCC, Geneva, Switzerland.* (First) (p. 184). Geneva, Switzerland: Intergovernmental Panel on Climate Change (IPCC). https://doi.org/10.59327/IPCC/AR6-9789291691647.

Jain, P., Barber, Q. E., Taylor, S. W., Whitman, E., Castellanos Acuna, D., Boulanger, Y., et al. (2024). Drivers and Impacts of the Record-Breaking 2023 Wildfire Season in Canada. *Nature Communications*, *15*(1), 6764. https://doi.org/10.1038/s41467-024-51154-7.

Jenness, J. (1949). Permafrost in Canada. *Arctic*, *2*(1), 13–27.

Johansson, T. (1999). Biomass production of Norway spruce (Picea abies (L.) Karst.) growing on abandoned farmland. *Silva Fennica*, *33*(4). https://doi.org/10.14214/sf.649.

Jorgenson, M. T., Kanevskiy, M., Roland, C., Hill, K., Schirokauer, D., Stehn, S., et al. (2022). Repeated Permafrost Formation and Degradation in Boreal Peatland Ecosystems in Relation to Climate Extremes, Fire, Ecological Shifts, and a Geomorphic Legacy. *Atmosphere*, *13*(8), 1170. https://doi.org/10.3390/atmos13081170.

Kokelj, S. V., & Jorgenson, M. T. (2013). Advances in Thermokarst Research. *Permafrost and Periglacial Processes*, *24*(2), 108–119. https://doi.org/10.1002/ppp.1779.

Kokelj, S. V., Gingras-Hill, T., Daly, S. V., Morse, P., Wolfe, S., Rudy, A. C. A., et al. (2023). The Northwest Territories Thermokarst Mapping Collective: A northern-driven mapping collaborative toward understanding the effects of permafrost thaw. *Arctic Science*, AS-2023-0009. https://doi.org/10.1139/AS-2023-0009.

Lambert, M.-C., Ung, C.-H., & Raulier, F. (2005). Canadian national tree aboveground biomass equations. *Canadian Journal of Forest Research*, *35*(8), 1996–2018. https://doi.org/10.1139/x05-112.

Lauerwald, R., Bastos, A., McGrath, M. J., Petrescu, A. M. R., Ritter, F., Andrew, R. M., et al. (2024). Carbon and Greenhouse Gas Budgets of Europe: Trends, Interannual and Spatial Variability, and Their Drivers. *Global Biogeochemical Cycles*, *38*(8), e2024GB008141. https://doi.org/10.1029/2024GB008141.

Lenton, T. M., Held, H., Kriegler, E., Hall, J. W., Lucht, W., Rahmstorf, S., & Schellnhuber, H. J. (2008). Tipping elements in the Earth's climate system. *Proceedings of the National Academy of Sciences*, *105*(6), 1786–1793. https://doi.org/10.1073/pnas.0705414105.

Loudermilk, E. L., O'Brien, J. J., Goodrick, S. L., Linn, R. R., Skowronski, N. S., & Hiers, J. K. (2022). Vegetation's influence on fire behavior goes beyond just being fuel. *Fire Ecology*, *18*(1), 9, s42408-022-00132–9. https://doi.org/10.1186/s42408-022-00132-9.

Mack, M., Connon, R., Makarieva, O., McLaughlin, J., Nesterova, N., & Quinton, W. (2021). Heterogenous runoff trends in peatland-dominated basins throughout the circumpolar North. *Environmental Research Communications*, *3*(7), 075006. https://doi.org/10.1088/2515-7620/ac11ed.

Mäkiranta, P., Laiho, R., Mehtätalo, L., Straková, P., Sormunen, J., Minkkinen, K., et al. (2018). Responses of phenology and biomass production of boreal fens to climate warming under different water-table level regimes. *Global Change Biology*, *24*(3), 944–956. https://doi.org/10.1111/gcb.13934.

Mekonnen, Z. A., Riley, W. J., Berner, L. T., Bouskill, N. J., Torn, M. S., Iwahana, G., et al. (2021). Arctic tundra shrubification: a review of mechanisms and impacts on ecosystem carbon balance. *Environmental Research Letters*, *16*(5), 053001. https://doi.org/10.1088/1748-9326/abf28b.

Millard, K., & Richardson, M. (2015). On the Importance of Training Data Sample Selection in Random Forest Image Classification: A Case Study in Peatland Ecosystem Mapping. *Remote Sensing*, *7*(7), 8489–8515. https://doi.org/10.3390/rs70708489.

Næsset, E., & Gobakken, T. (2008). Estimation of above- and below-ground biomass across regions of the boreal forest zone using airborne laser. *Remote Sensing of Environment*, *112*(6), 3079–3090. https://doi.org/10.1016/j.rse.2008.03.004.

Neigh, C. S. R., Nelson, R. F., Ranson, K. J., Margolis, H. A., Montesano, P. M., Sun, G., et al. (2013). Taking stock of circumboreal forest carbon with ground measurements, airborne and spaceborne LiDAR. *Remote Sensing of Environment*, *137*, 274–287. https://doi.org/10.1016/j.rse.2013.06.019.

Pan, Y., Birdsey, R. A., Fang, J., Houghton, R., Kauppi, P. E., Kurz, W. A., et al. (2011). A Large and Persistent Carbon Sink in the World's Forests. *Science*, *333*(6045), 988–993. https://doi.org/10.1126/science.1201609.

Patankar, R., Quinton, W., Hayashi, M., & Baltzer, J. (2015). Sap flow responses to seasonal thaw and permafrost degradation in a subarctic boreal peatland. *Trees*, *29*(1), 129–142. https://doi.org/10.1007/s00468-014-1097-8.

Price, D. T., Alfaro, R. I., Brown, K. J., Flannigan, M. D., Fleming, R. A., Hogg, E. H., et al. (2013). Anticipating the consequences of climate change for Canada's boreal forest ecosystems. *Environmental Reviews*, *21*(4), 322–365. https://doi.org/10.1139/er-2013-0042.

Quinton, W., Hayashi, M., & Chasmer, L. (2011). Permafrost-thaw-induced land-cover change in the Canadian subarctic: implications for water resources. *Hydrological Processes*, *25*(1), 152–158. https://doi.org/10.1002/hyp.7894.

Quinton, W., Berg, A., Braverman, M., Carpino, O., Chasmer, L., Connon, R., et al. (2019). A synthesis of three decades of hydrological research at Scotty Creek, NWT, Canada. *Hydrology and Earth System Sciences*, *23*(4), 2015–2039. https://doi.org/10.5194/hess-23-2015-2019.

Reisen, F., Duran, S. M., Flannigan, M., Elliott, C., & Rideout, K. (2015). Wildfire smoke and public health risk. *International Journal of Wildland Fire*, *24*(8), 1029. https://doi.org/10.1071/WF15034.

Ritter, S. M., Hoffman, C. M., Battaglia, M. A., Linn, R., & Mell, W. E. (2023). Vertical and Horizontal Crown Fuel Continuity Influences Group-Scale Ignition and Fuel Consumption. *Fire*, *6*(8), 321. https://doi.org/10.3390/fire6080321.

Rodrigues, I. S., Hopkinson, C., Chasmer, L., MacDonald, R. J., Bayley, S. E., & Brisco, B. (2024). Multi-decadal floodplain classification and trend analysis in the Upper Columbia River valley, British Columbia. *Hydrology and Earth System Sciences*, *28*(10), 2203–2221. https://doi.org/10.5194/hess-28-2203-2024.

Santoro, M., & Cartus, O. (2024). ESA Biomass Climate Change Initiative (Biomass CCI): Global datasets of forest above-ground biomass for the years 2010, 2015, 2016, 2017, 2018, 2019, 2020 and 2021 (Version 5.01) [Data set]. NERC EDS Centre for Environmental Data Analysis. https://doi.org/doi:10.5285/bf535053562141c6bb7ad831f5998d77.

Santoro, M., Cartus, O., Carvalhais, N., Rozendaal, D. M. A., Avitabile, V., Araza, A., et al. (2021). The global forest above-ground biomass pool for 2010 estimated from high-resolution satellite observations. *Earth System Science Data*, *13*(8), 3927–3950. https://doi.org/10.5194/essd-13-3927-2021.

Schuur, E. A. G., & Mack, M. C. (2018). Ecological Response to Permafrost Thaw and Consequences for Local and Global Ecosystem Services. *Annual Review of Ecology, Evolution, and Systematics*, *49*(1), 279–301. https://doi.org/10.1146/annurev-ecolsys-121415-032349.

See, C. R., Virkkala, A.-M., Natali, S. M., Rogers, B. M., Mauritz, M., Biasi, C., et al. (2024). Decadal increases in carbon uptake offset by respiratory losses across northern permafrost ecosystems. *Nature Climate Change*. https://doi.org/10.1038/s41558-024-02057-4.

Shur, Y. L., & Jorgenson, M. T. (2007). Patterns of permafrost formation and degradation in relation to climate and ecosystems. *Permafrost and Periglacial Processes*, *18*(1), 7–19. https://doi.org/10.1002/ppp.582.

Sniderhan, A., & Baltzer, J. (2016). Growth dynamics of black spruce (*Picea mariana*) in a rapidly thawing discontinuous permafrost peatland. *Journal of Geophysical Research: Biogeosciences*, *121*(12), 2988–3000. https://doi.org/10.1002/2016JG003528.

Sniderhan, A., Spence, C., Kokelj, S., & Baltzer, J. (2023). Evidence for unexpected net permafrost aggradation driven by local hydrology and climatic triggers. *Environmental Research Letters*, *18*(11), 115001. https://doi.org/10.1088/1748-9326/acff0f.

Spence, C., & Woo, M. (2003). Hydrology of subarctic Canadian shield: soil-filled valleys. *Journal of Hydrology*, *279*(1–4), 151–166. https://doi.org/10.1016/S0022-1694(03)00175-6.

The Canadian wetland classification system. (1987) (Provisional ed). Ottawa: Lands Conservation Branch, Canadian Wildlife Service, Environment Canada.

Thompson, D., Simpson, B., Whitman, E., Barber, Q., & Parisien, M.-A. (2019). Peatland Hydrological Dynamics as A Driver of Landscape Connectivity and Fire Activity in the Boreal Plain of Canada. *Forests*, *10*(7), 534. https://doi.org/10.3390/f10070534.

Waddington, J. M., Morris, P. J., Kettridge, N., Granath, G., Thompson, D. K., & Moore, P. A. (2015). Hydrological feedbacks in northern peatlands. *Ecohydrology*, *8*(1), 113–127. https://doi.org/10.1002/eco.1493.

Wang, J., & Friedl, M. (2019). The role of land cover change in Arctic-Boreal greening and browning trends. *Environmental Research Letters*, *14*(12), 125007. https://doi.org/10.1088/1748-9326/ab5429.

Wang, J., Farina, M., Baccini, A., & Friedl, M. (2021a). ABoVE: Annual Aboveground Biomass for Boreal Forests of ABoVE Core Domain, 1984-2014. [Data set]. GeoTIFF, ORNL DAAC, Oak Ridge, Tennessee, USA. Retrieved from https://doi.org/10.3334/ORNLDAAC/1808.

Wang, J., Baccini, A., Farina, M., Randerson, J., & Friedl, M. (2021b). Disturbance suppresses the aboveground carbon sink in North American boreal forests. *Nature Climate Change*, *11*(5), 435–441. https://doi.org/10.1038/s41558-021-01027-4.

Wang, T., Hamann, A., Spittlehouse, D., & Carroll, C. (2016). Locally Downscaled and Spatially Customizable Climate Data for Historical and Future Periods for North America. *PLOS ONE*, *11*(6), e0156720. https://doi.org/10.1371/journal.pone.0156720.

Wilcox, E. J., Keim, D., De Jong, T., Walker, B., Sonnentag, O., Sniderhan, A. E., et al. (2019). Tundra shrub expansion may amplify permafrost thaw by advancing snowmelt timing. *Arctic Science*, *5*(4), 202–217. https://doi.org/10.1139/as-2018-0028.

Wright, N., Quinton, W. L., & Hayashi, M. (2008). Hillslope runoff from an ice-cored peat plateau in a discontinuous permafrost basin, Northwest Territories, Canada. *Hydrological Processes*, *22*(15), 2816–2828. https://doi.org/10.1002/hyp.7005.

Wright, S., Thompson, L., Olefeldt, D., Connon, R., Carpino, O., Beel, C., & Quinton, W. (2022). Thaw-induced impacts on land and water in discontinuous permafrost: A review of the Taiga Plains and Taiga Shield, northwestern Canada. *Earth-Science Reviews*, *232*, 104104. https://doi.org/10.1016/j.earscirev.2022.104104.

CHAPTER 6: CONCLUSION

This thesis established a scaling and change detection framework to advance current understanding of gradual climate-mediated vegetation structural changes in a region identified as an important climate regulator yet also a source of critical uncertainty (IPCC, 2023). This was achieved by using field and bi-temporal airborne lidar data fusion with geospatial statistical analysis and machine learning techniques. By integrating short-stature vegetation in this framework and developing a single aboveground biomass model applicable across changing ecosystem types, ecosystem boundaries, and lidar technologies, this thesis has made significant contributions towards a holistic understanding of the effects of anthropogenic climate change and progressive permafrost thaw on successional states of ecosystems in the southern Taiga of western Canada. In addition, uncertainties in quantifying changing ecosystem carbon stocks were greatly reduced.

6.1. Contributions and recommendations

An increased abundance of short-stature vegetation in response to gradual anthropogenic climate change has been observed in boreal and tundra environments in Alaska and northern Canada (Myers-Smith et al., 2011, 2020; Orndahl et al., 2022) and in the rapidly changing ecotones between treed permafrost plateaus and adjacent peatlands in the southern Taiga of western Canada (Chasmer & Hopkinson, 2017; Dearborn & Baltzer, 2021; Germain Chartrand et al., 2023; Haynes et al., 2018). Short-stature vegetation is also the dominant vegetation structural type after wildfire disturbance (Goetz et al., 2007), which will increase in abundance as wildfire regimes change towards increased frequency and area burned (Flannigan et al., 2005; Kasischke & Turetsky, 2006).

However, changes in growth and spatial distribution of shrubs and short-stature trees and their contribution to changing aboveground biomass and plant carbon stocks remain largely unknown for boreal northwestern Canada due to a lack of regionally applicable allometric equations and measurements of aboveground biomass allocations to single plant components. In Chapter 2 (Flade et al., 2020) the derivation of regional short-stature plant allometric equations for five common boreal shrub and five common juvenile/short-stature tree genera/species, as well as multispecies allometric equations was elaborated. To develop these models, 1D, 2D, and 3D field measurements were compared to understand and improve the scaling relationships across shrubs and short-stature trees. 1D field measurements describe shrub and tree structures based on a single-length observation, such as diameter or stem length. 2D field measurements, such as cross-sectional area, represent two directions, while 3D measurements describe plant structures in three different directions (x, y, and z), such as volume. To improve modelling of aboveground biomass and aboveground carbon pools (determined as 50% of the dry weight of the plant), the proportion of aboveground biomass allocated to stem, branch, and leaf components was determined for genus/species specific, and multispecies allometric equations in Chapter 3 (Flade et al., 2021). The allometric equations were used to derive field-based aboveground biomass from vegetation mensuration data collected across the southern Northwest Territories, which served as input for airborne lidar-based aboveground biomass model development in Chapter 4. Aboveground biomass allocation to plant components was used to infer standing plant carbon stocks used in Chapter 5. This chapter discussed the quantification of aboveground biomass and carbon stock changes in common boreal ecosystem types in the southern Taiga of northwestern Canada.

Based on the analysis in Chapter 2 and 3, the recommendations for modelling aboveground biomass of shrubs with higher accuracies is to use a 3D field variable as predictor, such as volume. This requires the measurement of three variables (height, intercept-cover) in the field and may take more time to collect. For short-stature trees, this analysis suggests that aboveground biomass can be most accurately predicted with the stem diameter measured at 0.3 m stem length. Shrub AGB can be reconciled with small-stature tree AGB when using total stem cross-sectional area as the predictor variable, which can be useful when plant functional types cannot be distinguished e.g. by active remote sensing applications such as lidar (Chapter 2, Flade et al., 2020). Aboveground biomass allocations to stems, branches, and leaves were similar between shrubs and deciduous tree genera/species but differed to *Picea* spp. The plant component AGB allometric equations resulted in better model fits for predicting stem biomass compared to leaf (shrubs) and leaf and branch (trees) biomass (Chapter 3, Flade et al., 2021).

Short-stature vegetation was also integrated in the next step of this thesis, which explored the development of one bi-temporal lidar-based aboveground biomass model applicable to short-to-tall-stature vegetation structure at varying vertical and horizontal continuity and to data collected with an earlier generation lidar system (Chapter 4, Flade et al., 2024). A suite of different airborne lidar height and cover metrics were tested, and model transferability between a lower density single channel and a higher density multi-channel lidar sensor were assessed.

Comparisons of modelled aboveground biomass between sensors per lidar metric showed lower variances in modelled AGB using the average height of all lidar returns in a 5 m x 5 m area (for modelled values below 100 Mg ha^{-1}) and the 90^{th} height percentile of

all returns (for modelled values above 100 Mg ha^{-1}) as predictor variable. Both lidar metrics were therefore calibrated for the earlier lidar sensor and used in the final bi-temporal shrub-to-tree AGB model within a weighted approach as a function of modelled aboveground biomass. The development of one single model applicable across changing ecosystem types and advancing and receding of ecosystem boundaries is important for quantifying anthropogenic climate change effects on forest to peatland ecotones, which are changing most rapidly (Chasmer & Hopkinson, 2017). The ability to transfer the model between different lidar sensors was also important, as this enabled future research of spatially explicit changes of aboveground biomass (Chapter 5) and provides an example for future studies aiming to compare AGB products amongst different generations of lidar systems. The resulting maps of aboveground biomass and aboveground biomass change could also aid in the validation of spaceborne aboveground biomass products (Chapter 5).

Finally, combining results from Chapters 2 to 4, decadal short-to-tall-stature vegetation structural and plant carbon changes were quantified and analysed at the plot level for a wide range of ecosystem types and changes were examined in relation to local/proximal environmental to regional hydroclimatic drivers (Chapter 5). Vegetation structural changes were quantified using overlapping airborne lidar data in 2010 and 2019. Changes were assessed through the following indicators of the cumulative impacts of multiple, interacting feedbacks occurring within the system: lidar-based aboveground biomass (Chapters 2 and 4); carbon stored in aboveground woody plant components (stems including bark and branches, Chapter 3); and vegetation height.

Results of this analysis (Chapter 5) showed that increases in short-stature vegetation greatly reduced or offset losses from tall-stature vegetation mortality. In total, up to 20% of

the areas sampled shifted from non-woody (open) to short-stature vegetation (> 0.5 m and ≤ 4.5 m in height). These shifts occurred most dominantly as short-stature vegetation densification within permafrost plateaus in low lying peatland complexes, and along bedrock outcrops and in floating fens around ponds/lakes in areas underlain by Precambrian Shield, sampled by the lidar data. Across the study region, permafrost plateaus gained 15 times as much aboveground biomass and plant carbon compared to upland forests on dominantly mineral soils. Bogs and fens changed towards similar vegetation structure in 2019, due to a similar increase in short-stature vegetation in previously open areas. Overall, the results suggest that shifts from the intermediate stages of collapse scar wetland expansion to the later stages of expedited drainage, hummock formation, and forest growth (absence of permafrost) in low lying peatland complexes occurred faster than expected (within a decade as opposed to half a century (Carpino et al., 2021)). In the majority of areas underlain by Precambrian shield, permafrost aggradation was not observed and needs to be further investigated, also in other areas.

The aboveground biomass and plant carbon changes and successional shifts towards woody vegetation were generally more importantly related to local to proximal topographical drivers, which relate to the distribution of plant available water in the landscape. However, drivers related to regional hydroclimatic changes were also important and differed across the study region with a greater importance of total annual precipitation trends in the west at lower latitudes (in Lee of several mountain ranges) and mean annual air temperature trends in the east at higher latitudes (in Lee of the Great Slave Lake).

The results of this study will provide a baseline from which to compare future vegetation structural changes and successional shifts due to the continued climate change

effects on these systems. The increased aboveground biomass densities and distributions found in this study (Chapter 5) increased the fuel connectivity between upland forests and peatland complexes. This information about wildland fire fuel dynamics could aid in the investigation of the large areas burned due to the abnormally dry 2022 and 2023 wildland fire years and in the mapping of fire refugia. Overall, the quantified changes in these systems over larger areas is important for improving our understanding of accelerating ecosystem succession, feedbacks to the global carbon-climate system, and the implications of changing aboveground biomass and wildland fire fuels to northern communities.

6.2. Outlook

This thesis has shown that integration of short-stature vegetation, from field data and allometric equations to the final models used to infer aboveground biomass and plant carbon is important for improving understanding of anthropogenic climate change effects on ecosystems in the southern Taiga of western Canada. Future research needs to integrate short-stature vegetation in bottom-up modelling frameworks as shown in this thesis. Although this is difficult with regional to global products, such as Landsat imagery, which may or may not indicate shrub-to-tree vegetation changes relative to soil moisture, landscape position, and understory influences, these data provide an unparalleled long-term record of environmental change. The use of field and bi-temporal airborne lidar data fusion as shown in this study could be used to consistently calibrate and validate Landsat imagery and current/future spaceborne lidar (e.g. Ice, Cloud, and Land Elevation Satellite 2 (National Aeronautics and Space Administration (NASA)), Biomass mission (European Space Agency), Multi-footprint Observation LIDAR and Imager mission (Japan Aerospace Exploration Agency)) and radar (e.g. NASA-ISRO SAR Mission (NASA and Indian Space

Research Organization)) aboveground biomass products at coincident locations (Duncanson et al., 2019; Wulder et al., 2012). Ultimately, the integration of transect-wide airborne lidar data in carbon reporting frameworks could aid in scaling shrub-to-tree aboveground biomass from forest inventory plots to the globe (Castilla et al., 2022; Wulder et al., 2020). This could reduce uncertainty in regional to global estimates of aboveground biomass stocks and carbon sink strength of boreal ecosystems and broaden the scope in carbon reporting obligations to unmanaged forest and peatland areas. With regards to changes in the Canadian wildland fire regime, an integrated framework of field data, airborne lidar data, and spaceborne data could aid in the modelling and quantification of vertical and lateral wildland fire fuel dynamics, predicting and managing of fire behaviour and carbon losses/pollution, and could inform for example indigenous-led cultural burning practices (Christianson et al., 2022) and FireSmart activities around remote northern communities.

6.2. References

Carpino, O., Haynes, K., Connon, R., Craig, J., Devoie, É., & Quinton, W. (2021). Long-term climate-influenced land cover change in discontinuous permafrost peatland complexes. *Hydrology and Earth System Sciences*, *25*(6), 3301–3317. https://doi.org/10.5194/hess-25-3301-2021.

Castilla, G., Hall, R. J., Skakun, R., Filiatrault, M., Beaudoin, A., Gartrell, M., et al. (2022). *The Multisource Vegetation Inventory (MVI): A Satellite-Based Forest Inventory for the Northwest Territories Taiga Plains* (p. 1108). Retrieved from https://www.mdpi.com/2072-4292/14/5/1108.

Chasmer, L., & Hopkinson, C. (2017). Threshold loss of discontinuous permafrost and landscape evolution. *Global Change Biology*, *23*(7), 2672–2686. https://doi.org/10.1111/gcb.13537.

Christianson, A. C., Sutherland, C. R., Moola, F., Gonzalez Bautista, N., Young, D., & MacDonald, H. (2022). Centering Indigenous Voices: The Role of Fire in the Boreal Forest of North America. *Current Forestry Reports*, *8*(3), 257–276. https://doi.org/10.1007/s40725-022-00168-9.

Dearborn, K., & Baltzer, J. (2021). Unexpected greening in a boreal permafrost peatland undergoing forest loss is partially attributable to tree species turnover. *Global Change Biology*, *27*(12), 2867–2882. https://doi.org/10.1111/gcb.15608.

Duncanson, L., Armston, J., Disney, M., Avitabile, V., Barbier, N., Calders, K., et al. (2019). The Importance of Consistent Global Forest Aboveground Biomass Product Validation. *Surveys in Geophysics*, *40*(4), 979–999. https://doi.org/10.1007/s10712-019-09538-8.

Flade, L., Hopkinson, C., & Chasmer, L. (2020). Allometric Equations for Shrub and Short-Stature Tree Aboveground Biomass within Boreal Ecosystems of Northwestern Canada. *Forests*, *11*(11), 1207. https://doi.org/10.3390/f11111207.

Flade, L., Hopkinson, C., & Chasmer, L. (2021). Aboveground Biomass Allocation of Boreal Shrubs and Short-Stature Trees in Northwestern Canada. *Forests*, *12*(2), 234. https://doi.org/10.3390/f12020234.

Flade, L., Hopkinson, C., & Chasmer, L. (2024). A Bi-Temporal Airborne Lidar Shrub-to-Tree Aboveground Biomass Model for the Taiga of Western Canada: Un Modèle Bitemporal de Biomasse Aérienne D'arbuste à D'arbre Pour le Lidar Aéroporté Pour la Taïga du L'ouest du Canada. *Canadian Journal of Remote Sensing*, *50*(1), 2379915. https://doi.org/10.1080/07038992.2024.2379915.

Flannigan, M. D., Logan, K. A., Amiro, B. D., Skinner, W. R., & Stocks, B. J. (2005). Future Area Burned in Canada. *Climatic Change*, *72*(1–2), 1–16. https://doi.org/10.1007/s10584-005-5935-y.

Germain Chartrand, P., Sonnentag, O., Sanderson, N. K., & Garneau, M. (2023). Recent peat and carbon accumulation on changing permafrost landforms along the Mackenzie River valley, Northwest Territories, Canada. *Environmental Research Letters*, *18*(9), 095002. https://doi.org/10.1088/1748-9326/ace9ed.

Goetz, S., Mack, M. C., Gurney, K. R., Randerson, J. T., & Houghton, R. A. (2007). Ecosystem responses to recent climate change and fire disturbance at northern high latitudes: observations and model results contrasting northern Eurasia and North America. *Environmental Research Letters*, *2*(4), 045031. https://doi.org/10.1088/1748-9326/2/4/045031.

Haynes, K. M., Connon, R. F., & Quinton, W. (2018). Permafrost thaw induced drying of wetlands at Scotty Creek, NWT, Canada. *Environmental Research Letters*, *13*(11), 114001. https://doi.org/10.1088/1748-9326/aae46c.

IPCC. (2023). *IPCC, 2023: Climate Change 2023: Synthesis Report. Contribution of Working Groups I, II and III to the Sixth Assessment Report of the Intergovernmental Panel on Climate Change [Core Writing Team, H. Lee and J. Romero (eds.)]. IPCC, Geneva, Switzerland.* (First) (p. 184). Geneva, Switzerland: Intergovernmental Panel on Climate Change (IPCC). https://doi.org/10.59327/IPCC/AR6-9789291691647.

Kasischke, E. S., & Turetsky, M. R. (2006). Recent changes in the fire regime across the North American boreal region—Spatial and temporal patterns of burning across Canada and Alaska. *Geophysical Research Letters*, *33*(9), 2006GL025677. https://doi.org/10.1029/2006GL025677.

Myers-Smith, I. H., Forbes, B. C., Wilmking, M., Hallinger, M., Lantz, T., Blok, D., et al. (2011). Shrub expansion in tundra ecosystems: dynamics, impacts and research priorities. *Environmental Research Letters*, *6*(4), 045509. https://doi.org/10.1088/1748-9326/6/4/045509.

Myers-Smith, I. H., Kerby, J. T., Phoenix, G. K., Bjerke, J. W., Epstein, H. E., Assmann, J. J., et al. (2020). Complexity revealed in the greening of the Arctic. *Nature Climate Change*, *10*(2), 106–117. https://doi.org/10.1038/s41558-019-0688-1.

Orndahl, K. M., Macander, M. J., Berner, L. T., & Goetz, S. J. (2022). Plant functional type aboveground biomass change within Alaska and northwest Canada mapped using a 35-year satellite time series from 1985 to 2020. *Environmental Research Letters*, *17*(11), 115010. https://doi.org/10.1088/1748-9326/ac9d50.

Wulder, M. A., White, J. C., Bater, C. W., Coops, N. C., Hopkinson, C., & Chen, G. (2012). Lidar plots — a new large-area data collection option: context, concepts, and case study. *Canadian Journal of Remote Sensing*, *38*(5), 600–618. https://doi.org/10.5589/m12-049.

Wulder, M. A., Hermosilla, T., White, J. C., Coops, N. C., Hopkinson, C., & Chen, G. (2020). Biomass status and dynamics over Canada's forests: Disentangling disturbed area from associated aboveground biomass consequences. *Environmental Research Letters*, *15*(9), 094093. https://doi.org/10.1088/1748-9326/ab8b11.

Appendix

Supplementary material Chapter 2

Table S2.1 and S2.2 provide the descriptive statistics of the measured shrub and tree structural information.

Table S2.1. Descriptive statistic by shrub species and genus by plant compartment (range of values in parentheses, followed by average ± standard deviation).

	No. of samples	Max Height (m)	Max Basal Diameter (cm)	Volume (m^3)	No. of branches	Total AGB (g)	ABG Stems (g)	AGB Leaves (g)
Alnus spp.	33	[0.2; 3.2]	[0.3; 2.3]	[0.004; 10.4]	[1; 18]	[1.3; 2057.1]	[0.6; 1856]	[0.4; 289.7]
		1.3 ± 0.7	1.0 ± 0.4	1.7 ± 2.5	4.5 ± 4.3	311.4 ± 470.9	264.8 ± 401.8	46.7 ± 68.0
Betula spp.	46	[0.2; 2.1]	[0.3; 3.1]	[0.004; 3.8]	[1; 66]	[4.0; 1154.1]	[2.2; 1057.2]	[1.3; 154.7]
		1.1 ± 0.4	0.8 ± 0.3	0.7 ± 0.7	8.7 ± 12.0	232.7 ± 261.1	188.2 ± 228.4	44.5 ± 42.3
Dasiphora fruticosa	20	[0.2; 0.9]	[0.2; 2.1]	[0.004; 1.3]	[1; 24]	[5.1; 530.8]	[3.6; 434.6]	[1.5; 96.2]
		0.6 ± 0.4	0.6 ± 0.3	0.3 ± 0.4	7.0 ± 6.2	117.6 ± 127.9	96.2 ± 105.8	21.4 ± 22.7
Salix spp.	79	[0.3; 2.8]	[0.2; 3.5]	[0.004; 10.4]	[1; 24]	[0.8; 1503.7]	[0.4; 1381.4]	[0.4; 284.8]
		0.9 ± 0.5	0.7 ± 0.4	0.7 ± 1.5	7.0 ± 6.2	143.3 ± 302.5	118.4 ± 261.1	24.9 ± 47.0
Shepherdia canadensis	28	[0.3; 1.7]	[0.3; 1.4]	[0.001; 4.4]	[1; 11]	[7.1; 552.0]	[5.7; 484.0]	[1.1; 127.0]
		0.8 ± 0.4	0.6 ± 0.2	0.6 ± 0.9	4.2 ± 2.9	121.5 ± 158.9	99.5 ± 134.9	22.0 ± 28.6
Universal Shrubs	206	[0.2; 3.2]	[0.2; 3.5]	[0.004; 10.4]	[1; 66]	[0.8; 2057.1]	[0.4; 1856]	[0.4; 289.7]
		0.9 ± 0.5	0.7 ± 0.4	0.8 ± 1.5	5.7 ± 7.5	184.7 ± 307.4	152.7 ± 265.8	32.0 ± 47.6

Table S2.2. Descriptive statistic by tree species by plant compartment (range of values in parentheses, followed by average ± standard deviation).

	No. of samples	Max Height (m)	D 0.3 m [cm]	DBH (cm)	No. of Branches	Total AGB (g)	AGB Stems (g)	AGB Branches (g)	AGB Leaves (g)
Betula papyrifera	15	[0.7, 3.4]	[0.3; 2.4]	[0.1; 1.9]	[7; 71]	[4.2; 596.2]	[2.6; 444.9]	[0.8; 95.7]	[0.8; 55.6]
		2.0 ± 0.8	1.1 ± 0.6	0.9 ± 0.5	25.7 ± 17.9	127.7 ± 162.2	93.0 ± 122.4	22.0 ± 26.1	12.7 ± 14.8
Picea glauca	14	[0.4; 3.8]	[0.3; 4.8]	[0.7; 4.1]	[17; 217]	[10.5; 3021.8]	[3.4; 1789.6]	[1.2; 739.4]	[5.9; 947.8]
		1.8 ± 1.2	2.4 ± 1.4	2.3 ± 1.3	80.4 ± 51.7	865.0 ± 992.4	426.1 ± 545.6	212.5 ± 247.8	226.4 ± 270.5
Picea mariana	15	[0.4; 3.6]	[0.3; 4.9]	[0.8; 3.3]	[33; 204]	[12.5; 2968.9]	[4.3; 1269.6]	[3.1; 1103.6]	[5.1; 595.7]
		1.6 ± 0.9	2.2 ± 1.2	2.3 ± 0.9	78.5 ± 47.7	668.5 ± 801.2	326.0 ± 412.2	195.2 ± 270.4	157.1 ± 152.2
Populus balsamifera	31	[0.2; 4.2]	[0.1; 2.3]	[0.1; 1.8]	[0; 39]	[1.0; 380.9]	[0.7; 294.9]	[0.3; 53.1]	[0.04; 47.0]
		1.7 ± 1.1	1.0 ± 0.6	1.0 ± 0.5	12.0 ± 10.7	85.7 ± 103.3	65.7 ± 81.3	11.3 ± 13.7	10.1 ± 11.1
Populus tremuloides	30	[0.4; 3.9]	[0.1; 2.2]	[0.1; 1.8]	[0; 45]	[1.1; 329.2]	[0.5; 233.7]	[0.04; 52.4]	[0.2; 58.1]
		1.8 ± 0.9	1.0 ± 0.6	0.8 ± 0.4	14.0 ± 12.4	67.8 ± 84.3	50.2 ± 58.7	8.6 ± 13.2	10.9 ± 14.0
Softwood (*Picea* spp.)	29	[0.4;3.8]	[0.3; 4.9]	[0.7; 4.1]	[17; 217]	[10.5; 3021.8]	[3.4; 1789.6]	[1.2; 1103.6]	[5.1; 947.8]
		1.7±1.0	2.3 ± 1.3	2.3 ± 1.1	79.4 ± 49.7	766.8 ± 95.6	376.0 ± 66.7	203.9 ± 11.3	191.8 ± 59.0
Hardwood	76	[0.2;4.2]	[0.1; 2.4]	[0.1; 1.9]	[0; 71]	[1.0; 596.2]	[0.5; 444.9]	[0.04; 95.7]	[0.04; 58.1]
		1.8±1.0	1.0 ± 0.6	0.9 ± 0.5	15.5 ± 14.1	86.9±113.2	65.2 ± 85.5	12.5 ± 17.6	10.9 ± 13.1
Universal Trees	105	[0.2;4.2]	[0.1; 4.9]	[0.1; 4.1]	[0; 217]	[1.0; 3021.8]	[0.5; 1789.6]	[0.04; 1103.6]	[0.04; 947.8]
		1.8±1.0	1.4 ± 1.0	1.2 ± 0.9	33.3 ± 40.7	273.8 ± 571.3	151.4 ± 299.6	67.9 ± 165.3	60.6 ± 141.4

Tables S2.3 and S2.4 provide volume-based regression coefficients and error statistics for shrub and tree genera/species and for the pooled data.

Table S2.3. Volume-based regression coefficient estimates with error statistics to be input Equation 2.4 – 2.7 as appropriate to derive shrub AGB.

			Coefficients							
			LN(β)	**β**	**SE (β)**	**α**	**SE (α)**	**CF**	**RMSE [g]**	**R^2**
***Alnus* spp.**	Total AGB	LLRC	5.296	199.5371		0.9065		1.1764	172.10	0.879
		NLS		185.0650	35.9639	0.9760	0.0976		160.04	0.882
***Betula* spp.**	Total AGB	LLRC	5.644	282.5908		0.7678		1.166	149.26	0.682
		NLS		342.4160	30.3336	0.8386	0.1082		146.70	0.684
Dasiphora fruticosa	Total AGB	LLRC	5.522	250.1348		0.7211		1.1573	72.93	0.679
		NLS		311.5860	37.4226	0.8450	0.1990		71.92	0.684
***Salix* spp.**	Total AGB	LLRC	5.383	217.6743		0.8522		1.1191	139.13	0.79
		NLS		262.4690	27.8660	0.7850	0.0590		137.50	0.794
Shepherdia canadensis	Total AGB	LLRC	5.294	199.1384		0.7457		1.0908	80.31	0.747
		NLS		232.2120	22.508	0.6290	0.0876		77.56	0.765
Pooled Taiga Plains	Total AGB	LLRC	5.432	228.6060		0.7806		1.1668	160.33	0.738
		NLS		270.2610	20.8187	0.7990	0.0490		159.78	0.738
Pooled Taiga Shield	Total AGB	LLRC	5.498	244.2030		0.9032		1.1417	150.78	0.869
		NLS		270.6400	18.9745	0.7620	0.0380		102.81	0.882
Multi-species Shrubs	Total AGB	LLRC	5.452	233.2241		0.8291		1.1668	144.12	0.788
		NLS		272.1160	14.8934	0.7780	0.0326		141.04	0.790

Table S2.4. Cross-sectional area-based regression coefficient estimates with error statistic to be input into Equation 2.4 – 2.7 as appropriate to calculate tree AGB.

			Coefficients							
			LN(β)	**β**	**SE (β)**	**α**	**SE (α)**	**CF**	**RMSE [g]**	**R^2**
Betula papyrifera	Total AGB	LLRC	4.339	76.6309		1.1870		1.0485	53.06	0.904
		NLS		61.6474	16.0751	1.4718	0.1999		47.18	0.917
Picea glauca	Total AGB	LLRC	4.756	116.2799		1.0410		1.0327	209.30	0.984
		NLS		95.3486	18.4689	1.1745	0.0709		120.51	0.985
Picea mariana	Total AGB	LLRC	4.953	141.5991		0.8995		1.0944	246.61	0.981
		NLS		96.4484	8.0496	1.1711	0.0317		56.43	0.995
Populus balsamifera	Total AGB	LLRC	4.104	60.5821		1.1320		1.1564	29.22	0.928
		NLS		63.1474	6.7808	1.2899	0.0966		27.04	0.931
Populus tremuloides	Total AGB	LLRC	4.086	59.5014		1.0280		1.0512	27.52	0.940
		NLS		53.9702	4.1524	1.3612	0.0698		16.27	0.964
Softwood	Total AGB	LLRC	4.859	128.8952		0.9719		1.0712	223.97	0.984

(*Picea* spp.)		NLS		95.9904	9.3193	1.1724	0.0360		93.06	0.989
Hardwood	Total AGB	LLRC	4.151	63.4975		1.1000		1.1001	41.29	0.897
		NLS		56.0728	4.9062	1.4360	0.0738		32.9	0.917
Multi-species Trees	Total AGB	LLRC	4.320	75.1886		1.1360		1.1352	133.68	0.987
		NLS		79.6818	3.9366	1.2396	0.0186		62.25	0.988

Table S2.5. Cross-sectional area-based regression coefficients with error statistic to be input into Equation 2.4 – 2.7 as appropriate to calculate general shrub and tree AGB.

			Coefficients							
			LN(β)	**β**	**SE (β)**	**α**	**SE (α)**	**CF**	**RMSE [g]**	**R^2**
General Shrubs and Trees	Total AGB	LLRC	4.553	94.9167		1.0840		1.1773	206.37	0.770
		NLS		128.8020	10.5595	0.9790	0.0340		94.80	0.776

Tables S2.6 and S2.7 provide model accuracies per predictor variable of each shrub and tree genus/species.

Table S2.6. Model performances for shrub total ABG prediction per genus/species. (All p values < 0.001).

Species	Dimension & Model	Input Variable	Total Error (%)	RMSE (g)	R^2
***Alnus* spp.**	1D LLR	Max Stem Length	-32.77	436.83	0.174
	1D LLRC	Max Stem Length	24.96	503.54	0.174
	1D NLS	Max Stem Length	1.86	412.34	0.210
	1D LLR	Max Basal Diameter	-29.06	354.05	0.486
	1D LLRC	Max Basal Diameter	4.24	334.06	0.486
	1D NLS	Max Basal Diameter	-2.55	332.52	0.486
	2D LLR	Cross-sectional Area Basal	-5.79	174.75	0.870
	2D LLRC	Cross-sectional Area Basal	4.51	168.05	0.870
	2D NLS	Cross-sectional Area Basal	-6.66	159.25	0.885
	3D LLR	Volume	-5.64	163.89	0.879
	3D LLRC	Volume	11.01	172.10	0.879
	3D NLS	Volume	-4.12	160.04	0.882
***Betula* spp.**	1D LLR	Max Stem Length	-31.65	251.66	0.153
	1D LLRC	Max Stem Length	12.72	257.47	0.153
	1D NLS	Max Stem Length	1.25	237.41	0.174
	1D LLR	Max Basal Diameter	-29.93	264.76	0.108
	1D LLRC	Max Basal Diameter	17.60	302.44	0.108
	1D NLS	Max Basal Diameter	2.67	236.92	0.180
	2D LLR	Cross-sectional Area Basal	-2.88	212.89	0.445
	2D LLRC	Cross-sectional Area Basal	14.35	237.76	0.445
	2D NLS	Cross-sectional Area Basal	5.54	178.42	0.540
	3D LLR	Volume	-16.33	160.52	0.682
	3D LLRC	Volume	-2.44	149.26	0.682
	3D NLS	Volume	1.36	146.70	0.684
Dasiphora fruticosa	1D LLR	Max Stem Length	-42.38	139.00	0.005
	1D LLRC	Max Stem Length	19.40	142.13	0.005
	1D NLS	Max Stem Length	0.59	126.15	0.029
	1D LLR	Max Basal Diameter	-30.76	119.75	0.224
	1D LLRC	Max Basal Diameter	27.13	144.00	0.224
	1D NLS	Max Basal Diameter	3.81	108.09	0.292

	2D LLR	Cross-sectional Area Basal	-18.74	83.10	0.639
	2D LLRC	Cross-sectional Area Basal	5.47	77.17	0.639
	2D NLS	Cross-sectional Area Basal	-3.17	76.36	0.645
	3D LLR	Volume	-13.82	77.20	0.679
	3D LLRC	Volume	-0.27	72.93	0.679
	3D NLS	Volume	-1.54	71.92	0.684
***Salix* spp.**	1D LLR	Max Stem Length	-30.54	289.10	0.204
	1D LLRC	Max Stem Length	11.02	356.09	0.204
	1D NLS	Max Stem Length	13.86	250.19	0.325
	1D LLR	Max Basal Diameter	-9.44	472.84	0.141
	1D LLRC	Max Basal Diameter	39.72	709.00	0.141
	1D NLS	Max Basal Diameter	15.69	251.75	0.320
	2D LLR	Cross-sectional Area Basal	-1.95	186.27	0.691
	2D LLRC	Cross-sectional Area Basal	6.37	200.18	0.691
	2D NLS	Cross-sectional Area Basal	13.40	150.88	0.757
	3D LLR	Volume	-9.62	140.63	0.790
	3D LLRC	Volume	1.15	139.13	0.790
	3D NLS	Volume	5.17	137.50	0.794
Shepherdia canadensis	1D LLR	Max Stem Length	-30.86	128.07	0.433
	1D LLRC	Max Stem Length	0.04	119.93	0.433
	1D NLS	Max Stem Length	-2.54	119.76	0.433
	1D LLR	Max Basal Diameter	-25.91	93.65	0.803
	1D LLRC	Max Basal Diameter	-2.11	74.60	0.803
	1D NLS	Max Basal Diameter	-0.25	69.50	0.809
	2D LLR	Cross-sectional Area Basal	-16.69	92.02	0.727
	2D LLRC	Cross-sectional Area Basal	-6.51	86.18	0.727
	2D NLS	Cross-sectional Area Basal	-3.22	81.44	0.738
	3D LLR	Volume	-11.23	81.16	0.747
	3D LLRC	Volume	-3.17	80.31	0.747
	3D NLS	Volume	5.41	77.56	0.765

Table S2.7. Model performances for tree total ABG prediction per genus/species. (All p values < 0.001).

Species	Dimension & Model	Input Variable	Total Error (%)	RMSE (g)	R^2
Betula papyrifera	1D LLR	Stem Length	-15.61	72.32	0.898
	1D LLRC	Stem Length	-9.17	65.41	0.898
	1D NLS	Stem Length	-4.73	44.93	0.925
	1D LLR	Diameter at 0.3 m	-8.18	56.24	0.904
	1D LLRC	Diameter at 0.3 m	-3.73	53.13	0.904
	1D NLS	Diameter at 0.3 m	-4.64	47.18	0.917
	2D LLR	Cross-sectional Area at 0.3 m	-8.09	56.15	0.904
	2D LLRC	Cross-sectional Area at 0.3 m	-3.64	53.06	0.904
	2D NLS	Cross-sectional Area at 0.3 m	-4.64	47.18	0.917
Picea spp.	1D LLR	Stem Length	0.12	458.52	0.766
	1D LLRC	Stem Length	7.88	488.66	0.766
	1D NLS	Stem Length	3.87	415.77	0.791
	1D LLR	Diameter at 0.3 m	-13.82	278.27	0.984
	1D LLRC	Diameter at 0.3 m	-7.69	223.99	0.984
	1D NLS	Diameter at 0.3 m	0.39	93.06	0.989
	2D LLR	Cross-sectional Area at 0.3 m	-13.81	278.23	0.984
	2D LLRC	Cross-sectional Area at 0.3 m	-7.68	223.97	0.984
	2D NLS	Cross-sectional Area at 0.3 m	0.39	93.06	0.989
Populus balsamifera	1D LLR	Stem Length	-9.78	33.77	0.914
	1D LLRC	Stem Length	-3.27	31.02	0.914
	1D NLS	Stem Length	2.13	30.33	0.914
	1D LLR	Diameter at 0.3 m	-13.88	37.03	0.928
	1D LLRC	Diameter at 0.3 m	-0.14	29.24	0.928
	1D NLS	Diameter at 0.3 m	-0.07	27.04	0.931
	2D LLR	Cross-sectional Area at 0.3 m	-13.82	36.98	0.928
	2D LLRC	Cross-sectional Area at 0.3 m	-0.34	29.22	0.928
	2D NLS	Cross-sectional Area at 0.3 m	-0.07	27.04	0.931
Populus tremuloides	1D LLR	Stem Length	-10.43	35.13	0.884
	1D LLRC	Stem Length	-3.05	32.01	0.884
	1D NLS	Stem Length	-2.51	25.42	0.910
	1D LLR	Diameter at 0.3 m	-11.25	30.27	0.940
	1D LLRC	Diameter at 0.3 m	-6.71	27.55	0.940
	1D NLS	Diameter at 0.3 m	-3.10	16.27	0.964

2D LLR	Cross-sectional Area at 0.3 m	-11.24	30.24	0.940
2D LLRC	Cross-sectional Area at 0.3 m	-6.69	27.52	0.940
2D NLS	Cross-sectional Area at 0.3 m	-3.10	16.27	0.964

Supplementary material Chapter 5

Figure S5.1 provides the trends in downscaled and gridded ClimateNA data (described in Chapter 5.3.8.). Trends in MAAT and TAP were derived from 1989 to 2019, including the last 10 years of the field/lidar-based change detection analysis. The slopes of the trends through annual deviations from the preceding 1961 to 1990 baseline period were derived for each sampled point and plotted as mean ± standard deviations.

Table S5.1 provides the number of sample points per ecoregion-specific ecosystem types.

Tables S5.2 and S5.3 provide the distribution of sampled aboveground biomass change per level of organization.

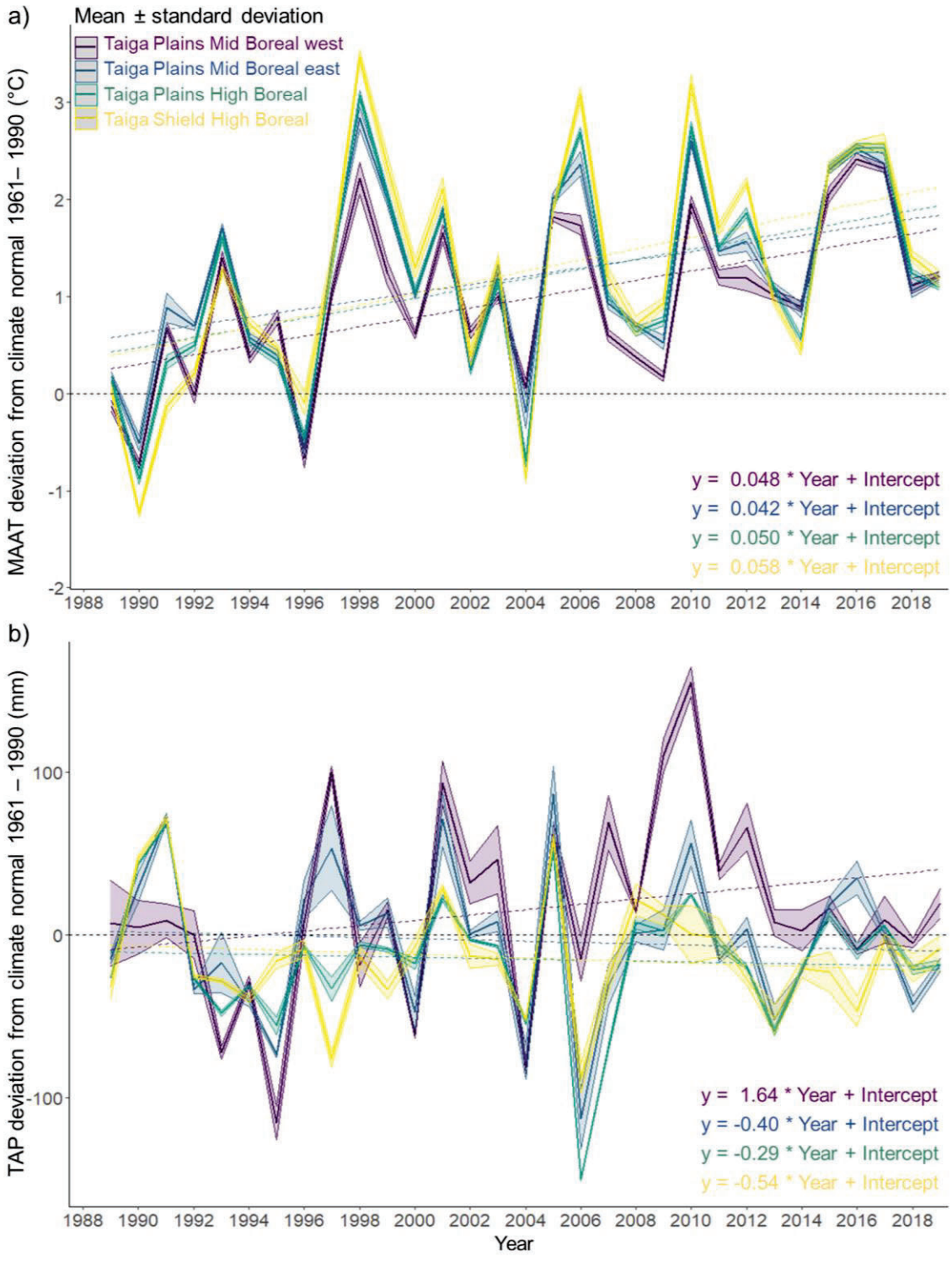

Figure S5.1. Trends in downscaled and gridded ClimateNA data of a) mean annual air temperatures (MAAT) and b) total annual precipitation (TAP) from 1998 to 2019 for ecoregions within the southern Northwest Territories on sporadic to discontinuous permafrost. Trends derived as slopes of linear trendlines plotted through annual climate variable deviations from climate normals (1961 to 1990) on a per grid-cell basis. Mean trends (± standard deviations) derived as averages of sampled grid cells per ecoregion.

Table S5.1. Random sample points (n) per ecoregion-specific ecosystem types

	Taiga Plains Mid Boreal	Taiga Plains High Boreal	Taiga Shield High Boreal	All ecoregions
Main ecosystem types				
Upland 'treed'	458	232	202	892
Peatland complex	1540	441	833	2814
Permafrost plateau	350		210	560
Ecotone UF to Peatland	164	131	92	387
Ecotone PF to Peatland	534		236	770
Peatland	492	310	295	1097
Bog	245	95	56	396
Fen	247	215	239	701
Ecotone & peatland class and form				
Ecotone UF to Bog	93	17	38	148
Ecotone UF to Fen	71	114	54	239
Ecotone PF to Bog	287		56	344
Ecotone PF to Fen	247		179	426
Ecotone UF to Bog 'open'	55	13	38	106
Ecotone UF to Bog 'treed'	38	4		42
Ecotone UF to Fen 'open'	60	93	50	203
Ecotone UF to Fen 'treed'	11	21	4	36
Ecotone PF to Bog 'open'	242		56	298
Ecotone PF to Bog 'treed'	45		See Ecotone PF to Bog	46
Ecotone PF to Fen 'open'	206		168	374
Ecotone PF to Fen 'treed'	41		11	52
Bog 'open'	144	45	See Bog	245
Bog 'treed'	101	50		151
Fen 'open'	166	143	155	464
Fen 'treed'	81	72	84	237

Table S5.2. Distribution of sampled aboveground biomass change (dAGB) for ecoregion-specific ecotones and peatland class and form.

	ΔAGB (Mg ha^{-1} a^{-1})	ΔAGB (Mg ha^{-1})			ΔAGB relative to 2010 (%)		Δ plant C (Mg C ha^{-1})	
Stratum	Mean	Mean	SD	IQR	Mean	IQR	Mean	SD
Ecoregion-specific ecosystem types: Taiga Plains Mid Boreal								
Ecotone UF to Bog	0.16	1.4	9.3	-0.4	6	-2	0.6	3.9
Ecotone UF to Fen	-0.12	-1.1	19.3	-1.5	-3	-4	-0.5	8.0
Ecotone PF to Bog	0.23	2.1	7.6	-1.4	22	-10	0.9	3.2
Ecotone PF to Fen	0.33	3.0	9.7	1.1	19	8	1.2	4.0
Ecotone UF to Bog 'open'	0.10	0.9	8.5	3.3	4	15	0.4	3.5
Ecotone UF to Bog 'treed'	0.24	2.2	10.4	-0.7	8	-3	0.9	4.3
Ecotone UF to Fen 'open'	-0.01	-0.1	15.4	2.1	0	5	0.0	6.4
Ecotone UF to Fen 'treed'	-0.76	-6.8	34.2	2.0	-18	7	-2.8	14.3
Ecotone PF to Bog 'open'	0.27	2.4	7.5	-0.7	26	-5	1.0	3.1
Ecotone PF to Bog 'treed'	0.08	0.7	8.0	-2.9	5	-19	0.3	3.3
Ecotone PF to Fen 'open'	0.31	2.8	9.5	1.8	20	15	1.2	3.9
Ecotone PF to Fen 'treed'	0.43	3.9	10.9	-8.7	18	-37	1.6	4.6
Bog 'open'	0.16	1.4	2.1	1.8	154	370	0.6	0.9
Bog 'treed'	0.24	2.2	5.6	-1.1	22	-9	0.9	2.3
Fen 'open'	0.18	1.6	2.7	1.3	123	104	0.7	1.1
Fen 'treed'	0.44	4.0	10.1	3.8	40	32	1.7	4.2
Ecoregion-specific ecosystem types: Taiga Plains High Boreal								
Ecotone UF to Bog	-0.07	-0.6	8.5	-9.9	-2	-26	-0.3	3.5
Ecotone UF to Fen	-0.32	-2.9	14.6	-9.6	-7	-22	-1.2	6.1
Ecotone UF to Bog 'open'	0.17	1.5	8.4	7.7	5	39	0.6	3.5
Ecotone UF to Bog 'treed'	-0.84	-7.6	3.8	-2.1	-17	-14	-3.2	1.6
Ecotone UF to Fen 'open'	-0.34	-3.1	15.4	-5.2	-7	-12	-1.3	6.4
Ecotone UF to Fen 'treed'	-0.22	-2.0	10.8	-16.0	-5	-43	-0.8	4.5
Bog 'open'	-0.04	-0.4	4.2	0.1	-5	2	-0.2	1.8
Bog 'treed'	-0.01	-0.1	12.6	5.2	0	30	0.0	5.3
Fen 'open'	-0.16	-1.4	9.2	-1.0	-20	-14	-0.6	3.8
Fen 'treed'	-0.02	-0.2	8.4	-3.0	-1	-11	-0.1	3.5

IQR: Interquartile range (3rd quartile – 1st quartile); change derived as IQR 2019 – IQR 2010.

Table S5.2. Continued

Stratum	ΔAGB (Mg ha^{-1} a^{-1}) Mean	ΔAGB (Mg ha^{-1}) Mean	SD	IQR	ΔAGB relative to 2010 (%) Mean	IQR	Δ plant C (Mg C ha^{-1}) Mean	SD
Ecoregion-specific ecosystem types: Taiga Shield High Boreal								
Ecotone UF to Bog	0.39	3.5	6.0	1.4	33.1	12.4	1.5	1.8
Ecotone UF to Fen	0.59	5.3	8.0	9.8	31.4	60.9	2.2	3.2
Ecotone PF to Bog	0.21	1.9	4.3	-0.7	18.8	-4.3	0.8	2.5
Ecotone PF to Fen	0.50	4.5	7.6	3.2	26.4	17.7	1.9	3.3
Ecotone UF to Fen 'open'	0.64	5.8	7.8	10.0	35.6	62.8	2.4	3.2
Ecotone UF to Fen 'treed'	-0.09	-0.8	6.4	2.4	-3.3	16.6	-0.3	2.7
Ecotone PF to Fen 'open'	0.44	4	4	2.7	25.1	15.4	1.7	1.7
Ecotone PF to Fen 'treed'	1.32	11.9	9.6	12.7	36.1	52.6	5.0	4.0
Fen 'open'	0.11	1.0	2.3	0.6	45.8	38.9	0.4	1.0
Fen 'treed'	0.60	5.4	10.5	3.9	18.1	11.8	2.2	4.4

IQR: Interquartile range (3rd quartile – 1st quartile); change derived as IQR 2019 – IQR 2010.

Table S5.3. Distribution of sampled aboveground biomass change (dAGB) for ecotones and peatland class and form (pooled for all ecoregions).

	ΔAGB (Mg ha^{-1} a^{-1})	ΔAGB (Mg ha^{-1})			ΔAGB relative to 2010 (%)		Δ plant C (Mg C ha^{-1})	
Stratum	Mean	Mean	SD	IQR	Mean	IQR	Mean	SD
Pooled Ecosystem types								
Ecotone UF to Bog	0.19	1.7	8.5	3.6	8	17	0.7	3.5
Ecotone UF to Fen	-0.06	-0.5	15.3	-6.1	-1	-15	-0.2	6.4
Ecotone PF to Bog	0.23	2.1	7.2	-0.4	21	-3	0.9	3.0
Ecotone PF to Fen	0.40	3.6	8.9	-0.1	23	-1	1.5	3.7
Ecotone UF to Bog 'open'	0.21	1.9	7.7	5.6	10	32	0.8	3.2
Ecotone UF to Bog 'treed'	0.14	1.3	10.4	-1.3	4	-5	0.5	4.3
Ecotone UF to Fen 'open'	0.00	0.0	14.3	-3.3	0	-8	0.0	6.0
Ecotone UF to Fen 'treed'	-0.37	-3.3	20.3	-6.7	-9	-21	-1.4	8.5
Ecotone PF to Bog 'open'	0.26	2.3	7.0	0.0	25	0	1	2.9
Ecotone PF to Bog 'treed'	0.07	0.6	7.9	-3	5	-18	0.3	3.3
Ecotone PF to Fen 'open'	0.37	3.3	8.5	0.8	22	6	1.4	3.6
Ecotone PF to Fen 'treed'	0.62	5.6	11.1	1.4	23	6	2.3	4.6
Bog 'open'	0.10	0.9	2.6	1.3	39	113	0.4	1.1
Bog 'treed'	0.17	1.5	8.6	0.0	11	0.2	0.6	3.6
Fen 'open'	0.06	0.5	5.6	0.8	14	37	0.2	2.3
Fen 'treed'	0.36	3.2	10.0	5.0	16	22	1.3	4.2

IQR: Interquartile range (3rd quartile – 1st quartile); change derived as IQR 2019 – IQR 2010.